UNIVERSIDAD COMPLUTENSE DE MADRID
FACULTAD DE MEDICINA

TESIS DOCTORAL

El receptor de quimioquinas CCR7 induce ubiquitinación de proteínas en el núcleo de las células dendríticas

MEMORIA PARA OPTAR AL GRADO DE DOCTOR

PRESENTADA POR

Carolina Gómez Moreira

Director

José Luis Rodríguez Fernández

Madrid, 2019

Universidad Complutense de Madrid

Facultad de Medicina

Doctorado en Investigación Biomédica

El Receptor de Quimioquinas CCR7 Induce Ubiquitinación de Proteínas en el Núcleo de las Células Dendríticas

Memoria para optar al grado de doctor presentada por:

Carolina Gómez Moreira

Director:

José Luis Rodríguez Fernández

Madrid 2018

El Dr. José Luis Rodríguez Fernández, Investigador Científico del Centro de Investigaciones Biológicas (CIB – CSIC) de Madrid.

CERTIFICA

Que el trabajo titulado: "El Receptor de Quimioquinas CCR7 Induce Ubiquitinación de Proteínas en el Núcleo de las Células Dendríticas", que presenta Carolina Gómez Moreira para la obtención del Grado de Doctor por la Universidad Complutense de Madrid, ha sido realizado bajo mi dirección en el grupo de "Funciones de los receptores quimiotácticos y la sinapsis inmunológica en las células dendríticas" del CIB y reúne la calidad y contenidos suficientes para que sea presentado ante el tribunal correspondiente.

Para que así conste a los efectos oportunos, se expide el presente certificado en Madrid, 20 de marzo de 2018.

Dr. José Luis Rodríguez Fernández

"Research is not a systematic occupation
but an intuitive artistic vocation"

Albert Szent-Gyorgyi

A mi familia, y a tí, Paolo

AGRADECIMIENTOS

Si tuviera que hablar de toda la gente maravillosa con la que me he topado estos años, creo que ocuparía más que toda esta tesis. Sin poderles dedicar todo el espacio que se merecen, me gustaría dedicarles unas palabras.

José Luis, gracias por darme la oportunidad de formarme como investigadora en tu laboratorio, por tu respeto y por tu confianza. Siempre has hecho valer mi opinión tanto como la tuya, aun cuando mis conocimientos son muchísimo menores que los tuyos. Gracias por enseñarme lo bonito que es este trabajo y por contagiarme la pasión tan grande que tienes por la ciencia.

A mis compañeras de bata y de cultivos, creo que me hubiera vuelto loca si no os hubiera tenido a mi lado. Gracias por acogerme con tanto cariño. Me habéis levantado y animado a seguir, tantas veces, que no sé dónde estaría si no fuera por vuestro apoyo. Todas me habéis enseñado algo diferente, y no hablo solo de ciencia, sino de la vida. Esta tesis tiene un cachito de cada una de vosotras y espero que sigáis formando parte de mi vida siempre.

Gracias a los servicios técnicos del CIB, sin los cuales el desarrollo de este trabajo no hubiera sido posible.

Gracias al laboratorio de inmunooncología del Hospital Gregorio Marañón, por ayudarme a hacer frente a la tormenta, me llevo a gente maravillosa de allí.

También me gustaría agradecer al departamento de fisiología de la facultad de medicina. Gracias Soni, por ayudarme a dar mis primeros pasitos en la investigación. Ana, gracias por enseñarme todo lo que sabías. Anabel y Mª Ángeles, fuisteis como dos madres cuyo apoyo fue fundamental para mí en muchos momentos. Y a todo el departamento, un enorme GRACIAS.

Me siento una persona muy afortunada por la familia que tengo. Si algún día llego lejos, será porque he partido con ventaja. Me habéis apoyado en cada una de mis decisiones, sin importar lo descabelladas que fueran. Fer, Susa, sois las personas más luchadoras que conozco, sabéis buscarle caminos alternativos a cada problema que os plantea la vida, y os admiro tanto, que ojalá pueda llegar a ser como vosotros algún día. Gracias Martín, Yeya y Yaya.

Y a tí, Paolo, me completas y me haces feliz, gracias.

ABREVIATURAS Y ACRÓNIMOS

ACR	Atypical chemokine receptor
ADN	Ácido desoxirribonucleico
ADP	Adenosín-difosfato
AEBSF	4-(2-aminoethyl)benzenesulfonyl fluoride hydrochloride
AKT	Protein kinase B
AMP	Adenosín-monofosfato
APC	Anaphase promoting complex
ATP	Adenosin-trifosfato
BSA	Bovine serum albumin
BTB	Broad-Complex, Tramtrack and Bric a brac domain
CAND1	Cullin-associated and neddylation-dissociated 1
CCD	Charge-coupled device camera
CCL	Chemokine (C-C motif) ligand
CCR	Chemokine (C-C motif) receptor
CD14	Cluster of differentiation 14
CDs	Células dendríticas
CLSM	Microscopio Láser Confocal espectral
CMH	Complejo mayor de histocompatibilidad
CRL	Cullin-containing RING-E3 ligase
CSN	Señalosoma COP9
Cul-1	Cullin-1
CXCL	Chemokine (CXC motif) ligand
CXCR	Chemokine (CXC motif) receptor
DAMPS	Damage associated molecular patterns
DAPI	4 ',6-diamino-2-fenilindol
DCAF	DDB1- and CUL4-associated factor
DCN1	Defective in cullin neddylation protein 1
DCUN1D1	DCN1-like protein 1
DDB1	DNA damage-binding protein 1
DEN1	Deneddylase 1
DRY	Aspárico, arginina, tirosina
DTT	Ditiotreitol
ECL	Enhanced chemiluminescence
EDTA	Ácido etilen-diamino-tetracético
EGTA	Ácido etilenbis(oxietilennitrilo)tetracético
ELC	Epstein-Barr virus-induced molecule 1 ligand chemokine
ERK	Extracellular signal-regulated kinase
FBS	Fetal Bovine Serum
FITC	Isotiocianato de fluoresceína (verde)
FL1	Fluorescence laser 1
FOXO	Forkhead box protein O
GAG	Glicosaminoglicano
GDP	Guanosín difosfato

GM-CSF	Granulocyte macrophage colony-stimulating factor
GMP	Guanosín monofosfato
GPCRs	Receptor acoplado a proteína G
GRK	G-receptor coupled kinase
GTP	Guanosín trifosfato
Gαi	Subunidad αi de la proteína G
Gα13	Subunidad α13 de la proteína G
Gβ2	Subunidad β2 de la proteína G
HCD	Colisión de alta energía
HECT	Homologous to E6-AP carboxyterminus
Hepes	2-[4-(2-hydroxyethyl)piperazin-1-yl]ethanesulfonic acid
HLA	Human Leukocyte Antigen
HLA-DR	Human Leukocyte Antigen - antigen D Related
HRP	Horseradish peroxidase
IgG	Inmunoglobulina G
IL-4	Interleukina 4
IκBα	Inhibitor of NfκB protein α
JNK	c-Jun N-terminal kinase
K	Lisina
KO	Knock out
LAT	Linker for activation of T cells
LC	Cromatografía líquida
LDH	Lactato deshidrogenasa
LIMK	LIM domain kinase
M	Metionina
MEK	Mitogen-activated protein kinase kinase
MHC	Major histocompatibility complex
MLC	Myosin Light Chain
MS	Espectrometría de masas
Mst1	Mammalian Sterile 20-like 1 Kinase
mTORC	Mammalian target of rapamycin complex
MYPT1	Myosin phosphatase target subunit 1
NAE	Nedd-activating enzyme 1
Nedd8	Neural precursor cell expressed developmentally down-regulated 8
NFκB	Nuclear factor kappa-light-chain-enhancer of activated B cells
NK	Célula natural killer
NP-40	Nonidet p-40
p65	Transcription factor p65 (NFκB)
PAGE	Electroforesis en gel de poliacrilamida
PAMPS	Pathogen Associated Molecular Patterns
PBMCs	Células mononucleares de sangre periférica
PBS	Phosphate buffered saline
PCR	Reacción en cadena de la polimerasa
PFA	Paraformaldehido
PHD	Plant homeo domain
PI3K	Phosphoinositide 3-kinase
PKA	Protein kinase A

PKC	Protein kinase C
PLA	Proximity Ligation Assay
ppm	Partes por millón
PVDF	Polifluoruro de vinilideno
PYK2	Protein Tyrosine Kinase 2 Beta
RAF	Rapidly Accelerated Fibrosarcoma Kinase
Rbl2	Retinoblastoma-like protein 2
Rbx1	RING-box protein 1
Rbx2	RING-box protein 2
Rho A	Ras homolog gene family, member A
RING	Really interesting new gene
ROCK	Rho-associated protein kinase
RPMI	Medio Roswell Park Memorial Institute
SCF	Skp1-Cul1-Fbox complex
SDS	Dodecilsulfato sódico
SDS-PAGE	Electroforesis en gel de acrilamida con SDS
siRNA	Small interfering RNA
SI	Sistema inmunológico
Skp1	S-Phase kinase associated protein 1
Skp2	S-Phase kinase associated protein 2
SLC	Secondary lymphoid-tissue chemokine
SOCS	Suppressor of cytokine signaling
TBS	Tris-buffered saline
TBST	Tween Tris-buffered saline
TCR	T Cell receptor
TNFα	Tumor necrosis factor α
Tris-HCl	Tris ácido clorhídrico
TRITC	Tetrametilrodamina
TSC2	Tuberous Sclerosis Complex 2
UBA1	Ubiquitin activating enzyme 1
Ub	Ubiquitina
UBA1	Ubiquitin C-Terminal Hydrolase L3
UCHL3	Ubiquitin activating enzyme 1
ULM	Ubiquitin like modifier proteins
UPS	Ubiquitin proteasome system
Zn	Zinc
4EBP1	Eukaryotic Translation Initiation Factor 4E Binding Protein 1

ÍNDICE

RESUMEN

Las células dendríticas (CDs) son células presentadoras de antígenos que desempeñan un papel crucial en el comienzo de la respuesta inmunológica adaptativa. En los tejidos y antes de su encuentro con el antígeno, las CDs se encuentran en un estado inmaduro, sin embargo, cuando las CDs inmaduras se exponen a patógenos u otras "señales de peligro", sufren un proceso denominado maduración o activación durante el cual, entre otros cambios, se produce el incremento en la expresión del receptor de quimioquinas CCR7. Este receptor controla la migración de las CDs maduras desde el foco de inflamación hacia los ganglios linfáticos, siguiendo un gradiente de concentración sus ligandos, CCL19 y CCL21. En los ganglios, las CDs presentarán los antígenos endocitados a los linfocitos T específicos para generar una respuesta adaptativa. Además de la quimiotaxis, CCR7 regula otras funciones en las CDs, como la maduración, la supervivencia, la endocitosis, la citoarquitectura y la velocidad migratoria.

El complejo SCF es un complejo enzimático con actividad E3 ubiquitin ligasa encargado de la ubiquitinación de numerosas proteínas en la célula para posteriormente ser degradadas por el proteasoma. Este complejo está compuesto por Skp1, Rbx1 y Cul-1. Para que el complejo se active, es necesario que la proteína de ensamblaje Cul-1 sea modificada covalentemente por Nedd8, una molécula homóloga a la ubiquitina, mediante un proceso denominado nedilación.

En este trabajo estudiamos si CCR7 podía estar induciendo nedilación, y consecuente activación, de la ubiquitin ligasa SCF en las CDs y también investigamos las consecuencias funcionales de dicha activación. En primer lugar, observamos que la estimulación de CCR7 con CCL21 inducía nedilación de Cul-1 a través de la señalización mediada por la familia de proteínas de Gαi. Posteriormente analizamos si dicha nedilación podía estar mediando alguna de las funciones reguladas por CCR7 en las células dendríticas. Sin embargo, observamos que la inhibición farmacológica de la nedilación con MLN4924 (MLN) no afectaba a las funciones reguladas por CCR7, incluyendo, la supervivencia, quimiotaxis, velocidad migratoria, endocitosis o la citoarquitectura de estas células.

Sorprendentemente, observamos que la nedilación de Cul-1 ocurría en el núcleo de las CDs. En este sentido, se comprobó que Cul-1 se encontraba en el núcleo formando parte del complejo SCF con Skp1 y Rbx1. En este trabajo también observamos que la estimulación de CCR7 indujo poliubiquitinación tipo K48 (Poli-Ub-K48), relacionada con la degradación proteasomal, en el núcleo de las CDs. Dicho incremento en Poli-Ub-K48 se inhibió cuando las células fueron pretratadas con MLN. La reducción en los niveles de Cul-1 mediante un siRNA tuvo un efecto similar sobre la Poli-Ub-K48 inducida por CCR7.

Estos resultados sugieren que CCR7 induce la Poli-Ub-K48 de proteínas a través de la nedilación de Cul-1, lo cual induce activación de la E3 ligasa SCF en el núcleo de las CDs. Apoyando este concepto, nuestros estudios indican que la ubiquitina (Ub) colocaliza con Nedd8 en el núcleo de las CDs y además la Ub

nuclear desaparece cuando se inhibe la nedilación con MLN o cuando se silencia Cul-1 mediante un siRNA.

Finalmente, analizamos si la degradación de las proteínas ubiquitinadas podía estar ocurriendo en el mismo núcleo de las CDs. Nuestros estudios mostraron la presencia de un componente del proteasoma 26S en el núcleo de las CDs y su posible cercanía con el complejo SCF, sugiriendo que la degradación de las proteínas ubiquitinadas en respuesta a CCR7 podría darse en el núcleo de las CDs. Con el fin de averiguar qué proteínas se ubiquitinan en respuesta a la estimulación de CCR7, se realizaron estudios de proteómica precipitando Cul-1 de extractos de proteínas nucleares. El análisis del interactoma de Cul-1 sugiere que esta proteína puede estar participando en el metabolismo de proteínas, y, posiblemente, en el mantenimiento de la proteostasis nuclear.

En conclusión, nuestros resultados indican que CCR7 puede inducir otros tipos de modificaciones post-traduccionales diferentes a la fosforilación, como es la nedilación y la ubiquitinación. Este trabajo describe una nueva vía de señalización regulada por CCR7 que induce la nedilación de Cul-1 y la activación de SCF en el núcleo de las CDs. Este complejo es responsable de la Poli-Ub-K48 de proteínas nucleares. La presencia de proteasomas y su cercanía a SCF sugieren que la degradación de proteínas puede darse en el núcleo de las CDs. En este sentido, los datos obtenidos permiten especular que CCR7 podría estar participando en el mantenimiento de la proteostasis nuclear.

SUMMARY

Dendritic cells (DCs) are potent antigen presenting cells, key for the development of an adaptive immune response. DCs are found in peripheral tissues in an immature state, but when these cells encounter a pathogen or a "danger signal", they undergo a process called maturation, in which, they upregulate the expression of chemokine receptor CCR7. This receptor controls the migration of DCs from the inflammation site to the lymph nodes, following the concentration gradient of its ligands, chemokines CCL19 and CCL21. In the lymph nodes, DCs will present the antigens endocyted to specific T cells to activate an adaptive response. In addition to chemotaxis, CCR7 controls other functions in DCs, such as maturation, survival, endocytosis, cytoarchitecture and migratory speed.

The SCF complex (Skp1-Cul-1-Fbox containing complex) is an E3 ubiquitin ligase enzyme that mediates the ubiquitination of a large number of proteins in the cell to induce their degradation by the ubiquitin proteasome system. This complex contains the proteins Skp1, Rbx1 and Cul-1. For SCF to be activated, Cul-1 has to be modified covalently by Nedd8, an ubiquitin-like protein. This process is called neddylation.

In this study we wanted to find out if CCR7 could induce neddylation of the SCF and the functional significance of this process in DCs. First, we observed that stimulation of CCR7 with CCL21 induces neddylation of Cul-1 through Gαi protein signaling. Next, we analyzed if this neddylation could be controlling CCR7-regulated functions in DCs. In this regard, we inhibited neddylation with a

drug called MLN4924 (MLN), but we observed no effect of this inhibition in CCR7 induced survival, chemotaxis, migratory speed, endocytosis or cytoarchitecture changes in DCs.

We later found that neddylation of Cul-1 was occurring in the nucleus of DCs and we confirmed that Cul-1 was part of the SCF complex, along with Skp1 and Rbx1 in the nucleus.

Upon CCR7 stimulation, we observed an increase in K48 polyubiquitination (K48-Poly-Ub), known to direct proteins for their degradation by the proteasome, in the nucleus of DCs. This increase was prevented by MLN treatment. A similar result was observed when Cul-1 levels were reduced with a siRNA. These results indicate that CCR7 is inducing K48-Poly-Ub of proteins in the nucleus of DCs through SCF Neddylation/activation. Consistent with these results, fluorescence microscopy analysis showed Ub was found concentrated in the nucleus of DCs co-localizing with Nedd8. Upon MLN treatment or Cul-1 reduction by a siRNA, Ub levels decreased in the nucleus of DCs. We could also detect proximity between Nedd8 and Ub, abolished when DCs were treated with MLN.

Likewise, we wondered whether degradation also could be taking place in the nucleus of DCs. Our studies show there are proteasomes in the nucleus of DCs and these superstructures seem to be close to the SCF complex, suggesting degradation of ubiquitinated proteins in response to SCF could also take place in the nucleus of DCs.

To find out which proteins are being ubiquitinated in response to CCR7, we carried out proteomic studies of the nuclear interactome of Cul-1. Our results indicate Cul-1 could participate in proteins metabolism, and, possibly, in the maintenance of nuclear proteostasis.

In conclusion, we have observed that CCR7 can induce other types of posttranslational modifications, different from phosphorylation, such as neddylation and ubiquitination. We describe a new signaling pathway in which CCR7 induces neddylation of Cul-1 and the activation of the SCF complex. This takes place largely in the nucleus of DCs and it is responsible for the K48-Poly-Ub of proteins in this compartment. Degradation also could be taking place in the nucleus of DCs, as the presence of proteasomes seems to indicate. In this regard, we speculate CCR7 could be participating in the maintenance of nuclear proteostasis.

RESUMEN GRÁFICO

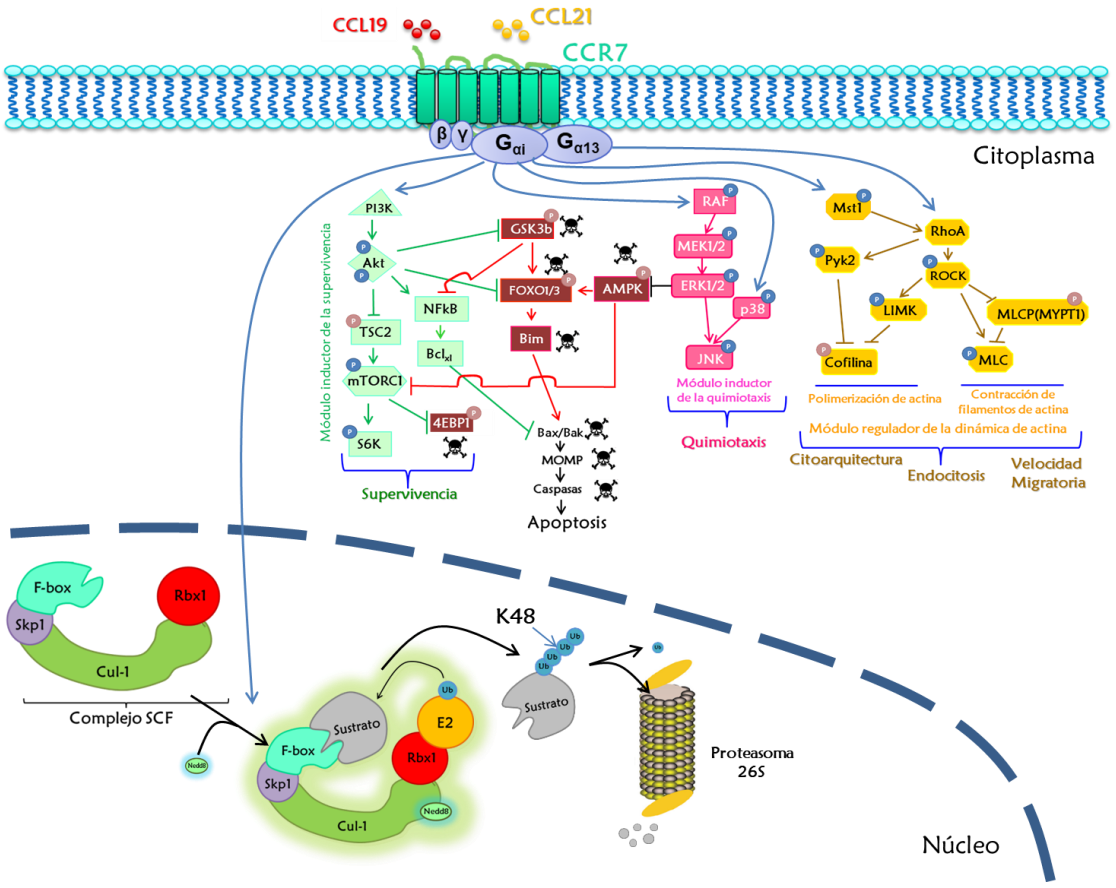

Modelo actualizado de la señalización intracelular activada por CCR7. La estimulación de CCR7 con sus ligandos, CCL19 y CCL21, induce un aumento de la supervivencia, la quimiotaxis, la velocidad migratoria y la endocitosis, así como cambios la citoarquitectura de las CDs. Los resultados obtenidos en esta tesis sugieren una nueva vía de señalización en la que la estimulación de CCR7 induce la nedilación de Cul-1 en el núcleo, activando así al complejo SCF, que induce poliubiquitinación tipo K48 de proteínas nucleares, para ser degradadas posteriormente por el proteasoma.

INTRODUCCIÓN

1. El sistema inmunológico

El sistema inmunológico (SI) protege al organismo frente a múltiples amenazas, incluyendo patógenos, agentes físicos y químicos o células tumorales, gracias a la coordinación de dos tipos de respuestas inmunológicas: la respuesta innata y la respuesta adaptativa. La respuesta inmunológica innata constituye la primera línea de defensa del organismo y es la encargada de reconocer las amenazas y actuar de manera inmediata y, relativamente, inespecífica para eliminarlas (Dudek, Martin et al. 2013). Las células del sistema inmune innato y otras células del organismo expresan receptores que reconocen estructuras microbianas conservadas denominadas "patrones moleculares asociados a patógenos" ("pathogen associated molecular patterns (PAMPs), u otras "señales de peligro", "patrones moleculares asociados al daño" ("damage associated molecular patterns (DAMPs))(Medzhitov 2001), que activan una respuesta inflamatoria en estas células.

La respuesta inmunológica adaptativa se desencadena de manera muy específica contra agentes que son reconocidos como antígenos. Comparada con la inmunidad innata, la inmunidad adaptativa se produce de manera más tardía (tras varios días). Está mediada principalmente por los linfocitos T y los linfocitos B, que tras ser activados por células de la inmunidad innata, maduran y generan clones de linfocitos específicos contra el antígeno (Iwasaki and Medzhitov 2015). Estos clones serán los responsables de generar la llamada "memoria

inmunológica", que consiste en la capacidad del sistema inmune de reaccionar de manera rápida y específica si se expone nuevamente a un antígeno con el que ya haya estado en contacto previamente (Dudek, Martin et al. 2013).

Aunque hasta ahora se pensaba que la memoria inmunológica era exclusiva del SI adaptativo, recientemente se ha descubierto que el SI innato posee una capacidad similar, a la que se ha denominado "inmunidad entrenada" ("trained immunity"). Este tipo de "memoria" confiere a las células del SI innato la capacidad de responder de manera más rápida y eficiente frente a un determinado antígeno con el que ya han estado en contacto anteriormente (Franceschi, Salvioli et al. 2017; Lee, Geng et al. 2017).

Para que se inicie la respuesta inmune adaptativa, es necesario que los linfocitos reconozcan al antígeno, que se expone sobre moléculas del complejo mayor de histocompatibilidad (CMH en ratón o HLA en humano) en la superficie de las células presentadoras de antígenos. Las células dendríticas son las más potentes y eficaces células presentadoras de antígenos.

2. Ciclo biológico y función de las células dendríticas

Las células dendríticas (CDs) juegan un papel clave en la iniciación de la respuesta inmunológica adaptativa, así como en la inducción de memoria inmunológica y tolerancia periférica (Mellman 2013).

Al igual que los monocitos y los macrófagos, las CDs derivan de progenitores hematopoyéticos de la médula ósea con un potencial de diferenciación mieloide.

Dichos progenitores mieloides dan lugar, tras sucesivas etapas de diferenciación, a pre-CDs que pasan al torrente circulatorio para posteriormente extravasarse a los tejidos periféricos (Geissmann, Manz et al. 2010). En estos tejidos, las CDs se encuentran en una fase de diferenciación denominada "inmadura" (figura 1). Las CDs inmaduras realizan una labor de "vigilantes" frente a patógenos invasores o señales de peligro. Este estado inmaduro se caracteriza por una alta capacidad endocítica, principalmente mediante macropinocitosis y fagocitosis, y una capacidad de presentación antigénica relativamente baja (Mellman 2013).

Cuando las CDs inmaduras se exponen a patógenos, PAMPs o citoquinas inflamatorias, experimentan una serie de cambios fenotípicos y funcionales, un proceso denominado maduración o activación (figura 1). Durante la maduración se reduce drásticamente la capacidad de capturar antígenos, aunque permanece la capacidad endocítica mediada por receptores (Yanagawa and Onoe 2003; Platt, Ma et al. 2010). Además, se activa la maquinaria de procesamiento antigénico y se incrementa la expresión de moléculas coestimuladoras como CD80 y CD86, y HLA (CMH) (Dudek, Martin et al. 2013). También, durante este proceso disminuye la expresión de receptores de quimioquinas inflamatorias (CCR1, 2, 5 y CXCR1 y 2) y se incrementa considerablemente la expresión del receptor de quimioquinas CCR7. Este receptor controla la migración de las CDs maduras desde el foco de la inflamación hacia los ganglios linfáticos, siguiendo un gradiente de concentración de sus dos ligandos, las quimioquinas CCL21 y CCL19.

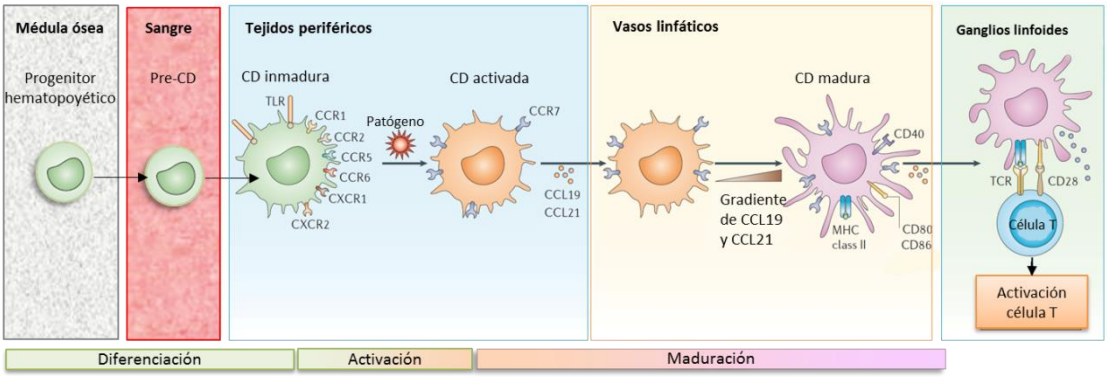

Figura 1. Ciclo biológico de las células dendríticas. Las células dendríticas (CDs) se originan en la médula ósea a partir de progenitores hematopoyéticos. Estos progenitores migran a través de los vasos sanguíneos a los tejidos periféricos, y durante este trayecto se produce su diferenciación a CDs inmaduras. En los tejidos periféricos, las CDs inmaduras actúan como "centinelas" que detectan microorganismos patógenos, PAMPS o DAMPS. Al activarse se modifica la expresión de sus receptores de membrana, disminuyendo la expresión de receptores inflamatorios (CCR1, 2, 5, 6 y CXCR1 y 2) y aumentando la expresión de CCR7, MHCII (CMHII), CD40, CD80 y CD86. CCR7 dirige las CDs a los ganglios linfáticos siguiendo el gradiente de concentración de los ligandos CCL19 y CCL21. En los ganglios, las CDs presentarán los antígenos endocitados previamente a las células T para comenzar una respuesta adaptativa. Modificado a partir de (Bachmann, Kopf et al. 2006).

Las CDs maduras, una vez localizadas en las zonas ricas en linfocitos T de los ganglios, presentarán los antígenos capturados en su fase inmadura a los linfocitos T que posean el receptor TCR específico para dichos antígenos. Estos linfocitos T se activarán, comenzarán a proliferar y migrarán al foco inflamatorio donde las CDs captaron previamente los antígenos, generando así una respuesta adaptativa contra esos antígenos (Mempel, Henrickson et al. 2004; Krummel, Bartumeus et al. 2016).

Durante un proceso inflamatorio, los monocitos de sangre periférica pueden migrar a las zonas inflamadas y diferenciarse en CDs que contribuyen a la respuesta inmune contra la amenaza detectada (Qu, Brinck-Jensen et al. 2014). Además, existe un subtipo de CDs inmaduras que, aunque no han sido activadas por señales inflamatorias, expresan CCR7, lo que les permite migrar a los ganglios linfáticos continuamente transportando antígenos propios o agentes

ambientales inocuos. De esta manera presentan los antígenos a las células T junto con las señales necesarias para que éstas se conviertan en linfocitos T reguladores (tolerogénicos) (Mellman 2013). Por lo tanto, las CDs desempeñan un papel clave en la regulación del sistema inmunológico y la adquisición de tolerancia periférica.

3. Las quimioquinas y sus receptores

3.1 Las quimioquinas

Las quimioquinas (citoquinas quimiotácticas) son pequeños péptidos (8-14 KDa) que actúan como quimioatrayentes celulares. Mediante la unión a sus receptores específicos, las quimioquinas inducen la activación de diversas vías de transducción de señales intracelulares que regulan la migración y otras múltiples funciones celulares (Luster 1998; Lopez-Cotarelo, Gomez-Moreira et al. 2017). Debido a este importante papel, son necesarias para el correcto desarrollo y homeostasis de las células del sistema inmunológico (Griffith, Sokol et al. 2014). Las quimioquinas generalmente son secretadas al medio extracelular, a excepción de CX3CL1 (fractalquina), que es una proteína de membrana. Muchos de estos péptidos pueden unirse a proteínas sialiladas presentes en la superficie celular o a los proteoglicanos sulfatados que se presentan en la matriz extracelular. Debido a su afinidad por los proteoglicanos, al ser secretadas al exterior celular, pueden oligomerizar y permanecer concentradas localmente formando gradientes estables (Li, Pettersson et al. 2014).

Las quimioquinas constituyen una amplia familia compuesta por alrededor de 50 miembros que se clasifican atendiendo a la posición relativa de dos de sus cuatro residuos de cisteína (C) muy conservados, que se encuentran próximos al extremo N-terminal. De acuerdo con esta clasificación existen 4 familias de quimioquinas: CXC-, CC-, C- o y CX_3C-. Donde X representa a cualquier aminoácido (figura 2).

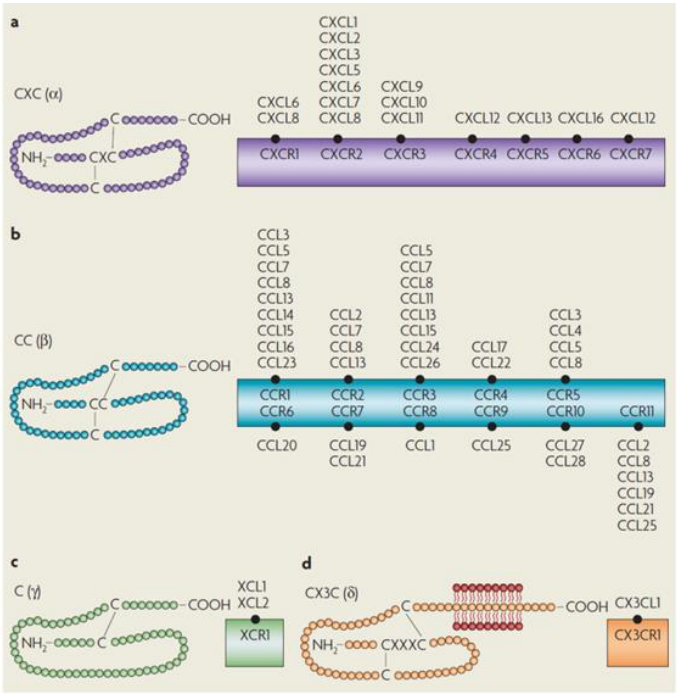

Figura 2. **Tipos de quimioquinas.** Las quimioquinas se clasifican en cuatro grupos, atendiendo a la posición relativa de dos de sus cuatro cisteínas más conservadas, en el extremo N-terminal: Quimioquinas tipo (CXC) (a), (CC) (b), (C) (c) y (CX3C) (d). A la derecha de cada tipo se indican las quimioquinas descritas y sus receptores.(Rostene, Kitabgi et al. 2007).

Las quimioquinas CXC presentan un aminoácido no conservado entre ambas cisteínas y son quimioatrayentes de neutrófilos, linfocitos T, linfocitos B y células Natural Killer (NK). Las quimioquinas CC-, en las cuales las cisteínas son adyacentes, son quimioatrayentes de monocitos, macrófagos, basófilos, linfocitos T y eosinófilos. Las quimioquinas C son aquellas que presentan sólo dos cisteínas

conservadas en lugar de cuatro (Kelner, Kennedy et al. 1994) y los únicos miembros de esta familia son la linfotactina α y la β, quimioatrayentes de linfocitos T. Por último, existe una quimioquina CX3C, con tres aminoácidos no conservados entre las dos primeras cisteínas, denominada fractalquina (Rollins 1997; Rostene, Kitabgi et al. 2007). Esta clasificación permite estandarizar la nomenclatura de estas moléculas de acuerdo con el grupo al que pertenecen (CC-, C-, CXC- o CX3C-), seguido de una L (ligando), todo ello seguido de un número (Bacon, Baggiolini et al. 2002) (figura 2).

Desde un punto de vista funcional, las quimioquinas además pueden agruparse en homeostáticas o inflamatorias, dependiendo de si regulan, a través de sus respectivos receptores, funciones celulares homeostáticas básicas o relacionadas con un proceso inflamatorio (Lopez-Cotarelo, Gomez-Moreira et al. 2017). Las quimioquinas homeostáticas controlan funciones como la migración constitutiva de los leucocitos y la organización de los órganos linfoides secundarios, mientras que las inflamatorias son secretadas en focos de inflamación, de manera transitoria, para reclutar a las células del sistema inmune encargadas de resolver dicho proceso inflamatorio (Lopez-Cotarelo, Gomez-Moreira et al. 2017).

3.2 Los receptores de quimioquinas

Las quimioquinas controlan las funciones celulares mediante su unión a receptores específicos en la superficie de las células. Los receptores de quimioquinas pertenecen a la familia de los receptores acoplados a proteínas G (*Guanine nucleotide binding proteins*) heterotriméricas (GPCR's o *G-protein-*

coupled-receptors). Los receptores de quimioquinas se clasifican en 4 grupos distintos atendiendo al tipo de quimioquina que unen: CCR-, CR-, CXCR- o CX3CR-, donde R significa receptor. Estos receptores se expresan en una gran cantidad de células (Zlotnik and Yoshie 2012; Lopez-Cotarelo, Gomez-Moreira et al. 2017) .

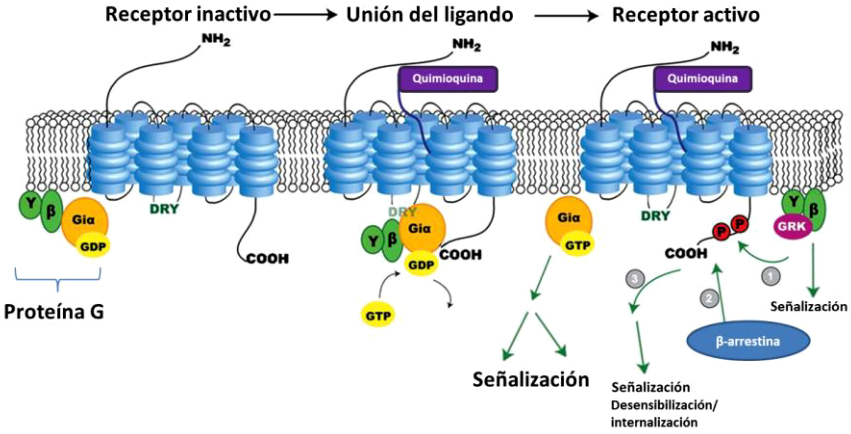

Figura 3. **Estructura de un receptor de quimioquinas acoplado a proteína G.** El receptor está formado por siete hélices alfa transmembrana. El extremo N-terminal está orientado hacia el exterior, donde interacciona con su ligando. La unión del ligando desencadena la interacción entre la proteína G acoplada y el receptor, a través motivo DRY y el extremo C-terminal, desencadenando la separación de las proteínas G_{α} y $G_{\beta\gamma}$, iniciando la cascada de señalización hacia el interior celular. Moléculas como la β-arrestina regulan la internalización y desensibilización del receptor. Modificado a partir de (O'Hayre, Salanga et al. 2008).

Los receptores de quimioquinas están formados por siete hélices alfa que se encuentran insertadas en la membrana citoplasmática con un extremo N-terminal y tres bucles orientados hacia el exterior celular y un extremo C-terminal y otros tres bucles orientados hacia el citosol (figura 3). Las quimioquinas se unen a la región N-terminal (extracelular) del receptor, y el extremo C-terminal está relacionado con la internalización del receptor (Nibbs, Gilchrist et al. 2007). La capacidad de los receptores de quimioquinas de señalizar tras la unión del ligando reside fundamentalmente en la presencia de un motivo DRY (Aspártico, Arginina, Tirosina). Este motivo, que se encuentra cerca de la tercera región

transmembrana en el segundo bucle intracelular, está situado cerca de la zona de acoplamiento de la proteína G. El motivo DRY se encuentra muy conservado y su ausencia o mutación impide la señalización intracelular del receptor a través de la proteína G (Allen, Crown et al. 2007).

Las proteínas G heterotriméricas acopladas a los GPCR's transducen y amplifican la señal de la quimioquina al interior celular (figura 3). Éstas están constituidas por tres subunidades: una subunidad α, una subunidad β y una subunidad γ, de las cuales existen una gran variedad de subtipos. Sin embargo, las subunidades β y γ forman un dímero muy estable que sólo puede ser disociado en condiciones desnaturalizantes, por lo que $G_{\beta\gamma}$ constituye una unidad funcional. La subunidad G_{α} se encuentra unida, por un lado, a los bucles citosólicos del receptor de quimioquinas, y, por otro lado, al complejo $G_{\beta\gamma}$. Las proteínas G heterotriméricas se clasifican en cuatro familias dependiendo de la subunidad α que contienen: α_{s}, $\alpha_{i/0}$, $\alpha_{q/11}$, $\alpha_{12/13}$. La subunidad G_{α} contiene un dominio GTPasa que determina la conformación y estado de activación de la proteína G (Vogler, Barcelo et al. 2008). Las proteínas G alternan dos estados: un estado inactivo unido a GDP y un estado activo unido a GTP. La unión del ligando al receptor GPCR desencadena el intercambio de GDP por GTP, en la subunidad α, lo que produce un cambio conformacional en G_{α} –GTP que separa dicha subunidad del dímero $G_{\beta\gamma}$, y ambas se liberan hacia el citoplasma, donde inician cascadas de señalización intracelular. La subunidad G_{α} posteriormente hidrolizará el GPT a GDP y volverá a su conformación inactiva, induciéndose la reasociación de las subunidad $G_{\beta\gamma}$, lo que termina con la señalización efectora (McCudden, Hains et al. 2005).

Los receptores de quimioquinas pueden regularse mediante un proceso de internalización y desensibilización que depende de unas proteínas adaptadoras denominadas β-arrestinas (figura 3). Se ha observado que la estimulación del receptor con su ligando induce que las proteínas GRK (G-receptor coupled kinase), PKA o PKC, fosforilen la región C-terminal del receptor creando un sitio de unión con las β-arrestinas, que inducen la internalización del receptor, e impiden que interaccione con la proteína G (Kohout and Lefkowitz 2003).

Existen unos receptores de quimioquinas denominados atípicos (Atypical Chemokine Receptors, ACRs) que carecen de motivos DRY o presentan motivos DRY alterados, de modo que no señalizan a través de las proteínas G. Se piensa que los receptores ACRs actúan como receptores "basurero" (*scavenger*) que regulan los niveles locales de quimioquinas (Ulvmar, Hub et al. 2011; Graham, Locati et al. 2012); aunque recientemente se ha descrito que algunos de estos ACRs pueden dimerizar con los receptores típicos regulando así su función (Nibbs and Graham 2013).

4. Las quimioquinas CCL19 y CCL21 y su receptor CCR7

4.1 CCL19 y CCL21

Las quimioquinas CCL19 y CCL21 son los únicos ligandos conocidos de CCR7 y se expresan de manera constitutiva en los órganos linfoides secundarios. A pesar de que ambas quimioquinas se unen a CCR7 con afinidad similar y se expresan en los órganos linfoides, CCL19 y CCL21 difieren ligeramente en su estructura. También se han encontrado algunas diferencias en cuanto al tipo de

señalización que inducen al unirse a CCR7 (Bardi, Lipp et al. 2001; Kohout, Nicholas et al. 2004; Sanchez-Sanchez, Riol-Blanco et al. 2006; Byers, Calloway et al. 2008; Comerford, Harata-Lee et al. 2013).

CCL21 es una molécula de 14,5 KDa que posee una cola polibásica en su región C-terminal, la cual le permite unirse a glicosaminoglicanos (GAGs) de la matriz extracelular y al ácido polisiálico de la superficie celular (Weber, Hauschild et al. 2013). Por ello, esta quimioquina, además de encontrarse de forma soluble, se encuentra también adherida a la matriz extracelular de las células endoteliales, siendo capaz de inducir adhesión, fundamental para el proceso de extravasación (Comerford, Harata-Lee et al. 2013). En ratón se expresan dos isoformas de CCL21, como consecuencia de una duplicación génica, que difieren en un aminoácido (Leu o Ser) en posición 65 (CCL21 Leu 65 y CCL21 Ser 65) (Vassileva, Soto et al. 1999) y tienen un patrón de expresión distinto en el organismo (Nakano and Gunn 2001). Sin embargo, en humanos sólo existe el gen que codifica para la forma CCL21-Leu y se expresa en las células endoteliales de los vasos linfáticos aferentes de los ganglios linfáticos y en los vasos linfáticos de algunos órganos no linfoides, además de en las células estromales de la zona T de los ganglios y en las células epiteliales de la medula del timo (Comerford, Harata-Lee et al. 2013).

CCL19 es una molécula más pequeña, de 11 KDa, y comparte un 32% de homología de secuencia peptídica con CCL21, pero no presenta la extensión o cola polibásica en su extremo C-terminal, por lo que se encuentra de manera soluble y con una disponibilidad más local. CCL19 se produce en las células

reticulares del área T de los ganglios linfáticos y en las células epiteliales de la médula del timo, además, las propias CDs maduras secretan CCL19 (Sallusto, Palermo et al. 1999).

El patrón de expresión de CCL19 y CCL21 permite que las células que expresan CCR7 migren desde los tejidos periféricos a los órganos linfoides a través de los vasos linfáticos aferentes. Aunque CCR7 es el receptor típico de CCL19 y CCL21, pueden unirse también a ACKR4 (previamente denominado CCR11 o CCX-CKR), que se expresa en las células reticulares de los ganglios linfáticos, las células epidérmicas y las epiteliales del timo. Se sabe poco acerca de la función de este receptor, pero se ha sugerido que, como todos los receptores de quimioquinas atípicos, ejerce una función de secuestro de estas quimioquinas como mecanismo regulador y parece tener un papel importante en el desarrollo y la selección de los linfocitos T (Heinzel, Benz et al. 2007; Bunting, Comerford et al. 2013).

4.2 CCR7

Este receptor se expresa en múltiples células, incluyendo linfocitos B, linfocitos T, células dendríticas, macrófagos, neutrófilos, y una subpoblación de NKs. CCR7 se expresa además, de manera patológica, en diversas células cancerígenas (Mashino, Sadanaga et al. 2002; Ding, Shimada et al. 2003; Takanami 2003; Takeuchi, Fujimoto et al. 2004; Gunther, Leier et al. 2005; Muller, Sonkoly et al. 2006; Fang, Lee et al. 2008).

Los ratones KO para CCR7 (*Ccr7-/-*) presentan órganos linfoides con una arquitectura y compartimentalización aberrante. Estos resultados sugieren que

CCR7 está implicado en el desarrollo y la organización de los órganos linfoides secundarios, debido a que regula la migración hacia los ganglios de leucocitos que son importantes para la organización de estas estructuras.

Se ha demostrado que la migración mediada por CCR7 en el timo es necesaria para el desarrollo de la **tolerancia central**. CCR7 regula la migración de los timocitos dentro del timo, necesaria para eliminación de células autorreactivas. Es por ello que en ratones KO para CCR7 se observa una elevada incidencia de autoinmunidad espontánea (Comerford, Harata-Lee et al. 2013).

Además de controlar la tolerancia central, CCR7 modula también la **tolerancia periférica**. La tolerancia periférica está relacionada con la continua migración constitutiva de las células dendríticas, cargadas con antígenos propios, desde los tejidos periféricos a los ganglios linfáticos para activar a las células T reguladoras, que inhiben a los linfocitos autoreactivos (Schneider, Meingassner et al. 2007; Maldonado and von Andrian 2010).

En los modelos KO para CCR7 también se observa un retraso en la inducción de una **respuesta inmunológica adaptativa**, debido nuevamente a la disminución en el número de CDs y linfocitos T que migran a los ganglios (Forster, Schubel et al. 1999).

5. Funciones reguladas por CCR7 en las CDs y vías de señalización intracelulares.

El receptor de quimioquinas CCR7 ha sido clásicamente estudiado como un receptor que regula la quimiotaxis; sin embargo, desde hace unos años se ha ido observando que regula otras funciones celulares importantes para el funcionamiento de las CDs y el desarrollo de una respuesta inmunológica adaptativa. Entre estas nuevas funciones se incluyen la inducción de la maduración (Marsland, Battig et al. 2005), el control de la supervivencia (Sanchez-Sanchez, Riol-Blanco et al. 2004; Escribano, Delgado-Martin et al. 2009) y la regulación del citoesqueleto de actina, del que dependen algunas funciones como la endocitosis (Yanagawa and Onoe 2003; Torres-Bacete, Delgado-Martin et al. 2015), los cambios en citoarquitectura (Yanagawa and Onoe 2002; Torres-Bacete, Delgado-Martin et al. 2015) y en la velocidad migratoria de las células (Riol-Blanco, Sanchez-Sanchez et al. 2005).

Numerosos trabajos en los últimos años han ido elucidando la red de interacciones moleculares que controlan las funciones reguladas por CCR7 en las CDs (figura 4). Las diversas cascadas de señalización activadas por CCR7 se pueden agrupar en tres módulos de señalización: el módulo regulador de la quimiotaxis, el módulo regulador de la supervivencia y el módulo regulador de la dinámica de la actina. Estos módulos presentan un alto grado de independencia porque se ha observado que cuando se inhibe uno de ellos, el resto de las funciones no se ven alteradas (Riol-Blanco, Sanchez-Sanchez et al.

2005; Torres-Bacete, Delgado-Martin et al. 2015). Hasta el momento sólo se ha identificado una conexión entre el módulo regulador de la quimiotaxis y el módulo de la supervivencia (Lopez-Cotarelo, Escribano-Diaz et al. 2015).

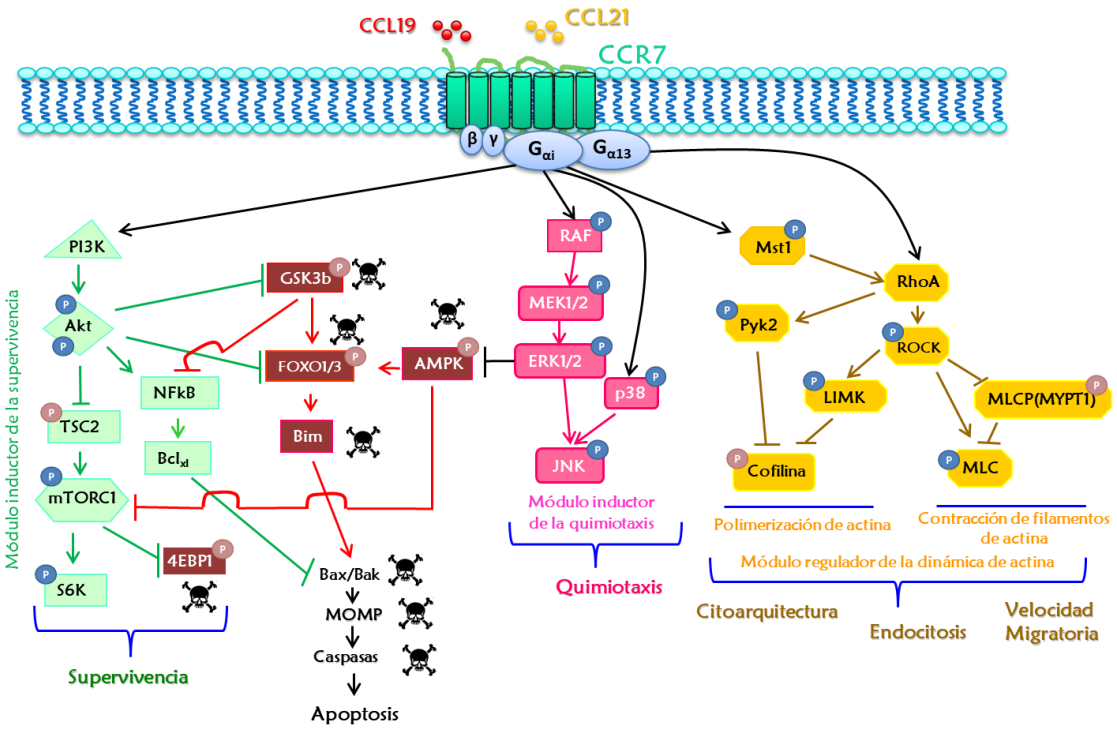

Figura 4. Esquema de las rutas de señalización intracelular activadas por CCR7 en las CDs. CCR7 controla tres complejos módulos de señalización que regulan la supervivencia, la quimiotaxis y la dinámica de la actina, que gobierna procesos de endocitosis, cambios en citoarquitectura y cambios en velocidad migratoria. P = fosforilación activadora, P = fosforilación inhibitoria.

5.1 CCR7 y la regulación de la quimiotaxis

La función clásica de CCR7, la quimiotaxis, está regulada por la vía de las MAP-quinasas (figura 4) (Riol-Blanco, Sanchez-Sanchez et al. 2005). CCR7, a través de la subunidad Gαi, induce una cascada de fosforilaciones que lleva a la activación secuencial de RAF (resultados no publicados) y MEK1/2, que fosforila y activa a ERK1/2. Por otra parte, CCR7 induce la activación de p38. ERK1/2 y p38 confluyen en la fosforilación y activación de JNK. Esta vía de señalización

controla la direccionalidad de las CDs y permite que las células se dirijan hacia la fuente productora de la quimioquina.

5.2 CCR7 y la regulación de la supervivencia de las CDs

La estimulación de CCR7 inhibe la apoptosis e induce supervivencia en las CDs (Sanchez-Sanchez, Riol-Blanco et al. 2004; Escribano, Delgado-Martin et al. 2009; Lopez-Cotarelo, Escribano-Diaz et al. 2015).

CCR7 activa a través de Gαi a PI3K (figura 4), que estimula la activación de la quinasa AKT mediante su fosforilación en la treonina 308, mediada por PDK1 (no mostrado). También se induce la fosforilación de AKT en la serina 473, mediada por mTORC2 (no mostrado). Una vez fosforilada en ambos residuos y activa, AKT fosforila e inhibe a una serie de moléculas con efectos pro-apoptóticos en las CDs, como los factores de transcripción FOXO1/3 y la proteína GSK3β (Escribano, Delgado-Martin et al. 2009; Lopez-Cotarelo, Escribano-Diaz et al. 2015). FOXO1/3 regula la transcripción de genes pro-apoptóticos como Bim y activa la cascada de caspasas, induciendo finalmente la apoptosis. Por otro lado, AKT también previene la apoptosis al fosforilar de manera inhibitoria a TSC2, permitiendo la activación de mTORC1. Este complejo de señalización induce supervivencia a través de la activación de la quinasa S6k y el bloqueo de 4EBP1, un inhibidor de la traducción (Lopez-Cotarelo, Escribano-Diaz et al. 2015).

Por otra parte, AKT activa directamente la ruta de NFκB, que promueve supervivencia (Sanchez-Sanchez, Riol-Blanco et al. 2004). AKT regula la

fosforilación de IκBα, proteína que secuestra a NFκB. La fosforilación de IκBα desencadena su ubiquitinación y degradación por el proteasoma (Sanchez-Sanchez, Riol-Blanco et al. 2004). Una vez que NFκB se encuentra libre, se trasloca al núcleo, donde activa la transcripción de genes relacionados con la supervivencia, como Bcl_{xl} (Escribano, Delgado-Martin et al. 2009).

Aunque hemos mencionado que los módulos activados por CCR7 presentan un alto grado de independencia, existe una conexión entre los módulos que regulan la quimiotaxis y la supervivencia a través de la proteína AMPK. Esta quinasa puede promover apoptosis induciendo la activación de FOXO1/3. Además, se sabe que AMPK también inhibe a mTORC1, que induce supervivencia en las CDs. Tras la estimulación de CCR7, ERK1/2 fosforila de manera inhibitoria a AMPK en la serina 485. Dicha inhibición impide que AMPK, por un lado, active a FOXO1/3 y, por otro lado, inhiba a mTORC1, contribuyendo en aproximadamente el 20% supervivencia inducida por CCR7 en las CDs (Lopez-Cotarelo, Escribano-Diaz et al. 2015).

5.3 CCR7 y la regulación del citoesqueleto de actina

El receptor CCR7, además de estar acoplado con la subunidad de la proteína Gαi, también se acopla a la subunidad Gα13. La subunidad Gα13 activa una ruta de señalización que está implicada en la regulación de la dinámica de la actina (figura 4). Esta regulación del citoesqueleto de actina es necesaria para que tengan lugar los cambios morfológicos y el movimiento celular necesarios para que la migración celular se produzca correctamente.

Tras la unión de sus ligandos, CCR7 se activa y estimula la ruta de la GTPasa RhoA, por un lado, a través de la proteína acoplada Gαi, que activa Mst1 (Torres-Bacete, Delgado-Martin et al. 2015) y, por otro lado, a través de la subunidad Gα13 acoplada a CCR7. Posteriormente, RhoA regula la actividad de las quinasas Pyk2 y ROCK, que activa a la quinasa LIMK. Ambas vías (Pyk2 y ROCK) convergen en la fosforilación inhibitoria de la cofilina-1, que resulta en una inhibición de su capacidad despolimerizadora de actina. Esta ruta, por tanto, impide la despolimerización de actina, pero, además, ROCK induce también la contracción de filamentos de actina al fosforilar y activar directamente a MLC, a la vez que bloquea a su inhibidor, la fosfatasa MYPT1. Estos efectos sobre la actina son fundamentales para que la célula lleve a cabo cambios en citoarquitectura, incremento la velocidad migratoria y la endocitosis activa de partículas (Torres-Bacete, Delgado-Martin et al. 2015).

6. El sistema ubiquitina-proteasoma (UPS)

La degradación de proteínas debe ser un mecanismo perfectamente coordinado, eficiente y rápido en su ejecución para asegurar que una célula funcione correctamente. Las células eucariotas cuentan con una maquinaria que permite controlar la degradación proteica de manera eficiente, el Sistema Ubiquitina-Proteasoma (UPS) (figura 5). La especificidad y selectividad de este sistema radica en el marcaje de las moléculas destinadas a la degradación con una pequeña proteína denominada ubiquitina. La unión de varias moléculas de ubiquitina o poliubiquitinación de una proteína permite "etiquetarla", generalmente, para ser degradada por un complejo molecular con actividad proteolítica denominado

proteasoma 26S (Hershko, Eytan et al. 1982; Hershko and Ciechanover 1998; Murata, Yashiroda et al. 2009; Tanaka 2009; Inobe and Matouschek 2014). El proceso de reconocimiento y "etiquetado" de una proteína con ubiquitina comprende 3 etapas con 3 tipos de enzimas (E1, E2 y E3).

El UPS es responsable de la degradación de entre el 80 y el 90% de las proteínas de la célula (Rock, Gramm et al. 1994). La desregulación del sistema UPS puede dar lugar a inestabilidad genómica y descontrol del ciclo celular, entre otros procesos, pudiendo desencadenar patologías como el cáncer, trastornos inmunológicos y neurológicos (Nakayama and Nakayama 2006; Paul 2008; Schmidt and Finley 2014; Skaar, Pagan et al. 2014).

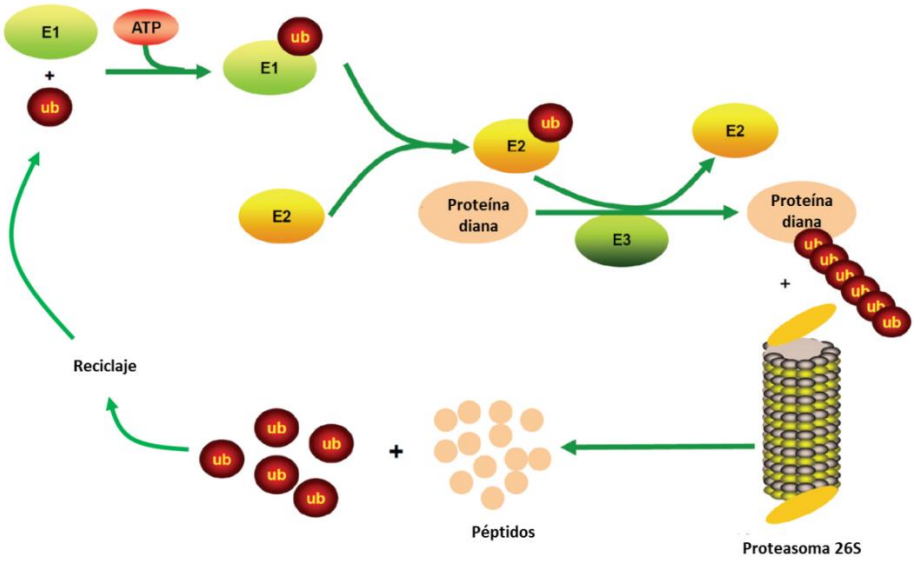

Figura 5. **Sistema Ubiquitina-Proteasoma (UPS).** El sistema UPS está encargado de la degradación a través del proteasoma de proteínas "etiquetadas" con ubiquitina (Ub). El marcaje de la proteína diana se realiza en tres pasos por enzimas activadoras E1, conjugadoras E2 y ligasas E3 de Ub. Una vez que la proteína es degradada a pequeños péptidos por el proteasoma 26S, las Ub son recicladas para ser utilizadas nuevamente. Modificado de (Tu, Chen et al. 2012).

6.1 La ubiquitinación

a) Estructura y función de la ubiquitina

La ubiquitina (Ub) es una proteína de 76 aminoácidos y 8,5KDa muy conservada a lo largo de la evolución (Jentsch, Seufert et al. 1991). La ubiquitina presenta una glicina (G76) en su extremo C-terminal a través de la cual forma un enlace covalente con un grupo amino de un residuo presente en la proteína diana (figura 6). Además, la ubiquitina presenta siete residuos de lisina (K o Lys) (K6, K11, K27, K29, K33, K48 y K63), altamente conservados, a través de los cuales establece enlaces con la G76 de otras ubiquitinas y genera las cadenas de poliubiquitina (Pickart and Eddins 2004; Pickart and Fushman 2004) (ilustrado más adelante en la figura 8).

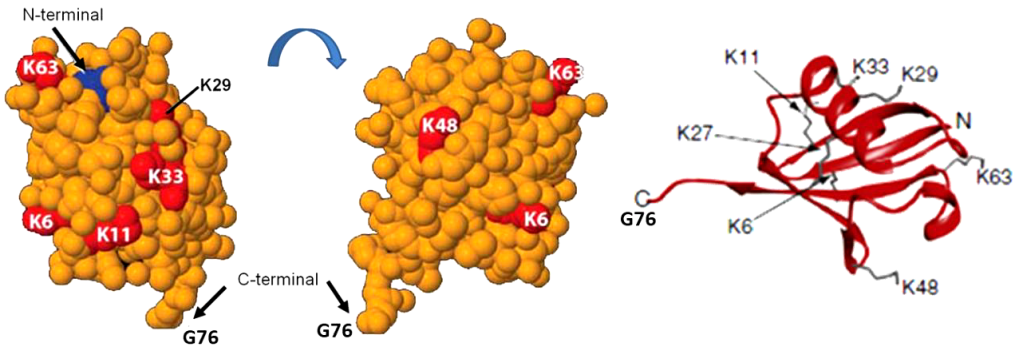

Figura 6. **Estructura de la Ubiquitina.** La ubiquitina presenta una estructura globular en la cual son fundamentales un residuo de glicina en el extremo C-terminal (G76) y siete residuos de lisina conservados (K6, K11, K27, K29, K33, K48 y K63), necesarios para la interacción con el sustrato y la formación de cadenas de poliubiquitina. Modificado a partir de (Neutzner and Neutzner 2012) y (Metzger, Pruneda et al. 2014).

b) Las proteínas similares a Ubiquitina (ULMs)

A lo largo de la evolución se ha generado una familia de proteínas, conocidas como proteínas similares a ubiquitina (ubiquitin-like modifier proteins o ULMs),

que comparten cierta similitud en secuencia y estructura con la ubiquitina (Cappadocia and Lima 2017). Estas proteínas no solo comparten parte de su secuencia de aminoácidos, sino también la capacidad de formar enlaces isopeptídicos entre la glicina de su extremo C-terminal y un grupo amino de la proteína diana (Pickart and Fushman 2004). La familia de proteínas ULMs está formada por alrededor de 20 miembros involucrados en la modificación post-traduccional de proteínas (Hochstrasser 2009; van der Veen and Ploegh 2012). Entre este grupo de proteínas se encuentra **Nedd8** ("Neural precursor cell Expressed Developmentally Downregulated protein 8"), una pequeña proteína de 81 aminoácidos y 9 KDa que presenta un ~60% de identidad con la secuencia de la ubiquitina (Kumar, Yoshida et al. 1993; Kamitani, Kito et al. 1997; Pickart and Eddins 2004; Soucy, Dick et al. 2010; Enchev, Schulman et al. 2015).

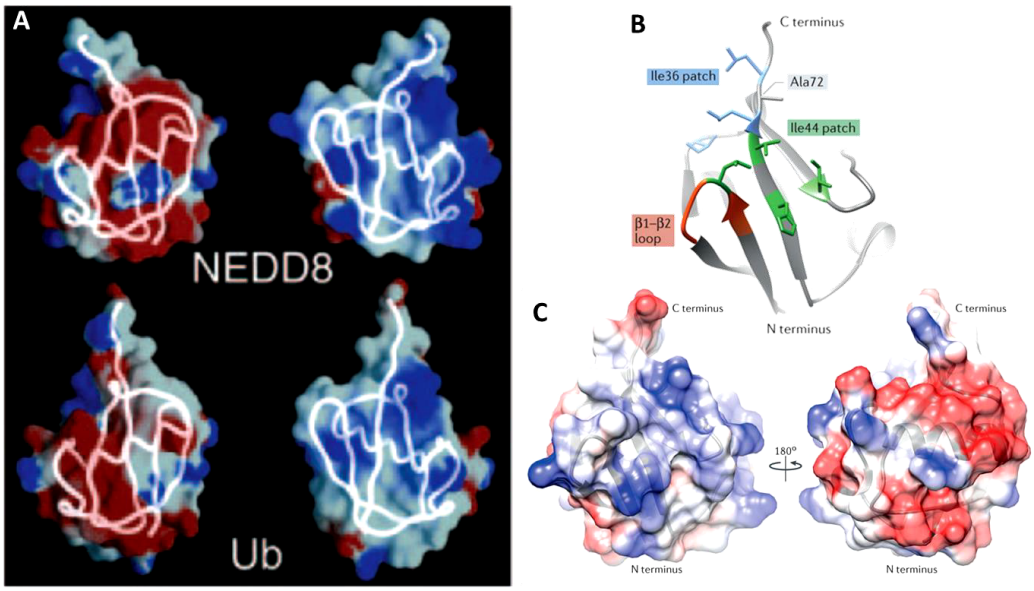

Figura 7. **Estructura de Nedd8 destacando su similitud con la ubiquitina. (A)** Representación tridimensional de las estructuras de Nedd8 y Ubiquitina ilustrando su potencial electrostático (negativo en rojo y positivo en azul). Se observa una gran similitud entre ambas proteínas. (Herrmann, Lerman et al. 2007) **(B)** y **(C)** Estructura de Nedd8. Nedd8 consiste en una estructura globular con dos parches hidrofóbicos (*patch*), Ile44 e Ile36 que median la interacción con otras proteínas y dos lazos (*loop*), β1 y β2. (Enchev, Schulman et al. 2015)

Nedd8 se compone de una cola C-terminal que finaliza con dos glicinas, a través de las cuales se forma el enlace covalente con la molécula diana (Enchev, Schulman et al. 2015) (figura 7). El cuerpo globular posee dos parches hidrofóbicos, de carga neutra, que existen también en la ubiquitina, y son los encargados de mediar interacciones con otras proteínas, y un lazo entre las láminas β1 y β2 (figura 7B). También posee unas regiones polares que no están presentes en la ubiquitina y que probablemente influencian las funciones específicas de Nedd8 (figura 7A). Aunque se asemeja mucho a la Ub en secuencia y estructura, la unión de Nedd8 a las proteínas (o nedilación) no induce directamente su degradación por el proteasoma, sino que se ha visto relacionada con la modificación de la conformación una proteína, su estabilidad o su capacidad para formar enlaces con otras moléculas, regulando así su función (Rabut and Peter 2008; Deshaies and Joazeiro 2009; Enchev, Schulman et al. 2015).

c) Proceso de ubiquitinación

Para que se lleve a cabo la ubiquitinación, es necesario que la molécula precursora de la ubiquitina sufra un corte proteolítico en una zona del extremo C-terminal que permite exponer el residuo de G76, de tal manera que puede ser ligada a una proteína diana.

La unión de ubiquitinas a un sustrato (figura 8) requiere tres tipos de enzimas, que actúan de manera secuencial: las enzimas activadoras de ubiquitina (E1), las enzimas conjugadoras de ubiquitina (E2) y las enzimas ligasas de ubiquitina

(E3)(Pickart and Eddins 2004). El genoma humano codifica 2 enzimas E1, 37 enzimas E2 y unas 600 ligasas E3 de ubiquitina, que catalizan la transferencia de una molécula de ubiquitina a la proteína diana (Bulatov and Ciulli 2015).

- **Enzimas activadoras de ubiquitina (E1):** Estas enzimas se encargan de adenilar a la ubiquitina en su extremo C-terminal, utilizando una molécula de ATP. Este proceso permite la formación de un enlace tioéster entre una cisteína del centro activo de la E1 y el residuo de glicina (G76) del extremo C-terminal de la ubiquitina, activándose la ubiquitina (Handley, Mueckler et al. 1991; Groen and Gillingwater 2015).
- **Enzimas conjugadoras de ubiquitina (E2):** Reciben la ubiquitina activada de la E1 y forman de nuevo un enlace tioéster entre su centro activo y la ubiquitina. Las E2 funcionan como un intermediario entre las E1 y las E3. El mecanismo de acción de las E2 depende del tipo de E3 con el que han de interaccionar. Cada enzima E2 puede interaccionar con varias E3 (Glickman and Ciechanover 2002; Lecker, Goldberg et al. 2006).
- **Enzimas ligasas de ubiquitina (E3):** Las denominaremos E3 ligasas a lo largo de esta tesis. Catalizan la "ligación" de la ubiquitina a la proteína diana, y lo pueden hacer de dos maneras distintas. Directamente, recibiendo la ubiquitina de la E2, uniéndola, y transfiriéndola a la proteína diana, o indirectamente, reclutando a la proteína diana y permitiendo que la E2 le transfiera la ubiquitina (ver más adelante en la figura 10). En este proceso se forma un enlace covalente isopeptídico entre la ubiquitina y el grupo ε-amino de un residuo de lisina de la proteína diana. Aunque la lisina es el residuo aceptor

más común, es también posible que otros residuos funcionen como sitios de ubiquitinación, como los residuos de cisteína y serina (Herrmann, Lerman et al. 2007; McDowell and Philpott 2013).

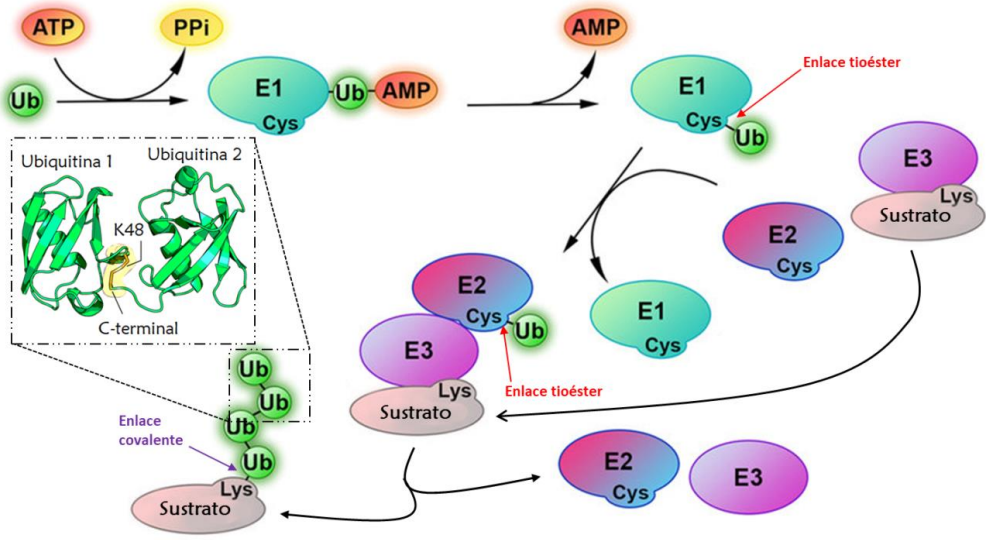

Figura 8. **Esquema del proceso de ubiquitinación.** La ubiquitina es activada por enzima E1 mediante un proceso de adenilación con consumo de ATP. La ubiquitina forma un enlace tioéster con la cisteína del centro activo de la E1, que la transfiere del mismo modo a una cisteína en la enzima E2 y, por último, la ubiquitina se transfiere al sustrato, acoplado a una enzima E3 ligasa, mediante la formación de un enlace covalente con una lisina del mismo. Posteriormente, se lleva a cabo la adición de más moléculas de ubiquitina o poliubiquitinación. Modificado a partir de (Valimberti, Tiberti et al. 2015)

La poliubiquitinación o elongación de las cadenas de ubiquitina se produce mediante la formación de un enlace isopeptídico entre el residuo G76 en posición C-terminal de una ubiquitina y el grupo ε-amino de un residuo de lisina (K) de la siguiente molécula de ubiquitina. Puesto que las ubiquitinas poseen 7 lisinas conservadas (K6, K11, K27, K29, K33, K48, K63), se pueden formar muchos tipos de enlaces con otras ubiquitinas o con proteínas diana. Cada tipo de enlace se ha visto relacionado con un destino específico de la proteína diana, hablándose de un "código de ubiquitinación" (Komander 2009; McDowell and Philpott 2013) (figura 9). La degradación de proteínas en el proteasoma depende

principalmente de cadenas de ubiquitina unidas a través de la K48 (Hershko and Ciechanover 1998; Thrower, Hoffman et al. 2000), aunque también puede ocurrir a través de la K11 (Jin, Williamson et al. 2008).

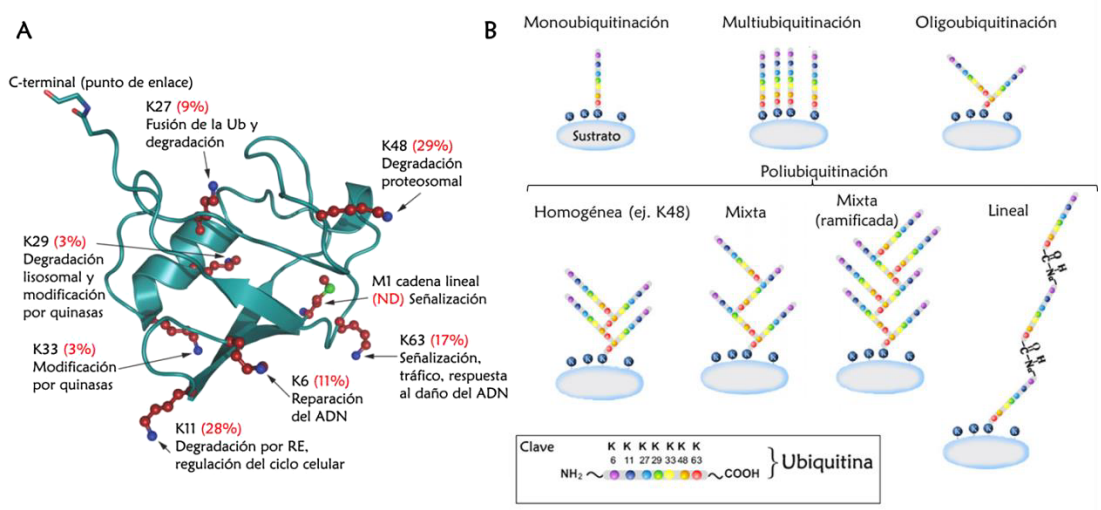

Figura 9. **Tipos de ubiquitinación y destino de las proteínas ubiquitinadas. (A)** Las ubiquitinas (Ub) pueden formar enlaces a través de sus 7 lisinas conservadas. Cada tipo de enlace se ha visto relacionado con diferentes destinos para una proteína. En la figura se detalla la abundancia relativa con la que se encuentra cada tipo de ubiquitinación. **(B)** La clave de colores representa los distintos residuos de Ub. Las proteínas pueden ser marcadas por una Ub (monoubiquitinación), varias moléculas de Ub en diferentes residuos de lisina (multiubiquitinación), cadenas cortas Ub (oligoubiquitinación) o cadenas más largas (poliubiquitinación) que pueden ser, tanto homogéneas como heterogéneas. También se puede dar la elongación de cadenas de Ub de manera lineal, unidas entre sí a través de su extremo N-terminal. Modificado de (Komander 2009)(A) y (Kravtsova-Ivantsiv and Ciechanover 2012)(B).

Otros residuos, como la ubiquitinación en K63, ha sido asociados mayormente con la modificación de la función de las proteínas, pudiendo estar involucrados en múltiples vías, como la respuesta al daño en el ADN (Glickman and Ciechanover 2002; Komander 2009), aunque recientemente se ha sugerido que K63, también puede estar involucrada en la degradación a través del proteosoma (Ohtake, Tsuchiya et al. 2018). Además, existen otros tipos de ubiquitinación menos comunes, como las cadenas de poliubiquitina de tipo mixto, combinando uniones de ubiquitinas a través de diferentes lisinas (Emmerich, Ordureau et al. 2013; Meyer and Rape 2014; Kristariyanto, Abdul

Rehman et al. 2015), la formación de cadenas de ubiquitina ramificadas, la multiubiquitinación, o la ubiquitinación lineal a través de la metionina 1 (M1) del extremo N-terminal (Rieser, Cordier et al. 2013).

Se ha demostrado que para que una proteína sea degradada por el proteasoma requiere llevar unida una cadena de al menos 4 moléculas de ubiquitina (Thrower, Hoffman et al. 2000).

6.2 Las ligasas E3 de ubiquitina

Como se ha mencionado anteriormente, las enzimas E3 ligasas son las encargadas de seleccionar específicamente las proteínas destinadas a ser ubiquitinadas. Estas moléculas reconocen modificaciones en las proteínas, como fosforilaciones, que las hacen más susceptibles de ser ubiquitinadas y degradadas (Lucas and Ciulli 2017).

a) Tipos de ligasas E3 de ubiquitina

Las enzimas E3 ligasas se clasifican en 4 grupos atendiendo al motivo estructural que poseen: ligasas E3 con dominios HECT (Kee and Huibregtse 2007; Metzger, Hristova et al. 2012), ligasas E3 con dominio PHD-finger (Pascual, Martinez-Yamout et al. 2000; Coscoy and Ganem 2003; Bienz 2006), ligasas E3 con dominios U-box (Hatakeyama and Nakayama 2003; Hatakeyama and Nakayama 2003; Metzger, Pruneda et al. 2014) y ligasas E3 con dominio RING-finger. En esta tesis nos centramos en las ligasas E3 con dominio RING-finger.

Ligasas E3 con dominio RING-finger

Estas enzimas contienen un dominio RING ("Really Interesting New Gene") formado por entre 40 y 100 aminoácidos con 8 residuos conservados de cisteína e histidina que coordinan dos átomos de Zn2+ formando una estructura de abrazaderas cruzadas ("zinc-finger"). Esta zona crea una plataforma que sirve de anclaje para las E2 ligasas (Yi and Ehlers 2007). En las E3 ligasas de tipo RING-finger, a diferencia de otras, como las HECT, la E2 cargada con ubiquitina se ancla en una región de la E3, mientras que el sustrato se ancla en otra zona de la E3, de modo que la E2 transfiere la ubiquitina directamente al sustrato sin pasar por la E3, es decir, sin formarse ningún enlace entre la E3 y la ubiquitina (figura 10).

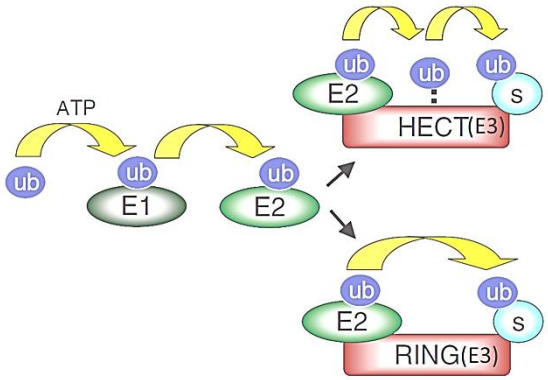

Figura 10. Ligasas E3 de ubiquitina tipo HECT y tipo RING-finger. Ambas ligasas reciben la ubiquitina de una enzima E2; sin embargo, mientras las E3 tipo HECT forman un enlace con la ubiquitina antes de transferirla al sustrato (s), las de tipo RING no establecen ningún enlace con la ubiquitina, sino que la transfieren directamente de la E2 al sustrato. Modificado a partir de (Nethe and Hordijk 2010)

Dentro de las E3 ligasas de tipo RING-finger, puede ocurrir que la E2 y el sustrato se anclen dentro de la misma proteína RING-finger (como muestra la figura 10), o que la proteína RING-finger se encuentre formando un conjunto con otras proteínas dando lugar a un Complejo E3 ligasa (Metzger, Pruneda et al. 2014) (figura 11), donde se requiere la actividad catalítica de la RING-finger y la presencia de una serie de adaptadores. Al segundo grupo, de tipo multimérico,

pertenecen los complejos E3 ligasa mejor descritos, los complejos tipo CRL ("Cullin-containing RING-E3 ligase") y el complejo APC ("Anaphase promoting complex").

Los **CRL** son complejos E3 ligasa que están formados, de manera general, por una E3 ligasa tipo RING-finger, una proteína que reconoce al sustrato (receptora del sustrato), una proteína adaptadora y una proteína de ensamblaje de la familia Cullin, que sirve como soporte a las dos anteriores para permitir la interacción de la E2-Ub con el sustrato a ubiquitinar (Zheng, Schulman et al. 2002)(figura 11).

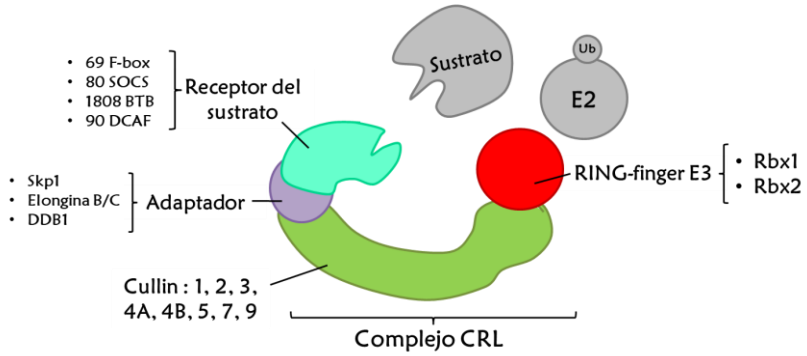

Figura 11. **Los complejos E3-ligasa tipo CRL.** Los complejos CRL están formados por una proteína de ensamblaje de la familia Cullin que ancla por un lado una proteína adaptadora que lleva unida una proteína receptora del sustrato, encargada de reconocer y unir el sustrato. Por el otro lado, Cullin se encuentra unida a la enzima RING-finger, que interacciona con la enzima E2 cargada con ubiquitina para que pueda producirse la ubiquitinación del sustrato.

Las proteínas de la familia Cullin se caracterizan por un dominio de homología *cullin* muy conservado ("cullin-repeat domain") de unos 150 aminoácidos en su región C-terminal y se denominaron así por su pertenencia a un complejo capaz de "seleccionar" y ubiquitinar proteínas ("to cull"="to choose in a negative way, discard") (Sarikas, Hartmann et al. 2011). Este dominio es responsable de la interacción con la RING-finger E3 (Zheng, Schulman et al. 2002), mientras que el

extremo N-terminal es el encargado de anclarse a otras proteínas adaptadoras. Existen 8 tipos de complejos CRL (CRL1, 2, 3, 4A, 4B, 5, 7 y 9) dependiendo de la proteína Cullin que posean (Cul-1, -2, -3, -4A, -4B, -5, -7 y -9/PARC).

Además, estos CRLs varían según la RING-finger E3 y las proteínas adaptadoras que posean. En humanos existen 2 componentes RING-finger E3 (Rbx1 y Rbx2), y 4 proteínas adaptadoras, Skp1 (para Cul-1 y -7), Elongina B/C (para Cul-2 y -5) y DDB1 (para Cul-4A/B)(Zhao and Sun 2013).

Las proteínas adaptadoras son las que se anclan a la proteína Cullin e interaccionan con las proteínas encargadas del reconocimiento del sustrato. Éstas últimas son muy variables, y en ellas radica la especificidad de las E3-ligasas. Existen 69 proteínas de tipo **F-box** (Jin, Cardozo et al. 2004) para CRL-1 (CRL con Cul-1), 80 proteínas **SOCS** para CRL-2 y -5, aproximadamente 180 proteínas **BTB** para CRL-3 y unas 90 proteínas **DCAF** para CRL-4A y -4B (Linossi and Nicholson 2012). Por lo tanto, las más de 400 proteínas se combinan para dar lugar a infinidad de complejos CRL encargados de ubiquitinar alrededor del 20% de las proteínas celulares degradadas en el proteasoma (Deshaies and Joazeiro 2009; Sarikas, Hartmann et al. 2011; Skaar, Pagan et al. 2014).

6.3 El complejo SCF (CRL-1)

El complejo CRL-1 ha sido el complejo CRL más estudiado ya que contiene a Cul-1 (gen conocido también como Cdc53) la proteína de la familia Cullin mejor caracterizada (Kipreos, Lander et al. 1996; Willems, Lanker et al. 1996). CRL-1 es

conocido también como SCF (Skp1-Cul-1-Fbox) y con ese nombre nos referiremos a él a partir de ahora.

El complejo SCF (figura 12), está formado por 3 componentes invariables, Rbx1 (la E3 ligasa tipo RING-finger), Cullin-1 (proteína de ensamblaje, Cul-1) y Skp1 (proteína adaptadora), que se une a un componente variable, la proteína receptora del sustrato, de la familia de proteínas F-box (Cenciarelli, Chiaur et al. 1999; Craig and Tyers 1999; Winston, Koepp et al. 1999; Zhao and Sun 2013; Bulatov and Ciulli 2015; Zheng, Zhou et al. 2016; Reitsma, Liu et al. 2017). Las proteínas Skp1 y F-box, son las responsables del reconocimiento del sustrato y de la especificidad del proceso de ubiquitinación por las E3.

En humanos se han descrito 69 proteínas F-box, pero solo el 5% de estas proteínas ha sido estudiado. Las proteínas F-box reconocen modificaciones en los sustratos (fosforilación, glicosilación, hidroxilación, acetilación, etc.) que les permiten interaccionar con ellos para que se lleve a cabo el proceso de ubiquitinación (Skaar, Pagan et al. 2013; Wang, Liu et al. 2014; Lucas and Ciulli 2017). De este modo, la proteólisis mediada por SCF depende tanto de la disponibilidad de las proteínas F-box, como de las modificaciones que presenten los sustratos (Nakayama and Nakayama 2006).

El complejo SCF posee una estructura (figura 12) en la cual Cul-1 aparece como una plataforma central elongada que une, por su extremo N-terminal al complejo formado por Skp1-F-box ("módulo de reconocimiento del sustrato"), y por su extremo C-terminal a la E3 Rbx1 (Zheng, Schulman et al. 2002). La región

N-terminal de Cul-1 está muy conservada entre especies, pero no con otras proteínas de la familia Cullin (Bulatov and Ciulli 2015). Rbx1, la E3 ligasa de tipo RING-finger asociada a SCF, se incorpora en la región C-terminal de Cul-1 y posee una región RING-finger un poco diferente al resto, puesto que, además de los dos átomos de Zn^{2+} que normalmente presentan estas enzimas, posee una inserción de 20 residuos que permiten la unión de un tercer átomo de Zn^{2+} y la formación de un tercer zinc finger (Zheng, Schulman et al. 2002).

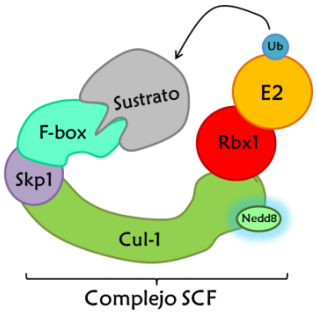

Figura 12. **El complejo SCF.** El complejo SCF está formado por Cul-1, que hace de plataforma conectora entre Skp1, F-box y el sustrato con la E3-RING finger, Rbx1, que entra en contacto con la enzima E2 cargada con ubiquitina. Para que la transferencia de ubiquitina ocurra, Cul-1 debe encontrarse nedilado.

6.4 Regulación de la actividad de SCF

La regulación de la actividad de SCF es muy compleja, pues depende de la disponibilidad y estabilidad de todos los componentes necesarios para el ensamblaje del SCF, así como de la disponibilidad de la E2 ligasa cargada con ubiquitina y de los sustratos a ubiquitinar. Estos últimos, además deben encontrarse con las modificaciones postraduccionales necesarias para poder ser reconocidos por las F-box (Lucas and Ciulli 2017). Por otro lado, la regulación de SCF depende de la existencia de componentes que activen o inactiven el complejo. Se trata de un equilibrio muy complejo de unión y separación de unidades que puede desviarse hacia un destino u otro, dependiendo de la disponibilidad y estado de dichas unidades.

a) Activación de SCF por nedilación

Todos las CRLs son activados mediante la modificación de un residuo de lisina (K) en la proteína Cullin. Esta modificación consiste en la unión covalente de Nedd8, un proceso conocido como nedilación. De este modo, el complejo SCF se activa cuando Cul-1 es nedilado (figura 12) (Duda, Borg et al. 2008). La nedilación estimula la actividad de SCF a través de varios mecanismos. La nedilación de Cul-1 ayuda a reclutar a la E2 cargada con ubiquitina gracias a la capacidad que tiene Nedd8 de unirse, además de a Cul-1, a la E2 cargada con Ub (Read, Brownell et al. 2000; Kawakami, Chiba et al. 2001; Petroski and Deshaies 2005; Sakata, Yamaguchi et al. 2007). Sin embargo, el reclutamiento de la E2-Ub y de los adaptadores de reconocimiento del sustrato no son suficientes para que la ubiquitinación del sustrato se lleve a cabo, debido a que, de manera constitutiva, el complejo (Rbx1, Cul1, Skp1-Fbox-sustrato) se encuentra en una conformación más o menos rígida que mantiene un espacio de 50Å entre la E2-Ub y el sustrato, una distancia que no permite que se transfiera la ubiquitina al mismo (figura 13). En este sentido, la unión de Nedd8 a Cul-1 provoca un cambio conformacional en el complejo SCF que le aporta flexibilidad, sobre todo a la región E3-E2-Ub, de modo que es capaz de reorientarse, acercarse al sustrato y transferirle la ubiquitina (Merlet, Burger et al. 2009).

La ubiquitinación se lleva a cabo en dos pasos, primero se produce la transferencia de la primera ubiquitina a un residuo de K del sustrato y después la unión de más ubiquitinas a la primera ubiquitina, esto es, la elongación de la cadena de poliubiquitinas. Se sabe que la unión de Nedd8 a Cul-1 estimula

ambos procesos (Petroski and Deshaies 2005; Duda, Borg et al. 2008; Merlet, Burger et al. 2009; Boh, Ng et al. 2011; Duda, Scott et al. 2011; Onel, Sumbul et al. 2017).

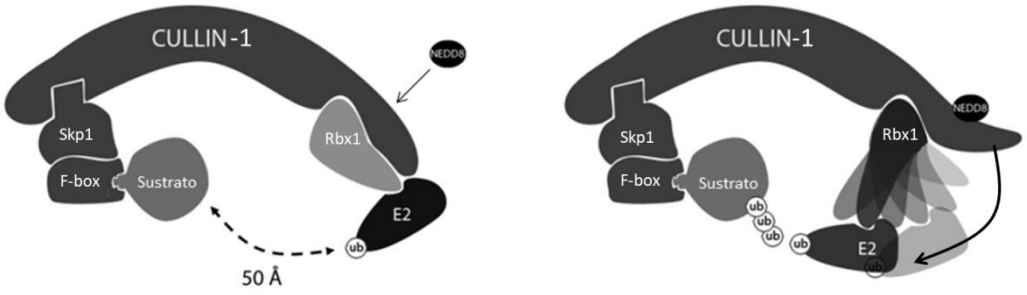

Figura 13. **Activación de SCF por nedilación de Cul-1.** Cuando Cul-1 es nedilado, sufre un cambio conformacional que modifica su interacción con Rbx (RING)-E2-Ub haciéndola más flexible y permitiendo que se reoriente hacia el sustrato. Esto provoca que se cierre el espacio de 50Å existente entre la E2 y el sustrato, permitiendo así la transferencia de ubiquitina. Modificado de (Merlet, Burger et al. 2009)

Nedilación

Nedd8 es una proteína similar a ubiquitina y el proceso de nedilación es análogo al proceso de ubiquitinación (Liakopoulos, Doenges et al. 1998; Cappadocia and Lima 2017). Al igual que la ubiquitina, Nedd8 debe sufrir un procesamiento inicial (Linghu, Callis et al. 2002; Coleman, Bekes et al. 2017). La enzima proteolítica UCHL3 procesa tanto a la ubiquitina como a Nedd8 (Wada, Kito et al. 1998), aunque otra enzima, DEN1 (llamada también SENP8), procesa exclusivamente a Nedd8 y además tiene la capacidad de desacoplarlo de algunos sustratos (Kurihara, Semenova et al. 2000; Chan, Yoon et al. 2008).

La nedilación, al igual que la ubiquitinación, depende de 3 pasos en los que participan una enzima E1, una enzima E2 y una enzima E3 (figura 14). La E1 o

NAE ("Nedd8 Activation Enzyme"), es un heterodímero formado por **Ula1** (NAE1 o APPBP1) y **Uba3**, la E2 o NCE ("Nedd Conjugation Enzyme"), es **Ubc12**, y la Nedd-E3-ligasa, en el caso de SCF, es **DCN1-like protein 1 (DCUN1D1)** (Dcn1 en levaduras) (Kurz, Chou et al. 2008; Chung and Dellaire 2015; Keuss, Thomas et al. 2016). También se ha demostrado que Rbx1 es esencial para que la nedilación se lleve a cabo, puesto que Rbx1 es capaz de unirse tanto a la Nedd8-E2, Ubc12, como a la Nedd8-E3, DCUN1D1, que catalizan el proceso de transferencia de Nedd8 a Cul-1 (Kamura, Conrad et al. 1999; Morimoto, Nishida et al. 2003; Yang, Zhou et al. 2007).

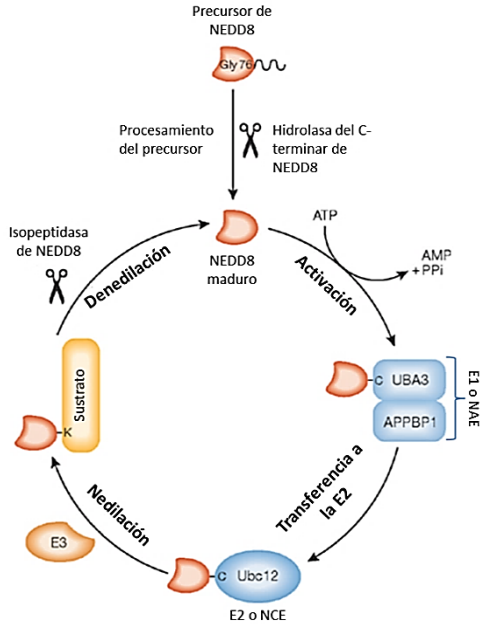

Figura 14. Mecanismo de la nedilación. El mecanismo es similar al de la ubiquitinación, esto es, consta de tres etapas en las que intervienen tres tipos de enzimas. Inicialmente, la proteína precursora de Nedd8 tiene que sufrir un corte proteolítico en una zona del extremo C-terminal, que lleva a cabo DEN1 (SENP8). Posteriormente, Nedd8 se activa mediante un proceso mediado por la enzima E1, el dímero UBA3/APPBP1, para luego transferirse a una enzima E2, Ubc12, la cual, asistida por la enzima E3, transferirá la molécula de Nedd8 a la proteína diana. Modificado de (Rabut and Peter 2008).

Se ha observado que, del conjunto total de proteínas Cullin, solo una pequeña fracción se encuentra nedilada basalmente (~10%), lo que indica que solo una pequeña parte de los complejos CRLs se encuentra completamente activo (Bennett, Rush et al. 2010; Emberley, Mosadeghi et al. 2012). Además, se ha demostrado que el residuo K720 es fundamental para que se forme el enlace

entre Nedd8 y Cul-1, y, por tanto, para que el complejo SCF se active (Furukawa, Zhang et al. 2000; Yue, Ma et al. 2018).

b) Denedilación y secuestro Cul-1

La nedilación es un proceso reversible. Un mecanismo de regulación del complejo SCF consiste en la eliminación de Nedd8 de Cul-1, proceso conocido como denedilación. Este proceso lo lleva a cabo el señalosoma COP9 (CSN), un complejo multimérico con actividad metaloproteasa que cataliza la separación de Nedd8 de las proteínas Cullin, regulando así la actividad de las CRLs (Schmaler and Dubiel 2010; Chung and Dellaire 2015). Sin embargo, el efecto de CSN sobre SCF no es del todo inhibitorio puesto que diferentes estudios indican que los ciclos de nedilación y denedilación de SCF favorecen la renovación de sus componentes y el correcto funcionamiento de este complejo. Además, la función denedilante de CSN estabiliza las F-box previniendo la autoubiquitinación de SCF (Zhou, Wee et al. 2003; He, Cheng et al. 2005; Wee, Geyer et al. 2005; Bosu and Kipreos 2008).

En ausencia de nedilación, las proteínas Cullin (excepto Cul-7) pueden formar un complejo con la proteína Cand1 ("cullin associated Nedd8 dissociated protein 1"), que compite con Skp1 por la unión a Cul-1 y obstruye la región de unión de Cul-1 con el complejo Skp1-Fbox-sustrato. La nedilación de Cul-1 disocia a Cand1 y permite la asociación del complejo Skp1-F-box-sustrato y la formación del SCF (Liu, Furukawa et al. 2002; Zheng, Yang et al. 2002; Goldenberg, Cascio et al. 2004; Reitsma, Liu et al. 2017). También se ha observado que la presencia de

Skp1 y altas concentraciones de ATP pueden provocar la disociación de Cand1 de Cul-1 (Zheng, Yang et al. 2002). Al igual que en el caso del CSN, se ha descrito recientemente que el efecto de Cand-1 sobre SCF no es inhibitorio como se pensaba, sino que se ha demostrado que es necesaria la presencia de Cand1 para la degradación eficiente de los sustratos de SCF, además de para estabilizar al complejo y reclutar las enzimas de nedilación, proceso que luego provocará su separación de SCF (Liu, Reitsma et al. 2018).

En resumen, CSN y Cand1 median la remodelación continua del complejo SCF, que sufre ciclos de nedilación, denedilación por CSN, secuestro por Cand1, nedilación, liberación de Cand1 y formación del nuevo complejo SCF activo. Este ciclo permite el correcto funcionamiento de la E3 ligasa de Ub.

c) Inhibición de la nedilación

El fármaco MLN4924 (también llamado Pevonedistat, de Millennium Pharmaceuticals, Inc. Takeda Oncology Company, Cambridge, MA, USA) inhibe la nedilación a nivel de la E1 (NAE) (Soucy, Smith et al. 2009) y ha sido ampliamente usado para la inhibición general de los complejos CRLs (Soucy, Dick et al. 2010; Nawrocki, Griffin et al. 2012; Zhao and Sun 2013; Zhao, Morgan et al. 2014). Durante el proceso de nedilación en presencia de MLN4924, aunque la NAE lleva a cabo el primer paso de adenilación de Nedd8, dependiente de ATP, debido a la similitud del MLN4924 con la molécula de AMP, se forma un aducto entre Nedd8 y MLN4924. Este aducto es similar al Nedd8 adenilado que debería formarse en condiciones normales, pero con la

diferencia de que permanece adherido al centro activo de la NAE (figura 15) bloqueando la actividad de la enzima e impidiendo que continúe el proceso de nedilación (mostrado en la figura 14) (Brownell, Sintchak et al. 2010). De este modo se bloquea de manera específica la nedilación de los complejos CRL (Soucy, Smith et al. 2009). La degradación de numerosos reguladores del ciclo celular depende de la nedilación y activación de los complejos CRL (Frescas and Pagano 2008), es por ello que MLN4924 ha mostrado tener propiedades antitumorales y actualmente se están llevando a cabo los primeros ensayos clínicos con esta molécula (Soucy, Smith et al. 2009; Soucy, Smith et al. 2009; Nawrocki, Griffin et al. 2012; Bulatov and Ciulli 2015; Bhatia, Pavlick et al. 2016; Paiva, Godbersen et al. 2017; Picco, Petti et al. 2017; Wong, Micel et al. 2017).

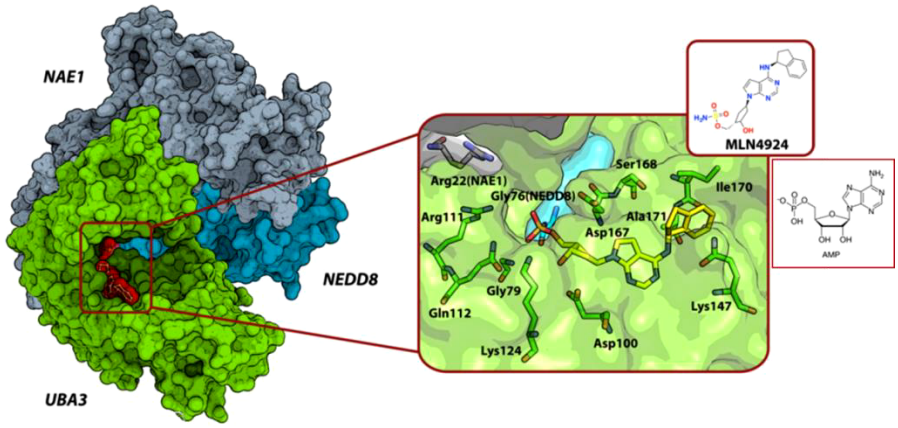

Figura 15. **Reconstrucción tridimensional de la interacción entre NAE1, NEDD8 y UBA3.** Se destaca el sitio de unión de MLN (en rojo). Debido a su similitud con la molécula de AMP, MLN interfiere con la reacción de transferencia de NEDD8 desde NAE1 (E1) a UBA3 (E2), necesaria para que se lleve a cabo el primer paso de la reacción. Modificado a partir de (Bulatov and Ciulli 2015)

d) Regulación de SCF por dimerización de sus proteínas F-box

Otro mecanismo de regulación del complejo SCF depende de su capacidad para formar dímeros a través de sus proteínas F-box (Tang, Orlicky et al. 2007;

Merlet, Burger et al. 2009) (figura 16). Esto favorece el encuentro de la E3 con el sustrato y la enzima E2-Ub cuando la disponibilidad local de los mismos es baja. También puede facilitar el reconocimiento del sustrato al modificar la orientación de las lisinas del mismo que aceptarán la ubiquitina de la E2 y así puede adaptar a todo el complejo al tamaño y forma del sustrato.

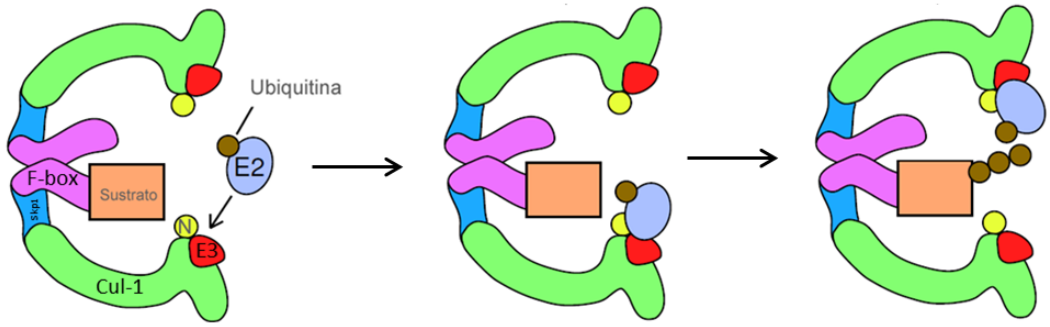

Figura 16: **Regulación de la actividad de SCF por dimerización de sus proteínas F-box.** En situaciones en las que la disponibilidad del sustrato y la E2 cargada sean limitados, se puede producir la dimerización de complejos E3-ligasa a través de sus subunidades F-box permitiendo la ubiquitinación de un sustrato en un SCF por parte de otro SCF que presente la E2 cargada con ubiquitina. Modificado a partir de (Bosu and Kipreos 2008).

Además, otro mecanismo regulador parece ser la existencia de "pseudosustratos" que pueden unirse a SCF, pero no son ubiquitinados. Se desconoce la función de estas proteínas pero se cree pueden desempeñar un papel regulador de la ubiquitinación compitiendo por afinidad con los sustratos del complejo SCF (Davis, Hatzubai et al. 2002).

6.5 Principales dianas conocidas del complejo SCF

Las proteínas F-box, la subunidad del complejo E3 ligasa que reconoce al sustrato, confieren especificidad al proceso de ubiquitinación. De las 69 proteínas F-box conocidas, sólo se han identificado los sustratos de unas 20 F-box (Frescas

and Pagano 2008; Zheng, Zhou et al. 2016). Los siguientes ejemplos son algunas F-box que interaccionan con Cul-1 dentro de SCF y algunos de los sustratos que reconocen:

- **SKP2:** reconoce para su ubiquitinación y, degradación, algunos reguladores negativos del ciclo celular, como p27, p21 y p57, otras proteínas supresoras de tumores como RBL2 y FOXO1. SKP2 reconoce a estos sustratos cuando se encuentran fosforilados en secuencias específicas (Frescas and Pagano 2008; Ravid and Hochstrasser 2008).
- **Fbw7:** induce la ubiquitinación de reguladores positivos del ciclo celular, como Myc, Jun, la Ciclina E, Notch, Presenilina 1/2 y SREBP1/2 (Welcker and Clurman 2008).
- **βTRCP:** reconoce a una gran variedad de sustratos como β-Catenina, IκBα, p100, IFNαR, SNAIL, y STAT1, y también a algunos reguladores del ciclo celular como Wee1, Emi1/2 y Cdc25A/B (Frescas and Pagano 2008).

6.6 El proteasoma 26s

El proteasoma 26S es una compleja maquinaria de proteólisis de 2.5 MDa encargada de la degradación de proteínas marcadas con cadenas de ubiquitina (Hershko and Ciechanover 1998; Murata, Yashiroda et al. 2009; Tanaka 2009; Inobe and Matouschek 2014). Se encarga de la degradación de toda clase de proteínas, desde proteínas reguladoras a estructurales, y también de la eliminación de proteínas defectuosas o desnaturalizadas que podrían interferir con el correcto funcionamiento de la célula (Hershko, Eytan et al. 1982).

Al proteosoma se le han atribuido, a su vez, funciones inmunológicas debido a que lleva a cabo el procesamiento de péptidos antigénicos para su presentación en moléculas del CMH (Kloetzel 2004). Por todo ello, el proteasoma participa en la homeostasis, la regulación del ciclo celular y la apoptosis, la diferenciación, la respuesta inmunológica y el metabolismo celular (Glotzer, Murray et al. 1991; Hershko, Ganoth et al. 1991; Kloetzel 2004; von Mikecz 2006; Konstantinova, Tsimokha et al. 2008) .

Este macrocomplejo está dividido estructuralmente y funcionalmente en dos subcomplejos (figura 17): un núcleo central catalítico 20S y una o dos partículas reguladoras 19S en los extremos, que se denominan así por su coeficiente de sedimentación. Cada subcomplejo está formado por anillos compuestos por múltiples subunidades que desempeñan distintas funciones durante el proceso de degradación. El proteasoma 19S está encargado del reconocimiento de las proteínas ubiquitinadas y de su desdoblamiento para penetrar en el proteasoma 20S, que posee la actividad proteolítica.

El **proteasoma 20S** está formado por 4 anillos apilados, dos interiores tipo β y dos exteriores tipo α, que forman una estructura de barril con un túnel central. Cada anillo está formado por 7 subunidades (α1-7, β1-7). Los anillos tipo β poseen las subunidades con actividad catalítica, β1, β2 y β5, cuyo extremo N-terminal, con capacidad hidrolítica, está orientado hacia el interior del túnel (Arendt and Hochstrasser 1997; Heinemeyer, Ramos et al. 2004). β1 posee actividad similar a caspasa, permitiendo el corte de la proteína a través de aminoácidos ácidos de su C-terminal. β2 posee actividad similar a tripsina al

cortar las proteínas por sus aminoácidos básicos en el extremo C-terminal. Y β5 posee actividad similar a quimotripsina y permite cortar a las proteínas por sus residuos hidrofóbicos (Arendt and Hochstrasser 1997; Heinemeyer, Ramos et al. 2004; Murata, Yashiroda et al. 2009; Tanaka 2009). Los anillos periféricos α tienen una función reguladora sobre los anillos β puesto que los extremos N-terminal de las subunidades α pueden cerrarse y ocluir el paso hacia el túnel formado por los anillos β (Tanaka 2009). El mecanismo de apertura de las subunidades α no ha sido completamente elucidado, pero probablemente esté regulado por el proteasoma 19S. El núcleo catalítico 20S degrada las proteínas a oligopéptidos de entre 3 y 15 aminoácidos, que son posteriormente degradados a aminoácidos simples por oligopeptidasas y/o amino-carboxi peptidasas.

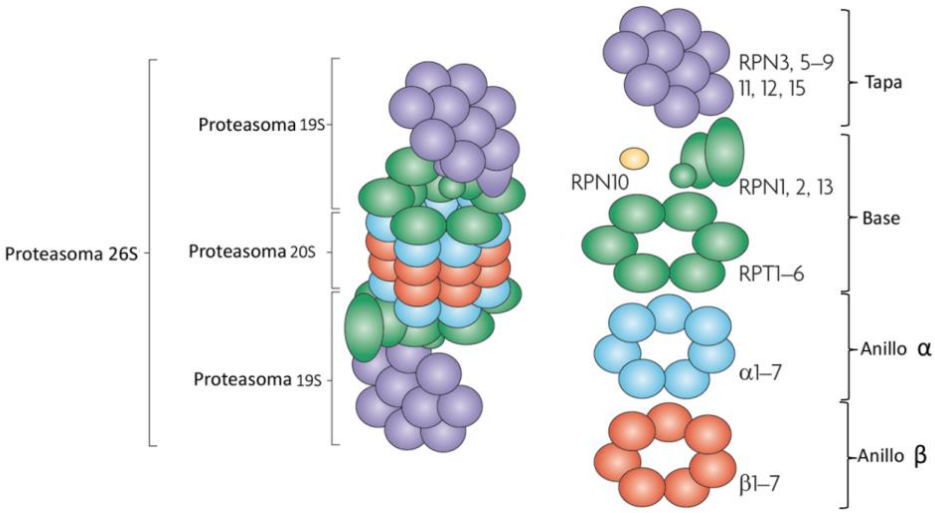

Figura 17. **Estructura del proteasoma 26S.** El proteasoma 26S está formado por un núcleo catalítico o proteasoma 20S compuesto por dos anillos α exteriores y dos anillos β internos, con actividad proteasa, y una partícula reguladora o proteasoma 19S en cada extremo del 20S, formado por una tapa y una base. El proteasoma 19S está compuesto por partículas reguladoras con capacidad ATPasa (RPT) y otras sin capacidad ATP-asa (RPN). Modificado a partir de (Murata, Yashiroda et al. 2009).

El **proteasoma 19S** es una unidad reguladora que cubre uno o ambos extremos del proteasoma 20S. Está formado por al menos 19 subunidades distintas denominadas partículas reguladoras (regulatory particles o RP) agrupadas en dos partes, una tapa y una base que interaccionan directamente con el núcleo catalítico 20S (Murata, Yashiroda et al. 2009). La degradación de proteínas por el proteasoma conlleva un gasto de ATP, por ello, el proteasoma 19S está formado por algunas subunidades reguladoras con actividad ATPasa, RPT (regulatory particle of triple-ATPase), y otras subunidades sin capacidad ATPasa, RPN (regulatory particle non-ATPase). La **tapa** está compuesta por las subunidades encargadas del reconocimiento del sustrato poliubiquitinado y de la deubiquitinación del mismo, que libera a la proteína para ser degradada y a las ubiquitinas para ser recicladas. Se ha demostrado que la unión de proteínas poliubiquitinadas estimula la actividad del proteasoma (Bech-Otschir, Helfrich et al. 2009; Li and Demartino 2009; Peth, Besche et al. 2009). La **base** está formada por 6 RPT y 4 RPN que están encargadas del desdoblamiento de la proteína, la apertura del canal α del proteasoma 20S y la traslocación de la proteína hacia el interior del mismo.

6.7 El sistema UPS en patología

El proteasoma 26S se localiza tanto en el citoplasma, ya sea independiente o asociado al retículo endoplasmático, como en el núcleo de las células eucariotas (Wojcik and DeMartino 2003; von Mikecz 2006). En este sentido, se ha sugerido que el correcto funcionamiento del proteasoma en el núcleo de las células es necesario para que se mantenga la proteostasis nuclear (homeostasis de proteínas

nucleares), puesto que la acumulación de proteínas aberrantes en el núcleo puede dar lugar a numerosas patologías neurodegenerativas (Gallagher, Oeser et al. 2014).

Como se ha mencionado, el sistema ubiquitina proteasoma regula múltiples procesos, por lo que un incorrecto funcionamiento del mismo puede dar lugar a patologías muy diversas, como el cáncer, patologías neurodegenerativas y patologías autoinmunes (Paul 2008). Es por ello que se han desarrollado inhibidores del proteasoma, como el Bortezomib (Paramore and Frantz 2003), que actualmente se utiliza para tratar el mieloma múltiple, la Lactacistina (Omura, Fujimoto et al. 1991) o el MG132, actualmente el más utilizado en investigación y que ha mostrado tener también propiedades antitumorales (Han and Park 2010; Guo and Peng 2013; Qiang, Sui et al. 2017).

Sin embargo, estos inhibidores actúan de manera inespecífica sobre la degradación de proteínas, y muchas patologías ya descritas se han asociado a disfunciones en ligasas E3, que llevan a la acumulación de proteínas como p53 o la ciclina E (Strohmaier, Spruck et al. 2001; Sakamoto 2002; Staropoli, McDermott et al. 2003). Es por ello que un abordaje más específico, como la inhibición de los complejos CRLs por parte el MLN4924 ha mostrado tener muy buenos resultados en cáncer (Soucy, Smith et al. 2009; Nawrocki, Griffin et al. 2012; Bulatov and Ciulli 2015; Bhatia, Pavlick et al. 2016; Paiva, Godbersen et al. 2017; Picco, Petti et al. 2017) o la enfermedad inflamatoria intestinal (Cheng, Hu et al. 2016). Sin embargo, es importante conocer cómo estos tratamientos

afectan al sistema inmunológico, fundamental para la resolución de las enfermedades.

Algunos estudios han destacado que la nedilación juega un papel crucial en el funcionamiento de algunas células del sistema inmunológico, como macrófagos, células T y CDs. Por ejemplo, la inhibición de la nedilación reprime la liberación de citoquinas proinflamatorias inducida por LPS en macrófagos (Chang, Reyna et al. 2012), e inducida por la activación del TCR en células T (Jin, Liao et al. 2013). Esto también ocurre en las CDs, humanas y murinas, donde la inhibición de la nedilación o la inactivación de SCF resulta en la supresión de la liberación de citoquinas proinflamatorias dependiente de LPS y otros estímulos, tanto infecciosos (ligandos de TLR1/2 y NOD2), como no infeccciosos (agonistas CD40L) (Mathewson, Toubai et al. 2013; Cheng, Hu et al. 2016). Además, también se ha demostrado que la inhibición de la nedilación en CDs inhibe su capacidad de estimular a las células T alogénicas para que éstas proliferen (Mathewson, Toubai et al. 2013; Cheng, Hu et al. 2016).

ANTECEDENTES

CCR7 regula una compleja red de señalización que le permite controlar múltiples funciones homeostáticas en las células dendríticas (CDs), incluyendo la quimiotaxis, supervivencia, velocidad migratoria, citoarquitectura, endocitosis o maduración (Yanagawa and Onoe 2002; Yanagawa and Onoe 2003; Sanchez-Sanchez, Riol-Blanco et al. 2004; Marsland, Battig et al. 2005; Riol-Blanco, Sanchez-Sanchez et al. 2005; Sanchez-Sanchez, Riol-Blanco et al. 2006; Lopez-Cotarelo, Escribano-Diaz et al. 2015; Torres-Bacete, Delgado-Martin et al. 2015). La mayoría de los estudios acerca de CCR7, y de los receptores de quimioquinas en general, se han centrado en el análisis del papel regulador de la fosforilación en el control de las funciones celulares mencionadas, pero los estudios de otros tipos de modificaciones post-traduccionales que pudieran ser importantes para la regulación de las funciones conocidas u otras funciones desconocidas de este receptor son escasos (Schaeuble, Hauser et al. 2012).

La nedilación, o unión de Nedd8 a una proteína, es un tipo de modificación post-traduccional que está involucrada en el control de algunas funciones de leucocitos del sistema inmune innato (Chang, Reyna et al. 2012; Li, Liu et al. 2013; Mathewson, Toubai et al. 2013; Cheng, Hu et al. 2016), y del sistema inmune adaptativo (Jin, Liao et al. 2013). La función más estudiada de la nedilación es la activación de las ligasas E3 de ubiquitina tipo CRL, entre ellas, la más estudiada es SCF (CRL-1) (Merlet, Burger et al. 2009).

La E3 ubiquitin ligasa SCF (Skp1-Cullin-1-F-Box) controla la ubiquitación de una gran cantidad de proteínas celulares para su degradación por el proteasoma y SCF se activa cuando su componente Cul-1 se nedila (Merlet, Burger et al. 2009). Por tanto, la nedilación regula la actividad E3 ubiquitin ligasa y la ubiquitinación de componentes celulares.

HIPÓTESIS

CCR7 controla en las células dendríticas humanas la ubiquitinación de proteínas mediante la estimulación, a través de nedilación, de la actividad de la ubiquitin-ligasa SCF (Skp1-Cullin1-F-Box).

OBJETIVOS

1. Analizar si la estimulación de CCR7 induce nedilación de Cullin-1 (Cul-1) en CDs humanas maduras y e identificar las proteínas G señalizadoras que median la nedilación de Cul-1.
2. Averiguar si se requiere nedilación para el control de las funciones reguladas por CCR7 (quimiotaxis, supervivencia, velocidad migratoria, endocitosis y cambios en citoarquitectura).
3. Examinar la localización subcelular de Cullin nedilado (Cul-1^{Nedd8}).
4. Comprobar si Cul-1^{Nedd8} forma parte del complejo SCF (Skp1-Cul-1-F-Box).
5. Estudiar si la nedilación de SCF, y la consecuente activación de esta ligasa, regula la ubiquitinación de proteínas en las CDs.
6. Identificar las proteínas que son ubiquitinadas por SCF tras la estimulación de CCR7.

MATERIALES Y MÉTODOS

Reactivos generales

Las quimioquinas CCL19, CCL21 y el TNF se adquirieron a PeproTech (Rocky Hill, NJ). Las citoquinas recombinantes humanas IL-4 y GM-CSF se obtuvieron de Immunotools.

El Ficoll (Lymphoprep) se obtuvo de Axis Shield (Oslo, Noruega). Los monocitos se purificaron con anticuerpos anti-CD14 unidos a bolitas magnéticas (Miltenyi Biotech, STEMCELL Technologies, GR, Francia).

El inhibidor MLN4924 se obtuvo de Active Biochemicals Co. (Wan Chai, Hong Kong,). El dextrano-FITC, la poli-L-ornitina, el Hoechst 33258, el colorante rojo Ponceau, la toxina pertúsica, el cocktail de inhibidores de proteasas, la Faloidina-TRITC, la proteína A-agarosa y el kit de PLA Duolink fueron adquiridos de Sigma-Aldrich (Merck, KGaA, Darmstadt, Alemania). La pepstatina A, la albúmina de suero bovino (BSA), la proteína G-agarosa y los anticuerpos secundarios de conejo, ratón y cabra acoplados a la peroxidasa (HRP) se adquirieron a Santa Cruz Biotechnology Inc. (Santa Cruz, CA).

Los anticuerpos secundarios conjugados con fluorocromos, anti-rabbit Alexa 568, anti-mouse Alexa 488 y anti-goat Alexa 488 se adquirieron a Molecular Probes (Thermo Fisher Scientific, Waltham, MA, EEUU).

La información sobre los anticuerpos primarios utilizados en esta tesis se detalla en la siguiente tabla.

Anticuerpo	Casa comercial	Especie	Concentración	Técnica	Concentración	Técnica	Concentración	Técnica
Actina β	Santa Cruz	Ms	0,2µg/ml	WB				
AKT p-Ser473	Cell Signalling	Rb	1µg/ml	WB				
AKT p-Thr308	Cell Signalling	Rb	1µg/ml	WB				
Cofilina p-Ser3	Santa Cruz	Rb	0,2µg/ml	WB				
Cullin-1	Biorbyt	Rb	1µg/ml	WB	10µg/ml	IF		
Cullin-1	Santa Cruz	Rb	2µg/ml	IP	4µg/ml	IF		
CD3ζ	Santa Cruz	Ms	2µg/ml	IP				
ERK1	Santa Cruz	Rb	0,2µg/ml	WB				
ERK2	Santa Cruz	Rb	0,2µg/ml	WB				
ERK1/2 p-Thr202/p-Tyr204	Cell Signalling	Rb	1µg/ml	WB				
Prot Gβ2	Santa Cruz	Rb	2µg/ml	IP				
IκBα	Biorbyt	Rb	1µg/ml	WB				
Lamina-β1	Cell Signalling	Rb	1µg/ml	WB				
LAT	Santa Cruz	Rb	10µg/ml	IP				
LDH	Sigma	Ms	1µg/ml	WB				
Nedd8	Cell Signalling	Rb	1µg/ml	WB	20µg/ml	IF		
Nedd8	Genetex	Rb	1µg/ml	WB	40µg/ml	IF		
PKCζ	Santa Cruz	Gt	10µg/ml	IP				
p65 (NFκB)	Santa Cruz	Rb	0,2µg/ml	WB				
Rbx1	Santa Cruz	Ms	0,2µg/ml	WB	2µg/ml	IF		
Rbx1	Biorbyt	Rb	1µg/ml	WB				
Rho-GDI	Santa Cruz	Rb	0,2µg/ml	WB				
Skp1	Santa Cruz	Gt	0,2µg/ml	WB	10µg/ml	IP		
Skp1	Cell Signalling	Rb	1µg/ml	WB				
Tubulina α	Rockland	Rb	1µg/ml	WB				
Ubiquitina	Santa Cruz	Ms	4µg/ml	IF	2µg/ml	IP	0,2µg/ml	WB
Ubiquitina K48	Millipore	Rb	1µg/ml	WB				
Vinculina	Sigma	Ms	2,5µg/ml	WB				
Proteasoma 20S β2	Santa Cruz	Gt	0,2µg/ml	WB	4µg/ml	IF		

Tabla 1: información de los anticuerpos utilizados en esta tesis y las concentraciones y técnicas para las que se usaron. Rb = conejo, Ms = ratón, Gt = cabra. WB = Western Blot, IP = inmunoprecipitación, IF = inmunofluorescencia.

Modelo experimental

Se utilizaron células dendríticas (CDs) humanas derivadas de monocitos de sangre periférica, obtenida de donantes sanos a través del Centro de Transfusiones de la Comunidad de Madrid. La sangre, obtenida en forma de concentrado leucoplaquetario, se diluyó en PBS para luego separar sus distintos componentes mediante centrifugación en gradiente de Ficoll. De este modo se separó la fracción de células mononucleares de sangre periférica (Peripheral Blood

Mononuclear Cells, PBMCs), que contiene mayormente monocitos, linfocitos T y B y células NK. A continuación, se purificaron los monocitos (células CD14+) mediante la utilización de anticuerpos anti-CD14 acoplados a bolitas magnéticas y un soporte imantado, siguiendo las instrucciones del proveedor (Miltenyi Biotech). Las células obtenidas, monocitos CD14+ (95%), se resuspendieron en RPMI con 10% de suero fetal bovino (FBS, Fetal Bovine Serum, Lonza Group Ltd, Basilea, Suiza) y se cultivaron a una concentración de 1 $x10^6$ células/ml en presencia de las citoquinas GM-CSF (1000 U/ml) y IL-4 (1000 U/ml). Las citoquinas, que se suministraron cada 2 días a partir del inicio del cultivo y durante 7 días, inducen la diferenciación de los monocitos hacia un fenotipo de CD inmadura. Las CDs inmaduras se maduraron añadiendo, además de las citoquinas GM-CSF e IL-4 a las concentraciones indicadas, la citoquina pro-inflamatoria TNF-α (50 ng/ml). Tras 3 días en cultivo, se obtuvo un porcentaje de células CD80+, CD86+, CD83+, CCR7+ y HLA-DR+ mayor del 85%, Estas células además dejaron de expresar CD14 (menos de 1% de células CD3+, CD14+, CD16+ o CD19+). Por tanto, las CDs maduras se utilizaron para los experimentos en el día 10 y 11 desde el momento de su purificación.

Experimentos de estimulación de CCR7

Para los experimentos se utilizaron las CDs maduras, que expresan el receptor CCR7. Para estudiar el efecto que ejerce la estimulación de CCR7 sobre la dinámica de activación de diferentes moléculas de señalización intracelular, se estimularon las CDs maduras con CCL21 a distintos tiempos. En primer lugar, es necesario reducir la actividad basal de las moléculas a estudiar. Por ello, las

células (10^6 células/ml) se trasladaron a un medio RPMI sin suero que incluye 0,1% de BSA, donde se dejaron aclimatar entre 30 y 45 minutos a 37ºC y 5% de CO_2. Posteriormente, las CDs se estimularon con CCL21 (18 nM) y se mantuvieron en el incubador durante tiempo indicado en la leyenda de las figuras. A continuación, las células se centrifugaron a las máximas revoluciones (~12.000 g) durante 30 segundos. Posteriormente, se retiró el sobrenadante y los pellets obtenidos se lisaron resuspendiéndolos en buffer de carga (SB) 2x (200 mM Tris-HCl, pH 6.8, 0,1 mM de ortovanadato sódico, 6% SDS, 1 mM EDTA, 4% β-mercaptoetanol, 10% glicerol y azul de bromofenol). Las muestras obtenidas se hirvieron durante 5 minutos para desnaturalizar las proteínas y, posteriormente, se mantuvieron a -20ºC hasta su análisis.

Experimentos con inhibidores

Se realizaron diversos experimentos en los que se bloqueó una determinada proteína o ruta de señalización. Los experimentos de inhibición se realizaron del mismo modo que los experimentos de estimulación mencionados arriba, solo que las células se incubaron con los inhibidores farmacológicos de interés, en ausencia de suero y a los tiempos indicados en la leyenda de las figuras, antes de la estimulación con CCL21.

Western Blot

Las muestras obtenidas de los experimentos se resolvieron mediante electroforesis en geles de poliacrilamida en condiciones reductoras (SDS-PAGE).

Los geles se transfirieron a membranas de PVDF (previamente activadas con metanol) mediante un sistema de transferencia húmedo. Tras la transferencia, se realizó una tinción de la membrana con rojo Ponceau para comprobar que la transferencia se había producido correctamente. Las membranas teñidas fueron escaneadas para conservar información sobre la carga de las proteínas. Tras ser desteñidas, las membranas se bloquearon durante 1h en TBST (TBS 0,1% Tween 20, pH 7,5) que incluye 5% de leche desnatada en polvo. Después, las membranas se incubaron durante 18 h a 4ºC con los anticuerpos primarios (Tabla 1) en TBST+ 5% BSA. Tras esta incubación, se realizaron 3 lavados con TBST y las membranas se incubaron con anticuerpos secundarios frente a la especie de interés (conejo, ratón, cabra) acoplado a peroxidasa (80 ng/ml en TBST) durante 1h. Por último, se lavaron 3 veces más con TBST y se procedió al revelado digital (Chemidoc, Bio-Rad Laboratories, CA, EEUU) o analógico (Curix 60, Agfa-Gevaert Group) de las bandas inmunoreactivas con ECL (Thermo Fisher Scientific, Waltham, MA, EEUU).

El densitometrado de las bandas se realizó con los softwares Multigauge de Fujifilm, Image Lab de Bio-rad e Image J, corrigiéndose los valores de las proteínas frente a un control de carga y normalizándolos respecto al punto no estimulado con CCL21, también llamado tiempo 0 ó (-), y frente al control sin tratar, en caso de tratamiento con inhibidores.

Para la eliminación de anticuerpos primarios y reincubación de membranas con nuevos anticuerpos, procedimiento conocido como "*stripping*" se utilizó un buffer compuesto por glicina (125 mM), 0,1% SDS, 1% Tween 20 pH 2.2. La

membrana se sometió a 2 lavados de 10 min en el buffer de stripping, después 2 lavados de 10min en PBS, 2 lavados de 5 min en TBST y fue bloqueada de nuevo e incubada con los anticuerpos primarios como se ha mencionado anteriormente.

Inmunofluorescencias

Las CDs maduras se resuspendieron en RPMI 0,1% BSA a una concentración de 10^6 CDs/ml. A continuación, se sembraron $5x10^5$ células en cristales de 10 mm de diámetro que habían sido previamente cubiertos con poli-L-ornitina (0,1 mg/ml) y se dejaron adherir durante 1h a 37ºC. Tras la estimulación con CCL21 (18 nM) las células se fijaron con PFA 4% (Santa Cruz Biotechnology Inc., Santa Cruz, CA) durante 15 min a temperatura ambiente. Tras un lavado con PBS, las células se permeabilizaron con metanol frío o Tritón X-100 al 0,2% en PBS durante 5 min. Tras otros 3 lavados con PBS, las preparaciones se bloquearon con IgG humana (1 µg/ml) durante 5 min. A partir de este momento, los lavados se hicieron con PBS 0,1% BSA. Las muestras se incubaron con los anticuerpos primarios diluidos en PBS 0,1% BSA durante 1h. Se hicieron 3 lavados y después se añadió la mezcla de anticuerpos secundarios diluidos en PBS 0,1% BSA junto con el colorante Hoechst 33258 durante 1h. Las muestras se lavaron 2 veces con PBS y 1 vez con agua destilada antes de ser montadas sobre portaobjetos con el medio de montaje Dako (Dakocytomation). Finalmente se analizaron con un Microscopio Láser Confocal espectral (CLSM) Leica TCS SP5. Se realizaron entre 10 y 20 fotografías de secciones confocales de 0,5 µm de grosor. Las imágenes se analizaron con el software de Leica LAS X y con Image J, con el que se realizaron

las animaciones en 3D. Las imágenes fueron preparadas con el software Adobe Photoshop CS.

Ensayo de ligación por proximidad: PLA (Proximity Ligation Assay)

La técnica del PLA permite analizar mediante microscopía de fluorescencia la proximidad de dos moléculas (Fredriksson, Gullberg et al. 2002; Soderberg, Gullberg et al. 2006). Con esta técnica se obtiene una señal fluorescente positiva cuando las dos moléculas analizadas se encuentran a una distancia menor a 40 nm, distancia a la cual la probabilidad de que estén interaccionando es muy alta.

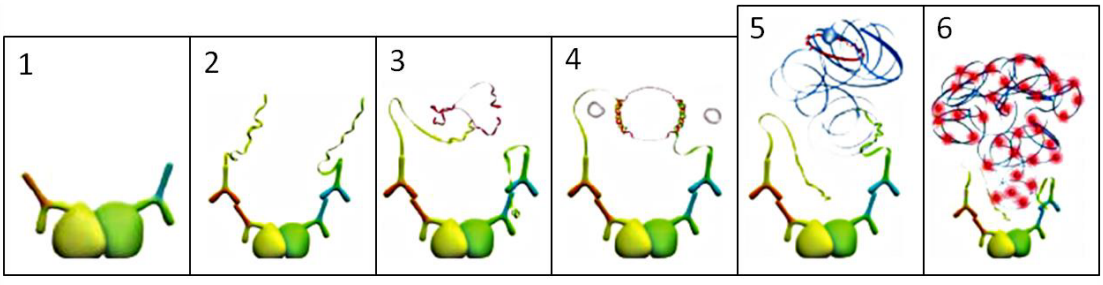

Figura 18. **La técnica PLA.** Esta técnica consiste en el marcaje de las proteínas cuya interacción quiere detectarse con sus respectivos anticuerpos primarios (1). A continuación, se añaden los anticuerpos secundarios que llevan acopladas unas sondas de ADN (2). Se añaden unas sondas complementarias y conectoras (3) y una ligasa de ADN, que produce la ligación de las sondas y la formación de un ADN circular (4). Se añade una ADN-polimerasa que amplifica el ADN circular (5) y gracias a la presencia de oligonucleótidos marcados fluorescentemente (6) se puede observar una señal fluorescente al microscopio, siempre y cuando las proteínas analizadas se encuentren a menos de 40 nm para que sondas acopladas a sus anticuerpos secundarios puedan hibridar. (Modificado del catálogo de Sigma).

Las CDs (5 x 10^4 células) se dejaron adherir sobre cristales cubiertos previamente de poli-L-ornitina y se fijaron del mismo modo que se hizo para las inmunofluorescencias. Las muestras se permeabilizaron con 0,2% Triton X-100 ó metanol frío (Panreac), se bloquearon con IgG humana y se incubaron con los anticuerpos primarios. A continuación, en lugar de utilizarse anticuerpos secundarios, se llevó a cabo el PLA (figura 18), siguiendo las instrucciones del fabricante (Duolink II in situ PLA detection kit, Sigma). Las muestras se incubaron

con anticuerpos secundarios especiales conjugados con unas sondas de ADN (sondas PLUS y MINUS) que hibridan y generan un ADN circular gracias a una enzima ligasa y a oligos complementarios. Seguidamente, se lleva a cabo una amplificación del ADN circular mediante la adición de la enzima polimerasa. Finalmente se añadieron sondas de oligonucleótidos complementarios fluorescentes que se unen al ADN amplificado. Por último, las muestras se montaron con un medio que incluye el colorante DAPI (4',6-diamino-2-fenilindol) para el marcaje de los núcleos. La amplificación del ADN circular, indicativa de una señal positiva de PLA, se aprecia como un punteado fluorescente en las zonas donde las moléculas estudiadas se encuentran próximas entre sí. Las preparaciones se analizaron mediante microscopía confocal, del mismo modo que las inmunofluorescencias.

Fraccionamiento de proteínas citoplásmicas y nucleares

Para el fraccionamiento de proteínas citoplásmicas y nucleares se utilizaron $5x10^6$ CDs maduras por condición. Se llevó a cabo el experimento en RPMI 0,1% BSA y, al finalizar el mismo, las células se lavaron con PBS frío, manteniéndose en medio frío (4º) a partir de este momento. Las CDs se disolvieron en buffer de extracción de proteínas citoplásmicas (10 mM Hepes pH 7,6, 10 mM KCl, 0,1 mM EDTA, 0,1 mM EGTA, 1 mM DTT, 1 mM molibdato) suplementado con los inhibidores de proteasas: pepstatina A (10 µg/ml) y el cocktail de inhibidores Sigma (5 mg/ml), que incluye EDTA (1 mM), AEBSF (2 mM), Bestatin (130 µM), E64 (14 µM), Leupeptin (1 µM). Las células se incubaron en hielo durante 15 min y posteriormente se añadió NP-40 (Fluka, Sigma-Aldrich) al 10% y se agitó en un

aparato vortex 5 segundos. Los lisados se centrifugaron a las máximas revoluciones (~12.000 g) durante 5 min a 4ºC. Se separó el sobrenadante, que corresponde a la fracción citoplásmica, y se alicuotó y congeló a -80ºC. Los *pellets* (núcleos) se lavaron con PBS, se resuspendieron en buffer de extracción de proteínas nucleares (20 mM Hepes pH 7,6, 400 mM NaCl, 1 mM EDTA, 1 mM EGTA, 1 mM DTT, 1 mM molibdato, pepstatina A (10 µg/ml) y el cocktail de inhibidor de proteasas de Sigma) y a continuación se incubaron 30 min en hielo, agitando con el vortex cada 10 min. Los lisados se centrifugaron a máximas revoluciones (~12.000 g) durante 30 min y se transfirieron los sobrenadantes (fracción nuclear) a un tubo nuevo. Se alicuotaron y congelaron las muestras a -80ºC hasta su utilización.

La concentración proteica de los extractos citoplásmicos y nucleares se cuantificó mediante el método de Bradford utilizando el reactivo de la compañía Sigma. Tras la cuantificación se prepararon diluciones de las muestras a 2 mg/ml y se resuspendieron en buffer de carga 2x para ser analizadas por electroforesis (cargaron 15 µg de proteína por pocillo) y Western blot.

Inmunoprecipitaciones

Para estos ensayos se utilizó la mayor cantidad de CDs disponible (idealmente entre 15-30x10^6 células, equivalente a 2-4 mg de proteína total). Las células se resuspendieron en RPMI con 0,1% BSA y se dejaron estabilizar 45 min a 37º y 5% de CO_2. Posteriormente las células se estimularon con CCL21 durante 5 min, tras lo cual se lavaron con PBS frío para detener la reacción. Las células se

mantuvieron a 4ºC el resto del proceso. A continuación, las CDs se lisaron en un buffer de inmunoprecipitación (1% NP-40, 50 mM Tris pH 7.4, 100 mM NaCl, 2 mM MgCl2, 10% glicerol y cocktail de inhibidores de proteasas de Sigma (5 mg/ml)) y se incubaron con rotación durante 1 h. El lisado fue sonicado 5 min y centrifugado a ~12.000 g durante 90 min. Posteriormente, el sobrenadante se sometió a un pre-aclarado con agarosa unida a proteína A durante 18 h en rotación a 4ºC. Tras eliminarse por centrifugación la proteína A-agarosa, se añadieron los anticuerpos (2 µg/mg de proteína) y se incubaron durante 6 h. Después se incubó el lisado con 30 µl/ml de proteína A-agarosa durante 1h. Se recogió el *pellet* de agarosa, y, tras varios lavados, las muestras estuvieron listas para ser procesadas, bien mediante Western blot, resuspendiéndolas en buffer de carga 2x, o bien para su análisis por proteómica.

Inmunoprecipitación nuclear

En este trabajo se llevó a cabo, también, la inmunoprecipitación de proteínas nucleares. Para ello se realizó la extracción proteínas como se mencionó en el método de fraccionamiento de proteínas citoplásmicas y nucleares. Tras la separación de los extractos citoplásmicos, se lavaron los pellets nucleares 3 veces con PBS frío. Estos pellets se disolvieron en el buffer de inmunoprecipitación mencionado arriba, se sonicaron durante 5 min y se procedió con la inmunoprecipitación de la manera habitual. Una vez terminado el proceso, las muestras se procesaron para ser analizadas mediante Western blot o mediante proteómica.

Análisis proteómico

Las muestras obtenidas en la inmunoprecipitación nuclear fueron sometidas a un proceso de digestión con tripsina para obtenerse los péptidos que posteriormente se analizaron mediante cromatografía líquida (LC) y espectrometría de masas (MS).

Digestión con tripsina

Las muestras se resuspendieron en 50 mM de bicarbonato amónico pH 8.0, y se trataron con 1 µg de tripsina, manteniéndose durante 18 h a 37°C con agitación (700 rpm). Al final de este período se añadieron 0,5 µg de tripsina y se continuó la incubación durante otras 2 h en las mismas condiciones. Posteriormente las muestras se centrifugaron, y los péptidos trípticos (el sobrenadante) se pasaron a un tubo limpio. El *pellet* se lavó dos veces con 100 µL de agua de calidad HPLC, El sobrenadante resultante de los dos lavados se juntó con los péptidos recolectados anteriormente, y el *pellet* se desechó. La solución con péptidos se acidificó con 50% de ácido fórmico (FA) hasta tener una concentración final de FA del 2%. Las muestras se secaron en el concentrador de vacío SpeddVac (Eppendorf), se resuspendieron en 20 µL de FA al 5% y una tercera parte de las muestras se analizó en el espectrómetro de masas Q-Exactive.

Análisis LC-MS

Los péptidos se cargaron en una pre-columna Acclaim PepMap 100 (Thermo Scientific) y se eluyeron en una columna PepMap RSLC C18, de 15 cm de

longitud, 75 µm de diámetro interno y 3 µm de tamaño de partícula (Thermo Scientific). La separación de los péptidos se llevó a cabo en un nano Easy nLC 1000 (Proxeon) acoplado a una fuente iónica con nanoelectrospray (Thermo Scientific).

La velocidad de flujo de la fase móvil fue de 300 nL/min usando 0.1% de ácido fórmico en agua (tampón A) y 0.1% de ácido fórmico en acetonitrilo (tampón B). Se siguió un perfil de gradiente de 0–35% de tampón B durante 90 min, 35%-100% de tampón B durante 4 min y 100% de tampón B durante 8 min.

Los espectros de masas se obtuvieron en un espectrómetro de masas Q Exactive (Thermo Scientific) trabajando en modo positivo. Los espectros de masas correspondientes al espectro de barrido completo tenían una relación de masa carga (m/z) 400-1500 Th y se obtuvieron con una resolución de 70.000 y 36.000, respectivamente. De cada espectro se seleccionaron los 10 iones más intensos para su fragmentación mediante disociación por colisión de alta energía (HCD). Los iones con carga única o sin asignación de carga se desecharon. La ventana de exclusión dinámica se fijó en 20 s. Los archivos de espectros (*.raw) se enfrentaron a la base de datos *Homo sapiens* a través de Proteome Discoverer (versión 1.4.1.14, Thermo Scientific) utilizando MASCOT como motor de búsqueda. En los parámetros de búsqueda, la carbamidometilación de cisteínas y la oxidación de metionina se establecieron como modificaciones fijas. La tolerancia de la selección de los precursores y los iones producto se fijó en 10 ppm y 0,02 Da, respectivamente. La identificación de los péptidos se validó mediante el algoritmo Percolator usando un valor $q \leq 0{,}01$ (1).

El conjunto de proteínas identificadas, excluyendo aquellas que se encontraron en el control de inmunoprecipitación, se filtraron contrastándose con la base de datos CRAPome (Mellacheruvu, Wright et al. 2013), un repositorio online de proteínas identificadas que aparecen recurrentemente en los controles negativos de experimentos de purificación por afinidad acoplados a espectrometría de masas (AP-MS) y, por tanto, muy probablemente sean contaminantes. Se eliminaron aquellas proteínas que aparecieran en más del 60% de los controles negativos de los experimentos del CRAPome.

Las proteínas resultantes del filtrado se introdujeron en la base de datos STRING (http://string-db.org/) (Szklarczyk, Franceschini et al. 2011), que recoge la información disponible acerca las interacciones conocidas o probables entre las proteínas y las agrupa de acuerdo a distintos parámetros formando redes. Este software detecta, entre otras características, posibles clusters de proteínas pertenecientes a la misma ruta de señalización, o que realizan funciones similares. Además, se analizó el enriquecimiento en procesos biológicos del conjunto de proteínas mediante el software FunRich 3.0, una herramienta bioinformática que aporta información sobre el enriquecimiento funcional y el análisis de las redes de interacción entre las proteínas identificadas.

Nucleofecciones

Las CDs se transfectaron con siRNA frente a Cul-1 (ON-TARGET plus human CUL1 (8454) siRNA - SMART Pool de Dharmacon, Nº catálogo L-004086-00-0005) o siRNA control (ON-TARGET plus Non-targeting Pool, Dharmacon Nº

catálogo D-001810-10-05), mediante el método de nucleofección (Amaxa, Lonza Group Ltd Basilea, Suiza) utilizando un kit específico para células dendríticas (Nucleofector™ Kits for Human Dendritic Cells, Amaxa, Lonza Group Ltd) y siguiendo el protocolo recomendado por el fabricante. Brevemente, se utilizaron 2 µg de siRNA para nucleofectar $5x10^6$ de CDs maduras por condición. Se utilizó un aparato nucleofector (Amaxa, Lonza Group Ltd) utilizando el programa U2, que es específico para las CDs. Posteriormente, las células se cultivaron en un medio completo (+FBS) que incluye GM-CSF (1000U/ml) y IL-4 (1000U/ml) y se incubaron durante 48h a 37ºC y 5% de CO_2. Transcurrido este tiempo, las células se recolectaron y contaron mediante exclusión de la tinción con Azul Tripán, para excluir a las CDs muertas. Para comprobar que se había producido el silenciamiento del gen con el siRNA, se analizaron los niveles de la proteína de interés mediante Western blot, como se ha descrito previamente.

Ensayos de quimiotaxis

Los ensayos de quimiotaxis se realizaron en placas 6,5 mm con soportes permeables *Transwells* de 5 µm de diámetro de poro (Costar, Corning Incorporated, NY, EEUU). Se utilizaron 10^5 CDs disueltas en RPMI 0,1% BSA y se colocaron en la cámara superior permeable del pocillo. En el pocillo inferior, rellenado con RPMI 0,1% BSA, se añadió CCL21 (18 nM). Se reservaron alícuotas de las células como controles o inputs del número de células de partida. La placa se incubó durante 2h a 37º y 5% de CO_2. Tras este tiempo se recogió el medio del pocillo inferior y se contó el número de células que habían migrado a la

cámara inferior mediante citometría de flujo, estableciendo un contaje durante 60 segundos.

Ensayos de endocitosis

Para analizar la endocitosis en las CDs maduras se realizaron experimentos de captación de dextrano-FITC (1 mg/ml) y se analizó la incorporación de este reactivo mediante citometría de flujo. Para ello se utilizaron 3 x 10^5 CDs por condición que se resuspendieron en RPMI 10% FBS y HEPES (20 mM). Para el experimento es necesario un control de absorción pasiva de dextrano-FITC, que consiste en mantener a las células con dextrano-FITC a 4º durante todo el experimento. Las muestras donde se valoró la endocitosis activa se incubaron con dextrano-FITC a 37º y 5% de CO_2 el tiempo deseado, en presencia o ausencia de CCL21 (18 nM). Posteriormente las células se centrifugaron a 4ºC y se lavaron 5 veces con PBS 0,1% BSA frío. Por último, se resuspendieron en PBS frío para su análisis por citometría de flujo mediante un citómetro EPICS (Coulter Electronics) equipado con un láser de Argón que emite a una longitud de onda de 488 nm y recoge la fluorescencia del FITC con un filtro FL1 a 525 nm.

Análisis de la apoptosis

Para analizar la apoptosis de las CDs humanas se realizaron experimentos en los que se indujo la apoptosis mediante la privación de suero en células sin tratar o pre-tratadas con el inhibidor MLN4924, y que fueron mantenidas en presencia o ausencia de la quimioquina CCL21 (18 nM). Para ello se utilizó el mismo número

de células vivas, cuantificadas mediante la exclusión del colorante azul Tripán, mantenidas el tiempo indicado a 37º y 5% de CO_2 en RPMI 0,1% BSA.

Tras el experimento, se valoró la apoptosis de las CDs analizando la morfología de sus núcleos mediante tinción con Hoechst y microscopía de fluorescencia. Para ello, las CDs se adhirieron 45 min sobre cristales recubiertos de poli-L-ornitina, se fijaron con PFA 4% durante 15 min a temperatura ambiente. Las muestras se tiñeron con Hoechst 33258 en PBS con 0,1% BSA durante 5 min y se montaron con medio de montaje DAKO del mismo modo que las inmunofluorescencias.

Las preparaciones se analizaron usando un microscopio Axioplan Universal de Zeiss con una cámara CCD Digital Leica DFC 350 FX y un objetivo 63x de inmersión en aceite (Leica Microsystems, Mannheim). Se realizaron fotografías al azar de los núcleos de las CDs en distintos campos y se cuantificaron alrededor de 500 células de cada condición y donante, analizando el porcentaje de núcleos condensados (picnóticos) o fragmentados presentes en cada muestra.

Análisis de la citoarquitectura

Al igual que en las inmunofluorescencias, las CDs maduras se resuspendieron en RPMI 0,1% BSA a una concentración de 10^6 CDs/ml. A continuación, se sembraron $5x10^5$ de estas células en cristales de 10 mm de diámetro previamente cubiertos con poli-L-ornitina y se dejaron adherir durante 1h a 37ºC. Tras este tiempo las células se dejaron sin estimular o se estimularon con CCL21 (18 nM) durante 10 min. Posteriormente las células se fijaron con PFA (4%) (Santa Cruz

Biotechnology Inc., Santa Cruz, CA) durante 15 min, a temperatura ambiente. Tras un lavado con PBS, las células se permeabilizaron con Tritón X-100 (0,2% V/V) en PBS durante 5 min. Tras 3 lavados con PBS. Las muestras se incubaron con Faloidina-TRITC (Sigma-Aldrich) junto con el colorante Hoechst 33258 durante 1 h. Se hicieron 3 lavados con PBS 0,1% BSA una vez con agua antes de montar los cristales sobre portaobjetos con el medio de montaje Dako (Dakocytomation) y se analizaron con un Microscopio Láser Confocal espectral (CLSM) Leica TCS SP5. Las imágenes se analizaron con el software Image J, con el que se analizó la morfología de las CDs maduras tras ser estimuladas con CCL21, a través de la medición de su diámetro mayor. Las imágenes fueron preparadas con el software Adobe Photoshop CS.

Análisis estadístico

Los datos representados en las gráficas muestran la media ± el error estándar de la media de experimentos que se realizaron en, al menos, 3 donantes sanos independientes. La evaluación de la significancia estadística entre tratamientos se calculó utilizándose la prueba t de Student para muestras pareadas. En los casos en los que la desviación era muy elevada se empleó la prueba no paramétrica de Wilcoxon-Mann-Whitney. En todos los casos, se consideraron significativos los p-valores inferiores a 0,05. Como prueba complementaria también se analizaron los intervalos de confianza. "ns" indica diferencias no significativas entre dos tratamientos, mientras que "N" hace referencia al número de experimentos independientes realizados, es decir, número de donantes independientes analizados.

RESULTADOS

1. La estimulación de CCR7 en las células dendríticas induce nedilación de Cullin-1 mediada por Gαi.

En primer lugar, quisimos averiguar si la activación de CCR7 podía inducir nedilación en las células dendríticas (CDs). La nedilación se puede analizar mediante Western blot (WB) usando anticuerpos frente Nedd8.

En la figura 19 se puede observar que, la estimulación de CCR7 con CCL21 durante 5 min produjo un incremento significativo en la nedilación (Nedd8) (figura 19A) de una proteína de un peso molecular de ~85 KDa. Este peso molecular es similar al de la proteína Cul-1, la diana de nedilación mayoritaria y mejor caracterizada en diferentes tipos celulares, incluyendo las CDs (Mathewson, Toubai et al. 2013; Enchev, Schulman et al. 2015; Cheng, Hu et al. 2016). La unión de Nedd8 a Cul-1 provoca un cambio de movilidad electroforética de esta proteína ("shift") que permite observar una señal de doble banda en el WB frente a Cul-1, siendo la banda superior, Cul-1-nedilada (Cul-1^{Nedd8}) y la banda inferior, Cul-1 sin modificar. Tras someter la membrana anterior a un lavado (*stripping*, ver Material y Métodos), se reincubó con un anticuerpo frente a Cul-1 y se observó que la banda nedilada detectada previamente, correspondía con Cul-1^{Nedd8} (figura 19A).

Los experimentos de estimulación de las CDs con CCL21 a distintos tiempos confirmaron que se obtenía la máxima nedilación entre los 2 y los 10 min,

manteniéndose niveles altos de nedilación hasta, al menos, los 30 min después de la estimulación con CCL21 (figura 19B). Como el tiempo máximo de nedilación se alcanzó tras 5 min de estimulación CCL21, el resto de las estimulaciones se realizaron a este tiempo.

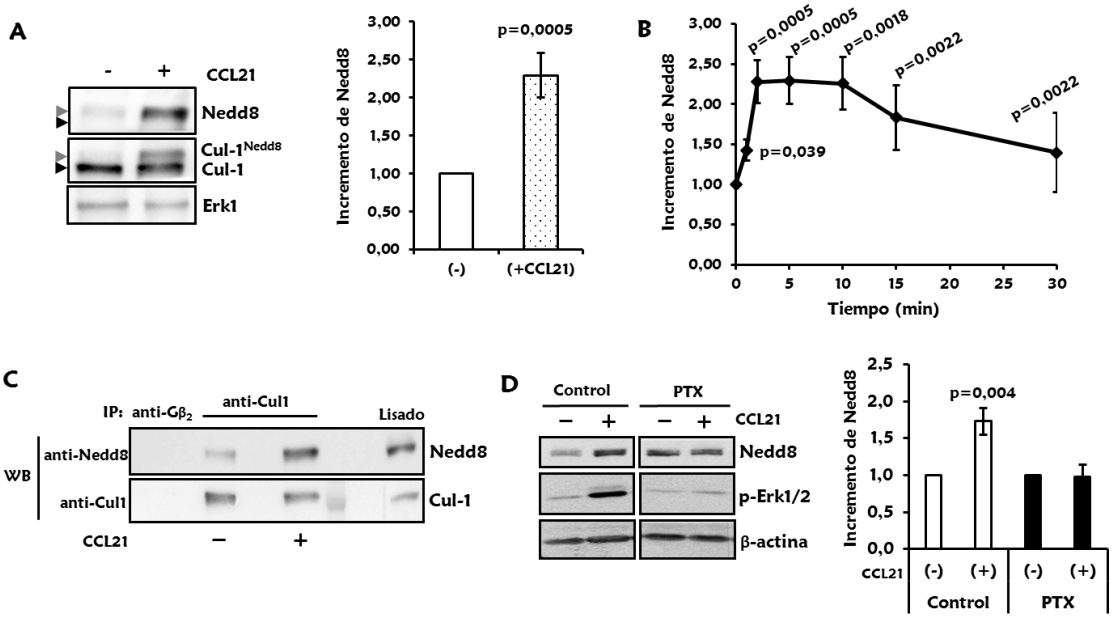

Figura 19. La estimulación CCR7 con CCL21 induce nedilación de Cul-1. (A) y (B) Las CDs (10^6celulas/ml) se resuspendieron en RPMI con 0,1% de BSA y se mantuvieron sin estimular (-) o se estimularon con CCL21 (18 nM), durante 5 min en (A) y los tiempos indicados en (B). Después las células se lisaron y analizaron mediante SDS-PAGE seguido de WB en los que se usaron anticuerpos frente a Nedd8. La banda de Nedd8 se cuantificó y se representa como incremento relativo respecto a las células sin estimular, a las que se asignó un valor arbitrario de 1. En (A) se muestra un WB representativo frente a los anticuerpos anti-Nedd8 y anti-Cul-1, empleándose Erk1 como control de carga. A continuación, se representa la media ± SEM (N=15). En la figura (B) se representa, al igual que en (A) la media ± SEM (N=6-15). **(C)** Las células (20-30 x 10^6 CDs) se trataron igual que en (A) con la diferencia de que, tras la estimulación con CCL21, las CDs se resuspendieron en buffer de lisis y, posteriormente, se inmunoprecipitó Cul-1. Las muestras se separaron mediante SDS-PAGE, y posteriormente se analizó mediante WB la presencia de Cul-1 y Nedd8. **(D)** Las células (10^6 CDs/ml) fueron tratadas como en (A), con la diferencia de que, previo a la estimulación con CCL21, las células fueron pre-tratadas con toxina pertúsica (PTX, 100ng/ml 3h). Posteriormente las CDs fueron estimuladas, lisadas, separadas mediante SDS-PAGE y analizadas mediante WB con anticuerpos frente a Nedd8 y p-ERK1/2. Se usó un anticuerpo frente β-actina para confirmar la igualdad de la carga. En el diagrama de barras se representa la media ± SEM (N=10).

Para confirmar que la proteína nedilada en respuesta a la estimulación de CCR7 es Cul-1, se realizó una inmunoprecipitación (IP) de Cul-1, seguida de un WB con un anticuerpo anti-Nedd8. Como se observa en la figura 19C, se produjo un aumento de la nedilación de Cul-1 tras la estimulación de las CDs con CCL21.

CCR7 induce señales intracelulares a través de las proteínas G heterotriméricas. Para analizar si tras la estimulación de CCR7, la familia $G_{\alpha i}$ media la nedilación observada, se trataron las CDs con la toxina pertúsica (PTX), un inhibidor selectivo de esta familia de proteínas G. Los resultados muestran que el tratamiento con PTX inhibió el efecto estimulante de CCR7 sobre la nedilación, lo que sugiere la participación de las proteínas $G_{\alpha i}$ (figura 19D) en este proceso.

2. Las funciones reguladas por CCR7 en las CDs no dependen de la nedilación

CCR7 regula, además de la quimiotaxis, varias funciones de las CDs, incluyendo la supervivencia, la velocidad migratoria, la endocitosis y los cambios en citoarquitectura (Yanagawa and Onoe 2002; Yanagawa and Onoe 2003; Sanchez-Sanchez, Riol-Blanco et al. 2004; Riol-Blanco, Sanchez-Sanchez et al. 2005; Torres-Bacete, Delgado-Martin et al. 2015). A continuación analizamos si la nedilación estaba implicada en la regulación de las funciones de CCR7 en las CDs. Para ello utilizamos un inhibidor farmacológico de la nedilación, MLN4924 (MLN), que actúa inhibiendo a la enzima NAE, que participa en el primero de los tres pasos de la transferencia de Nedd8 a las proteínas Cullin, o nedilación (Soucy, Smith et al. 2009).

2.1 La inhibición de la nedilación no afecta a la supervivencia inducida por CCR7

En numerosos tipos celulares, incluyendo leucocitos, la nedilación de las proteínas Cullin está implicada en la regulación la supervivencia celular (Li, Liu et al. 2013;

Wang, Luo et al. 2015; Cheng, Hu et al. 2016). Como CCR7 regula la supervivencia de las CDs (Sanchez-Sanchez, Riol-Blanco et al. 2004; Escribano, Delgado-Martin et al. 2009; Lopez-Cotarelo, Escribano-Diaz et al. 2015) analizamos si la nedilación de Cul-1 podía estar mediando estos efectos inductores de supervivencia. Para analizar la apoptosis las CDs se tiñeron con Hoechst (figura 20), un método que permite apreciar los núcleos condensados y/o fragmentados, típicos de las células apoptóticas, y compararlos con los de las células sanas, que son más grandes y mantienen su integridad (Sanchez-Sanchez, Riol-Blanco et al. 2004; Escribano, Delgado-Martin et al. 2009; Lopez-Cotarelo, Escribano-Diaz et al. 2015) (figura 20A). En la figura 20B(a) se puede observar que el cultivo de las CDs durante 48h en RPMI en ausencia de suero produjo un aumento en los niveles de apoptosis de las CDs, que se redujo significativamente cuando las células se mantuvieron en presencia CCL21, tal como se había reportado previamente (Sanchez-Sanchez, Riol-Blanco et al. 2004; Escribano, Delgado-Martin et al. 2009; Lopez-Cotarelo, Escribano-Diaz et al. 2015). Cuando se analizó la apoptosis de las CDs en las que se inhibió la nedilación mediante el tratamiento con MLN, se observó que, aunque la apoptosis aumentó tras el tratamiento, la estimulación de las CDs con CCL21 redujo el porcentaje de células apoptóticas de manera equivalente a la observada en el en el control sin MLN (figura 20B b). La figura 20C muestra que el tratamiento con MLN produjo un completo bloqueo de la nedilación. Los resultados indican que, aunque la inhibición de la nedilación induce apoptosis basal en las CDs, tal como se ha descrito previamente (Cheng, Hu et al. 2016), la estimulación de CCR7 induce supervivencia, aun cuando la nedilación se encuentra completamente inhibida.

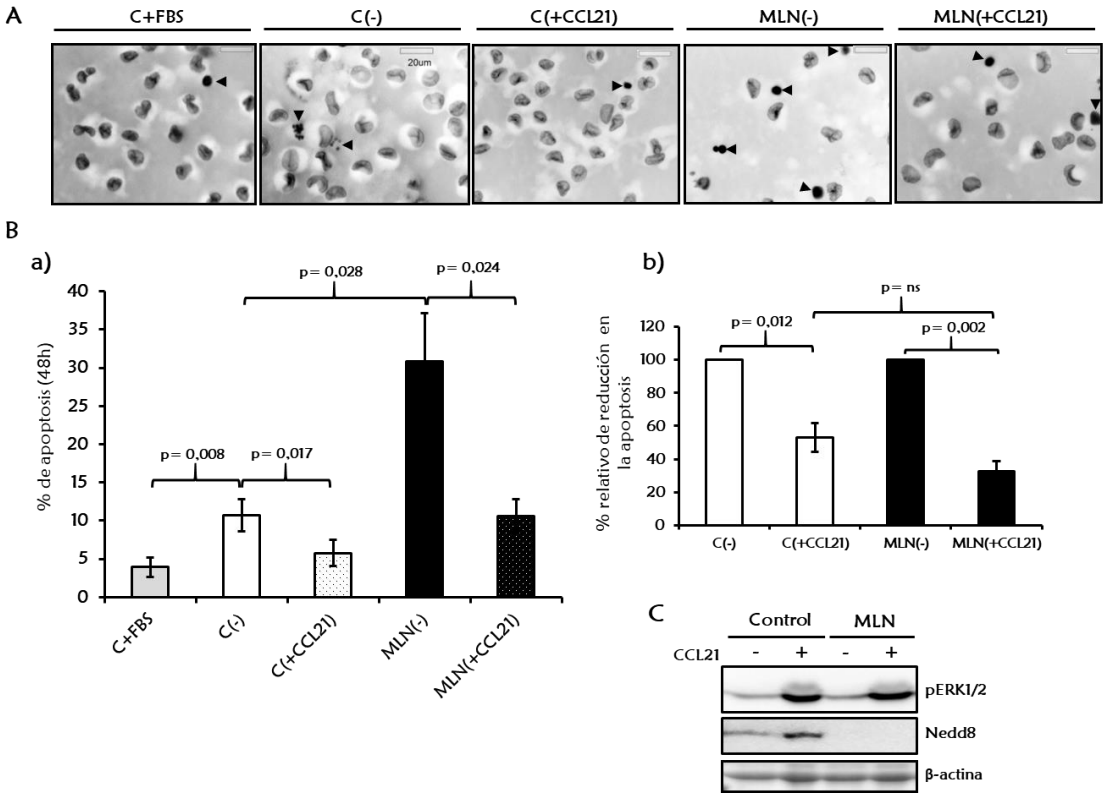

Figura 20. **La inhibición de la nedilación no afecta a la supervivencia inducida por CCR7.** Las CDs (10^6 celulas/ml) se resuspendieron en RPMI con 10% FBS (+FBS) o 0,1% de BSA (-) y se mantuvieron sin tratar (Control o C) o se trataron con MLN4924 (MLN, 0,5 μM 2h) tras lo cual las CDs se estimularon con CCL21 (18 nM) (+CCL21) y se mantuvieron en cultivo a 37ºC durante 48h, añadiéndose nuevamente CCL21 al medio cada 6h. Posteriormente las CDs se adhirieron durante 1 h en cristales previamente cubiertos con Poli-L-ornitina. Posteriormente las células se fijaron con PFA 4% y se tiñeron los núcleos con Hoechst33342. Las preparaciones se analizaron al microscopio y se fotografiaron. En **(A)** se muestra una fotografía representativa de cada tratamiento en la que las puntas de flecha señalan núcleos condensados o fragmentados que se corresponden con células apoptóticas. Los colores de las fotografías fueron invertidos porque así se puede apreciar mejor la condensación nuclear. **(B) a)** Se contaron alrededor de 500 células y se calculó el porcentaje de apoptosis (% medio ± SEM). **b)** Estos porcentajes se relativizaron respecto a las muestras no estimuladas para analizar el efecto de la quimioquina CCL21. **(C)** Una alícuota de estas muestras se analizó por SDS-PAGE seguido por WB con anticuerpos frente a Nedd8, pERK1/2 como control de estimulación de CCR7 y β-actina como control de carga. Se muestra que tras el tratamiento con MLN la nedilación (Nedd8) se encuentra totalmente inhibida (N=4).

La inhibición de la nedilación no afecta a la activación de la vía de NFkB inducida por CCR7.

Puesto que la activación de la vía de NFκB es uno de los mecanismos mediante los cuales CCR7 regula la supervivencia en las CDs (Sanchez-Sanchez, Riol-Blanco et al. 2004; Escribano, Delgado-Martin et al. 2009) y se ha descrito previamente que la nedilación de Cul-1 está implicada en la activación de NFκB en las CDs en

respuesta a LPS (Mathewson, Toubai et al. 2013), analizamos si la inhibición de la nedilación con MLN ejercía algún efecto sobre la activación de NFκB inducida por la estimulación de CCR7.

NFκB es un factor de transcripción que se encuentra en el citoplasma secuestrado por la proteína inhibitoria IκB. Sin embargo, diversos estímulos provocan la fosforilación de IκB, que induce su degradación, permitiendo que NFκB se trasloque al núcleo, donde regula la expresión de diversos genes promotores de supervivencia como Bcl_{xl}, un gen de la familia Bcl2 (Sanchez-Sanchez, Riol-Blanco et al. 2004; Escribano, Delgado-Martin et al. 2009). La medida de los niveles de IκB puede reflejar, de manera indirecta, el grado de activación de NFkB. Niveles elevados de IκB, indican que NFκB está inhibido, y, reducidos niveles de IκB implican que está activado. Para investigar si la nedilación juega un papel en la activación de NFkB, se analizó si la inhibición de la nedilación afecta la degradación de IκBα mediada por CCR7 y la traslocación de NFκB al núcleo de las CDs. Para ello se llevó a cabo el fraccionamiento de proteínas citoplásmicas y nucleares, en células pre-tratadas con MLN o sin pre-tratar, y estimuladas con CCL21 o sin estimular. Como control positivo se emplearon CDs tratadas con TNFα, un conocido activador de la ruta de NFκB (Sanchez-Sanchez, Riol-Blanco et al. 2004). Como se puede observar en la figura 21, la estimulación de CCR7 con CCL21, o con TNF-α, indujo la degradación de IκBα en el citoplasma de las CDs (figura 21A y 21B). La inhibición de la nedilación con MLN no afectó a la degradación de IκBα, lo que sugiere que la nedilación de Cul-1 no regula la degradación IκBα inducida por CCR7.

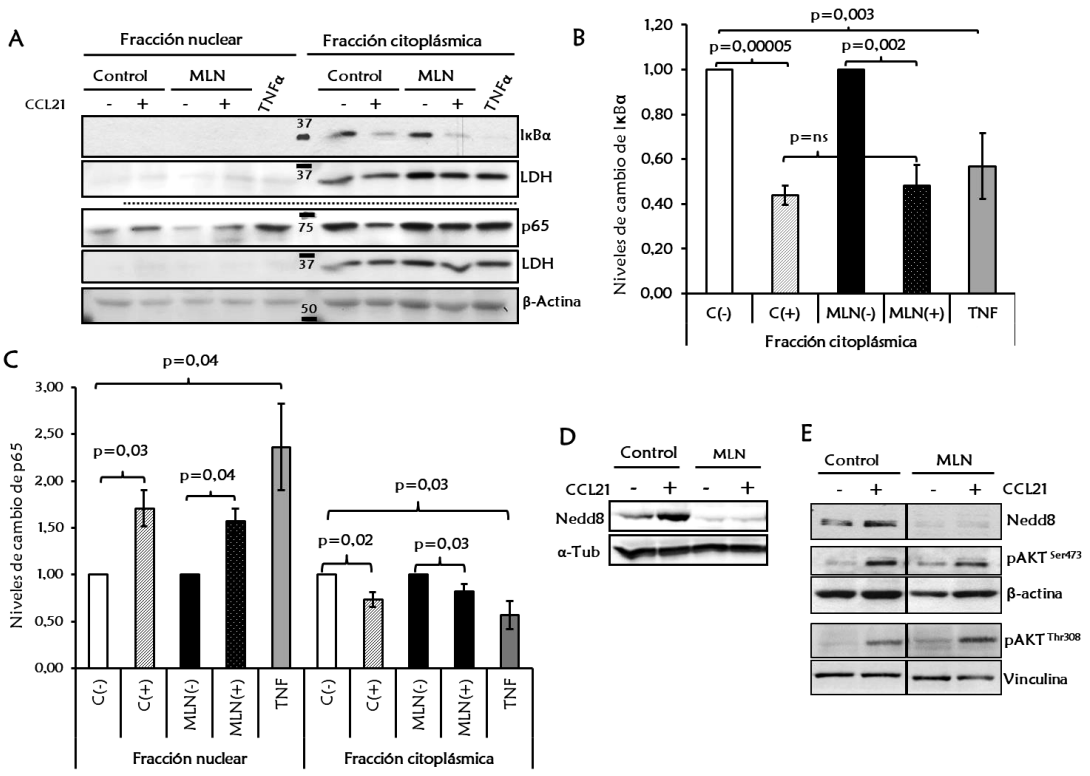

Figura 21. La inhibición de la nedilación no afecta a la activación de la vía de NFkB inducida por CCR7. Las CDs (5 x 10^6 células) se resuspendieron en RPMI con 0,1% de BSA y se mantuvieron sin tratar (Control o C) o se trataron con MLN4924 0,5 µM durante 2 h (MLN), posteriormente las células se mantuvieron sin estimular (-) o fueron estimuladas con CCL21 (18 nM) (+) o TNFα (100 ng/ml) durante 45 min. Transcurrido este tiempo, las células se lavaron en PBS frío y se llevó a cabo la extracción y fraccionamiento de proteínas citoplásmicas y nucleares. **(A)** Las muestras fueron analizadas mediante SDS-PAGE seguido de WB con anticuerpos frente a IκBα y p65. Como control de carga se analizaron los niveles β-Actina y de LDH. Este último se utilizó también como marcador de citoplasma. **(B)** Se representa la cuantificación de los niveles de proteína IκBα en la fracción citoplásmica estandarizados como incremento respecto a las muestras sin estimular [(-)] a las que se asigna un valor arbitrario de 1. **(C)** Se representa la cuantificación de los niveles de proteína p65 en la fracción citoplásmica y nuclear estandarizados como incremento respecto a las muestras sin estimular [(-)] a las que se asigna un valor arbitrario de 1. En las gráficas se representa la media ±SEM (N=6). **(D)** Se comprobó mediante WB que la nedilación se encontraba inhibida. **(E)** Las CDs (10^6 células/ml) se resuspendieron en RPMI con 0,1% de BSA y se mantuvieron sin tratar (Control o C) o se trataron con MLN4924 0,5 µM durante 2 h (MLN), posteriormente las células se mantuvieron sin estimular (-) o fueron estimuladas con CCL21 (18 nM) (+) durante 5 min. Transcurrido este tiempo, las muestras fueron lisadas y analizadas mediante SDS-PAGE seguido de WB con anticuerpos frente a Nedd8, p-AKT (Ser473) y p-AKT (Thr308). Se utilizaron β-Actina y vinculina como controles de carga (N=3).

Cuando se analizaron mediante WB los niveles de p65, una molécula de la familia NFκB, en el núcleo y el citoplasma (figura 21A y 21C), se observó que la estimulación de CCR7 con CCL21 o TNF-α indujo la traslocación de p65 al núcleo, como se sugiere por la observación de la caída en los niveles de p65 en el citoplasma y su aumento en el núcleo (figura 21C). Nuevamente, en las CDs pretratadas con MLN, CCL21 indujo los mismos efectos de caída del p65

citoplásmico y aumento del nuclear, indicando que la nedilación de Cul-1 parece no tener ningún efecto sobre la traslocación de p65 al núcleo tras la estimulación de CCR7. La figura 20D confirma que la nedilación se inhibió correctamente en el experimento de fraccionamiento. Los resultados obtenidos sobre NFkB concuerdan con lo observado en el caso de IκBα.

La ruta de AKT es la principal ruta inductora de la supervivencia activada por CCR7 en las CDs y es responsable de la activación de la ruta de NFκB (Sanchez-Sanchez, Riol-Blanco et al. 2004; Escribano, Delgado-Martin et al. 2009; Lopez-Cotarelo, Escribano-Diaz et al. 2015). En concordancia con estos resultados, se observó que MLN no afecta a la activación de AKT (fosforilación en serina 473 y en treonina 308) inducida por CCR7 (figura 21E).

2.2 La nedilación no regula la quimiotaxis inducida por CCR7

A continuación, estudiamos si la nedilación de Cul-1 podía estar involucrada en la regulación de la quimiotaxis, una función clave controlada por CCR7 en las CDs (Riol-Blanco, Sanchez-Sanchez et al. 2005). Para ello realizamos experimentos en el sistema *transwell*, que mide la migración de las células de un pocillo superior hacia un pocillo inferior, comunicados entre sí por poros. En los resultados de los experimentos en *transwell*, el signo (–) significa que no hay quimioquina y (+), que se incluye CCL21 en el medio (pocillo superior/pocillo inferior). De este modo, en la condición (-/-) no hay quimioquina en ningún compartimiento, de tal manera que las células que migran al pocillo inferior lo hacen de manera aleatoria. El punto (-/+) representa la migración quimiotáctica,

puesto que existe un gradiente de concentración de CCL21. Por último, el punto (+/+), en el que hay quimioquina en ambos compartimentos y, por tanto, no hay gradiente de concentración, representa una migración aleatoria, que en caso de ser mayor que (-/-) se debe a un incremento en la velocidad migratoria, puesto que la quimioquina está induciendo aceleración en las células.

En la figura 22A se puede observar un experimento en un *Transwell*, donde el establecimiento de un gradiente quimiotáctico de CCL21 (pocillo superior -/ pocillo inferior +) induce un importante aumento en la quimiotaxis de las CDs, como ya está descrito anteriormente (Riol-Blanco, Sanchez-Sanchez et al. 2005). Como se puede observar, el tratamiento con MLN no afecta a la quimiotaxis inducida por CCR7. Se comprobó que la nedilación de Cul-1 se bloquea completamente tras el tratamiento con MLN (figura 22B).

También puede apreciarse en las figuras 22C y 22D que, aunque el tratamiento con MLN aumenta basalmente la activación de ERK1/2, la principal proteína reguladora de la quimiotaxis en las CDs, su fosforilación dependiente de CCR7 no se vio afectada por el tratamiento con MLN.

En conjunto, estos resultados indican que el bloqueo de la nedilación no afecta ni a la activación de ERK1/2 ni a la quimiotaxis regulada por CCR7.

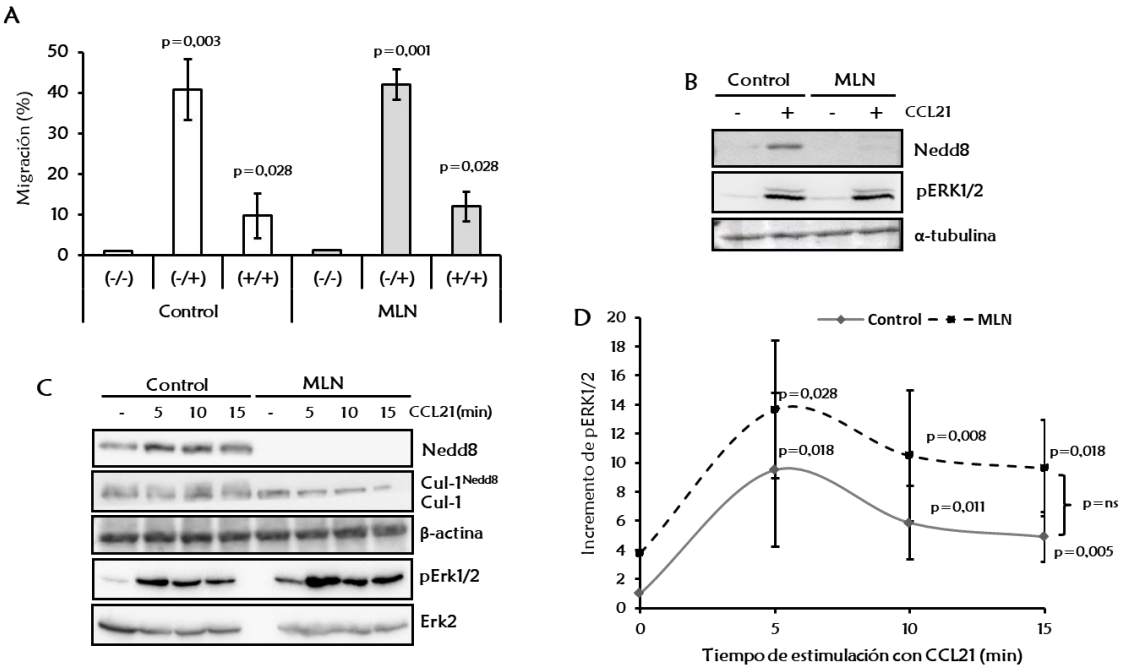

Figura 22. **La inhibición de la nedilación no afecta a la quimiotaxis inducida por CCR7. (A)** Las CDs (10^5 células/100 µL) disueltas en RPMI 0,1% BSA se mantuvieron sin tratar (Control) o se trataron con MLN4924 durante 2h (MLN, 0,5 µM). A continuación, las células se colocaron en el pocillo superior del Transwell. El pocillo inferior se rellenó con RPMI 0,1% BSA. El símbolo – representa ausencia de quimioquina y + significa que se añade CCL21 (18 nM) en el medio (pocillo superior/pocillo inferior). La placa se incubó durante 2 h a 37º. Tras este tiempo se contó el número de CDs que habían migrado a la cámara inferior y se normalizaron respecto a sus valores de partida. Los datos se representan como porcentaje de migración ± SEM (N=6). **(B)** Alícuotas tomadas del experimento (A) se analizaron mediante SDS-PAGE seguida de WB, con anticuerpos frente a Nedd8, pERK1/2 y α-tubulina, que fue usada como control de carga. **(C)** Las CDs (10^6 células/ml) se trataron igual que en (A) con MLN4924 (MLN), después las células se estimularon con CCL21 (18 nM) durante los tiempos indicados. Las muestras se lisaron y analizaron mediante SDS-PAGE seguida de WB con anticuerpos frente a Nedd8, Cul-1 y p-ERK1/2. ERK2 y β-actina fueron usados como controles de carga. Se cuantificaron los niveles de pERK1/2, representados en **(D)** y normalizados frente a las muestras control sin estimular (tiempo 0), a las que se asignó un valor arbitrario de 1 ± SEM (N=10).

A continuación se analizó si la nedilación juega algún papel en la regulación de otras funciones controladas por CCR7, como son la velocidad migratoria (Riol-Blanco, Sanchez-Sanchez et al. 2005), la endocitosis (Yanagawa and Onoe 2003), o la citoarquitectura celular (Yanagawa and Onoe 2002).

2.3 La nedilación no controla la velocidad migratoria inducida por CCR7

En el experimento de *transwell* mencionado anteriormente (figura 22A) se puede determinar, de manera indirecta, si se producen cambios en velocidad

migratoria de las CDs (Riol-Blanco, Sanchez-Sanchez et al. 2005). Como se explicó previamente, si se cuantifica el porcentaje de CDs que migran cuando se añade la quimioquina tanto en el pocillo superior e inferior del *transwell* (+/+) con respecto a aquel en donde no se pone quimioquinas (-/-) se evalúa la velocidad migratoria. Los datos obtenidos en las condiciones (-/-) y (+/+) de la figura 22A se representan en la figura 23.

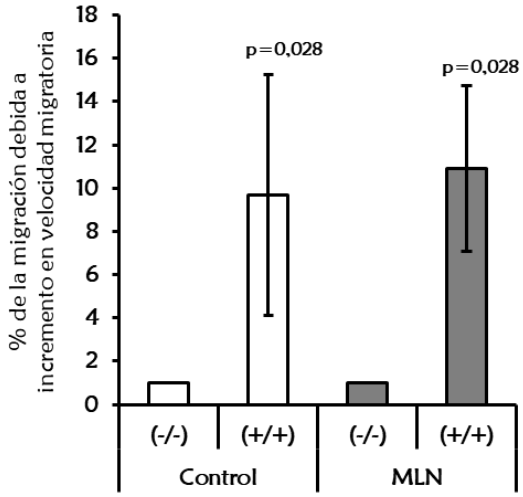

Figura 23. La inhibición de la nedilación no afecta a la velocidad migratoria inducida por CCR7. 10^5 CDs disueltas en RPMI 0,1% BSA se mantuvieron sin tratar (Control) o se trataron con MLN4924 durante 2 h (MLN, 0,5 µM). A continuación se colocaron en el pocillo superior permeable del Transwell. El pocillo inferior se rellenó con RPMI 0,1% BSA. (-/-) y (+/+) representan (pocillo superior/pocillo inferior), donde + significa que se añadió CCL21 (18 nM). La placa se incubó durante 2h a 37º y 5% de CO_2. Tras este tiempo se contó el número de células que habían migrado a la cámara inferior y se normalizaron respecto a sus valores de partida. Los datos se representan como porcentaje ± SEM (N=6).

Como se observa en esta figura, cuando se compara la migración de las CDs en los transwell (+/+) frente a (-/-), se observa que la estimulación de CCR7 indujo un aumento en la velocidad migratoria de las células, tal como hemos descrito previamente (Riol-Blanco, Sanchez-Sanchez et al. 2005; Torres-Bacete, Delgado-Martin et al. 2015). Si se analiza esta migración en las CDs control y las CDs tratadas con MLN, se observa que se produce un aumento similar en la velocidad migratoria en ambos casos (figura 23). Por tanto, los resultados indican que la nedilación no está implicada en la regulación de la velocidad migratoria inducida por la estimulación de CCR7 en las CDs.

2.4 La nedilación no regula la endocitosis dependiente de CCR7

CCR7 regula la endocitosis en las CDs (Yanagawa and Onoe 2003; Torres-Bacete, Delgado-Martin et al. 2015). En el siguiente experimento utilizamos dextrano-FITC para analizar la endocitosis en las CDs. Se considera endocitosis a aquella captación de dextrano que se produce cuando las células están a 37ºC, y ésta disminuye cuando disminuye la temperatura del medio, por lo que, la fluorescencia que observemos al mantener a las células 4ºC, se atribuye a la absorción pasiva de dextrano. Cuando las CDs mantenidas a 37º se estimularon con CCL21 durante 5 min, se observó un incremento en la cantidad de fluorescencia (figura 24A), esto es, en la endocitosis de dextrano-FITC, respecto a la fluorescencia de las células a 37ºC sin estimular, como ya está descrito previamente (Yanagawa and Onoe 2003; Torres-Bacete, Delgado-Martin et al. 2015). Este incremento refleja el aumento de la endocitosis dependiente de CCR7. Cuando analizamos la endocitosis a 37º (figura 24B), vemos que, tras la estimulación con CCL21, no se observaron diferencias entre las células tratadas con MLN y las células control. Por tanto, los datos indican que la endocitosis inducida por la activación de CCR7 no requiere de la nedilación. Se comprobó la inhibición de la nedilación mediante WB (figura 24C)

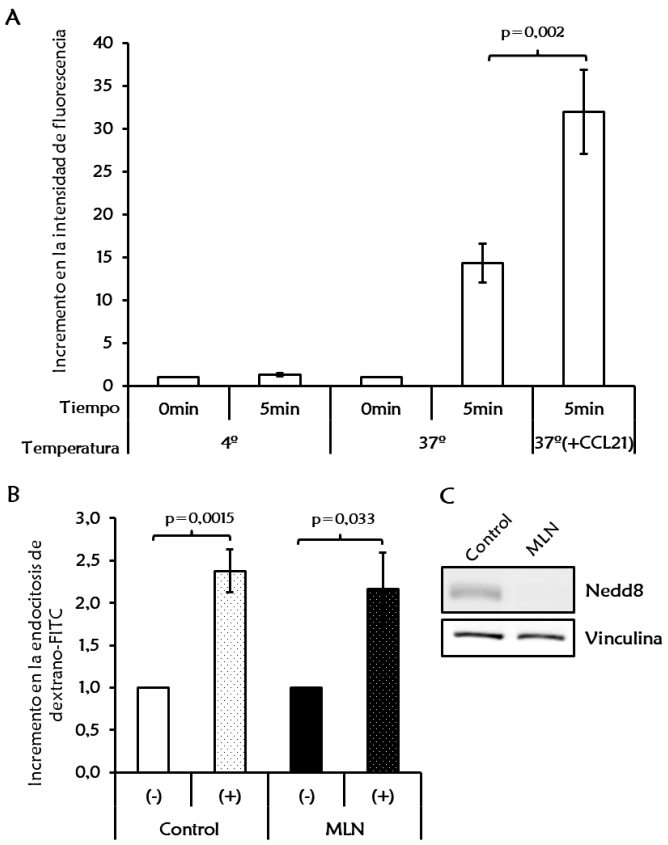

Figura 24. La nedilación no regula la endocitosis dependiente de CCR7. Se utilizaron 3 x 10^5 CDs resuspendidas en RPMI 10% FBS y HEPES 20 mM, que fueron incubadas con dextrano-FITC (1 mg/ml) durante los tiempos indicados. Como control de absorción pasiva de dextrano-FITC, las CDs se mantuvieron a 4º durante todo el experimento. Las muestras donde se valoró la endocitosis se incubaron con dextrano-FITC a 37º en el incubador en presencia o ausencia de CCL21 (18 nM). Posteriormente las CDs se lavaron varias veces en PBS 0,1% BSA y se re-suspendieron en PBS para su análisis por citometría de flujo. **(A)** muestra la intensidad de fluorescencia de las CDs en las distintas condiciones y permite distinguir la endocitosis de dextrano-FITC. En **(B)** se compara la endocitosis de dextrano-FITC en células sin tratar (Control) y pre-tratadas con MLN4924 (MLN, 0,5 µM 2 h) y estimuladas (+) o no (-) con CCL21. Los datos se representan como incremento en la intensidad de fluorescencia estandarizado frente a las células sin quimioquina, a las que se asigna un valor arbitrario de 1 ± SEM (N=7). **(C)** Se comprobó mediante WB que la nedilación estaba inhibida por el tratamiento con MLN.

2.5 La nedilación no está implicada en los cambios de morfología celular producidos por CCR7

Para que las CDs migren correctamente es necesario que experimenten cambios en citoarquitectura, particularmente, cambios en la configuración de la F-actina. En la figura 25A se muestran unas imágenes de microscopía de fluorescencia en las que se observa el citoesqueleto de actina de las CDs teñido con faloidina-TRITC. En esta figura se puede apreciar como al estimularse las células con CCL21 la morfología cambia de un fenotipo redondeado a un fenotipo expandido, que refleja el aplastamiento ("spreading") de las CDs sobre el sustrato (Yanagawa and Onoe 2002). Es posible cuantificar este fenómeno analizando la longitud del

diámetro mayor de estas células antes y después de la estimulación de las CDs (figura 25B). Como se observa en la gráfica, la longitud del diámetro mayor aumenta significativamente al exponer las células a la quimioquina CCL21. Además, tras la estimulación con CCL21, no se apreciaron diferencias en "spreading" entre las CDs no tratadas (Control) o tratadas con MLN4924 (MLN).

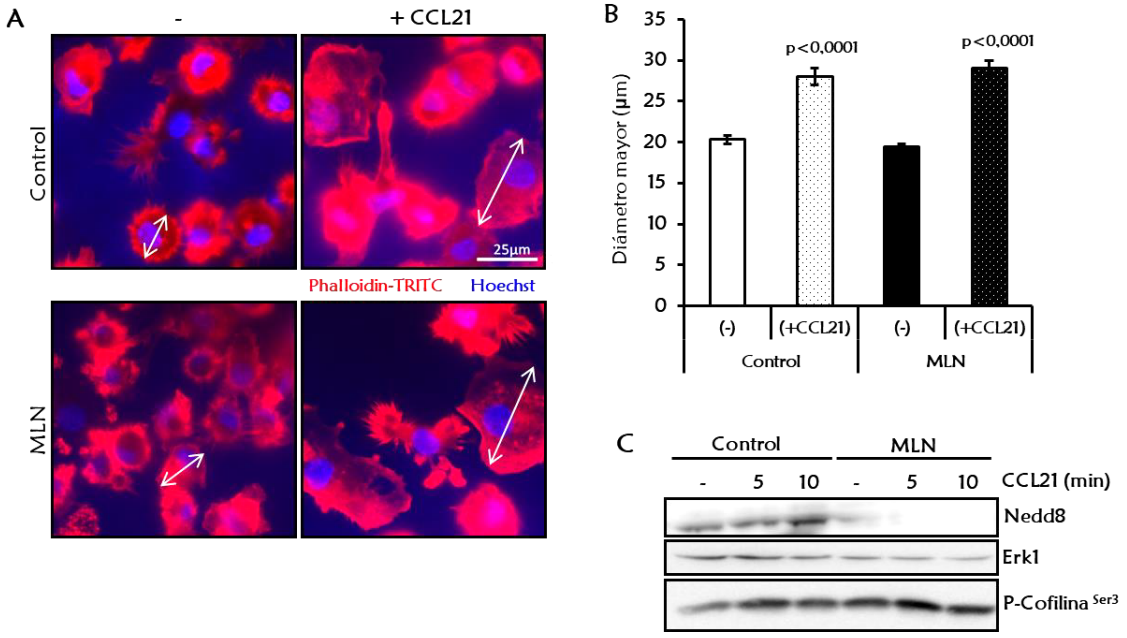

Figura 25. La nedilación no está implicada en los cambios de citoarquitectura inducidos por CCR7 en las CDs. Las CDs ($5x10^5$) se resuspendieron en RPMI 0,1% BSA y se trataron con MLN4924 (MLN, 0,5 µM) durante 2h o se mantuvieron sin tratar (Control). Posteriormente se sembraron en cristales recubiertos con poli-L-ornitina y se dejaron adherir durante 1 h a 37ºC, tras lo cual se estimularon con CCL21 (18 nM) durante 10 min, se fijaron con PFA 4% y se permeabilizaron con Tritón X-100 al 0,2% en PBS. Después, las muestras se tiñeron con Faloidina-TRITC (5 µg/ml) y Hoechst 33258 (10 µg/ml). **(A)** Las muestras se analizaron en el microscopio y se fotografiaron. **(B)** Las imágenes se analizaron para cuantificar la expansión de las CDs maduras (~120 CDs) tras ser estimuladas con CCL21, a través de la medición de su diámetro mayor, representado en valores absolutos (diámetro celular ± SEM). **(C)** Las CDs (10^6cel/ml) se resuspendieron en RPMI con 0,1% de BSA, se pretrataron con MLN como en (A) y se estimularon con CCL21 (18 nM) los tiempos indicados. Después las CDs se lisaron y analizaron mediante SDS-PAGE seguido de WB con anticuerpos frente a Nedd8, p-Cofilina-1 (Ser 3) o frente a Erk1, que fue usado como control de carga (N=3).

Una de las moléculas que regula la dinámica de la actina es la Cofilina-1. Tras la estimulación de CCR7, esta proteína se fosforila de manera inhibitoria en la serina 3. Si analizamos la fosforilación Cofilina-1 mediante WB (figura 25C), se observa que, tras la estimulación con CC21, dicha fosforilación no se encuentra

alterada por el pretratamiento con MLN. Por tanto, estos resultados indican que la nedilación no se requiere para que CCR7 induzca cambios en el citoesqueleto en las CDs.

3. Nedd8 se concentra en el núcleo de las células dendríticas

Los resultados negativos mencionados en el apartado 2, nos hicieron cuestionarnos acerca de la posible localización de la nedilación inducida por CCR7, pues, algunos de los mediadores activados por CCR7 actúan en el citoplasma de las CDs, pero otros ejercen su acción en el núcleo. En este sentido, llevamos a cabo experimentos de fraccionamiento de proteínas citoplásmicas y nucleares. En estos experimentos observamos, por WB, que Nedd8 o Cul-1 nedilada (Cul-1^{Nedd8}) se concentraba en el núcleo de las CDs (figuras 26A y 26B). Además, la estimulación de CCR7 indujo nedilación de Cul-1 en el núcleo de las células, que se vio bloqueada por el tratamiento con MLN. Sin embargo, los niveles de Cul-1 sin modificar son similares en el núcleo y el citoplasma de las CDs, aunque se vio una disminución de Cul-1 en el citoplasma de las células control tras la estimulación con CCL21. Los experimentos de inmunofluorescencia (IF), con anticuerpos frente a Nedd8 y Cul-1, mostraron un resultado similar (figura 26C), esto es, Cul-1 total se encuentra más homogéneamente distribuido por toda la célula, mientras que Nedd8 se concentra en el núcleo de las CDs.

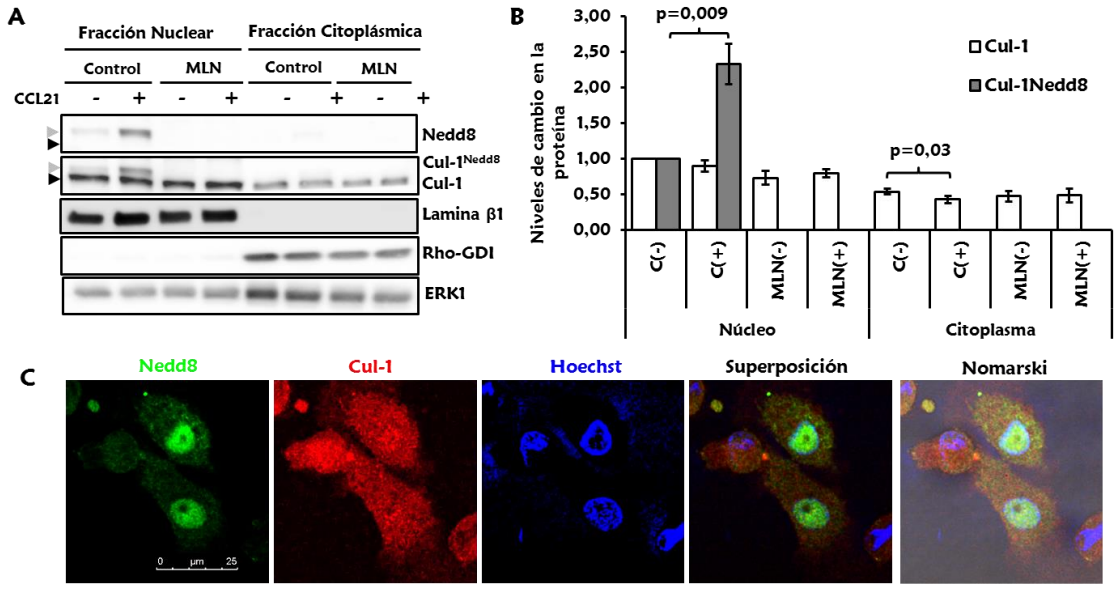

Figura 26. Nedd8 se concentra en el núcleo de las células dendríticas. Las CDs (5 x 10^6cel/ml) se resuspendieron en RPMI con 0,1% de BSA y se mantuvieron sin tratar (Control) o se trataron con MLN4924 durante 2 h (MLN). Posteriormente, las células fueron estimuladas con CCL21 (18 nM) (+) durante 5 min. Transcurrido este tiempo, las CDs se lavaron en PBS frío y se llevó a cabo la extracción y el fraccionamiento de proteínas citoplásmicas y nucleares. **(A)** Las muestras fueron analizadas mediante SDS-PAGE seguido de WB con anticuerpos frente a Nedd8, Cul-1 y Erk1, que fue usado como control de carga. Se emplearon anticuerpos frente a la proteína nuclear Lamina β1 y la proteína citoplasmática Rho-GDI, que fueron usadas como como controles de posible contaminación entre fracciones nuclear y citoplasmática **(B)** Se representa la cuantificación de los niveles relativos de Cul-1^{Nedd8} y Cul-1 en las CDs del apartado A, estandarizada respecto a la fracción nuclear (C-), a la que se asigna un valor arbitrario de 1 ± SEM (N=5). **(C)** 5 x 10^4 CDs resuspendidas en RPMI con 0,1% BSA dejaron adherir sobre cristales recubiertos de poli-L-ornitina. Las células se estimularon con CCL21 (18 nM) durante 5 min y luego se fijaron con PFA 4%, se permeabilizaron con metanol frío y se tiñeron con anticuerpos específicos frente a Nedd8 y Cul-1. Los núcleos se tiñeron con Hoechst 33342. Las preparaciones fueron montadas y analizadas mediante microscopía confocal. Se muestra una fotografía representativa de una sección confocal (N=4).

4. Cul-1^{Nedd8} forma parte de un complejo SCF en el núcleo.

Los resultados negativos obtenidos con relación a los efectos de la inhibición de la nedilación sobre las funciones descritas reguladas por CCR7 y el descubrimiento de que Nedd8 se encontraba fundamentalmente en el núcleo de las CDs nos llevaron a plantearnos si Cul-1^{Nedd8} formaba parte del complejo E3 ligasa SCF también en el núcleo o, por el contrario, podía estar ejerciendo una función independiente de SCF.

Como se ha comentado en la introducción, el complejo SCF consta de 3 proteínas invariables: Rbx1, Skp1 y Cul-1. En los siguientes experimentos nos centramos en el estudio de la localización de Rbx1 y Skp1 en las CDs, así como en el análisis de su interacción con Cul-1. Para ello, se realizaron experimentos de inmunofluorescencia (IF), ensayo de ligación por proximidad (Proximity ligation Assay, PLA) e IP.

En primer lugar, los experimentos de IF frente a Rbx1 y Skp1 (figura 27A), sugieren que ambos tienen una distribución similar a la de Nedd8, pues se encuentran concentrados en el núcleo de las CDs, aunque de manera menos acusada que Nedd8.

Una vez comprobado que Rbx1 y Skp1 están presentes también en el núcleo de las CDs, usamos la técnica PLA para analizar si ambas proteínas están lo suficientemente cercanas a Cul-1 (<40nm) como para sugerir que están interaccionando y formando un complejo. La técnica PLA se ha empleado previamente para estudiar la presencia de complejos moleculares analizando la cercanía entre sus componentes (Soderberg, Gullberg et al. 2006).

En la figura 27B puede observarse mediante microscopía de fluorescencia una fotografía de una sección confocal de un PLA entre Cul-1 y Rbx1 donde se aprecian puntos fluorescentes tanto en núcleo como en citoplasma. Del mismo modo se observa un PLA entre Cul-1 y Skp1 donde se aprecian puntos fluorescentes en el núcleo de las CDs.

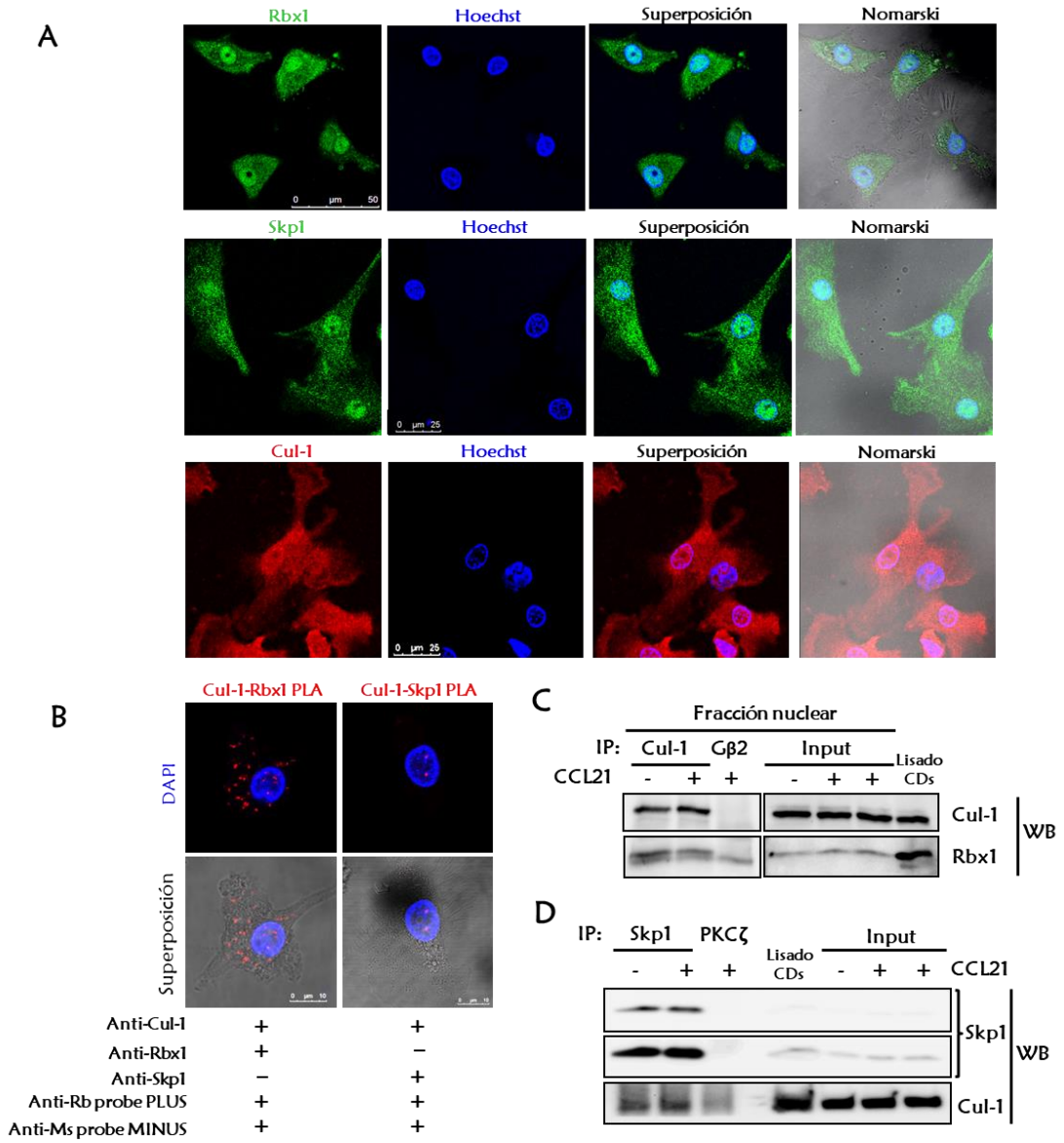

Figura 27. Cul-1^{Nedd8} forma parte del complejo SCF en el núcleo. (A) A las CDs resuspendidas en RPMI con 0,1% BSA (5 x 10^4) se les permitió adherirse sobre cristales recubiertos de poli-L-ornitina, se estimularon con CCL21 (18 nM) durante 5 min y se fijaron con PFA 4%, después fueron permeabilizadas con metanol frío y teñidas con anticuerpos específicos frente a Rbx1, Skp1 o Cul-1. Los núcleos se tiñeron con Hoechst 33342. Las preparaciones fueron montadas y analizadas mediante microscopía confocal. Se muestra una fotografía representativa de una sección confocal (N=3). **(B)** Las CDs fueron tratadas igual que en (A) hasta la incubación de las mismas con los anticuerpos primarios Cul-1 y Rbx1 o Cul-1 y Skp1, tras lo cual se llevó a cabo un PLA (ver Materiales y Métodos) con las sondas arriba mencionadas. Las muestras fueron analizadas por microscopía confocal y se muestra una fotografía representativa de una sección confocal. Los puntos fluorescentes rojos se representan una señal positiva del PLA (N=3). **(C)** Las CDs (20-30 x 10^6 CDs) se resuspendieron en RPMI con 0,1% de BSA y se mantuvieron sin estimular (-) o estimuladas con CCL21 (18 nM) durante 5 min (+) a 37º. Después, las CDs se lavaron en PBS frío y se llevó a cabo la extracción de proteínas citoplásmicas y la lisis de los núcleos en buffer de IP. Posteriormente se llevó a cabo la IP nuclear de Cul-1. Se tomaron alícuotas de las muestras antes de la IP para analizar la carga. Las muestras se analizaron mediante WB usando anticuerpos frente a Cul-1 y Rbx1. **(D)** Las CDs humanas maduras (20-30 x 10^6 CDs) se resuspendieron en RPMI con 0,1% de BSA y se mantuvieron sin estimular (-) o estimuladas con CCL21 (18 nM) durante 5 min (+) a 37º. Después, las células se lisaron resuspendiéndolas en buffer de lisis y se llevó a cabo la IP de Skp1. Las muestras fueron analizadas mediante SDS-PAGE y WB con anticuerpos frente a Cul-1 y Skp1.

Para confirmar que existe interacción entre Cul-1, Skp1 y Rbx se realizaron experimentos de IP. En la figura 27C se puede observar un experimento de IP de Cul-1 nuclear. Como se observa en la figura, el anticuerpo inmunoprecipitó a Cul-1 adecuadamente y se observó la co-inmunoprecipitación de Rbx1, sugiriendo que estas dos proteínas interaccionan entre sí.

Por otro lado, se realizó una IP con un anticuerpo frente a Skp1 (figura 27D). Observamos que Skp1 se inmunoprecipitó correctamente y que co-inmunoprecipitó con Cul-1.

Estos experimentos sugieren que los miembros del complejo SCF, Rbx1 y Skp1 se localizan en el núcleo y además que se encuentran interaccionando con Cul-1. Por tanto, Cul-1^{nedd8} parece estar formando el complejo E3 ligasa SCF en el núcleo de las CDs.

5. CCR7 induce nedilación/activación de SCF que estimula la ubiquitinación de proteínas en el núcleo de las CDs.

5.1 CCR7 estimula la poliubiquitinación de tipo K48 en el núcleo de las CDs a través de la nedilación.

Una vez confirmado que Cul-1 se encontraba nedilado y formando parte del complejo E3 ligasa SCF en el núcleo de las CDs, en los siguientes experimentos estudiamos si el complejo SCF se encontraba ubiquitinando proteínas nucleares. Como se ha mencionado anteriormente, existen distintos tipos de ubiquitinación dependiendo del residuo conservado de la ubiquitina (Ub) que media el enlace

con la siguiente molécula de ubiquitina en la cadena (McDowell and Philpott 2013). Se ha establecido que los distintos tipos de enlaces entre Ub's pueden determinar un destino diferente para la proteína marcada. El marcaje de una proteína por una cadena de al menos 4 Ub's unidas entre sí a través de la lisina 48 (K48) induce la degradación de dicha proteína por el proteasoma 26S (Thrower, Hoffman et al. 2000). Puesto que el complejo SCF participa en la ubiquitinación de proteínas que son posteriormente degradadas por el proteasoma, analizamos si la estimulación con CCR7 podía estar induciendo poliubiquitinación de tipo K48 y si este fenómeno podía estar mediado por la nedilación de Cul-1 y la consiguiente activación de SCF. Para ello se utilizó un anticuerpo que reconoce específicamente las moléculas de Ub unidas entre sí a través de la K48 (Poli-Ub-K48). En la figura 28 se representa un fraccionamiento de proteínas citoplásmicas y nucleares de células control y tratadas con MLN y estimuladas (+) o no (-) durante 5 min con CCL21. Cuando analizamos los resultados mediante WB, como se puede observar en la figura, la estimulación de las CDs con CCL21 induce un aumento en la nedilación de Cul-1 en el núcleo de las CDs y el tratamiento con MLN inhibe por completo la nedilación de Cul-1. Cuando analizamos las proteínas que se encuentran poliubiquitinadas con cadenas de ≥5 unidades de Ub (≥50 KDa) con uniones tipo K48, además de que se observa que existe una mayor cantidad de dichas proteínas en el núcleo de las CDs respecto al citoplasma, la estimulación con CCL21 induce un aumento significativo en los niveles de Poli-Ub-K48 en el núcleo de estas células. Además, dicho fenómeno se previene cuando las células son pre-tratadas con MLN,

sugiriendo que se requiere nedilación para que se produzca la ubiquitinación observada (figura 28A y 28B).

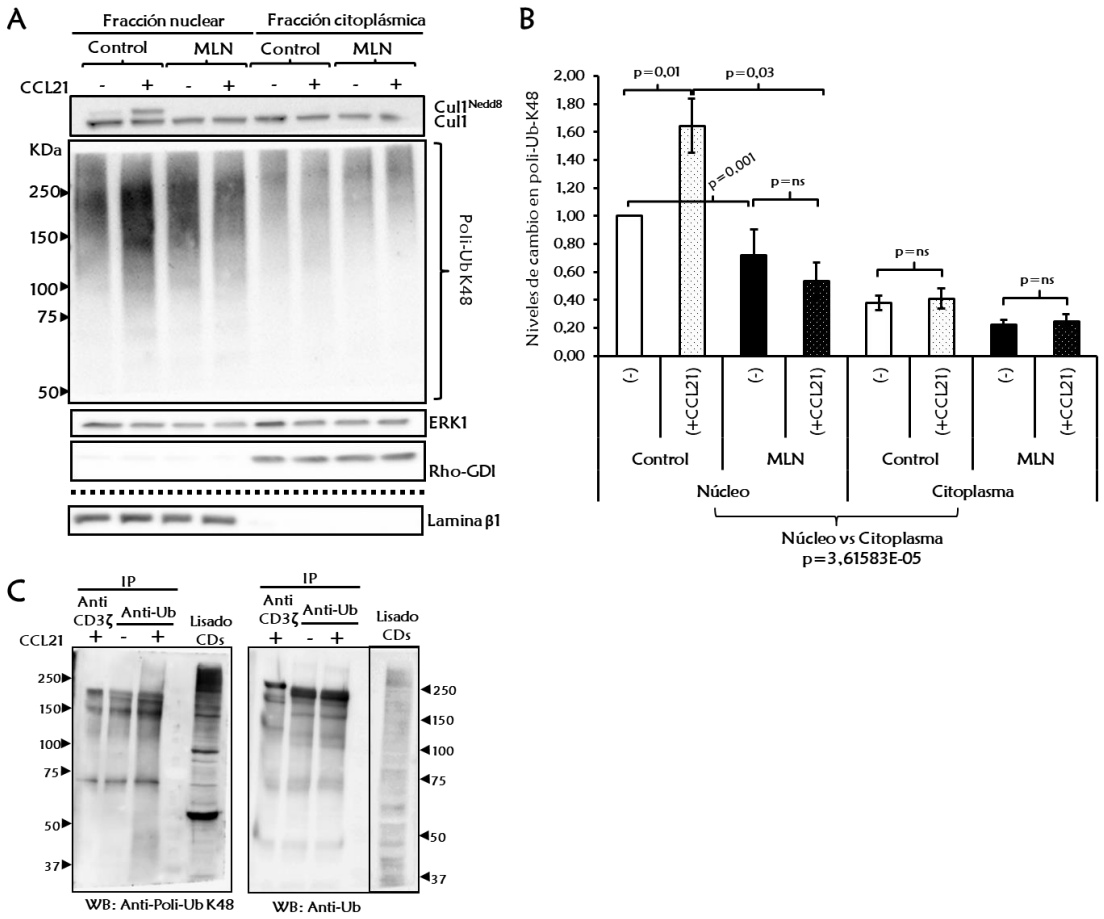

Figura 28. CCR7 estimula la poliubiquitinación de proteínas tipo K48 en el núcleo de las CDs a través de la nedilación. Las CDs (5 x 10^6cel/ml) se resuspendieron en RPMI con 0,1% de BSA y se mantuvieron sin tratar (Control) o se trataron con MLN4924 durante 2h (MLN, 0,5 μM), posteriormente las células fueron estimuladas con CCL21 (18 nM) (+) durante 5 min. Transcurrido este tiempo, las células se lavaron en PBS frío y se llevó a cabo la extracción y fraccionamiento de proteínas citoplásmicas y nucleares. **(A)** Las muestras fueron analizadas mediante SDS-PAGE seguido de WB con anticuerpos frente a Cul-1, Poli-Ub-K48, Erk1 como control de carga y Lamina β1 y Rho-GDI como controles de carga y de contaminación entre fracciones. **(B)** Se representa la cuantificación de los niveles de poliubiquitinación en las CDs del apartado A, estandarizados respecto a la fracción nuclear sin estimular, a la que se asigna un valor arbitrario de 1±SEM (N=8). **(C)** Las CDs humanas maduras (20-30 x 10^6 CDs) se resuspendieron en RPMI con 0,1% de BSA y se mantuvieron sin estimular (-) o estimuladas con CCL21 (18 nM) durante 5 min (+) a 37º. Después, las células se lisaron resuspendiéndolas en buffer de lisis y se llevó a cabo la IP de la ubiquitina total (Ub). Las muestras fueron analizadas mediante SDS-PAGE y WB con anticuerpos frente a la Poli-Ub K48 y la ubiquitina total (Ub).

A continuación, estudiamos si CCR7 producía un aumento en la ubiquitinación de manera general, o exclusivamente sobre la poliubiquitinación de tipo K48. Para ello, inmunoprecipitamos las proteínas ubiquitinadas con un anticuerpo que

reconoce tanto cadenas de Ub de los distintos tipos y tamaños, como ubiquitina libre. En la figura 28C observamos que se inmunoprecipitó la misma cantidad de Ub total en células estimuladas y sin estimular, pero dicho inmunoprecipitado se vio enriquecido en cadenas de Poli-Ub-K48 en células estimuladas con CCL21. Estos resultados indican que CCR7 induce un aumento en la Poli-Ub-K48 en el núcleo de las CDs y que dicho fenómeno requiere de la nedilación.

También analizamos mediante IF doble, si Nedd8 y Ubiquitina (Ub) co-localizan en el núcleo de las CDs, así como el efecto del tratamiento de estas células con MLN. Como se observa en la figura 29A, la Ub tiene una distribución mayormente nuclear en las CDs, coincidiendo con la distribución de Nedd8. Sin embargo, cuando las CDs son pre-tratadas con MLN, se observa una disminución de los niveles de Nedd8 en el núcleo, que va acompañada también de una disminución de los niveles de Ub nucleares. Estos resultados sugieren nuevamente que la nedilación es necesaria para que se produzca la ubiquitinación de las proteínas nucleares.

Para asegurarnos de que Nedd8 y la Ubiquitina se encontraban lo suficientemente cerca como para que SCF activo esté interaccionando con la ubiquitina, transfiriéndola a la proteína diana, se realizaron experimentos de PLA entre ambas proteínas en células pre-tratadas o no pre-tratadas con MLN y estimuladas con CCL21 (figura 29B). Después se cuantificó el número de puntos fluorescentes en núcleo y citoplasma de cada célula (figura 29C) y se observó que la señal fluorescente era mayormente nuclear, pues se observaron aproximadamente el doble de puntos fluorescentes PLA en el núcleo respecto al

citoplasma. Además, cuando las CDs, fueron tratadas con MLN, dichos puntos fluorescentes se redujeron drásticamente, hasta aproximadamente la mitad, coincidiendo con los resultados observados en la IF. Estos resultados indican que la cercanía de Nedd8 y Ub en el núcleo de las CDs depende de la existencia de nedilación.

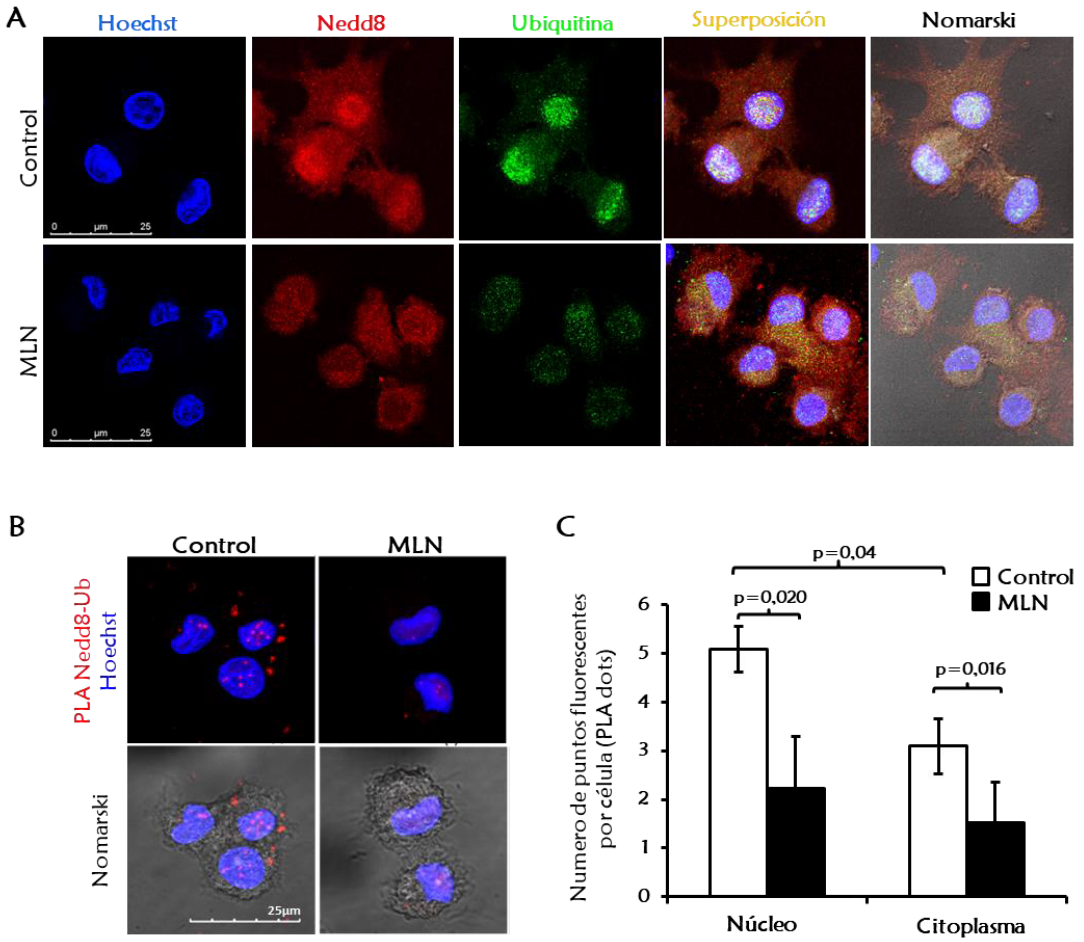

Figura 29. La ubiquitinación nuclear depende de nedilación en las CDs. (A) 5 x 10^4 CDs resuspendidas en RPMI con 0,1% BSA fueron tratadas con MLN4924 (0,5 µM 2h) y adheridas sobre cristales recubiertos de poli-L-ornitina. Las células fueron estimuladas con CCL21 (18 nM) durante 5 min, fijadas con PFA 4%, permeabilizadas con metanol frío y teñidas con anticuerpos específicos frente a Ubiquitina (Ub) y Nedd8. Los núcleos se tiñeron con Hoechst 33342. Las preparaciones fueron montadas y analizadas por microscopía confocal. Se muestra una fotografía representativa de una sección confocal (N=5). **(B)** Las CDs fueron tratadas igual que en (A) hasta la incubación de las mismas con los anticuerpos primarios Ub y Nedd8, tras lo cual se llevó a cabo un PLA (descrito en materiales y métodos). Las muestras fueron analizadas por microscopía confocal y se muestra una fotografía representativa de una sección confocal. Los puntos fluorescentes rojos se representan una señal positiva del PLA. **(C)** Las muestras del apartado (B) fueron analizadas y se cuantificó el número de puntos fluorescentes por célula en el núcleo y el citoplasma de las CDs, que se representa en valores absolutos ± SEM (N=4).

Tras la estimulación de las CDs con CCL21 no se observaron diferencias en los niveles de Ub mediante IF, en concordancia con los resultados de la IP de la figura 28C. Tampoco se observaron cambios significativos en cuanto al número de puntos fluorescentes en los experimentos de PLA (no mostrado).

5.2 La nedilación específica de Cul-1 regula la ubiquitinación inducida por CCR7 en CDs.

Puesto que MLN es un inhibidor del proceso de nedilación y hay otras proteínas que se nedilan además de Cul-1, quisimos confirmar nuestros resultados mediante la reducción de la expresión de Cul-1 con un siRNA. Para ello las CDs se nucleofectaron con un pool de siRNAs frente a Cul-1 y se analizaron los niveles de Cul-1 48h más tarde mediante WB e IF. Posteriormente se analizaron los niveles de ubiquitinación en respuesta a CCL21 en células silenciadas y control por ambas técnicas.

La figura 30A muestra 3 donantes sometidos a un silenciamiento de Cul-1. Como se puede observar, la reducción en los niveles de Cul-1 varió de un donante a otro (figura 30A a). La disminución en los niveles de Cul-1 se observó también mediante IF (figura 30A b).

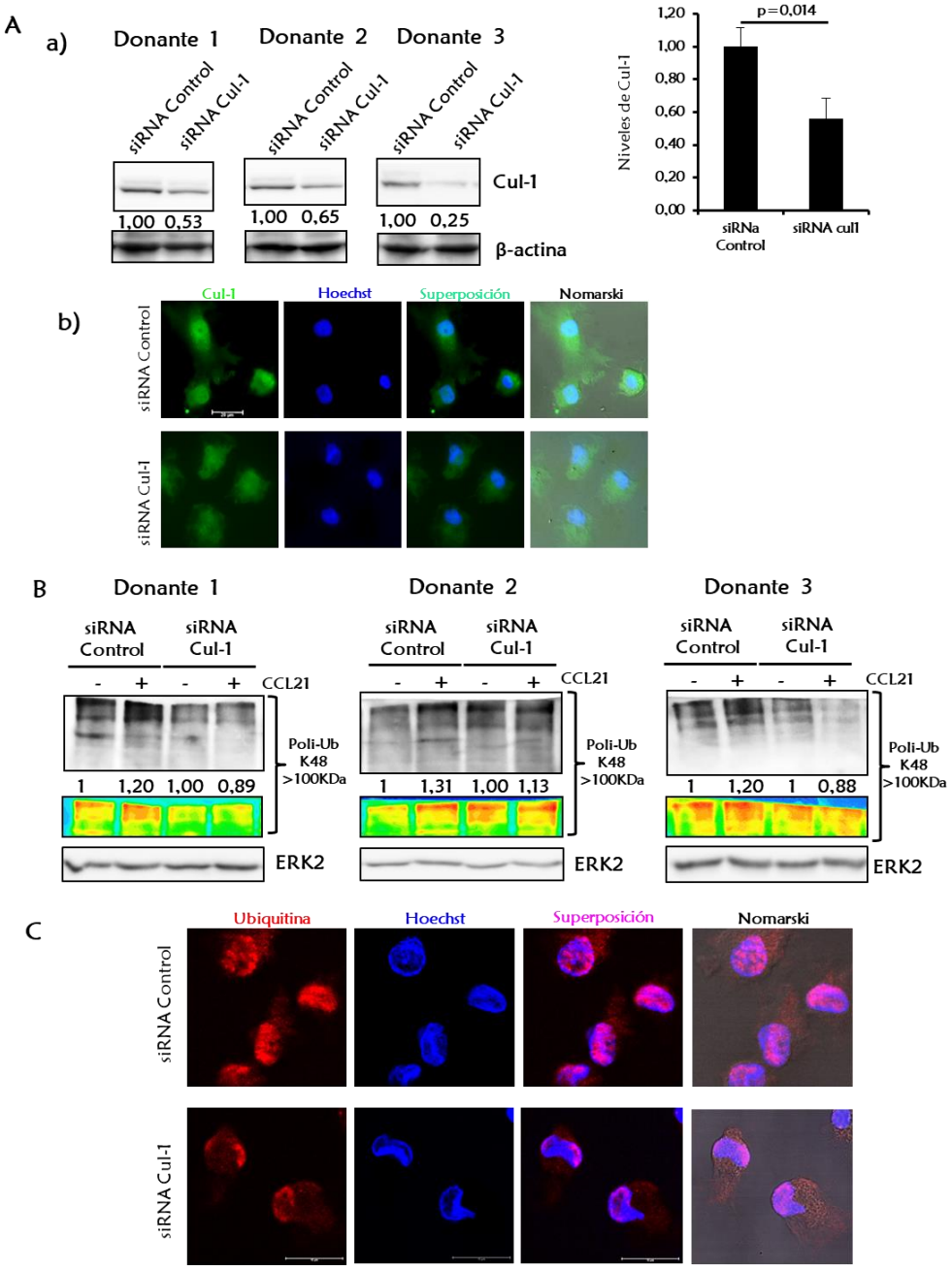

Figura 30. La reducción de los niveles de Cul-1 con un siRNA tiene los mismos efectos que MLN sobre la ubiquitinación. 5x10^6 CDs se nucleofectaron con un siRNA frente a Cul-1 (ver material y métodos). **(A)** 48h después de la nucleofección las CDs se resuspendieron en RPMI 0,1% BSA (10^6 cel/ml). **(a)** Las células del apartado (A) se lisaron y analizaron mediante SDS-PAGE seguido de WB con anticuerpos frente a Cul-1 y β-actina como control de carga. Se muestran 3 experimentos independientes en los cuales la reducción de Cul-1 fue diferente. **(b)** 5x10^5 CDs del apartado (A) se adhirieron sobre cristales recubiertos de poli-L-ornitina, después se fueron fijaron con PFA 4%, se permeabilizaron con metanol frío y se tiñeron con un anticuerpo específico frente a Cul-1. Los núcleos se tiñeron con Hoechst 33342. **(B)** 10x10^5 células del apartado A se estimularon con CCL21 (18 nM) durante 5 min a 37ºC. Después las CDs se lisaron y analizaron mediante SDS-PAGE seguido de WB con anticuerpos frente a Ub-k48 y Erk2, como control de carga. Las muestras aparecen cuantificadas y estandarizadas respecto a las muestras sin estimular, a las que se asignó un valor arbitrario de 1. **(C)** 5x10^5 CDs del apartado (A) se adhirieron sobre cristales recubiertos de poli-L-ornitina, después se fijaron con PFA 4%, se permeabilizaron con metanol frío y se tiñeron con un anticuerpo específico frente ubiquitina (Ub). Los núcleos se tiñeron con Hoechst 33342. Las preparaciones del apartado A(b) y C fueron montadas y analizadas por microscopía confocal. Se muestra una fotografía representativa de una sección confocal (N=3).

Al analizarse los niveles de Poli-Ub-K48, se puede apreciar que la reducción de Cul-1 produjo una reducción en el efecto estimulador de CCR7 sobre la Poli-Ub-K48 (figura 30B), de manera similar a lo observado en los estudios con MLN.

Por último, al analizarse la ubiquitina mediante IF también se observó un resultado equivalente al obtenido con MLN, la reducción en los niveles de Cul-1 por efecto del siRNA produjo una disminución de los niveles de ubiquitina en el núcleo de las CDs (figura 30C).

Los resultados mostrados, sugieren que la nedilación de Cul-1 regula la ubiquitinación de proteínas nucleares en CDs.

6. El proteasoma se localiza próximo a SCF en el núcleo de las CDs

El hecho de que CCR7 induzca ubiquitinación K48 en el núcleo de las CDs sugiere que podría estar ocurriendo la degradación de proteínas en este mismo compartimento. El proteasoma 26S se ha identificado previamente en el núcleo celular (Hugle, Kleinschmidt et al. 1983; Kleinschmidt, Hugle et al. 1983; Lee and Goldberg 1998; Pines and Lindon 2005; Rockel, Stuhlmann et al. 2005; von Mikecz 2006; Carmo-Fonseca, Berciano et al. 2010; Matsuo, Kishimoto et al. 2011; Gallagher, Oeser et al. 2014). En este sentido, también analizamos la localización del proteasoma en las CDs y si esta superestructura se encontraba cerca de SCF. Estudios de IF muestran la existencia del proteasoma (subunidad catalítica β2 del proteasoma 20S) en el núcleo de las CDs (figura 31A). También se realizaron estudios de PLA entre Cul-1 y la proteína 20S β2. Como se puede observar en la figura 31B, Cul-1 y el proteasoma 20S se encuentran próximos

tanto en el núcleo como en el citoplasma de las CDs. Estos resultados están en línea con resultados previos que muestran que SCF se asocia directamente con el proteasoma 26S (Bloom, Peschiaroli et al. 2006). Ante la posibilidad de que se encontraran interaccionando o formando parte del mismo complejo, se llevó a cabo la IP de Cul-1 y se analizó la posible interacción con 20S β2. Sin embargo, no se observó asociación entre estas proteínas (figura 31C).

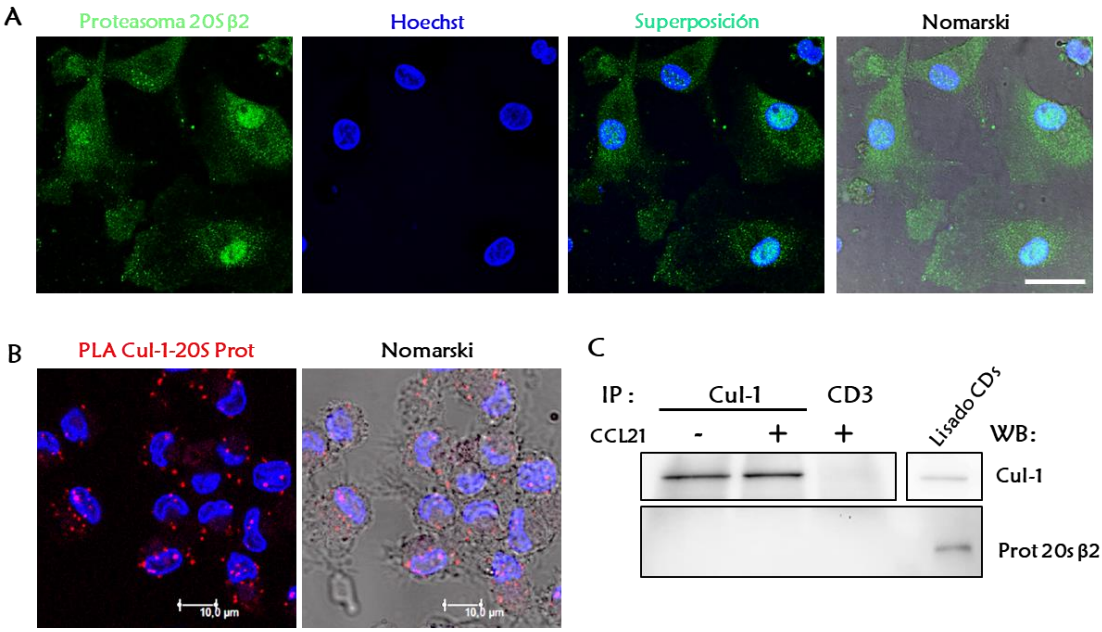

Figura 31. El proteasoma se localiza próximo a SCF en el núcleo de las CDs (A) 5 x 10^4 CDs resuspendidas en RPMI con 0,1% BSA fueron adheridas sobre cristales recubiertos de poli-L-ornitina. Las células fueron estimuladas con CCL21 (18 nM) durante 5 min. A continuación fueron fijadas con PFA 4%, permeabilizadas con metanol frío y teñidas con anticuerpos específicos frente a la subunidad β2 del proteasoma 20S. Los núcleos se tiñeron con Hoechst 33342. Las preparaciones fueron montadas y analizadas por microscopía confocal. Se muestra una fotografía representativa de una sección confocal (N=2). **(B)** Las CDs fueron tratadas al igual que en (A) salvo que tras la fijación y permeabilización, las células se incubaron con anticuerpos específicos frente a la subunidad β2 del proteasoma 20S y frente a Cul-1. A partir de entonces se llevó acabo la técnica PLA (ver sección de materiales y métodos). Las preparaciones fueron montadas y analizadas por microscopía confocal. Se muestra una fotografía representativa de una sección confocal (N=2). **(C)** Las CDs humanas maduras (20-30 x 10^6 CDs) se resuspendieron en RPMI con 0,1% de BSA y se mantuvieron sin estimular (-) o estimuladas con CCL21 (18 nM) durante 5 min (+) a 37º. Después, las células se lisaron resuspendiéndolas en buffer de lisis y se llevó a cabo la IP de Cul-1. Las muestras fueron analizadas mediante SDS-PAGE y WB con anticuerpos frente a Cul-1 y a la subunidad β2 del proteasoma 20S.

7. Posibles proteínas candidatas a ser ubiquitinadas bajo la estimulación de CCR7: Análisis del interactoma de Cul-1 en el núcleo de las CDs

El siguiente objetivo que nos planteamos en este estudio fue investigar qué proteínas podían ser ubiquitinadas por el complejo SCF activo en el núcleo en respuesta a la estimulación de CCR7. Esta información puede proporcionar una idea de si la ubiquitinación activada por CCR7 a través de la nedilación de Cul-1 podría estar regulando alguna función nueva para este receptor en el núcleo de las CDs.

Para intentar resolver esta pregunta, llevamos a cabo estudios de proteómica basados en espectrometría de masas. Decidimos llevar a cabo un fraccionamiento celular para obtener fracciones enriquecidas en proteínas citoplásmicas y fracciones enriquecidas en proteínas nucleares de células estimuladas con CCL21. Posteriormente inmunoprecipitamos Cul-1 de la fracción nuclear, donde se encuentra la mayor parte de Cul-1^{Nedd8}. Las muestras se analizaron mediante cromatografía líquida (LC) acoplada a espectrometría de masas (MS), en el espectrómetro de masas Q-Exactive, con el objetivo de identificar las proteínas que podrían estar interaccionando con Cul-1, y, por tanto, siendo reclutadas por el complejo SCF para su ubiquitinación.

En la figura 32 se observa el resumen de tres experimentos de IP de Cul-1 nuclear analizados mediante LC-MS. Aunque se identificó un reducido número de proteínas, se encontraron proteínas comunes en los tres experimentos realizados

(figura 32A). De las 40 proteínas identificadas en los tres experimentos, se eliminaron 11 tras el filtrado por el repositorio de contaminantes CRAPome (Mellacheruvu, Wright et al. 2013). Posteriormente, se analizaron las posibles interacciones entre las 29 proteínas resultantes mediante la herramienta bioinformática STRING v 9.0 (www.string-db.org) (Szklarczyk, Franceschini et al. 2011). De este modo, se encontraron interacciones descritas, representadas con líneas, entre 9 de las proteínas encontradas, aunque no se encontró ninguna interacción descrita o predicha entre proteínas identificadas y Cul-1 (figura 32B). El análisis funcional de las 29 proteínas mediante el programa FunRich (Pathan, Keerthikumar et al. 2015) reveló un enriquecimiento en los procesos biológicos metabolismo de proteínas (6 proteínas, incluyendo a Cul-1) y respuesta inmune (4 proteínas) (figura 32C). Se comprobó mediante WB (figura 32D) que la IP se llevó a cabo correctamente.

Estos resultados confirman nuevamente que el complejo SCF activado en respuesta a CCR7 puede estar involucrado en el control del metabolismo de proteínas en el núcleo de las CDs. Concretamente, destacamos varias proteínas involucradas en la síntesis de proteínas, como las proteínas ribosomales L27A, S5, 4X, el factor de elongación Ts mitocondrial (TSFM) y el complejo THO (ALYREF), implicado en la exportación nuclear de ARNm. Se puede encontrar más información sobre las proteínas identificadas en las tablas suplementarias incluidas en formato electrónico.

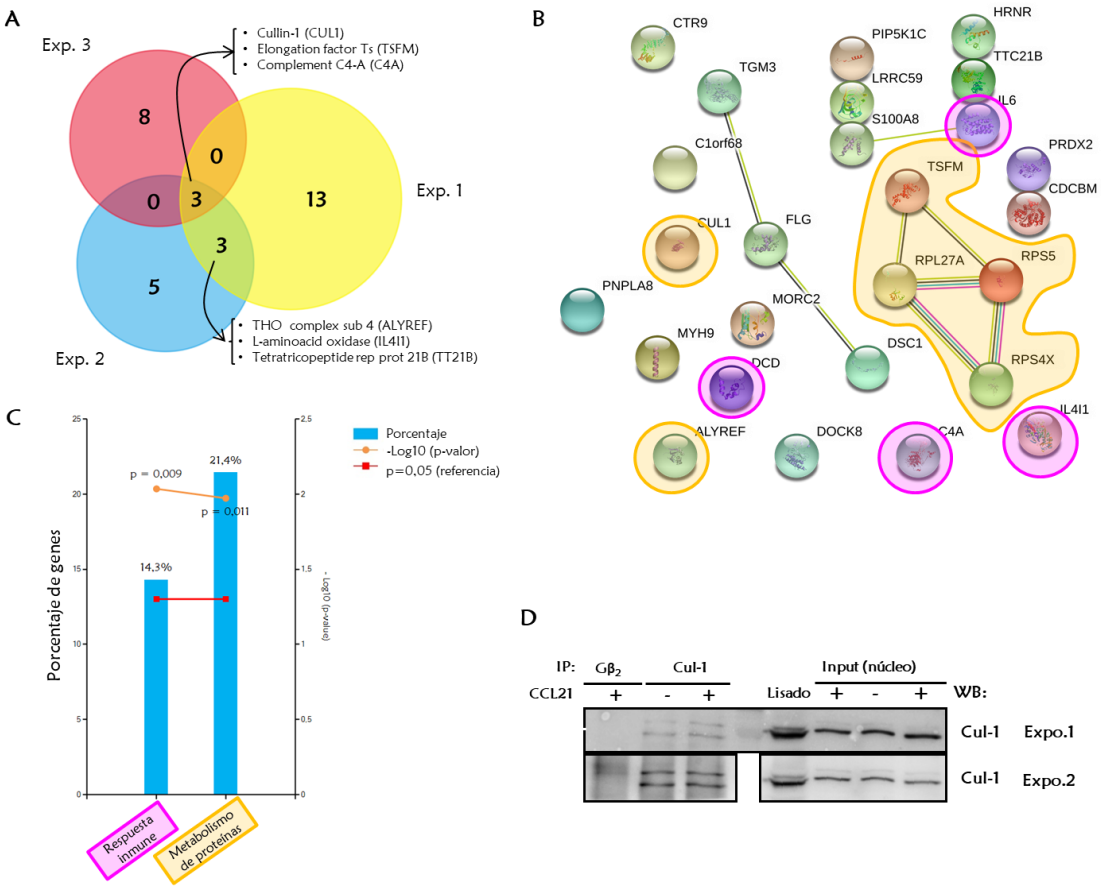

Figura 32. Estudio del interactoma de Cul-1 en el núcleo. Las CDs (20-30 x 10^6 CDs) se resuspendieron en RPMI con 0,1% de BSA y se mantuvieron sin estimular (-) o estimuladas con CCL21 (18 nM) durante 5 min (+) a 37º. Después, las CDs se lavaron en PBS frío y se llevó a cabo la extracción de proteínas citoplásmicas y la lisis de los núcleos en buffer de IP. Posteriormente se llevó a cabo la IP nuclear de Cul-1. Las muestras obtenidas fueron sometidas a una digestión con tripsina y se analizaron mediante LC-MS. **(A)** representa las proteínas obtenidas en 3 experimentos diferentes señalando las proteínas comunes a los experimentos, entre ellas, la propia Cul-1. **(B)** El análisis de las interacciones de estas proteínas mediante STRING revela interacciones conocidas entre 9 de las proteínas encontradas, pero ninguna interacción con Cul-1 descrita hasta ahora. **(C)** El análisis de los procesos biológicos en los que están implicados estas proteínas muestra un enriquecimiento significativo en los procesos de metabolismo de proteínas (marcado en amarillo) y respuesta inmune (marcado en rosa). **(D)** Se tomaron alícuotas de las muestras de la IP para analizar la carga y comprobar que la IP se había producido correctamente mediante WB usando anticuerpos frente a Cul-1 (se muestran dos exposiciones (Expo.) de un revelado del WB). (N=3 experimentos, 9 donantes)

DISCUSIÓN

CCR7 controla múltiples funciones en las CDs que contribuyen a una adecuada respuesta inmune adaptativa. Por ello, es importante conocer la señalización intracelular inducida por este receptor y cómo contribuye a regular las funciones celulares. La mayor parte de los estudios sobre la señalización de CCR7 se han centrado en el análisis de la fosforilación de proteínas, y los estudios centrados en otros tipos de modificaciones post-traduccionales son escasos (Schaeuble, Hauser et al. 2012). En este trabajo observamos que la estimulación de CCR7 induce nedilación de la E3 ligasa SCF en el núcleo de CDs, resultando en su activación y el consiguiente incremento de la poliubiquitinación nuclear de tipo K48.

En primer lugar, observamos que la estimulación de CCR7 produjo un aumento en la nedilación de Cul-1 (Cul-1$^{\text{-nedd8}}$), una de las dianas de nedilación más estudiadas (Enchev, Schulman et al. 2015). Estudios previos han mostrado que la nedilación juega un importante papel en la regulación de diferentes células del sistema inmunológico, como los macrófagos, las células T y las CDs (Chang, Reyna et al. 2012; Jin, Liao et al. 2013; Mathewson, Toubai et al. 2013; Cheng, Hu et al. 2016). Es por ello que, a continuación, estudiamos si la nedilación jugaba un papel en la señalización inducida por CCR7 en las CDs.

Hasta ahora, la mayoría de los trabajos en los que se estudia la nedilación, se centran en bloquear dicho proceso con el fármaco MLN4924 (MLN) y analizar qué efectos ejerce la inhibición sobre el funcionamiento de las células, pero

pocos estudios han analizado los cambios en nedilación producidos por la estimulación de un receptor. En relación con esto, se ha observado que la estimulación de células endoteliales microvasculares humanas con LPS induce un aumento en la nedilación de Cul-1 (Ehrentraut, Kominsky et al. 2013) y que la IL-β1 induce nedilación de Cul-3 en fibroblastos embrionarios de ratón (Lee, Kim et al. 2012). También, se ha observado en células HEK-293 que el daño en el ADN estimula la nedilación de proteínas, como la Histona 4 y la Histona 2 y que Nedd8 se encuentra localizada en los sitios dañados del ADN (Ma, Chen et al. 2013; Li, Guan et al. 2014; Brown, Lukashchuk et al. 2015). Además, se ha observado que incluso algunos receptores pueden nedilarse, como EGFR (Oved, Mosesson et al. 2006) o CXCR5 (Renaudin, Guervilly et al. 2014). Este trabajo se muestra, por primera vez, que un receptor de quimioquinas, induce nedilación en las CDs.

Los receptores de quimioquinas señalizan al interior celular a través de las proteínas G. Gαi media la señalización de la mayor parte de las rutas reguladas por CCR7 en las CDs (Riol-Blanco, Sanchez-Sanchez et al. 2005). En este sentido, nuestros estudios de inhibición con la toxina pertúsica mostraron que Gαi también controla el incremento de nedilación inducido tras la estimulación de CCR7.

A continuación, investigamos si la nedilación se requería para regular las funciones que controla CCR7 en las CDs. Para este fin, empleamos el inhibidor MLN.

CCR7 induce supervivencia en las CDs (Sanchez-Sanchez, Riol-Blanco et al. 2004; Riol-Blanco, Sanchez-Sanchez et al. 2005; Lopez-Cotarelo, Escribano-Diaz et al. 2015), y parte este incremento de la supervivencia se debe a la activación de la ruta de NFκB (Sanchez-Sanchez, Riol-Blanco et al. 2004; Escribano, Delgado-Martin et al. 2009). La estimulación de CCR7 induce degradación de IκBα por el proteasoma, lo que permite la traslocación de NFκB al núcleo, donde regula la expresión de genes reguladores de la supervivencia, como Bcl_{xl}. Está descrito que la nedilación de SCF regula la ruta de NFκB en diversos tipos celulares, incluyendo a las CDs (Mathewson, Toubai et al. 2013), puesto que IκBα es una diana del complejo SCF, que regula su ubiquitinación para su posterior degradación por el proteasoma (Winston, Strack et al. 1999; Read, Brownell et al. 2000). Es por ello que nos preguntamos si la nedilación de Cul-1 inducida por CCR7, podía regular la vía de NFκB al inducir la ubiquitinación y degradación de IκBα y, de esta manera, regular la supervivencia de las CDs.

En primer lugar, observamos que la inhibición de la nedilación mediante el tratamiento con MLN aumentó el porcentaje de apoptosis en las CDs con respecto a las células no tratadas. Este resultado concuerda con lo observado por Cheng et al., que previamente mostraron que el tratamiento con MLN induce apoptosis de CDs derivadas de médula ósea de ratón (Cheng, Hu et al. 2016). Puesto que la nedilación regula la supervivencia basal de las CDs, analizamos si podría contribuir a regular la supervivencia de las CDs tras la estimulación de CCR7. Sin embargo, observamos que en CDs pre-tratadas con MLN, la estimulación de CCR7 aún reducía la apoptosis hasta niveles similares a los de las

células sin tratamiento con MLN, indicando que la nedilación no juega un papel en la regulación de la supervivencia inducida por CCR7 en las CDs. Para confirmar estos resultados, analizamos directamente si la nedilación inducida por CCR7 estaba implicada en la regulación de la ruta de NFκB. Sin embargo, observamos que, en concordancia con lo observado en los experimentos de supervivencia inducida por CCR7, el tratamiento con MLN no afectó a la degradación de IκBα ni a la traslocación de NFκB al núcleo dependiente de CCR7. También observamos que, tras la estimulación de CCR7, la activación de AKT, necesaria para la activación de la vía de NFκB, tampoco estaba afectada por la inhibición de la nedilación. Por tanto, concluimos que el incremento de nedilación de Cul-1 observado tras la estimulación de CCR7 no regula la activación de la vía de NFκB, ni la supervivencia de las CDs.

A continuación, quisimos estudiar si la nedilación jugaba algún papel en el control del resto de las funciones que se sabe que están reguladas por CCR7 en CDs. Comenzamos analizando si la nedilación controlaba la quimiotaxis, la función clásica controlada por CCR7. Los experimentos de *transwell* mostraron que la inhibición de la nedilación no afectó a la quimiotaxis de las CDs, así como tampoco afectó a la activación de ERK1/2, un regulador clave de la esta ruta. Este resultado concuerda con trabajos previos que muestran que la inhibición de la nedilación no afecta a la vía de las MAP-quinasas (Mathewson, Toubai et al. 2013; Cheng, Hu et al. 2016). Por tanto, los resultados claramente indicaban que, tras la estimulación de CCR7, el incremento observado en la nedilación no está involucrado en el control de la quimiotaxis. Del mismo modo que en los

experimentos de *transwell* mencionados anteriormente, observamos que la inhibición de la nedilación tampoco afectó el al incremento de la velocidad migratoria regulada por CCR7.

También analizamos el posible papel de la nedilación en la regulación de la endocitosis inducida por CCR7 (Yanagawa and Onoe 2003). En relación a esto, observamos que la inhibición de la nedilación tampoco afectó al incremento en la endocitosis inducida por CCR7.

Como hemos mencionado, CCR7 también regula cambios en la citoarquitectura de las CDs (Yanagawa and Onoe 2002) que dependen de la inhibición, mediante fosforilación, de la proteína reguladora de actina Cofilina-1 (Torres-Bacete, Delgado-Martin et al. 2015). En este sentido, observamos, nuevamente, que la inhibición de la nedilación no afectó a los cambios en morfología, aplastamiento (spreading) celular, ni en la fosforilación de la Cofilina-1 en la Serina 3 inducida por la estimulación de CCR7.

Aunque estos resultados son interesantes, no aportan información acerca del significado funcional de la nedilación inducida por CCR7 en las CDs. Sin embargo, durante los experimentos de fraccionamiento de proteínas y Western blot (WB), y de inmunofluorescencias (IF) nos encontramos con un resultado interesante: A pesar de que Cul-1 total se observó repartido de manera similar entre el núcleo y citoplasma de las CDs; Nedd8 o Cul-1$^{\text{-nedd8}}$ se encontró mayormente concentrado en el núcleo de las CDs. La presencia nuclear de proteínas modificadas por Nedd8 ya había sido observado previamente

(Kamitani, Kito et al. 1997; Furukawa, Zhang et al. 2000; Jubelin, Taieb et al. 2010; Huang, Kaufman et al. 2011; Ma, Chen et al. 2013; Enchev, Schulman et al. 2015), aunque esto no se ha investigado hasta ahora en células del sistema inmunológico. Se ha sugerido que el extremo C-terminal de Cul-1 es responsable de su traslocación al núcleo y que el bloqueo de dicha traslocación disminuye la nedilación de Cul-1 (Furukawa, Zhang et al. 2000), sugiriendo que la nedilación se produce en el núcleo. En nuestro sistema celular nos encontramos con unos niveles de nedilación basales en el núcleo de las CDs y es allí donde aumenta la nedilación de Cul-1 en respuesta a la estimulación de CCR7. Además, se observa una disminución en los niveles de Cul-1 sin modificar en el citoplasma, tras la estimulación con CCR7, por lo que existe la posibilidad de que CCR7 esté induciendo la traslocación de Cul-1 al núcleo, donde sufre nedilación. Sin embargo, es necesario realizar experimentos de inhibición del transporte nuclear para averiguar si CCR7 tiene algún efecto sobre la traslocación de Cul-1.

Puesto que las proteínas Rbx1, Skp1, Cul-1 forman el núcleo invariable del complejo SCF, analizamos si estas proteínas podrían formar parte un complejo SCF nuclear. Los estudios de IF mostraron que Rbx1 tiene una distribución predominantemente nuclear, coincidiendo con la de Nedd8. Estos resultados coinciden con resultados previos que también indican una localización nuclear de Rbx1 (Wei and Sun 2010). Además, los análisis de PLA entre Cul-1 y Rbx1 sugieren que ambas moléculas se encuentran muy próximas en el interior del núcleo, aunque también se observó cercanía en el citoplasma, lo que señala la presencia de SCF tanto en el núcleo como en el citoplasma. El hecho de que la

nedilación/activación de SCF ocurra únicamente en el núcleo, plantea preguntas acerca de qué función puede estar desempeñando el complejo SCF sin nedilar en el citoplasma, o si Cul-1-Rbx1 se traslocan juntos al núcleo para activarse SCF. Se requieren futuros experimentos para resolver estas preguntas.

En cualquier caso, quisimos analizar la interacción en el núcleo entre Cul-1 y Rbx1 mediante IP nuclear de Cul-1 en CDs estimuladas o no con CCL21. En estos experimentos se observó que Rbx1 co-inmunoprecipitaba con Cul-1 en ambos casos, indicando que ambas proteínas forman parte de un mismo complejo. En su conjunto, los resultados del PLA y de la IP sugieren que ambas proteínas interaccionan en el núcleo.

En cuanto al otro componente invariable de SCF, la proteína adaptadora Skp1, los resultados de la IF muestran una distribución similar a la observada para Rbx1. Skp1 también aparece más concentrada en el núcleo de las CDs. Interesantemente, los experimentos de PLA muestran que Skp1 y Cul-1 se encuentran próximos exclusivamente en el núcleo de las CDs. Se ha descrito que cuando Cul-1 no se encuentra nedilado, su sitio de unión a Skp1-Fbox se encuentra bloqueado por la proteína Cand1; sin embargo, cuando Cul-1 se nedila, Cand1 se disocia, permitiendo la asociación de Skp1-Fbox a Cul-1 (Liu, Furukawa et al. 2002). Puesto que Cul-1^{-nedd8} se observa sólo en el núcleo, es de esperar que la señal positiva de PLA para Skp1-Cul-1 se observe sólo en el núcleo de las CDs.

A continuación, decidimos comprobar mediante inmunoprecipitación (IP) que estas moléculas interaccionaban. Se inmunoprecipitó Skp1 de lisados totales de CDs estimuladas y sin estimular con CCL21 y se comprobó, mediante WB, que co-inmunoprecipitaba con Cul-1.

En resumen, podemos afirmar que Cul-1 está formando un complejo con Rbx1 y Skp1 y, por tanto, que el complejo se encuentra completo en el núcleo de las CDs. En su conjunto, los resultados previos indican que, puesto que la mayoría de Cul-1^{-nedd8} se encuentra en el núcleo, el complejo SCF se encuentra activado en el núcleo de las CDs, y por tanto puede estar induciendo la ubiquitinación de proteínas en este compartimento.

Trabajos previos han demostrado que la E3 ligasa SCF controla la ubiquitinación de proteínas de tipo K48 (Petroski and Deshaies 2005). Además, este tipo de ubiquitinación se ha observado previamente también en el núcleo (Chen, Dai et al. 2006; Suresh, Ramakrishna et al. 2010; Ferreira, Soares et al. 2015). Por tanto, en los siguientes experimentos analizamos si CCR7 podía inducir la poliubiquitinación de tipo K48 (poli-Ub-K48). Observamos que la estimulación de CCR7 dio lugar a un aumento de la poli-Ub-K48 en el núcleo, sobre todo de cadenas largas de poliubiquitina (de más de 5 unidades, o peso superior a 50 KDa). Además, este incremento se bloqueó cuando las CDs se pretrataron con MLN. Estos resultados indican que la estimulación de CCR7 induce poliubiquitinación-K48 de proteínas en el núcleo de las CDs, y para que este proceso ocurra, se requiere nedilación.

Cuando se realizó una IP de las proteínas ubiquitinadas totales en las CDs, se observó que la estimulación de CCR7 no indujo un aumento general en la ubiquitinación, sino que provocó un enriquecimiento en cadenas de poliubiquitina tipo K48, indicando que la ubiquitinación inducida por CCR7 es específicamente ese tipo. Además, resultados preliminares (no mostrado) indican que la estimulación de CCR7, no modifica los niveles de ubiquitinación en K63.

Cuando analizamos la ubiquitina (Ub) mediante IF comprobamos que esta proteína se encuentra muy concentrada en el núcleo de las CDs. Sin embargo, cuando las CDs se pretrataron con MLN, se observó una disminución de la Ub dentro del núcleo. Por tanto, parece que la existencia de ubiquitinación en el núcleo de las CDs depende de la nedilación. Este resultado coincide el trabajo de Hughes et al., que observan, mediante IF, una reducción en la ubiquitinación tras el tratamiento con MLN (Hughes, Wood et al. 2015).

Trabajos previos de otros grupos han mostrado que el sitio de nedilación de Cul-1 se encuentra muy próximo al sitio de unión de la enzima E2, que porta consigo la Ub y, por otro lado, que la nedilación de Cul-1 favorece la interacción de SCF con la E2 cargada (Kawakami, Chiba et al. 2001; Sakata, Yamaguchi et al. 2007). Por tanto, si el complejo SCF nedilado/activo esta ubiquitinando a las proteínas nucleares, entonces Nedd8 se localizará cerca de la Ub. En los experimentos de IF mencionados anteriormente, se observó que la Ub colocaliza en el núcleo con Nedd8, y que ambos disminuyen cuando las células son pretratadas con MLN. Al realizar experimentos de PLA entre Ub y Nedd8, observamos señal fluorescente mayormente en el núcleo de las CDs, y el tratamiento con MLN, redujo

significativamente dicha señal fluorescente. Estos resultados sugieren que existe cercanía entre Nedd8 (Cul-1^{-nedd8}) y la Ub, y que dicha cercanía depende en gran medida de que Nedd8 esté unido a Cul-1.

El tratamiento con MLN inhibe la nedilación a nivel de la E1 (NAE), por lo que no solo inhibe la nedilación de Cul-1, sino también la de otras proteínas de la familia Cullin. Para comprobar que el efecto de CCR7 sobre la ubiquitinación se debe específicamente a Cul-1, decidimos reducir los niveles de Cul-1, mediante un siRNA.

La transfección de las CDs con material genético es un proceso con una eficiencia limitada, debido a que se trata de células terminalmente diferenciadas. Se redujeron los niveles de Cul-1 en tres donantes y se analizaron los efectos del silenciamiento sobre la ubiquitinación. En dichos donantes se observó una tendencia similar a la observada con MLN sobre la Poli-Ub-K48. Tras la estimulación de las CDs con CCL21, se observó un aumento en la Poli-Ub-K48 en las CDs transfectadas con el siRNA control, que no se observó en las CDs transfectadas con el siRNA de Cul-1.

Asimismo, se analizó la localización de la Ub mediante IF y se observó que el silenciamiento de Cul-1 produjo una disminución de la Ub en el núcleo de las CDs, de manera similar a lo observado en los experimentos con MLN. Estos resultados sugieren que la ubiquitinación de proteínas inducida por CCR7 en el núcleo de las CDs depende de la nedilación de Cul-1 y activación de SCF.

La ubiquitinación de tipo K48 está asociada a la degradación de proteínas mediante el proteasoma, y numerosos trabajos en los últimos años han mostrado ubiquitinación y degradación mediada por el proteasoma en el núcleo de las células eucariotas (Hugle, Kleinschmidt et al. 1983; Kleinschmidt, Hugle et al. 1983; Lee and Goldberg 1998; Pines and Lindon 2005; Rockel, Stuhlmann et al. 2005; von Mikecz 2006; Carmo-Fonseca, Berciano et al. 2010; Matsuo, Kishimoto et al. 2011; Gallagher, Oeser et al. 2014). En el caso de las CDs, mostramos mediante inmunofluorescencia que el proteasoma también se expresa en el núcleo, usando un anticuerpo frente a la subunidad catalítica β2, perteneciente al subcomplejo 20S del proteasoma 26S.

Además, experimentos de PLA nos permitieron observar que existe cercanía entre Cul-1 y la subunidad β2 del proteasoma 20S, tanto en el núcleo como en el citoplasma de las CDs, lo cual sugiere que en ambos compartimentos SCF y el proteasoma están cercanos. Interesantemente, un estudio ha reportado que existe una interacción directa entre SCF y el proteasoma (Bloom, Peschiaroli et al. 2006). Sin embargo, tras la IP de Cul-1, observamos que Cul-1 no coinmunoprecipita con la subunidad β2. El trabajo de Bloom et al. demuestra asociación entre Cul-1 y las subunidades α2 y α6, por lo que, es posible que la asociación entre Cul-1 y el proteasoma se dé únicamente en esas subunidades. Es por ello que es necesario analizar la co-inmunoprecipitación con dichas moléculas antes de afirmar que no existe unión entre SCF y el proteasoma 26S.

Para averiguar posibles dianas del complejo SCF y, puesto que Cul-1 es una proteína clave en este complejo, analizamos, mediante IP y proteómica, las proteínas que pudieran interaccionar con Cul-1.

Realizamos tres experimentos en los que inmunoprecipitamos Cul-1 del núcleo de las CDs e identificamos las proteínas acompañantes mediante proteómica. Aunque se comprobó que Cul-1 inmunoprecipitó correctamente, se obtuvo un bajo número de proteínas, debido probablemente a que las proteínas nucleares de las CDs constituyen entre un 8-10% de las proteínas totales (datos no publicados de nuestro laboratorio) y la eficiencia de la IP puede ser muy baja. La reproducibilidad en los 3 experimentos también fue bastante baja, debido posiblemente al bajo número de proteínas obtenidas. Al analizarse las posibles interacciones entre las proteínas identificadas, no se encontraron interacciones descritas entre Cul-1 y las proteínas identificadas. Sin embargo, el estudio funcional de procesos biológicos mostró un enriquecimiento significativo en proteínas relacionadas con la respuesta inmune, aunque sin una relación descrita entre ellas, y también en proteínas relacionadas con el metabolismo proteico, con interacciones descritas entre ellas. Concretamente, se encontraron varias proteínas ribosomales, una relacionada con la elongación traduccional y otra relacionada con la exportación nuclear de ARN mensajero. Estas proteínas sugieren que Cul-1 podía interaccionando, de algún modo, con la maquinaria de síntesis de proteínas. En este sentido, existen evidencias que indican la existencia de síntesis de proteínas en el núcleo de las células (Dahlberg, Lund et al. 2003; David, Dolan et al. 2012; Reid and Nicchitta 2012; Yewdell and David 2013) y se

sabe que durante la síntesis de proteínas se producen proteínas defectuosas o mal plegadas que deben ser eliminadas para asegurar el correcto funcionamiento de la célula (Goldberg 2003; Lelouard, Ferrand et al. 2004).

La estimulación de CCR7 induce activación de la ruta de mTORC1, cuyas dianas, S6K y 4EBP1, controlan la síntesis de proteínas (Haghighat, Mader et al. 1995; Hay and Sonenberg 2004). Por tanto, es posible que la activación por nedilación de SCF inducida por CCR7 en el núcleo de las CDs esté implicada en el control de calidad de las proteínas sintetizadas en respuesta a CCR7. Futuros experimentos permitirán determinar si CCR7 está regulando la traducción de proteínas.

En resumen, los resultados presentados en esta tesis demuestran, por primera vez, que un receptor de quimioquinas regula la activación por nedilación de SCF y la consecuente ubiquitinación de proteínas en el núcleo de las CDs. Estos resultados muestran que CCR7 está regulando una nueva función, además de las ya descritas, y aportan información sobre la regulación del UPS en el núcleo de las CDs, un compartimiento celular muy sensible al estrés, donde la acumulación de proteínas aberrantes pueden dar lugar a toxicidad y muerte celular, y originar numerosas patologías (Shibata and Morimoto 2014). Puesto que las CDs son fundamentales para el desarrollo de una respuesta inmune adaptativa, resulta crucial comprender con precisión los mecanismos que regulan la degradación de proteínas, así como las nuevas funciones reguladas por CCR7 en estas células, ya que pueden ser utilizadas como posibles dianas terapéuticas para la modulación de la respuesta inmunológica.

En la figura 33 se representan el modelo que incluye los resultados obtenidos en este trabajo, en conjunto con los resultados previos acerca de las funciones reguladas por CCR7 y la red de señalización controlada por este receptor en las CDs.

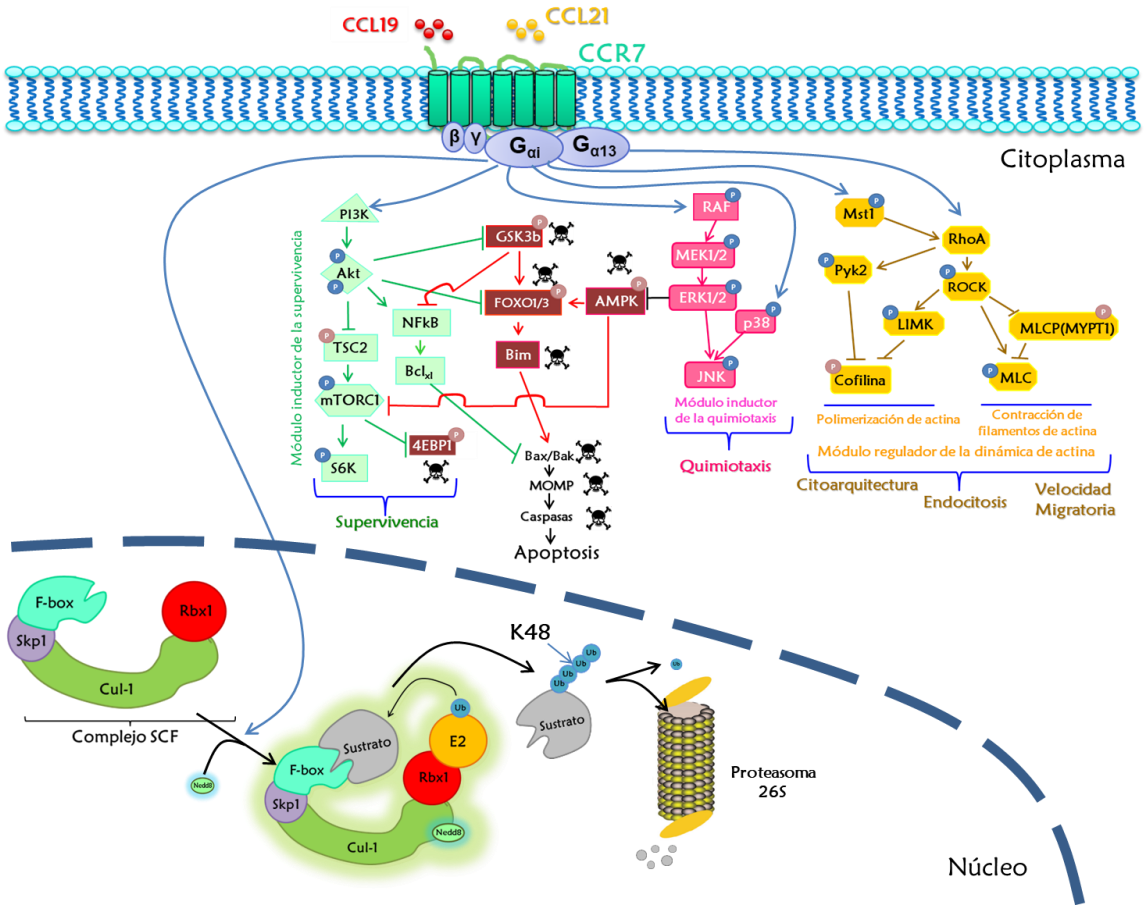

Figura 33. Modelo actualizado de la señalización intracelular activada por CCR7. La estimulación de CCR7 con sus ligandos, CCL19 y CCL21, induce un aumento de la supervivencia, la quimiotaxis, la velocidad migratoria y la endocitosis, así como cambios la citoarquitectura de las CDs. Los resultados obtenidos en esta tesis sugieren una nueva vía de señalización en la que la estimulación de CCR7 induce la nedilación de Cul-1 en el núcleo, activando así al complejo SCF, que induce poliubiquitinación tipo K48 de proteínas nucleares, para ser degradadas posteriormente por el proteasoma nuclear.

CONCLUSIONES

- La estimulación de CCR7 induce nedilación de Cullin-1 (Cul-1) en las CDs humanas maduras, que está mediada por la familia de proteínas Gαi.

- Esta nedilación no participa en el proceso regulatorio que conduce a la quimiotaxis, el incremento de supervivencia, la velocidad migratoria, la endocitosis o los cambios en citoarquitectura inducidos por CCR7 en las CDs.

- La nedilación de Cul-1 inducida por CCR7 se produce en el núcleo de las CDs, donde Cul-1^{Nedd8} forma parte del complejo SCF junto con las proteínas Rbx1 y Skp1.

- La nedilación/activación de SCF inducida por CCR7 promueve ubiquitinación (K48) de proteínas nucleares en las CDs.

- CCR7 podría controlar la degradación de proteínas mediada por el proteasoma en el núcleo de las CDs, contribuyendo a los mecanismos de la proteostasis nuclear.

BIBLIOGRAFÍA

Allen, S. J., S. E. Crown, et al. (2007). "Chemokine: receptor structure, interactions, and antagonism." Annu Rev Immunol **25**: 787-820.

Arendt, C. S. and M. Hochstrasser (1997). "Identification of the yeast 20S proteasome catalytic centers and subunit interactions required for active-site formation." Proc Natl Acad Sci U S A **94**(14): 7156-7161.

Bacon, K., M. Baggiolini, et al. (2002). "Chemokine/chemokine receptor nomenclature." J Interferon Cytokine Res **22**(10): 1067-1068.

Bachmann, M. F., M. Kopf, et al. (2006). "Chemokines: more than just road signs." Nat Rev Immunol **6**(2): 159-164.

Bardi, G., M. Lipp, et al. (2001). "The T cell chemokine receptor CCR7 is internalized on stimulation with ELC, but not with SLC." Eur J Immunol **31**(11): 3291-3297.

Bech-Otschir, D., A. Helfrich, et al. (2009). "Polyubiquitin substrates allosterically activate their own degradation by the 26S proteasome." Nat Struct Mol Biol **16**(2): 219-225.

Bennett, E. J., J. Rush, et al. (2010). "Dynamics of cullin-RING ubiquitin ligase network revealed by systematic quantitative proteomics." Cell **143**(6): 951-965.

Bhatia, S., A. C. Pavlick, et al. (2016). "A phase I study of the investigational NEDD8-activating enzyme inhibitor pevonedistat (TAK-924/MLN4924) in patients with metastatic melanoma." Invest New Drugs **34**(4): 439-449.

Bienz, M. (2006). "The PHD finger, a nuclear protein-interaction domain." Trends Biochem Sci **31**(1): 35-40.

Bloom, J., A. Peschiaroli, et al. (2006). "Modification of Cul1 regulates its association with proteasomal subunits." Cell Div **1**: 5.

Boh, B. K., M. Y. Ng, et al. (2011). "Inhibition of cullin RING ligases by cycle inhibiting factor: evidence for interference with Nedd8-induced conformational control." J Mol Biol **413**(2): 430-437.

Bosu, D. R. and E. T. Kipreos (2008). "Cullin-RING ubiquitin ligases: global regulation and activation cycles." Cell Div **3**: 7.

Brown, J. S., N. Lukashchuk, et al. (2015). "Neddylation promotes ubiquitylation and release of Ku from DNA-damage sites." Cell Rep **11**(5): 704-714.

Brownell, J. E., M. D. Sintchak, et al. (2010). "Substrate-assisted inhibition of ubiquitin-like protein-activating enzymes: the NEDD8 E1 inhibitor MLN4924 forms a NEDD8-AMP mimetic in situ." Mol Cell **37**(1): 102-111.

Bulatov, E. and A. Ciulli (2015). "Targeting Cullin-RING E3 ubiquitin ligases for drug discovery: structure, assembly and small-molecule modulation." Biochem J **467**(3): 365-386.

Bunting, M. D., I. Comerford, et al. (2013). "CCX-CKR deficiency alters thymic stroma impairing thymocyte development and promoting autoimmunity." Blood **121**(1): 118-128.

Byers, M. A., P. A. Calloway, et al. (2008). "Arrestin 3 mediates endocytosis of CCR7 following ligation of CCL19 but not CCL21." J Immunol **181**(7): 4723-4732.

Cappadocia, L. and C. D. Lima (2017). "Ubiquitin-like Protein Conjugation: Structures, Chemistry, and Mechanism." Chem Rev.

Carmo-Fonseca, M., M. T. Berciano, et al. (2010). "Orphan nuclear bodies." Cold Spring Harb Perspect Biol **2**(9): a000703.

Cenciarelli, C., D. S. Chiaur, et al. (1999). "Identification of a family of human F-box proteins." Curr Biol **9**(20): 1177-1179.

Coleman, K. E., M. Bekes, et al. (2017). "SENP8 limits aberrant neddylation of NEDD8 pathway components to promote cullin-RING ubiquitin ligase function." Elife **6**.
Comerford, I., Y. Harata-Lee, et al. (2013). "A myriad of functions and complex regulation of the CCR7/CCL19/CCL21 chemokine axis in the adaptive immune system." Cytokine Growth Factor Rev **24**(3): 269-283.
Coscoy, L. and D. Ganem (2003). "PHD domains and E3 ubiquitin ligases: viruses make the connection." Trends Cell Biol **13**(1): 7-12.
Craig, K. L. and M. Tyers (1999). "The F-box: a new motif for ubiquitin dependent proteolysis in cell cycle regulation and signal transduction." Prog Biophys Mol Biol **72**(3): 299-328.
Chan, Y., J. Yoon, et al. (2008). "DEN1 deneddylates non-cullin proteins in vivo." J Cell Sci **121**(Pt 19): 3218-3223.
Chang, F. M., S. M. Reyna, et al. (2012). "Inhibition of neddylation represses lipopolysaccharide-induced proinflammatory cytokine production in macrophage cells." J Biol Chem **287**(42): 35756-35767.
Chen, Y., X. Dai, et al. (2006). "Proteasome-dependent down-regulation of activated Stat5A in the nucleus." Blood **108**(2): 566-574.
Cheng, M., S. Hu, et al. (2016). "Inhibition of neddylation regulates dendritic cell functions via Deptor accumulation driven mTOR inactivation." Oncotarget **7**(24): 35643-35654.
Chung, D. and G. Dellaire (2015). "The Role of the COP9 Signalosome and Neddylation in DNA Damage Signaling and Repair." Biomolecules **5**(4): 2388-2416.
Dahlberg, J. E., E. Lund, et al. (2003). "Nuclear translation: what is the evidence?" RNA **9**(1): 1-8.
David, A., B. P. Dolan, et al. (2012). "Nuclear translation visualized by ribosome-bound nascent chain puromycylation." J Cell Biol **197**(1): 45-57.
Davis, M., A. Hatzubai, et al. (2002). "Pseudosubstrate regulation of the SCF(beta-TrCP) ubiquitin ligase by hnRNP-U." Genes Dev **16**(4): 439-451.
Deshaies, R. J. and C. A. Joazeiro (2009). "RING domain E3 ubiquitin ligases." Annu Rev Biochem **78**: 399-434.
Ding, Y., Y. Shimada, et al. (2003). "Association of CC chemokine receptor 7 with lymph node metastasis of esophageal squamous cell carcinoma." Clin Cancer Res **9**(9): 3406-3412.
Duda, D. M., L. A. Borg, et al. (2008). "Structural insights into NEDD8 activation of cullin-RING ligases: conformational control of conjugation." Cell **134**(6): 995-1006.
Duda, D. M., D. C. Scott, et al. (2011). "Structural regulation of cullin-RING ubiquitin ligase complexes." Curr Opin Struct Biol **21**(2): 257-264.
Dudek, A. M., S. Martin, et al. (2013). "Immature, Semi-Mature, and Fully Mature Dendritic Cells: Toward a DC-Cancer Cells Interface That Augments Anticancer Immunity." Front Immunol **4**: 438.
Ehrentraut, S. F., D. J. Kominsky, et al. (2013). "Central role for endothelial human deneddylase-1/SENP8 in fine-tuning the vascular inflammatory response." J Immunol **190**(1): 392-400.
Emberley, E. D., R. Mosadeghi, et al. (2012). "Deconjugation of Nedd8 from Cul1 is directly regulated by Skp1-F-box and substrate, and the COP9 signalosome inhibits deneddylated SCF by a noncatalytic mechanism." J Biol Chem **287**(35): 29679-29689.
Emmerich, C. H., A. Ordureau, et al. (2013). "Activation of the canonical IKK complex by K63/M1-linked hybrid ubiquitin chains." Proc Natl Acad Sci U S A **110**(38): 15247-15252.

Enchev, R. I., B. A. Schulman, et al. (2015). "Protein neddylation: beyond cullin-RING ligases." Nat Rev Mol Cell Biol **16**(1): 30-44.
Escribano, C., C. Delgado-Martin, et al. (2009). "CCR7-dependent stimulation of survival in dendritic cells involves inhibition of GSK3beta." J Immunol **183**(10): 6282-6295.
Fang, L., V. C. Lee, et al. (2008). "CCR7 regulates B16 murine melanoma cell tumorigenesis in skin." J Leukoc Biol **84**(4): 965-972.
Ferreira, J. V., A. R. Soares, et al. (2015). "K63 linked ubiquitin chain formation is a signal for HIF1A degradation by Chaperone-Mediated Autophagy." Sci Rep **5**: 10210.
Forster, R., A. Schubel, et al. (1999). "CCR7 coordinates the primary immune response by establishing functional microenvironments in secondary lymphoid organs." Cell **99**(1): 23-33.
Franceschi, C., S. Salvioli, et al. (2017). "Immunobiography and the Heterogeneity of Immune Responses in the Elderly: A Focus on Inflammaging and Trained Immunity." Front Immunol **8**: 982.
Fredriksson, S., M. Gullberg, et al. (2002). "Protein detection using proximity-dependent DNA ligation assays." Nat Biotechnol **20**(5): 473-477.
Frescas, D. and M. Pagano (2008). "Deregulated proteolysis by the F-box proteins SKP2 and beta-TrCP: tipping the scales of cancer." Nat Rev Cancer **8**(6): 438-449.
Furukawa, M., Y. Zhang, et al. (2000). "The CUL1 C-terminal sequence and ROC1 are required for efficient nuclear accumulation, NEDD8 modification, and ubiquitin ligase activity of CUL1." Mol Cell Biol **20**(21): 8185-8197.
Gallagher, P. S., M. L. Oeser, et al. (2014). "Cellular maintenance of nuclear protein homeostasis." Cell Mol Life Sci **71**(10): 1865-1879.
Geissmann, F., M. G. Manz, et al. (2010). "Development of monocytes, macrophages, and dendritic cells." Science **327**(5966): 656-661.
Glickman, M. H. and A. Ciechanover (2002). "The ubiquitin-proteasome proteolytic pathway: destruction for the sake of construction." Physiol Rev **82**(2): 373-428.
Glotzer, M., A. W. Murray, et al. (1991). "Cyclin is degraded by the ubiquitin pathway." Nature **349**(6305): 132-138.
Goldenberg, S. J., T. C. Cascio, et al. (2004). "Structure of the Cand1-Cul1-Roc1 complex reveals regulatory mechanisms for the assembly of the multisubunit cullin-dependent ubiquitin ligases." Cell **119**(4): 517-528.
Graham, G. J., M. Locati, et al. (2012). "The biochemistry and biology of the atypical chemokine receptors." Immunol Lett **145**(1-2): 30-38.
Griffith, J. W., C. L. Sokol, et al. (2014). "Chemokines and chemokine receptors: positioning cells for host defense and immunity." Annu Rev Immunol **32**: 659-702.
Groen, E. J. and T. H. Gillingwater (2015). "UBA1: At the Crossroads of Ubiquitin Homeostasis and Neurodegeneration." Trends Mol Med **21**(10): 622-632.
Gunther, K., J. Leier, et al. (2005). "Prediction of lymph node metastasis in colorectal carcinoma by expressionof chemokine receptor CCR7." Int J Cancer **116**(5): 726-733.
Guo, N. and Z. Peng (2013). "MG132, a proteasome inhibitor, induces apoptosis in tumor cells." Asia Pac J Clin Oncol **9**(1): 6-11.
Haghighat, A., S. Mader, et al. (1995). "Repression of cap-dependent translation by 4E-binding protein 1: competition with p220 for binding to eukaryotic initiation factor-4E." EMBO J **14**(22): 5701-5709.
Han, Y. H. and W. H. Park (2010). "MG132, a proteasome inhibitor decreased the growth of Calu-6 lung cancer cells via apoptosis and GSH depletion." Toxicol In Vitro **24**(4): 1237-1242.

Handley, P. M., M. Mueckler, et al. (1991). "Molecular cloning, sequence, and tissue distribution of the human ubiquitin-activating enzyme E1." Proc Natl Acad Sci U S A **88**(1): 258-262.
Hatakeyama, S. and K. I. Nakayama (2003). "U-box proteins as a new family of ubiquitin ligases." Biochem Biophys Res Commun **302**(4): 635-645.
Hatakeyama, S. and K. I. Nakayama (2003). "Ubiquitylation as a quality control system for intracellular proteins." J Biochem **134**(1): 1-8.
Hay, N. and N. Sonenberg (2004). "Upstream and downstream of mTOR." Genes Dev **18**(16): 1926-1945.
He, Q., P. Cheng, et al. (2005). "The COP9 signalosome regulates the Neurospora circadian clock by controlling the stability of the SCFFWD-1 complex." Genes Dev **19**(13): 1518-1531.
Heinemeyer, W., P. C. Ramos, et al. (2004). "The ultimate nanoscale mincer: assembly, structure and active sites of the 20S proteasome core." Cell Mol Life Sci **61**(13): 1562-1578.
Heinzel, K., C. Benz, et al. (2007). "A silent chemokine receptor regulates steady-state leukocyte homing in vivo." Proc Natl Acad Sci U S A **104**(20): 8421-8426.
Herrmann, J., L. O. Lerman, et al. (2007). "Ubiquitin and ubiquitin-like proteins in protein regulation." Circ Res **100**(9): 1276-1291.
Hershko, A. and A. Ciechanover (1998). "The ubiquitin system." Annu Rev Biochem **67**: 425-479.
Hershko, A., E. Eytan, et al. (1982). "Immunochemical analysis of the turnover of ubiquitin-protein conjugates in intact cells. Relationship to the breakdown of abnormal proteins." J Biol Chem **257**(23): 13964-13970.
Hershko, A., D. Ganoth, et al. (1991). "Methylated ubiquitin inhibits cyclin degradation in clam embryo extracts." J Biol Chem **266**(25): 16376-16379.
Hochstrasser, M. (2009). "Origin and function of ubiquitin-like proteins." Nature **458**(7237): 422-429.
Huang, G., A. J. Kaufman, et al. (2011). "SCCRO (DCUN1D1) promotes nuclear translocation and assembly of the neddylation E3 complex." J Biol Chem **286**(12): 10297-10304.
Hughes, D. J., J. J. Wood, et al. (2015). "NEDDylation is essential for Kaposi's sarcoma-associated herpesvirus latency and lytic reactivation and represents a novel anti-KSHV target." PLoS Pathog **11**(3): e1004771.
Hugle, B., J. A. Kleinschmidt, et al. (1983). "The 22 S cylinder particles of Xenopus laevis. II. Immunological characterization and localization of their proteins in tissues and cultured cells." Eur J Cell Biol **32**(1): 157-163.
Inobe, T. and A. Matouschek (2014). "Paradigms of protein degradation by the proteasome." Curr Opin Struct Biol **24**: 156-164.
Iwasaki, A. and R. Medzhitov (2015). "Control of adaptive immunity by the innate immune system." Nat Immunol **16**(4): 343-353.
Jentsch, S., W. Seufert, et al. (1991). "Genetic analysis of the ubiquitin system." Biochim Biophys Acta **1089**(2): 127-139.
Jin, H. S., L. Liao, et al. (2013). "Neddylation pathway regulates T-cell function by targeting an adaptor protein Shc and a protein kinase Erk signaling." Proc Natl Acad Sci U S A **110**(2): 624-629.
Jin, J., T. Cardozo, et al. (2004). "Systematic analysis and nomenclature of mammalian F-box proteins." Genes Dev **18**(21): 2573-2580.
Jin, L., A. Williamson, et al. (2008). "Mechanism of ubiquitin-chain formation by the human anaphase-promoting complex." Cell **133**(4): 653-665.
Jubelin, G., F. Taieb, et al. (2010). "Pathogenic bacteria target NEDD8-conjugated cullins to hijack host-cell signaling pathways." PLoS Pathog **6**(9): e1001128.

Kamitani, T., K. Kito, et al. (1997). "Characterization of NEDD8, a developmentally down-regulated ubiquitin-like protein." J Biol Chem **272**(45): 28557-28562.
Kamura, T., M. N. Conrad, et al. (1999). "The Rbx1 subunit of SCF and VHL E3 ubiquitin ligase activates Rub1 modification of cullins Cdc53 and Cul2." Genes Dev **13**(22): 2928-2933.
Kawakami, T., T. Chiba, et al. (2001). "NEDD8 recruits E2-ubiquitin to SCF E3 ligase." EMBO J **20**(15): 4003-4012.
Kee, Y. and J. M. Huibregtse (2007). "Regulation of catalytic activities of HECT ubiquitin ligases." Biochem Biophys Res Commun **354**(2): 329-333.
Kelner, G. S., J. Kennedy, et al. (1994). "Lymphotactin: a cytokine that represents a new class of chemokine." Science **266**(5189): 1395-1399.
Keuss, M. J., Y. Thomas, et al. (2016). "Characterization of the mammalian family of DCN-type NEDD8 E3 ligases." J Cell Sci **129**(7): 1441-1454.
Kipreos, E. T., L. E. Lander, et al. (1996). "cul-1 is required for cell cycle exit in C. elegans and identifies a novel gene family." Cell **85**(6): 829-839.
Kleinschmidt, J. A., B. Hugle, et al. (1983). "The 22 S cylinder particles of Xenopus laevis. I. Biochemical and electron microscopic characterization." Eur J Cell Biol **32**(1): 143-156.
Kloetzel, P. M. (2004). "The proteasome and MHC class I antigen processing." Biochim Biophys Acta **1695**(1-3): 225-233.
Kohout, T. A. and R. J. Lefkowitz (2003). "Regulation of G Protein-Coupled Receptor Kinases and Arrestins During Receptor Desensitization." Molecular Pharmacology **63**(1): 9-18.
Kohout, T. A., S. L. Nicholas, et al. (2004). "Differential desensitization, receptor phosphorylation, beta-arrestin recruitment, and ERK1/2 activation by the two endogenous ligands for the CC chemokine receptor 7." J Biol Chem **279**(22): 23214-23222.
Komander, D. (2009). "The emerging complexity of protein ubiquitination." Biochem Soc Trans **37**(Pt 5): 937-953.
Konstantinova, I. M., A. S. Tsimokha, et al. (2008). "Role of proteasomes in cellular regulation." Int Rev Cell Mol Biol **267**: 59-124.
Kravtsova-Ivantsiv, Y. and A. Ciechanover (2012). "Non-canonical ubiquitin-based signals for proteasomal degradation." J Cell Sci **125**(Pt 3): 539-548.
Kristariyanto, Y. A., S. A. Abdul Rehman, et al. (2015). "K29-selective ubiquitin binding domain reveals structural basis of specificity and heterotypic nature of k29 polyubiquitin." Mol Cell **58**(1): 83-94.
Krummel, M. F., F. Bartumeus, et al. (2016). "T cell migration, search strategies and mechanisms." Nat Rev Immunol **16**(3): 193-201.
Kumar, S., Y. Yoshida, et al. (1993). "Cloning of a cDNA which encodes a novel ubiquitin-like protein." Biochem Biophys Res Commun **195**(1): 393-399.
Kurihara, L. J., E. Semenova, et al. (2000). "Expression and functional analysis of Uch-L3 during mouse development." Mol Cell Biol **20**(7): 2498-2504.
Kurz, T., Y. C. Chou, et al. (2008). "Dcn1 functions as a scaffold-type E3 ligase for cullin neddylation." Mol Cell **29**(1): 23-35.
Lecker, S. H., A. L. Goldberg, et al. (2006). "Protein degradation by the ubiquitin-proteasome pathway in normal and disease states." J Am Soc Nephrol **17**(7): 1807-1819.
Lee, C., S. Geng, et al. (2017). "Programming and memory dynamics of innate leukocytes during tissue homeostasis and inflammation." J Leukoc Biol **102**(3): 719-726.
Lee, D. H. and A. L. Goldberg (1998). "Proteasome inhibitors: valuable new tools for cell biologists." Trends Cell Biol **8**(10): 397-403.

Lee, J., H. R. Kim, et al. (2012). "Autophagy suppresses interleukin-1beta (IL-1beta) signaling by activation of p62 degradation via lysosomal and proteasomal pathways." J Biol Chem **287**(6): 4033-4040.
Li, L., B. Liu, et al. (2013). "Neddylation pathway regulates the proliferation and survival of macrophages." Biochem Biophys Res Commun **432**(3): 494-498.
Li, S., U. S. Pettersson, et al. (2014). "Interference with glycosaminoglycan-chemokine interactions with a probe to alter leukocyte recruitment and inflammation in vivo." PLoS One **9**(8): e104107.
Li, T., J. Guan, et al. (2014). "RNF168-mediated H2A neddylation antagonizes ubiquitylation of H2A and regulates DNA damage repair." J Cell Sci **127**(Pt 10): 2238-2248.
Li, X. and G. N. Demartino (2009). "Variably modulated gating of the 26S proteasome by ATP and polyubiquitin." Biochem J **421**(3): 397-404.
Liakopoulos, D., G. Doenges, et al. (1998). "A novel protein modification pathway related to the ubiquitin system." EMBO J **17**(8): 2208-2214.
Linghu, B., J. Callis, et al. (2002). "Rub1p processing by Yuh1p is required for wild-type levels of Rub1p conjugation to Cdc53p." Eukaryot Cell **1**(3): 491-494.
Linossi, E. M. and S. E. Nicholson (2012). "The SOCS box-adapting proteins for ubiquitination and proteasomal degradation." IUBMB Life **64**(4): 316-323.
Liu, J., M. Furukawa, et al. (2002). "NEDD8 modification of CUL1 dissociates p120(CAND1), an inhibitor of CUL1-SKP1 binding and SCF ligases." Mol Cell **10**(6): 1511-1518.
Liu, X., J. M. Reitsma, et al. (2018). "Cand1-Mediated Adaptive Exchange Mechanism Enables Variation in F-Box Protein Expression." Mol Cell **69**(5): 773-786 e776.
Lopez-Cotarelo, P., C. Escribano-Diaz, et al. (2015). "A novel MEK-ERK-AMPK signaling axis controls chemokine receptor CCR7-dependent survival in human mature dendritic cells." J Biol Chem **290**(2): 827-840.
Lopez-Cotarelo, P., C. Gomez-Moreira, et al. (2017). "Beyond Chemoattraction: Multifunctionality of Chemokine Receptors in Leukocytes." Trends Immunol **38**(12): 927-941.
Lucas, X. and A. Ciulli (2017). "Recognition of substrate degrons by E3 ubiquitin ligases and modulation by small-molecule mimicry strategies." Curr Opin Struct Biol **44**: 101-110.
Luster, A. D. (1998). "Chemokines--chemotactic cytokines that mediate inflammation." N Engl J Med **338**(7): 436-445.
Ma, T., Y. Chen, et al. (2013). "RNF111-dependent neddylation activates DNA damage-induced ubiquitination." Mol Cell **49**(5): 897-907.
Maldonado, R. A. and U. H. von Andrian (2010). "How tolerogenic dendritic cells induce regulatory T cells." Adv Immunol **108**: 111-165.
Marsland, B. J., P. Battig, et al. (2005). "CCL19 and CCL21 induce a potent proinflammatory differentiation program in licensed dendritic cells." Immunity **22**(4): 493-505.
Mashino, K., N. Sadanaga, et al. (2002). "Expression of chemokine receptor CCR7 is associated with lymph node metastasis of gastric carcinoma." Cancer Res **62**(10): 2937-2941.
Mathewson, N., T. Toubai, et al. (2013). "Neddylation plays an important role in the regulation of murine and human dendritic cell function." Blood **122**(12): 2062-2073.
Matsuo, Y., H. Kishimoto, et al. (2011). "Nuclear protein quality is regulated by the ubiquitin-proteasome system through the activity of Ubc4 and San1 in fission yeast." J Biol Chem **286**(15): 13775-13790.

McCudden, C. R., M. D. Hains, et al. (2005). "G-protein signaling: back to the future." Cell Mol Life Sci **62**(5): 551-577.
McDowell, G. S. and A. Philpott (2013). "Non-canonical ubiquitylation: mechanisms and consequences." Int J Biochem Cell Biol **45**(8): 1833-1842.
Medzhitov, R. (2001). "Toll-like receptors and innate immunity." Nat Rev Immunol **1**(2): 135-145.
Mellacheruvu, D., Z. Wright, et al. (2013). "The CRAPome: a contaminant repository for affinity purification-mass spectrometry data." Nat Methods **10**(8): 730-736.
Mellman, I. (2013). "Dendritic cells: master regulators of the immune response." Cancer Immunol Res **1**(3): 145-149.
Mempel, T. R., S. E. Henrickson, et al. (2004). "T-cell priming by dendritic cells in lymph nodes occurs in three distinct phases." Nature **427**(6970): 154-159.
Merlet, J., J. Burger, et al. (2009). "Regulation of cullin-RING E3 ubiquitin-ligases by neddylation and dimerization." Cell Mol Life Sci **66**(11-12): 1924-1938.
Metzger, M. B., V. A. Hristova, et al. (2012). "HECT and RING finger families of E3 ubiquitin ligases at a glance." J Cell Sci **125**(Pt 3): 531-537.
Metzger, M. B., J. N. Pruneda, et al. (2014). "RING-type E3 ligases: master manipulators of E2 ubiquitin-conjugating enzymes and ubiquitination." Biochim Biophys Acta **1843**(1): 47-60.
Meyer, H. J. and M. Rape (2014). "Enhanced protein degradation by branched ubiquitin chains." Cell **157**(4): 910-921.
Morimoto, M., T. Nishida, et al. (2003). "Nedd8-modification of Cul1 is promoted by Roc1 as a Nedd8-E3 ligase and regulates its stability." Biochem Biophys Res Commun **301**(2): 392-398.
Muller, A., E. Sonkoly, et al. (2006). "Chemokine receptors in head and neck cancer: association with metastatic spread and regulation during chemotherapy." Int J Cancer **118**(9): 2147-2157.
Murata, S., H. Yashiroda, et al. (2009). "Molecular mechanisms of proteasome assembly." Nat Rev Mol Cell Biol **10**(2): 104-115.
Nakano, H. and M. D. Gunn (2001). "Gene duplications at the chemokine locus on mouse chromosome 4: multiple strain-specific haplotypes and the deletion of secondary lymphoid-organ chemokine and EBI-1 ligand chemokine genes in the plt mutation." J Immunol **166**(1): 361-369.
Nakayama, K. I. and K. Nakayama (2006). "Ubiquitin ligases: cell-cycle control and cancer." Nat Rev Cancer **6**(5): 369-381.
Nawrocki, S. T., P. Griffin, et al. (2012). "MLN4924: a novel first-in-class inhibitor of NEDD8-activating enzyme for cancer therapy." Expert Opin Investig Drugs **21**(10): 1563-1573.
Nethe, M. and P. L. Hordijk (2010). "The role of ubiquitylation and degradation in RhoGTPase signalling." J Cell Sci **123**(Pt 23): 4011-4018.
Neutzner, M. and A. Neutzner (2012). "Enzymes of ubiquitination and deubiquitination." Essays Biochem **52**: 37-50.
Nibbs, R. J., D. S. Gilchrist, et al. (2007). "The atypical chemokine receptor D6 suppresses the development of chemically induced skin tumors." J Clin Invest **117**(7): 1884-1892.
Nibbs, R. J. and G. J. Graham (2013). "Immune regulation by atypical chemokine receptors." Nat Rev Immunol **13**(11): 815-829.
O'Hayre, M., C. L. Salanga, et al. (2008). "Chemokines and cancer: migration, intracellular signalling and intercellular communication in the microenvironment." Biochem J **409**(3): 635-649.

Ohtake, F., H. Tsuchiya, et al. (2018). "K63 ubiquitylation triggers proteasomal degradation by seeding branched ubiquitin chains." Proc Natl Acad Sci U S A **115**(7): E1401-E1408.
Omura, S., T. Fujimoto, et al. (1991). "Lactacystin, a novel microbial metabolite, induces neuritogenesis of neuroblastoma cells." J Antibiot (Tokyo) **44**(1): 113-116.
Onel, M., F. Sumbul, et al. (2017). "Cullin neddylation may allosterically tune polyubiquitin chain length and topology." Biochem J **474**(5): 781-795.
Oved, S., Y. Mosesson, et al. (2006). "Conjugation to Nedd8 instigates ubiquitylation and down-regulation of activated receptor tyrosine kinases." J Biol Chem **281**(31): 21640-21651.
Paiva, C., J. C. Godbersen, et al. (2017). "Pevonedistat, a Nedd8-activating enzyme inhibitor, sensitizes neoplastic B-cells to death receptor-mediated apoptosis." Oncotarget.
Paramore, A. and S. Frantz (2003). "Bortezomib." Nat Rev Drug Discov **2**(8): 611-612.
Pascual, J., M. Martinez-Yamout, et al. (2000). "Structure of the PHD zinc finger from human Williams-Beuren syndrome transcription factor." J Mol Biol **304**(5): 723-729.
Pathan, M., S. Keerthikumar, et al. (2015). "FunRich: An open access standalone functional enrichment and interaction network analysis tool." Proteomics **15**(15): 2597-2601.
Paul, S. (2008). "Dysfunction of the ubiquitin-proteasome system in multiple disease conditions: therapeutic approaches." Bioessays **30**(11-12): 1172-1184.
Peth, A., H. C. Besche, et al. (2009). "Ubiquitinated proteins activate the proteasome by binding to Usp14/Ubp6, which causes 20S gate opening." Mol Cell **36**(5): 794-804.
Petroski, M. D. and R. J. Deshaies (2005). "Function and regulation of cullin-RING ubiquitin ligases." Nat Rev Mol Cell Biol **6**(1): 9-20.
Petroski, M. D. and R. J. Deshaies (2005). "Mechanism of lysine 48-linked ubiquitin-chain synthesis by the cullin-RING ubiquitin-ligase complex SCF-Cdc34." Cell **123**(6): 1107-1120.
Picco, G., C. Petti, et al. (2017). "Efficacy of NEDD8 Pathway Inhibition in Preclinical Models of Poorly Differentiated, Clinically Aggressive Colorectal Cancer." J Natl Cancer Inst **109**(2).
Pickart, C. M. and M. J. Eddins (2004). "Ubiquitin: structures, functions, mechanisms." Biochim Biophys Acta **1695**(1-3): 55-72.
Pickart, C. M. and D. Fushman (2004). "Polyubiquitin chains: polymeric protein signals." Curr Opin Chem Biol **8**(6): 610-616.
Pines, J. and C. Lindon (2005). "Proteolysis: anytime, any place, anywhere?" Nat Cell Biol **7**(8): 731-735.
Platt, C. D., J. K. Ma, et al. (2010). "Mature dendritic cells use endocytic receptors to capture and present antigens." Proc Natl Acad Sci U S A **107**(9): 4287-4292.
Qiang, W., F. Sui, et al. (2017). "Proteasome inhibitor MG132 induces thyroid cancer cell apoptosis by modulating the activity of transcription factor FOXO3a." Endocrine **56**(1): 98-108.
Qu, C., N. S. Brinck-Jensen, et al. (2014). "Monocyte-derived dendritic cells: targets as potent antigen-presenting cells for the design of vaccines against infectious diseases." Int J Infect Dis **19**: 1-5.
Rabut, G. and M. Peter (2008). "Function and regulation of protein neddylation. 'Protein modifications: beyond the usual suspects' review series." EMBO Rep **9**(10): 969-976.
Ravid, T. and M. Hochstrasser (2008). "Diversity of degradation signals in the ubiquitin-proteasome system." Nat Rev Mol Cell Biol **9**(9): 679-690.

Read, M. A., J. E. Brownell, et al. (2000). "Nedd8 modification of cul-1 activates SCF(beta(TrCP))-dependent ubiquitination of IkappaBalpha." Mol Cell Biol **20**(7): 2326-2333.
Reid, D. W. and C. V. Nicchitta (2012). "The enduring enigma of nuclear translation." J Cell Biol **197**(1): 7-9.
Reitsma, J. M., X. Liu, et al. (2017). "Composition and Regulation of the Cellular Repertoire of SCF Ubiquitin Ligases." Cell **171**(6): 1326-1339 e1314.
Renaudin, X., J. H. Guervilly, et al. (2014). "Proteomic analysis reveals a FANCA-modulated neddylation pathway involved in CXCR5 membrane targeting and cell mobility." J Cell Sci **127**(Pt 16): 3546-3554.
Rieser, E., S. M. Cordier, et al. (2013). "Linear ubiquitination: a newly discovered regulator of cell signalling." Trends Biochem Sci **38**(2): 94-102.
Riol-Blanco, L., N. Sanchez-Sanchez, et al. (2005). "The chemokine receptor CCR7 activates in dendritic cells two signaling modules that independently regulate chemotaxis and migratory speed." J Immunol **174**(7): 4070-4080.
Rock, K. L., C. Gramm, et al. (1994). "Inhibitors of the proteasome block the degradation of most cell proteins and the generation of peptides presented on MHC class I molecules." Cell **78**(5): 761-771.
Rockel, T. D., D. Stuhlmann, et al. (2005). "Proteasomes degrade proteins in focal subdomains of the human cell nucleus." J Cell Sci **118**(Pt 22): 5231-5242.
Rollins, B. J. (1997). "Chemokines." Blood **90**(3): 909-928.
Rostene, W., P. Kitabgi, et al. (2007). "Chemokines: a new class of neuromodulator?" Nat Rev Neurosci **8**(11): 895-903.
Sakamoto, K. M. (2002). "Ubiquitin-dependent proteolysis: its role in human diseases and the design of therapeutic strategies." Mol Genet Metab **77**(1-2): 44-56.
Sakata, E., Y. Yamaguchi, et al. (2007). "Direct interactions between NEDD8 and ubiquitin E2 conjugating enzymes upregulate cullin-based E3 ligase activity." Nat Struct Mol Biol **14**(2): 167-168.
Sallusto, F., B. Palermo, et al. (1999). "Distinct patterns and kinetics of chemokine production regulate dendritic cell function." Eur J Immunol **29**(5): 1617-1625.
Sanchez-Sanchez, N., L. Riol-Blanco, et al. (2004). "Chemokine receptor CCR7 induces intracellular signaling that inhibits apoptosis of mature dendritic cells." Blood **104**(3): 619-625.
Sanchez-Sanchez, N., L. Riol-Blanco, et al. (2006). "The multiple personalities of the chemokine receptor CCR7 in dendritic cells." J Immunol **176**(9): 5153-5159.
Sarikas, A., T. Hartmann, et al. (2011). "The cullin protein family." Genome Biol **12**(4): 220.
Schaeuble, K., M. A. Hauser, et al. (2012). "Ubiquitylation of the chemokine receptor CCR7 enables efficient receptor recycling and cell migration." J Cell Sci **125**(Pt 19): 4463-4474.
Schmaler, T. and W. Dubiel (2010). "Control of Deneddylation by the COP9 Signalosome." Subcell Biochem **54**: 57-68.
Schmidt, M. and D. Finley (2014). "Regulation of proteasome activity in health and disease." Biochim Biophys Acta **1843**(1): 13-25.
Schneider, M. A., J. G. Meingassner, et al. (2007). "CCR7 is required for the in vivo function of CD4+ CD25+ regulatory T cells." J Exp Med **204**(4): 735-745.
Shibata, Y. and R. I. Morimoto (2014). "How the nucleus copes with proteotoxic stress." Curr Biol **24**(10): R463-474.
Skaar, J. R., J. K. Pagan, et al. (2013). "Mechanisms and function of substrate recruitment by F-box proteins." Nat Rev Mol Cell Biol **14**(6): 369-381.
Skaar, J. R., J. K. Pagan, et al. (2014). "SCF ubiquitin ligase-targeted therapies." Nat Rev Drug Discov **13**(12): 889-903.

Soderberg, O., M. Gullberg, et al. (2006). "Direct observation of individual endogenous protein complexes in situ by proximity ligation." Nat Methods **3**(12): 995-1000.
Soucy, T. A., L. R. Dick, et al. (2010). "The NEDD8 Conjugation Pathway and Its Relevance in Cancer Biology and Therapy." Genes Cancer **1**(7): 708-716.
Soucy, T. A., P. G. Smith, et al. (2009). "An inhibitor of NEDD8-activating enzyme as a new approach to treat cancer." Nature **458**(7239): 732-736.
Soucy, T. A., P. G. Smith, et al. (2009). "Targeting NEDD8-activated cullin-RING ligases for the treatment of cancer." Clin Cancer Res **15**(12): 3912-3916.
Staropoli, J. F., C. McDermott, et al. (2003). "Parkin is a component of an SCF-like ubiquitin ligase complex and protects postmitotic neurons from kainate excitotoxicity." Neuron **37**(5): 735-749.
Strohmaier, H., C. H. Spruck, et al. (2001). "Human F-box protein hCdc4 targets cyclin E for proteolysis and is mutated in a breast cancer cell line." Nature **413**(6853): 316-322.
Suresh, B., S. Ramakrishna, et al. (2010). "K48- and K63-linked polyubiquitination of deubiquitinating enzyme USP44." Cell Biol Int **34**(8): 799-808.
Szklarczyk, D., A. Franceschini, et al. (2011). "The STRING database in 2011: functional interaction networks of proteins, globally integrated and scored." Nucleic Acids Res **39**(Database issue): D561-568.
Takanami, I. (2003). "Overexpression of CCR7 mRNA in nonsmall cell lung cancer: correlation with lymph node metastasis." Int J Cancer **105**(2): 186-189.
Takeuchi, H., A. Fujimoto, et al. (2004). "CCL21 chemokine regulates chemokine receptor CCR7 bearing malignant melanoma cells." Clin Cancer Res **10**(7): 2351-2358.
Tanaka, K. (2009). "The proteasome: overview of structure and functions." Proc Jpn Acad Ser B Phys Biol Sci **85**(1): 12-36.
Tang, X., S. Orlicky, et al. (2007). "Suprafacial orientation of the SCFCdc4 dimer accommodates multiple geometries for substrate ubiquitination." Cell **129**(6): 1165-1176.
Thrower, J. S., L. Hoffman, et al. (2000). "Recognition of the polyubiquitin proteolytic signal." EMBO J **19**(1): 94-102.
Torres-Bacete, J., C. Delgado-Martin, et al. (2015). "The Mammalian Sterile 20-like 1 Kinase Controls Selective CCR7-Dependent Functions in Human Dendritic Cells." J Immunol **195**(3): 973-981.
Tu, Y., C. Chen, et al. (2012). "The Ubiquitin Proteasome Pathway (UPP) in the regulation of cell cycle control and DNA damage repair and its implication in tumorigenesis." Int J Clin Exp Pathol **5**(8): 726-738.
Ulvmar, M. H., E. Hub, et al. (2011). "Atypical chemokine receptors." Exp Cell Res **317**(5): 556-568.
Valimberti, I., M. Tiberti, et al. (2015). "E2 superfamily of ubiquitin-conjugating enzymes: constitutively active or activated through phosphorylation in the catalytic cleft." Sci Rep **5**: 14849.
van der Veen, A. G. and H. L. Ploegh (2012). "Ubiquitin-like proteins." Annu Rev Biochem **81**: 323-357.
Vassileva, G., H. Soto, et al. (1999). "The reduced expression of 6Ckine in the plt mouse results from the deletion of one of two 6Ckine genes." J Exp Med **190**(8): 1183-1188.
Vogler, O., J. M. Barcelo, et al. (2008). "Membrane interactions of G proteins and other related proteins." Biochim Biophys Acta **1778**(7-8): 1640-1652.
von Mikecz, A. (2006). "The nuclear ubiquitin-proteasome system." J Cell Sci **119**(Pt 10): 1977-1984.

Wada, H., K. Kito, et al. (1998). "Cleavage of the C-terminus of NEDD8 by UCH-L3." Biochem Biophys Res Commun **251**(3): 688-692.
Wang, Y., Z. Luo, et al. (2015). "Targeting protein neddylation with an NEDD8-activating enzyme inhibitor MLN4924 induced apoptosis or senescence in human lymphoma cells." Cancer Biol Ther **16**(3): 420-429.
Wang, Z., P. Liu, et al. (2014). "Roles of F-box proteins in cancer." Nat Rev Cancer **14**(4): 233-247.
Weber, M., R. Hauschild, et al. (2013). "Interstitial dendritic cell guidance by haptotactic chemokine gradients." Science **339**(6117): 328-332.
Wee, S., R. K. Geyer, et al. (2005). "CSN facilitates Cullin-RING ubiquitin ligase function by counteracting autocatalytic adapter instability." Nat Cell Biol **7**(4): 387-391.
Wei, D. and Y. Sun (2010). "Small RING Finger Proteins RBX1 and RBX2 of SCF E3 Ubiquitin Ligases: The Role in Cancer and as Cancer Targets." Genes Cancer **1**(7): 700-707.
Welcker, M. and B. E. Clurman (2008). "FBW7 ubiquitin ligase: a tumour suppressor at the crossroads of cell division, growth and differentiation." Nat Rev Cancer **8**(2): 83-93.
Willems, A. R., S. Lanker, et al. (1996). "Cdc53 targets phosphorylated G1 cyclins for degradation by the ubiquitin proteolytic pathway." Cell **86**(3): 453-463.
Winston, J. T., D. M. Koepp, et al. (1999). "A family of mammalian F-box proteins." Curr Biol **9**(20): 1180-1182.
Winston, J. T., P. Strack, et al. (1999). "The SCFbeta-TRCP-ubiquitin ligase complex associates specifically with phosphorylated destruction motifs in IkappaBalpha and beta-catenin and stimulates IkappaBalpha ubiquitination in vitro." Genes Dev **13**(3): 270-283.
Wojcik, C. and G. N. DeMartino (2003). "Intracellular localization of proteasomes." Int J Biochem Cell Biol **35**(5): 579-589.
Wong, K. M., L. N. Micel, et al. (2017). "Targeting the protein ubiquitination machinery in melanoma by the NEDD8-activating enzyme inhibitor pevonedistat (MLN4924)." Invest New Drugs **35**(1): 11-25.
Yanagawa, Y. and K. Onoe (2002). "CCL19 induces rapid dendritic extension of murine dendritic cells." Blood **100**(6): 1948-1956.
Yanagawa, Y. and K. Onoe (2003). "CCR7 ligands induce rapid endocytosis in mature dendritic cells with concomitant up-regulation of Cdc42 and Rac activities." Blood **101**(12): 4923-4929.
Yang, X., J. Zhou, et al. (2007). "Structural basis for the function of DCN-1 in protein Neddylation." J Biol Chem **282**(34): 24490-24494.
Yewdell, J. W. and A. David (2013). "Nuclear translation for immunosurveillance." Proc Natl Acad Sci U S A **110**(44): 17612-17613.
Yi, J. J. and M. D. Ehlers (2007). "Emerging roles for ubiquitin and protein degradation in neuronal function." Pharmacol Rev **59**(1): 14-39.
Yue, Y., Y. Ma, et al. (2018). "Catalytic Mechanism of the Ubiquitin-Like NEDD8 Transfer in RING E3-E2 approximately NEDD8-Target Complex from QM/MM Free Energy Simulations." J Chem Inf Model.
Zhao, Y., M. A. Morgan, et al. (2014). "Targeting Neddylation pathways to inactivate cullin-RING ligases for anticancer therapy." Antioxid Redox Signal **21**(17): 2383-2400.
Zhao, Y. and Y. Sun (2013). "Cullin-RING Ligases as attractive anti-cancer targets." Curr Pharm Des **19**(18): 3215-3225.
Zheng, J., X. Yang, et al. (2002). "CAND1 binds to unneddylated CUL1 and regulates the formation of SCF ubiquitin E3 ligase complex." Mol Cell **10**(6): 1519-1526.

Zheng, N., B. A. Schulman, et al. (2002). "Structure of the Cul1-Rbx1-Skp1-F boxSkp2 SCF ubiquitin ligase complex." Nature **416**(6882): 703-709.
Zheng, N., Q. Zhou, et al. (2016). "Recent advances in SCF ubiquitin ligase complex: Clinical implications." Biochim Biophys Acta **1866**(1): 12-22.
Zhou, C., S. Wee, et al. (2003). "Fission yeast COP9/signalosome suppresses cullin activity through recruitment of the deubiquitylating enzyme Ubp12p." Mol Cell **11**(4): 927-938.
Zlotnik, A. and O. Yoshie (2012). "The chemokine superfamily revisited." Immunity **36**(5): 705-716.

ANEXO

Publicaciones relacionadas con el trabajo de esta tesis:

- López-Cotarelo P*, **Gómez-Moreira C***, Criado-García O*, Sánchez L, Rodríguez-Fernández JL. Beyond Chemoattraction: Multifunctionality of Chemokine Receptors in Leukocytes. Trends Immunol. 2017 Dec;38(12):927-941. Epub 2017 Sep 19. Review. * Contributed similarly to the study.

- Torres-Bacete J, Delgado-Martín C, **Gómez-Moreira C**, Simizu S, Rodríguez-Fernández JL. The Mammalian Sterile 20-like 1 Kinase Controls Selective CCR7-Dependent Functions in Human Dendritic Cells. J Immunol. 2015 Aug 1; 195 (3):973-81.

- López-Cotarelo P, Escribano-Díaz C, González-Bethencourt IL, **Gómez-Moreira C**, Deguiz ML, Torres-Bacete J, Gómez-Cabañas L, Fernández-Barrera J, Delgado-Martín C, Mellado M, Regueiro JR, Miranda-Carús ME, Rodríguez-Fernández JL. A novel MEK-ERK-AMPK signaling axis controls chemokine receptor CCR7-dependent survival in human mature dendritic cells. J Biol Chem. 2015 Jan 9; 290 (2):827-40.

Colaboraciones

- Gómez-SanMiguel AB*, **Gomez-Moreira C***, Nieto-Bona MP, Fernández-Galaz C, Villanúa MÁ, Martín AI, López-Calderón A. Formoterol decreases muscle wasting as well as inflammation in the rat model of rheumatoid arthritis. Am J Physiol Endocrinol Metab. 2016 Jun 1; 310 (11): E925-37. *Contributed similarly to the study.

- Martín AI, Gómez-SanMiguel AB, **Gómez-Moreira C**, Villanúa MÁ, López-Calderón A. αMSH blunts endotoxin-induced MuRF1 and atrogin-1 upregulation in skeletal muscle by modulating NF-κB and Akt/FoxO1 pathway. Mediators Inflamm. 2014; 2014:179368.

- Martin AI, Nieto-Bona MP, Castillero E, Fernandez-Galaz C, Lopez-Menduina M, Gomez-Sanmiguel AB, **Gomez-Moreira C**, Villanua MA, Lopez-Calderon A. Effect of cyclooxygenase-2 inhibition by meloxicam, on atrogin-1 and myogenic regulatory factors in skeletal muscle of rats injected with endotoxin. J Physiol Pharmacol. 2012 Dec; 63(6):649-59.

Trends in Immunology

CellPress
REVIEWS

Review

Beyond Chemoattraction: Multifunctionality of Chemokine Receptors in Leukocytes

Pilar López-Cotarelo,[1,3] Carolina Gómez-Moreira,[1,3] Olga Criado-García,[1,3] Lucas Sánchez,[2] and José Luis Rodríguez-Fernández[1,*]

The word chemokine is a combination of the words chemotactic and cytokine, in other words cytokines that promote chemotaxis. Hence, the term chemokine receptor refers largely to the ability to regulate chemoattraction. However, these receptors can modulate additional leukocyte functions, as exemplified by the case of CCR7 which, apart from chemotaxis, regulates survival, migratory speed, endocytosis, differentiation and cytoarchitecture. We present evidence highlighting that multifunctionality is a common feature of chemokine receptors. Based on the activities that they regulate, we suggest that chemokine receptors can be classified into inflammatory (which control both inflammatory and homeostatic functions) and homeostatic families. The information accrued also suggests that the non-chemotactic functions controlled by chemokine receptors may contribute to optimizing leukocyte functioning under normal physiological conditions and during inflammation.

Trends

Chemoattraction controlled by chemokine receptors is crucial for the correct positioning of leukocytes during the immune response.

Most studies on chemokine receptors have focused on their ability to regulate chemoattraction, but there is accumulating evidence that chemokines receptors regulate additional functions in leukocytes.

Gaining information on these non-chemoattractive functions may provide a better understanding of the role of these receptors in the immune system and facilitate the development of immunomodulatory tools.

'What's in a name? That which we call a rose by any other name would smell as sweet.'
Romeo and Juliet (II, ii, 1–2)

Chemokine Receptors: What's in a Name?

Chemokines constitute a large family of peptides that are characterized by their relatively high degree of similarity in their amino acid sequences, small molecular weights, and the presence of cysteines at conserved positions resulting in a characteristic 3D structure [1]. A common function for this family of proteins emerged in 1987 when it was found that interleukin-8 (IL-8, later renamed CXCL8) displayed potent **chemoattractive** (see Glossary) activity for neutrophils, leading to the groundbreaking discovery that most members of this family of molecules promote directional **migration** [2]. In 1992, considering the high number of these ligands that were able to attract leukocytes, they were officially called chemokines, a combination of the words 'chemotactic' and 'cytokine', i.e., cytokines that promote **chemotaxis**. Studies on IL-8 showed very early that chemokines are able to regulate several functions in leukocytes in addition to chemotaxis, including respiratory burst, cell shape changes, and exocytosis [3]. However, soon the field focused on chemotaxis, a function that is crucial for the control of the positioning of leukocytes during the immune response. In this regard, most work performed on chemokine receptors has focused on their ability to control chemotaxis. It could be that the

[1]Molecular Microbiology and Infection Biology Department, Centro de Investigaciones Biológicas, Consejo Superior de Investigaciones Científicas, Madrid, Spain
[2]Cellular and Molecular Biology Department, Centro de Investigaciones Biológicas, Consejo Superior de Investigaciones Científicas, Madrid, Spain
[3]Equal first authors

*Correspondence: rodrifer@cib.csic.es (J.L. Rodríguez-Fernández).

The Mammalian Sterile 20–like 1 Kinase Controls Selective CCR7-Dependent Functions in Human Dendritic Cells

Jesús Torres-Bacete,* Cristina Delgado-Martín,* Carolina Gómez-Moreira,* Siro Simizu,[†,1] and José Luis Rodríguez-Fernández*

The chemokine receptor CCR7 directs mature dendritic cells (mDCs) to the lymph nodes where these cells control the initiation of the immune response. CCR7 regulates chemotaxis, endocytosis, survival, migratory speed, and cytoarchitecture in mDCs. The molecular mechanisms used by CCR7 to regulate these functions in mDCs are not completely understood. The mammalian sterile 20–like 1 kinase (Mst1) plays a proapoptotic role under stress conditions; however, recently, it has been shown that Mst1 can also control homeostatic cell functions under normal conditions. In this study, we show that stimulation of CCR7 in mDCs induces $G_{\alpha i}$-dependent activation of Mst1, suggesting the involvement of this kinase in the control of CCR7-dependent functions. Analysis of the mDCs in which Mst1 expression levels were reduced with small interfering RNA shows that this kinase mediates CCR7-dependent effects on cytoarchitecture, endocytosis and migratory speed but not on chemotaxis or survival. In line with these results, biochemical analysis indicates that Mst1 does not control key signaling regulators of CCR7-dependent chemotaxis or survival. In contrast, Mst1 regulates downstream of CCR7 and, of note, independently of $G_{\alpha 13}$, the RhoA pathway. Reduction of Mst1 inhibits CCR7-dependent phosphorylation of downstream targets of RhoA, including cofilin, myosin L chain, and myosin L chain phosphatase. Consistent with the role of the latter molecules as modulators of the actin cytoskeleton, mDCs with reduced Mst1 also displayed a dramatic reduction in actin barbed-end formation that could not be recovered by stimulating CCR7. The results indicate that the kinase Mst1 controls selective CCR7-dependent functions in human mDCs. ***The Journal of Immunology*****, 2015, 195: 973–981.**

Mature dendritic cells (mDCs) play a key role in the initiation of the immune response (1). These cells express the chemokine receptor CCR7, which directs them to the lymph nodes (LNs), where they present Ags to naive T cells (2). In addition to chemotaxis, CCR7 controls in mDCs several functions, including cytoarchitecture, migratory speed, endocytosis, and survival (2–8), which contribute to the efficient functioning of these cells during the adaptive immune response (3, 9). The adequate functioning of CCR7 in mDCs is necessary to elicit an efficient immune response. Therefore, it is crucial to understand the mechanisms used by this receptor to regulate its different functions in these cells (2, 9–11). Recent studies suggest that CCR7-dependent functions can be controlled in mDCs through the regulation of function-specific signaling modules that display some degree of independence (2). In this regard, before we have shown that CCR7 uses the kinase Akt to regulate survival (2, 3, 5), the kinases Mek1/2–Erk1/2 to control chemotaxis (2, 4), and the axis RhoA–cofilin to regulate migratory speed (2, 4).

The active form of the small GTPase RhoA (RhoA–GTP) regulates actin organization, through its downstream target, the Rho-associated coiled-coil–containing protein kinase (ROCK). This serine/threonine kinase induces activation of LIM kinase, which phosphorylates and inhibits cofilin, an actin-binding protein with severing and depolymerizing activities (12, 13). Active cofilin severs actin fibers resulting in the generation of free barbed ends. At these sites takes place the assembly of actin filaments, which drive membrane protrusions required for cell migration and other actin-dependent processes (12, 13). LIM kinase–mediated phosphorylation inhibits the actin-binding activity of cofilin, resulting in more stable F-actin filaments and inhibition of actin-free barbed formation (12, 13). Apart from controlling cofilin activity, ROCK also promotes actin filament contraction through two alternative mechanisms. First, by phosphorylating/activating the myosin L chain (MLC) (12, 14) and, second, through the phosphorylation of myosin phosphatase target subunit 1 (MYPT1), the regulatory/myosin binding subunit of the MLCP, the enzyme that dephosphorylates MLC, resulting in the inhibition of this phosphatase (12, 15). The net result of this process is an increase in the phosphorylation of the MLC, which leads to an increase in cross-bridge cycling and the rate of tension development.

The mammalian sterile 20 (Ste20)–like kinase 1 (Mst1) is a serine–threonine kinase included in the germinal center kinase

*Departamento de Microbiología Molecular y Biología de las Infecciones, Centro de Investigaciones Biológicas, Consejo Superior de Investigaciones Científicas, 28040 Madrid, Spain; and [†]Chemical Biology Department, RIKEN Advanced Science Institute, 230-0045 Kanagawa, Japan

[1]Current address: Department of Applied Chemistry, Faculty of Science and Technology, Keio University, Yokohama, Japan.

Received for publication August 5, 2014. Accepted for publication May 25, 2015.

This work was partially supported by Ministerio de Ciencia e Innovación Grant SAF2008-01468, Ministerio de Economía y Competitividad Grants SAF2011-23890 and SAF2014-53151-R, "Redes Temáticas de Investigación Cooperativa en Salud" Program/Instituto de Salud Carlos III (Red de Inflamación y Enfermedades Reumáticas [RIER]) Grant RD08/0075, and Consejería de Educación y Empleo from Comunidad de Madrid Grant (Raphyme) S2010/BMD-2350. J.T.-B. was supported by a Junta de Ampliación de Estudios Doctores contract conferred by the Consejo Superior de Investigaciones Cientificas, which is cofinanced by the European Social Fund. C.D.-M. was partially supported by a Formación de Personal Investigador Fellowship, conferred by the Ministerio de Educación y Ciencia (Spain) and by a contract associated with Grant RD08/0075 (RIER). C.G.-M. was supported by a contract associated with Grant Raphyme S2010/BMD-2350 (Consejería de Educación y Empleo, Comunidad de Madrid).

Address correspondence and reprint requests to Dr. José Luis Rodríguez-Fernández, Centro de Investigaciones Biológicas, Consejo Superior de Investigaciones Científicas, Calle de Ramiro de Maeztu 9, 28040 Madrid, Spain. E-mail address: rodrifer@cib.csic.es

The online version of this article contains supplemental material.

Abbreviations used in this article: DC, dendritic cell; mDC, mature DC; MLC, myosin L chain; MLCP, MLC phosphatase; Mst1, mammalian sterile 20–like kinase 1; MYPT1, myosin phosphatase target subunit 1; PTX, pertussis toxin; ROCK, Rho-associated coiled-coil–containing protein kinase; siRNA, small interfering RNA; Ste20, sterile 20.

group II of proteins, a family of MAPK-related kinases that are homologous to the yeast Ste20 kinase (16, 17). Under stress conditions, Mst1 plays proapoptotic roles in multiple cells types (18, 19). Recently, it has been shown that under homeostatic conditions Mst1 can regulate several additional cell functions in lymphocytes, including adhesion, proliferation, cell morphology, and chemotaxis (20–24). The studies on nonapoptotic functions of Mst1 have focused largely on lymphocytes, and there is no information on other leukocytes (25). These studies are important to define the functions of this kinase in the immune system. We have analyzed the involvement of Mst1 in the control of CCR7-mediated functions in human mDCs and found differences in the role played by Mst1 in these cells compared with lymphocytes. Our results indicate that CCR7 uses in mDCs Mst1 to regulate endocytosis, cytoarchitecture, and migratory speed but not chemotaxis or survival. To our knowledge, this is the first published study on the role of Mst1 in DCs. The information obtained can be useful to develop strategies for efficient modulation of the functions of CCR7 during the immune response.

Materials and Methods

Reagents and materials

Fibronectin, polyornithine, LY294002, pertussis toxin, Hoechst 33342, and FITC–phalloidin were from Sigma-Aldrich. Biotin–G-actin was from Cytoskeleton (Denver, CO). CCL19 and CCL21 were obtained from PeproTech (London, U.K.). FITC-conjugated anti-biotin Ab was from Jackson ImmunoResearch Laboratories. Akti-1/2 and UO126 were from Calbiochem (Nottingham, U.K.). The rabbit polyclonals anti–phospho-Akt (S473), anti–phospho-Erk1/2 (T202/Y204), and anti–phospho-myosin L chain 2 (T18/S19) and the rabbit monoclonals anti–phospho-Mek1/2 (S217/221) and anti–phospho-Mst1 (T183) were from Cell Signaling Technology (Beverly, MA). The mouse monoclonal anti–Dock-8, the goat polyclonal anti-Mst2, the rabbit polyclonals anti–Erk-2 (C14), anti–phospho-MYPT1 (T853), anti–phospho-cofilin1 (S3), and the mouse monoclonals anti-RhoA and anti–β-actin were from Santa Cruz Biotechnology (Santa Cruz, CA). The rabbit monoclonal recognizing Mst1 and phospho-Mst1 (T183)/Mst2 (T180) were from Epitomics (Burlingame, CA).

Cells and culture conditions

Human PBMCs were isolated from buffy coats from normal donors over a Lymphoprep (Nycomed) and monocyte induced to differentiate to DCs by adding GM-CSF and IL-4 for 7 d as described previously (3–5, 26, 27). Briefly, monocytes were resuspended at 0.5–1 $\times$ 10^6 cells/ml and cultured in complete medium (RPMI 1640 [Life Technologies BRL; Life Technologies, Paisley, U.K.]) containing 10% heat-inactivated FBS, including GM-CSF (1000 U/ml) and IL-4 (1000 U/ml). Cells were cultured for 7–8 d, with cytokine addition every second day to obtain a population of immature DCs ($CD14^{low}$, $CD83^-$, $CD1a^+$, and $HLA\text{-}DR^+$). GM-CSF, IL-4, and 50 ng/ml TNF-α were added to the cells for an additional 72-h period to induce their maturation. Analysis by flow cytometry showed that the treatment yielded a homogeneous population of mDCs ($CD1a^+$, $DC\text{-}SIGN^+$, $CD14^{low/-}$, $HLA\text{-}DR^{high}$, $CD83^+$, and $CCR7^+$ expressing cells).

Rho activity

DCs (5 $\times$ 10^6 cells) were dissolved in Rho-lysis buffer (25 mM HEPES [pH 7.5], 150 mM NaCl, 1% Igepal CA-630, 10 mM $MgCl_2$, 1 mM EDTA, 2% glycerol, 5 mM sodium fluoride, 0.2 mM sodium orthovanadate, and protease inhibitors). Active Rho (Rho·GTP) was isolated directly on glutathione–agarose beads using GST-tagged Rhotekin Rho binding domain (Cytoskeleton). The bead pellets were washed in Rho-lysis buffer, suspended in SDS-PAGE sample buffer, and boiled as indicated below. Samples were separated by SDS-PAGE and subjected to Western blotting with an anti-RhoA Ab.

Measurement of chemotaxis and random migratory speed of mDCs

Chemotaxis in response to chemokines was determined by measuring the number of migrated cells through a polycarbonate filter with 5-μm pore size in 24-well Transwell chambers (COSTAR, Costar Europe, Badhoevedorp, the Netherlands) as indicated previously (4, 14, 27). Briefly, the upper chamber of the Transwells included 1 $\times$ 10^5 mDCs suspended in 100 μl RPMI 1640 medium containing 0.1% BSA, and the lower chamber contained 600 μl of the same medium with or without CCL21 (18 nM). The mDCs that migrate to the bottom chamber (after 2 h at 37°C) were counted by flow cytometry using the CellQuest software (BD Biosciences). The migratory speed of mDCs was measured by videomicroscopy. DCs suspended in 0.1% BSA in RPMI 1640 medium were allowed to attach for 30 min onto 0.5 μg/ml fibronectin-coated well μ-Slides (IBIDI, Martinsried, Germany), and then movement of the mDCs in the absence (random spontaneous migration) or in the presence of CCL21 (chemokinesis) was followed for 2 h using a Leica DMI6000B microscope coupled to a high-resolution monochrome Hamamatsu CCD C9100-02 camera. Tracks of individual cells were analyzed using the manual tracking plugin of the ImageJ 1.47 software (National Institutes of Health, Bethesda, MD). As a complement to the time-lapse microscopy experiments, we also assessed indirectly the effects of CCL21, or the reduction of Mst1, on the migratory speed of the mDCs using a checkerboard setting (Fig. 7D). For this purpose, we included, or not, CCL21 in the upper and lower chambers of the Transwell setting described above and then counted the number of DCs that randomly migrate to the bottom chamber. Under these conditions, the percentage of mDCs migrating to the bottom well is an indicator of the speed of the cells.

Assays of apoptotic damage

An equal number of viable DCs (determined by exclusion on trypan blue staining) were incubated in RPMI 1640 for 30 h in the absence or the presence of CCL21 (18 nM). The cells were then fixed with cold methanol, and apoptotic nuclear morphology was assessed using Hoechst33342 staining as indicated previously (3, 5, 26–28).

Endocytosis

The cells (0.5–1 $\times$ 10^5 DCs) were incubated in 10% FBS RPMI 1640 medium including 20 mM HEPES. FITC–dextran was added to a final concentration of 1 mg/ml. CCL21 was added to the mDCs at a final concentration of 18 nM. Endocytosis of the tracer was halted at 5 min by addition of ice-cold PBS and rapid cooling of the cells on ice. The cells were extensively washed with ice-cold PBS. The fluorescence intensity of the cells was analyzed by flow cytometry using an EPICS flow cytometer (Coulter Electronics). Incubation of cells with the endocytic tracer on ice was used as a background control. The mean fluorescence intensity, after subtracting the background fluorescence of the control from each experimental sample, multiplied by the percentage of mDCs that display fluorescence indicates the amount of tracer incorporated by the cell population.

Immunofluorescence

Immunofluorescence and confocal microscopy analysis were performed as previously described (29) with small changes. Briefly, DCs (5 $\times$ 10^4 cells), suspended in 0.1% BSA in RPMI 1640 medium, were incubated 30 min at 37°C onto coverslips coated with poly-ornithine (20 μg/ml). Cells were fixed in 4% paraformaldehyde in PBS (10 min at room temperature) and permeabilized with 0.2% Triton X-100 (10 min at room temperature). Before processing for immunofluorescence, the cells were treated with 1% BSA (15 min) to block unspecific binding. Coverslips were mounted in fluorescent mounting medium (DakoCytomation), and representative fields of cells were photographed through oil immersion lens. Confocal microscopy was performed using an MRC-1000 Confocal Laser Scanning System (Bio-Rad) connected to a Nikon Diaphot 200 inverted microscope. Images were acquired with the Bio-Rad COMOS graphical user interface and software. Image analysis was performed using Adobe Photoshop 5.0 (Adobe Systems) and Image software.

Barbed-end detection and quantification

The procedure was performed as described elsewhere (30) with slight changes. DCs (3 $\times$ 10^5 DCs/300 μl RPMI 1640 medium) stimulated or not for 5 min with CCL21 (18 nM) were suspended for 45 s at 37°C in permeabilization buffer (5 mM KCl, 137 mM NaCl, 4 mM $NaHCO_3$, 0.4 mM KH_2PO_4, 1.1 mM Na_2HPO_4, 2 mM $MgCl_2$, 5 mM PIPES [pH 7.2], 2 mM EGTA, 5.5 mM glucose, 0.04 mg/ml saponin, and 1% BSA) containing 0.02 mg/ml biotin–G-actin. The reaction was stopped by adding permeabilizing buffer, without saponin and BSA. Subsequently, the DCs were fixed for 10 min with 3.7% paraformaldehyde in permeabilizing buffer. Finally, the mDCs were incubated for 10 min with permeabilizing buffer containing 0.1 M glycine; blocked for 20 min in TBS buffer containing 1% BSA, 1% FBS, and 5 μg/ml phalloidin; and incubated for 1 h with FITC-conjugated anti-biotin Ab. The mDCs were extensively washed with TBS buffer containing 1% BSA. Coverslips were mounted in fluorescent mounting medium (DakoCytomation), and representative fields of cells were photographed through oil immersion lens. It has been shown that

fluorescent intensity is proportional to the number of barbed-end present in the compartment analyzed (31). Therefore, we analyzed the fluorescent intensity in annuli outside the cell periphery and extending inside the cell using Fujifilm Multi Gauge. The images were always collected at sensitivities such that none of the pixels in the image were saturated.

Cell stimulation, cell lysis, and immunoblotting

This process was performed as indicated previously (4, 5, 27). Briefly, mDCs (3×10^5 cells/300 μl RPMI 1640 medium) were stimulated or not with the chemokines for indicated periods of time. The stimulation was terminated by solubilizing the cells in 2× SDS-PAGE buffer (250 mM Tris/HCl [pH 6.8], 0.1 μM sodium orthovanadate, 6% SDS, 2 mM EDTA, 4% 2-ME [v/v], and 10% glycerol [v/v]) and boiled. The samples were fractionated by SDS-PAGE and transferred to nitrocellulose membranes. The membranes were blocked with 5% nonfat milk protein in TBS (pH 7.5) and then incubated with the indicated Abs in TBST (TBS plus 0.1% Tween 20). Proteins were visualized with the appropriate HRP-conjugated secondary Abs (Santa Cruz Biotechnology) and ECL substrate (Pierce) detection system.

Expression constructs and transfections

Control-, Mst1-, and α_{13}-siRNA were all from Applied Biosystems/Ambion (Austin, TX). Two different siRNAs–Mst1s were used to reduced Mst1 (Mst1–siRNA catalog number 4390824, sense (5′–3′), GGCGACUUGAAUACCUUCAUtt, and antisense (5′–3′), AUGAAGGUAUUCAAGUCCCtt; and Mst1–siRNA catalog number AM51331, sense (5′–3′), CAGUGAUAGGAACACCAUUtt, and antisense (5′–3′), AAUGGUGUUCCUAUCACUGTa). Two siRNAs–controls were used with similar results (catalog numbers 4390843 and AM4613 [sequences not provided by Ambion]). Expression plasmids pCI-neo and pCI-Human Mst2 have been described (32) (5 μg DNA in both cases), or siRNA–Control-, siRNA–Mst1-, and siRNA–α_{13} (0.9 μg in all cases) were transfected in the mDCs ($3–5 \times 10^6$ DCs) using a nucleofactor (AMAXA, Koeln, Germany), following the manufacturer's instructions. When the siRNAs were nucleofected, the DCs were collected and analyzed 48 h after nucleofection.

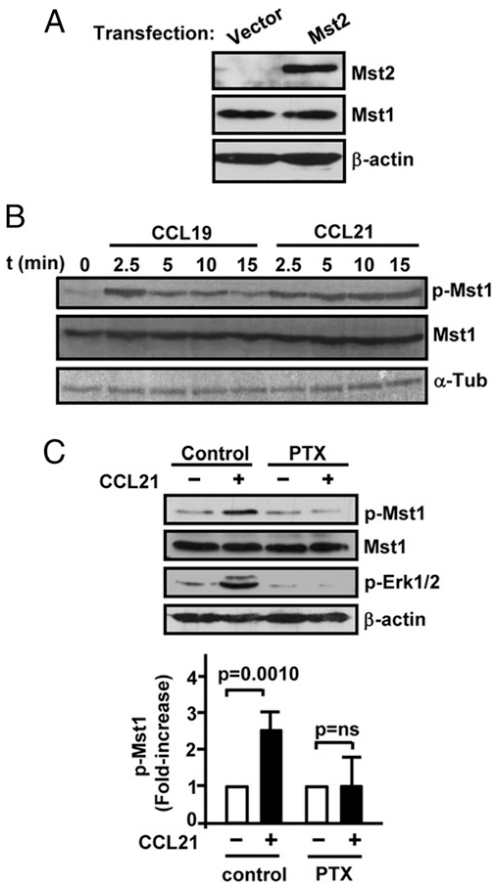

FIGURE 1. Stimulation of CCR7 in human mDCs induces G_i-mediated activation of Mst1. (**A**) DCs (3×10^6 DCs) were nucleofected either with pCI (vector) or pCI/Mst2 expression vector (Mst2). Aliquots including similar numbers of live vector– and Mst2-transfected mDCs were analyzed by Western blot for the presence of Mst2 and Mst1. The blots were also probed with an Ab against β-actin to show equal loading of the gels. One of three representative experiments is shown. (**B**) DCs were stimulated with CCL19 (18 nM) or CCL21 (18 nM) for the indicated times. Aliquots were taken to analyze the level of phosphorylated/active Mst1 (T183) (p-Mst1) and total Mst1. α-Tubulin (α-Tub) shows equal loading. One of three representative experiments is shown. (**C**) *Upper panel*, DCs were left untreated (control) or pretreated with PTX (100 ng/ml) in 10% FBS/RPMI 1640 medium for 2 h. Subsequently, the mDCs were transferred to RPMI 1640 medium and then stimulated or not with CCL21 (18 nM) for 5 min. Then, aliquots were taken to analyze the level of phospho-Mst1 (T183) (p-Mst1), total Mst1, and phosphorylated Erk1/2 (T202/Y204) (p-Erk1/2) by Western blotting. β-Actin levels show equal loading. One of four representative experiments is shown. *Lower panel*, The phosphorylation of Mst1 in control and PTX-treated mDCs, unstimulated (−) or stimulated with CCL21 (+), were analyzed. Phosphorylation levels of Mst1 in unstimulated control and PTX-treated DCs, normalized for β-actin, were given an arbitrary value of 1, and phosphorylation levels of the CCL21-stimulated DCs were referred to this value. Results shown represent the mean ± SD (n = 3 independent experiments).

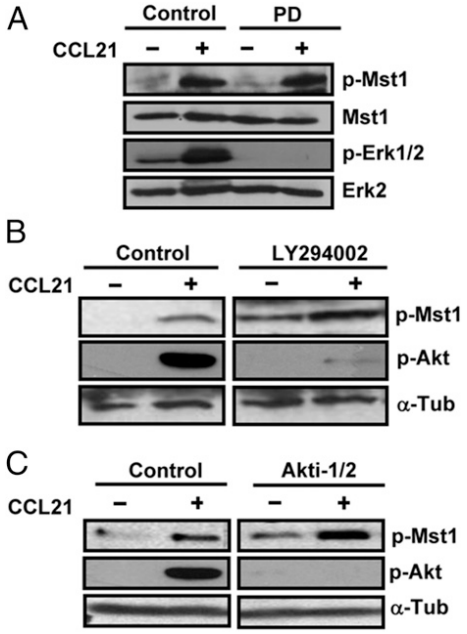

FIGURE 2. CCR7-dependent activation of Mst1 in human mDCs is not mediated by Erk1/2 or PI3K/Akt. (**A**) DCs (1×10^6 mDCs/ml RPMI 1640 medium) were either left untreated (control) or pretreated for 60 min with 1 μM PD0325901 (PD). Subsequently, the mDCs were stimulated (+) or not (−) with CCL21 (18 nM) for 5 min. The mDCs were then lysed and analyzed by Western blotting with Abs against phospho-Mst1 (T183) (p-Mst1) or total Mst1. To analyze the phosphorylation/activation of Erk1/2, the membranes were also probed with an anti–phospho-Erk1/2 (T202/Y204) (p-Erk1/2). To show equal loading, the membrane were probed with anti-Erk2. (**B**) DCs (1×10^6 DCs/ml RPMI 1640 medium) were either left untreated (control) or pretreated with LY294002 (100 μM) for 60 min. The mDCs were subsequently stimulated (+) or not (−) with CCL21 for 5 min and then subjected to Western blot with anti–phospho-Mst1 (T183) (p-Mst1) or phospho-Akt (S473) (p-Akt). α-Tubulin (α-Tub) levels show equal loading of the gels. One of three representative experiments is shown. (**C**) DCs suspended as in (A) were either left untreated (control) or pretreated with Akti-1/2 inhibitor (5 μM) for 60 min. The mDCs were stimulated (+) or not (−) with CCL21 for 5 min and then lysed, and aliquots were subjected to Western blot with anti–phospho-Mst1 (T183) (p-Mst1) or anti–phospho-Akt (S473) (p-Akt) Abs. α-Tubulin (α-Tub) levels show equal loading of the gels. One of three representative experiments is shown.

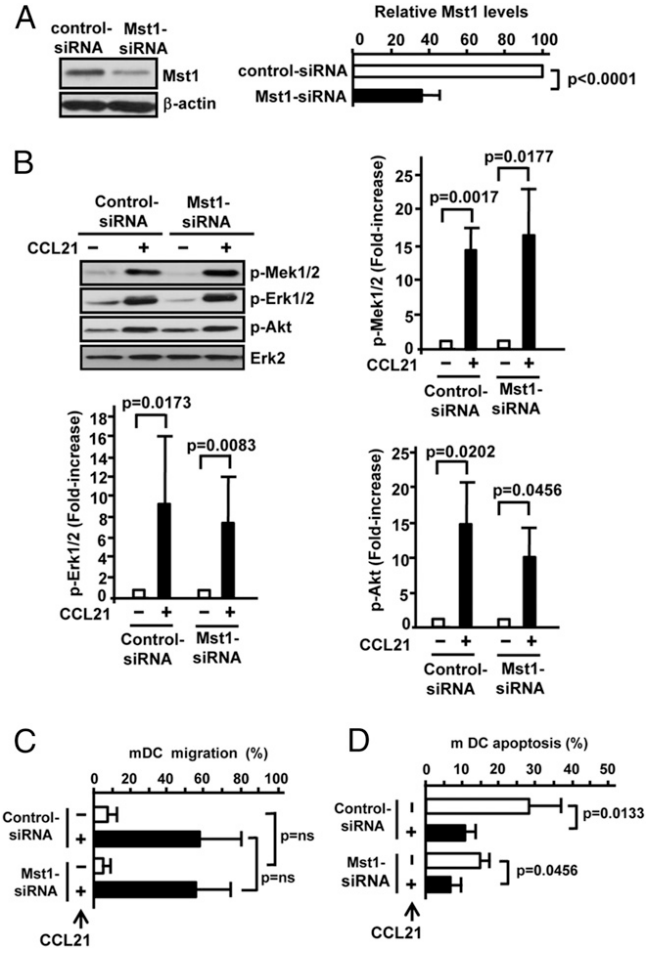

FIGURE 3. Mst1 does not mediate CCR7-dependent activation of Erk1/2 or Akt. (**A**) *Left panel*, DCs (3×10^6 DCs) were nucleofected with control- or Mst1-siRNA. Thirty-six hours after nucleofection, samples were washed in RPMI 1640 medium, and then an equal number of live DCs, determined by trypan blue exclusion, were extracted in 2× sample buffer and analyzed by Western blotting with an anti-Mst1 Ab. To confirm equal loading, the blots were reprobed with an Ab reacting with β-actin. One representative example is shown. *Right panel*, Bar diagrams showing the quantification of the relative levels of Mst1 in control– and Mst1–siRNA nucleofected mDCs. The quantity of Mst1 observed in the immunoblots was normalized against the levels of β-actin observed in each sample. The levels of Mst1 in the control–siRNA nucleofected DCs were given an arbitrary value of 100. Results shown represent the mean ± SD ($n = 7$). (**B**) *Upper left panel*, Samples of DCs nucleofected either with control– or Mst–siRNA were washed in RPMI 1640 medium, and then an equal number of live DCs, as determined by trypan blue exclusion, were stimulated or not for 5 min with CCL21 (18 nM). Subsequently, the cells were lysed, and aliquots were subjected to Western blot with Abs against phosphorylated/active Mek1/2 (S217/221) (p-Mek1/2), Erk1/2 (T202/Y204) (p-Erk1/2), or Akt (S473) (p-Akt). Erk2 levels show equal loading of the gels. One of three representative experiments is shown. The bar diagrams represent the fold increase in phosphorylation of Mek1/2 (*upper right panel*), Erk1/2 (*lower left panel*), and Akt (*lower right panel*) in control– and Mst1–siRNA nucleofected mDCs upon stimulation with CCL21. The phosphorylation levels of all the proteins examined were normalized with respect to the total levels of Erk2. The normalized phosphorylation was referred to the phosphorylation levels in the unstimulated control– and Mst1–siRNA nucleofected mDCs, which were given a value of 1. Results shown represent the mean ± SD ($n = 3$, for p-Mek1/2; $n = 6$, for p-Erk1/2; and $n = 3$, for p-Akt). (**C**) The mDCs were nucleofected with control– or Mst1–siRNA as indicated in (A). A total of 100×10^3 of controls or Mst1–siRNA nucleofected mDCs was suspended in 0.1% BSA/RPMI 1640 medium and placed in the upper chambers of a Transwell setting and then allowed to migrate to the bottom chamber, which includes (+) or not (−) CCL21. The values represent the percentage of mDCs migrating to the lower chambers. Results shown represent the mean ± SD ($n = 3$). (**D**) The mDCs were nucleofected with control– or Mst1–siRNA as indicated in (A). A total of 5×10^4 of live, control–, or Mst1–siRNA nucleofected mDCs, were suspended in 0.1% BSA/RPMI 1640 medium and left in the incubator for 30 h in the presence or absence of CCL21 as indicated. The cells were supplemented with CCL21 every 10 h. Subsequently, the mDCs were fixed and stained with Hoechst to analyze the percentage of apoptotic cells as indicated in *Materials and Methods*. Results shown represent the mean ± SD ($n = 3$).

Statistics

Data are expressed as mean ± SD, with the "n," indicating the number of experiments performed. Significance of differences between two series of results was assessed using the Student t test. The p values ≤ 0.05 were considered significant. The p values > 0.05 were denoted as ns, nonsignificant.

Results

Stimulation of CCR7 in human mDCs induces $G_{\alpha i}$-dependent activation of Mst1

We studied whether stimulation of CCR7 induces activation of Mst in mDCs. For this purpose, we used an Ab that recognizes phosphorylated/active Mst1/2. Because the Ab used recognizes both active Mst1 (T183) and Mst2 (T180) (33, 34), we tested whether the human monocyte–derived mDCs used in our experiments express endogenously both Mst isoforms. As shown in Fig. 1A, the mDCs express endogenously Mst1 but not Mst2. We could only detect Mst2 when we overexpressed this kinase (Fig. 1A). Therefore, hereafter, the results obtained with the anti–phospho-Mst1/2 Ab used in the experiments will refer only to phosphorylated/active Mst1 (T183). We studied whether the stimulation of CCR7 in mDCs induces phosphorylation/activation of Mst1. Time-course experiments showed that both CCL19 and CCL21 induced phosphorylation of Mst1 (Fig. 1B). Because similar activations were obtained with CCL19 and CCL21, we decided to use CCL21 to stimulate the cells in the rest of the experiments. Next, we analyzed the signaling pathways downstream of CCR7 involved in the activation of Mst1. Inhibition of Gi by pretreating the mDCs with pertussis toxin (PTX) blocked CCR7-dependent phosphorylation of Mst1, indicating that Gi mediates CCR7-dependent phosphorylation of this kinase (Fig. 1C).

Mst1 does not mediate CCR7-dependent chemotaxis or survival in human mDCs

Previously, we have shown that CCR7 uses in mDCs the key regulators Mek1/2–Erk1/2 (2, 4) and Akt (2, 3, 5) to control chemotaxis and survival, respectively. We analyzed whether Mst1 could be a component of the signaling pathway that controls these two CCR7-dependent functions in mDCs. Inhibition of the activity of Mek1/2–Erk1/2—by treating the DCs with PD0325901 (Fig. 2A, see Supplemental Fig. 1) or UO126 (data not shown), two highly selective inhibitors of Mek1/2 (35) and, consequently, of Erk1/2, the only known downstream targets of Mek1/2 (36)—failed to block CCR7-dependent phosphorylation of Mst1. Moreover, inhibition of PI3K—by treating the cells with LY294002 (Fig. 2B) or Akt by using the selective Akt inhibitor Akti-1/2 (37) (Fig. 2C)—failed to inhibit CCR7-induced activation of Mst1. Note that in these experiments, inhibition of PI3K/Akt increased the basal activity of Mst1, consistent with prior results indicating that active Akt keeps Mst1 basally inhibited (38). Finally, we knocked down Mst1 by nucleofecting the mDCs with either of two different siRNAs (see *Materials and Methods*). Both siRNAs for Mst1 were able to reduce Mst1 at similar levels and gave similar results in functional and biochemical experiments (Fig. 3A and results not shown; see also

Materials and Methods); therefore, we used them interchangeably in all the subsequent experiments. As shown in Fig. 3A, reduction of Mst1 with siRNA in DCs failed to affect CCR7-dependent activation of the Mek1/2, Erk1/2, or Akt (Fig. 3B, see also Supplemental Fig. 1). The results obtained suggest that downstream of CCR7 the signaling pathways that induce activation of Mst1 are independent of those that induce activation of Mek1/2–Erk1/2 or Akt. Consistent with the biochemical results, reduction of Mst1 in mDCs using siRNA failed to affect CCR7-induced chemotaxis (Fig. 3C). Furthermore, although the knocking down of Mst1 reduced the basal number of mDCs that became apoptotic, however, it did not inhibit the prosurvival effects induced by the stimulation of CCR7 (Fig. 3D). In summary, the results indicate that CCR7 induces activation of Mst1 in mDCs independently of the pathways used by this receptor to regulate survival and chemotaxis (Supplemental Fig. 1).

Mst1 mediates CCR7-induced activation of the RhoA pathway independently of $G_{\alpha 13}$ in human mDCs

We analyzed whether Mst1 could mediate RhoA activation in mDCs. First, we analyzed the kinetics of RhoA activation upon stimulation of CCR7. Stimulation of mDCs with CCL21 induced activation of RhoA, which starts after 0.5 min, reaches maximal activity after 2 min, and decays after 5 min (Fig. 4A). Consistent with these results, stimulation of CCR7 also induced changes in the phosphorylation of three well-known targets downstream of RhoA, namely, MLC, MYPT1, which is the regulatory/myosin binding subunit of the MLCP, and cofilin (Fig. 4B). MLC was phosphorylated on T18/S19, which leads to its activation (Fig. 4B) (14), MYPT1 was phosphorylated on T696, which results in the inhibition of the activity of MLCP (Fig. 4B) (15), and cofilin was phosphorylated on S3, which results in the inactivation of its actin severing activity (12). Taking into account these biochemical results, next we analyzed whether Mst1 could mediate CCR7-dependent activation of RhoA in mDCs. For this purpose, we analyzed the effect that the reduction of Mst1 exerted on CCR7-induced phosphorylation of the RhoA downstream targets. After knocking down of Mst1 by nucleofecting the mDCs with siRNA (see Fig. 3A), it was observed that the reduction of Mst1 blocked the phosphorylation of MYPT1, MLC, and cofilin (Fig. 5A), suggesting that Mst1 modulates the activation of the RhoA pathway downstream of CCR7 (see Supplemental Fig. 1).

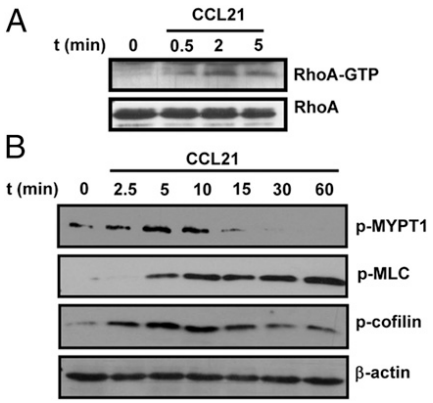

FIGURE 4. Stimulation of CCR7 induces phosphorylation of RhoA downstream targets. (**A**) DCs (5×10^6 cells) were stimulated with CCL21 (18 nM) for the indicated time. The DCs were then lysed, and active Rho (Rho·GTP) was pulled down using GST-tagged Rho binding domain (RBD) bound to glutathione–agarose beads. The level of RhoA–GTP isolated on the beads was assessed by Western blotting with an anti-RhoA Ab. An aliquot of the cells lysed before the pull down was used to perform a Western blot with the anti-RhoA Ab. The results are representative of three independent experiments. (**B**) DCs (1×10^6 mDCs/ml RPMI 1640 medium) were stimulated for the indicated times with CCL21, and subsequently, aliquots were taken to analyze the level of phosphorylated MYPT1 (T696) (p-MYPT1), MLC (T18/S19) (p-MLC), and cofilin (S3) (p-cofilin) by Western blotting. β-Actin levels show equal loading of the gels. One of three representative experiments is shown.

As Mst1 regulates the RhoA-dependent pathway and it has been shown that the $G_{\alpha 12/13}$ family of G proteins can mediate the effects of G protein–coupled receptors on this pathway (39–41), we analyzed whether $G_{\alpha 13}$ could mediate the effects of CCR7 on Mst1. However, it was observed that the reduction of $G_{\alpha 13}$ using siRNA (Fig. 5B) failed to inhibit the increase in the phosphorylation of Mst1 upon stimulation of CCR7 (Fig. 5C, Supplemental Fig. 1), which indicates that $G_{\alpha 13}$ does not mediate the activation of Mst1 downstream of this receptor. The interference with $G_{\alpha 13}$-mediated signaling using siRNA blocked the CCR7-dependent activation of the RhoA signaling pathway, including the phosphorylation of MYPT1, MLC, and cofilin (Supplemental Fig. 2), confirming that $G_{\alpha 13}$ can also mediate the activation of RhoA downstream of CCR7 (Supplemental Fig. 1). Finally, as both $G_{\alpha 13}$ (Supplemental Fig. 2) and Mst1 (Fig. 5) regulate, downstream of CCR7, the RhoA-dependent pathway, we analyzed whether RhoA could be upstream of Mst1. For this purpose, we inhibited RhoA by treating the mDCs with C3–exoenzyme, which irreversibly inhibits the activity of this small GTPase (Fig. 5D) (29, 42). Although this treatment blocked the RhoA pathway as expected (Fig. 5D), however, it failed to block CCR7-dependent activation of Mst1 (Fig. 5D), suggesting that RhoA is not upstream of Mst1. Because, as shown above, Mst1 is downstream of Gi (Fig. 1C), together the results point out the existence in mDCs of two signaling axes, namely CCR7-$G_{\alpha 13}$ and CCR7-G_i-Mst1, which independently converge in RhoA (Supplemental Fig. 1).

Finally, interestingly, the inhibition of RhoA (Fig. 5D) or the decrease in the expression of $G_{\alpha 13}$ (Supplemental Fig. 2B) did not affect the CCR7-induced increase in the phosphorylation of the survival regulator Akt (Supplemental Fig. 2B; data not shown) or the chemotaxis regulator Erk1/2 (Fig. 5D, Supplemental Fig. 2B). These results emphasize that downstream of CCR7 the signaling pathways that converge on RhoA are independent of those regulating chemotaxis and survival (Supplemental Fig. 1).

Mst1 is required for actin-free barbed-end formation in human mDCs

The extension of an actin cytoskeletal network requires the development of F-actin–rich protrusions, which depends on the formation of free barbed end, from where F-actin filaments can grow. Because new barbed-end formation requires the activity of the actin-severin protein cofilin (12), which, as shown above (Fig. 5A), was phosphorylated/inhibited downstream of Mst1, we hypothesized that the inhibition of this kinase could block free barbed-end formation (Supplemental Fig. 1). We reduced Mst1 by nucleofecting mDCs with siRNA (Fig. 6A) and then analyzed barbed-end formation in the mDCs (Fig. 6B). As shown in Fig. 6B, reduction of Mst1 dramatically blocked barbed-end formation in both unstimulated and CCL21-stimulated mDCs, indicating that normal levels of Mst1 are required for barbed-end formation in mDCs.

Mst1 mediates the effects of CCR7 on endocytosis, cytoarchitecture, and migratory speed in human mDCs

Because Mst1 regulates barbed-end formation, consequently, F-actin organization, we analyzed other CCR7-dependent functions that could be regulated by Mst1 in mDCs. Because CCR7 regulates the cytoarchitecture of mDC (4, 6), we reduced Mst1 in

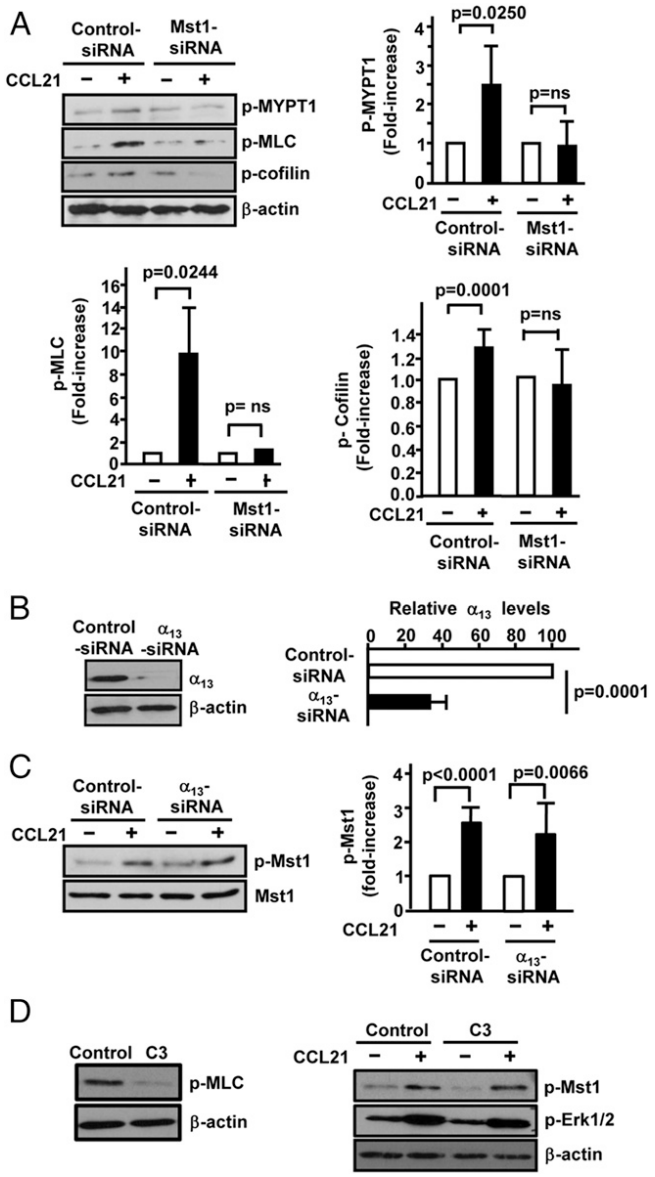

FIGURE 5. Mst1 regulates CCR7-induced activation of the RhoA pathway independently of $G_{\alpha 13}$. (**A**) The experiments were performed with mDCs obtained in the nucleofections shown in Fig. 3A. *Upper right panel*, Live control– and Mst1–siRNAs nucleofected mDCs were suspended in RPMI 1640 medium and then stimulated (+) or not (−) for 5 min with CCL21. The cells were subjected to a Western blot as in Fig 3A. The following Abs were used, namely, anti-phosphorylated MYPT1 (T696) (p-MYPT1), MLC (T18/S19) (p-MLC), and cofilin (S3) (p-cofilin). β-Actin shows equal loading of the gels. One of three representative experiments is shown. The bar diagrams represent the fold increase in the phosphorylation of MYPT1 (*upper right panel*), MLC (*lower left panel*), and cofilin (*lower right panel*) in control– and Mst1–siRNA nucleofected mDCs upon stimulation with CCL21. The phosphorylation levels of all the proteins examined were normalized with respect to β-actin. The phosphorylation levels in the unstimulated control– and Mst1–siRNA nucleofected DCs were given a value of 1. Results shown represent the mean ± SD ($n = 4$, for p-MYPT1; $n = 3$ for p-MLC; and $n = 9$ for p-cofilin). (**B**) *Left panel*, DCs (3×10^6 cells) were nucleofected either with control– or $G_{\alpha 13}$–siRNA and the levels of $G_{\alpha 13}$ analyzed by immunoblotting. β-Actin shows equal loading of the gels. *Right panel*, The relative levels of expression $G_{\alpha 13}$ in mDCs nucleofected with control– or Mst1–siRNA were determined as indicated in Fig. 3A. Results shown represent the mean ± SD ($n = 8$). (**C**) *Left panel*, Samples of the control– or $G_{\alpha 13}$–siRNA nucleofected mDCs obtained in (B) were stimulated (+) or not (−) for 5 min with CCL21. The mDCs were lysed, and aliquots were subjected to Western blot with an anti-phosphorylated Mst1 (T183) (p-Mst1). The blots were striped and analyzed with an Ab against Mst1 to show equal loading. One of three representative experiments is shown. *Right panel*, The level of phosphorylated Mst1 was normalized against the total Mst1 and referred to the values observed in unstimulated control– or $G_{\alpha 13}$–siRNA nucleofected mDCs, which were given an arbitrary value of 1. Results shown represent the mean ± SD ($n = 7$). (**D**) *Left panel*, DCs (300×10^3 DCs) were left untreated (control) or pretreated with C3–exoenzyme (50 ng/ml) for 16 h. Then, the cells were lysed and aliquots subjected to Western blot with an anti-phosphorylated MLC (T18/S19) (p-MLC). *Right panel*, DCs pretreated with C3 exoenzyme as in the *left panel* were stimulated (+) or not (−) with CCL21 (18 nM) for 3 min. Aliquots were taken to analyze the level of phosphorylated-Mst1 (T183) (p-Mst1) and Erk1/2 (T202/Y204) (p-Erk1/2). β-Actin shows equal loading of the gels. One of four representative experiments is shown.

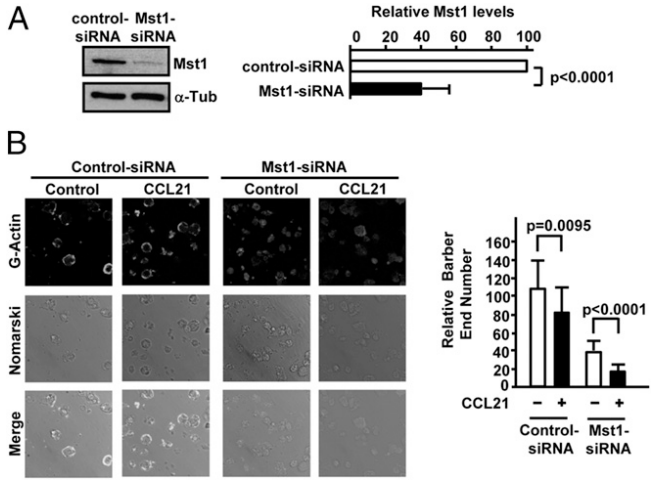

FIGURE 6. Mst1 controls barbed end formation in mDCs. (**A**) *Left panel*, DCs were nucleofected with control– or Mst1–siRNA, and Western blots were performed as indicated in the legend to Fig. 3A. α-Tubulin shows equal loading of the gels. *Right panel*, The relative levels of $G_{\alpha 13}$ in DCs nucleofected either with control or with Mst1–siRNA were determined as indicated in Fig. 3A. Results shown represent the mean ± SD ($n = 6$). (**B**) *Left panel*, Aliquots of control– or Mst1–siRNA nucleofected mDCs as indicated in (A) were stimulated or not with CCL21. The mDCs were partially permeabilized and processed to analyze barbed-end formation as indicated in *Materials and Methods*. One representative experiment is shown. *Right panel*, Incorporation of FITC-labeled actin monomers was quantified by fluorescence intensity measurement using Multigauge version 3.0. Data representing the number of free barbed ends are expressed as arbitrary units of fluorescence intensity and represent means ± SD.

mDCs by nucleofecting cells with siRNA (Fig. 7A) and then analyzed the morphology of the mDCs both in the presence or absence of CCL21 (Fig. 7B). Analysis of the polarization indexes (Fig. 7B), which quantify the degree of morphological polarization of the cells, showed that mDCs with reduced expression of Mst1, both unstimulated or CCL21-stimulated, displayed a rounder morphology (i.e., higher polarization indexes) when compared with control–siRNA nucleofected mDCs, which presented more elongated morphologies (lower polarization indexes) (Fig. 7B). Staining of the actin cytoskeleton with phalloidin–FITC also showed that the mDCs that presented reduced levels of Mst1 displayed smaller dendritic extensions and the F-actin was largely localized at the cell periphery (see insets in Fig. 7B).

Because stimulation of CCR7 induces endocytosis of mDCs (7), we tested whether Mst1 could also modulate this function. DCs nucleofected with control– or Mst1–siRNAs (Fig. 7A) were incubated with FITC–dextran and then stimulated or not with CCL21 to study the degree of incorporation of this polysaccharide

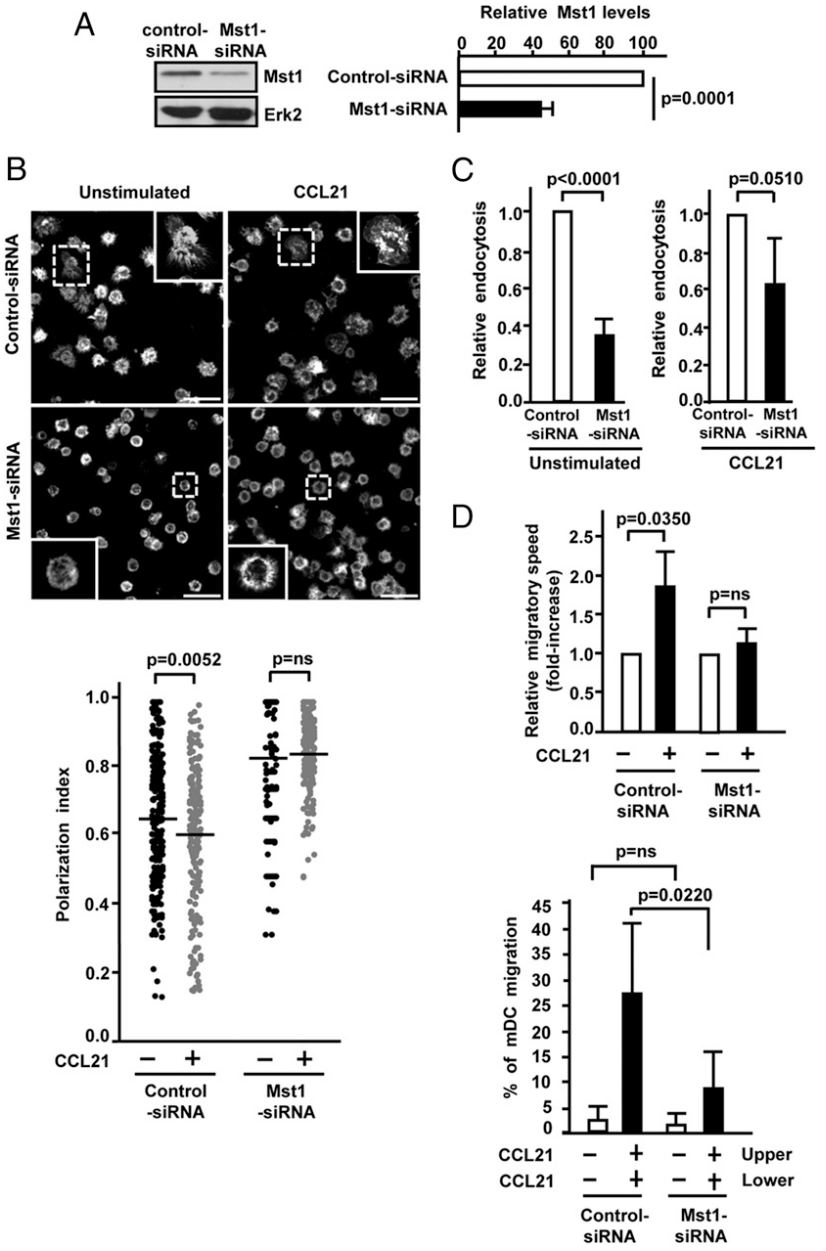

FIGURE 7. Mst1 controls CCR7-dependent cytoarchitecture, endocytosis, and migratory speed in human mDCs. (**A**) *Left panel*, DCs were nucleofected either with control– or Mst1–siRNA, and Western blots were performed as indicated in Fig. 3A. Erk2 shows equal loading of the gels. *Right panel*, Mst1 levels in mDCs nucleofected either with control– or with Mst1–siRNA were quantified as indicated in Fig. 3A. Results shown represent the mean ± SD (n = 11). (**B**) *Upper panel*, Samples of mDCs nucleofected with control– or Mst1–siRNA were plated on polyornithine-coated dishes and allowed to adhere for 30 min at 37°C in the incubator. Subsequently, the cells were stimulated or not with CCL21 (18 nM) for 5 min. The cells were treated and stained with FITC–phalloidin as indicated in *Materials and Methods*. Scale bar indicates 50 μm. *Inset* shows a representative mDC under the conditions indicated. *Lower panel*, The polarization index of the cells was calculated as the ratio of X to Y, where Y is the longest distance across cells, and X is the greatest width perpendicular to Y. (**C**) Samples of control– or Mst1–siRNA nucleofected mDCs (50–100 × 10^3 cells), suspended in complete medium, in the presence of FITC–dextran (1 mg/ml), were left unstimulated (*left panel*) or stimulated (*right panel*) for 5 min with CCL21. The bar diagrams represent the amount of FITC–dextran internalized by the mDCs after 5 min. The relative levels of incorporation of FITC–dextran in Mst1–siRNA nucleofected mDCs both in unstimulated (*left panel*) or CCL21-stimulated (*right panel*) were referred to the levels of endocytosis observed in unstimulated (*left panel*) or CCL21-stimulated (*right panel*) control–siRNA nucleofected mDCs. Results shown represent the mean ± SD (n = 3). (**D**) *Upper panel*, Relative migratory speed in control– and Mst1–siRNA nucleofected mDCs both unstimulated (−) or stimulated with CCL21 (+). Unstimulated control– and Mst1–siRNA were given an arbitrary value of 1. *Lower panel*, Checkerboard setting to assess random motility of control– and Mst1–siRNA nucleofected mDCs were performed as indicated in *Materials and Methods*. CCL21 included (+) or not (−) in the upper or lower wells of the Transwell setting as indicated in the figure.

by flow cytometry. As shown in Fig. 7C, the reduction in the expression of Mst1 curtails the ability to internalize FITC–dextran in unstimulated and in CCL21-stimulated mDCs. The effects of the reduction of Mst1 on the endocytic ability of the mDCs were less potent in the CCL21-stimulated than in the unstimulated mDCs, suggesting the existence of alterative, Mst1-independent pathways that may contribute to regulate CCR7-dependent endocytosis.

We have shown before that stimulation of CCR7 results in an increase in the migratory speed of the mDCs (4). Because migration involves changes in the actin cytoskeleton, we analyzed whether the reduction of Mst1 could also affect the migratory speed of the mDCs (Fig. 7D). For this purpose, first we analyzed by time-lapse videomicroscope the relative migratory speed of mDCs stimulated or not with CCL21 (Fig. 7D). Alternatively, we used a Transwell setting where we included or not CCL21 in the upper and lower chambers (Fig. 7D). As in this setting, there is no gradient of chemokines, the number of mDCs that migrate to the lower chambers of provides information on the random motility of the cells, in the absence or in the presence of CCL21. As shown in Fig. 7D, both time-lapse videomicroscopy and the Transwell setting experiments showed that the reduction of Mst1 did not affect the migratory speed of the mDC in the absence of chemokines. In contrast, in the presence of CCL21, mDCs with reduced levels of Mst1 presented a significant reduction of their migratory speed. The results indicate that upon stimulation of CCR7, the kinase Mst1 regulates the migratory speed of the mDCs.

Discussion

CCR7 directs mDCs to the lymph nodes, where takes place the initiation of the immune response, implying that an adequate functioning of this receptor during this process is of critical importance (2). CCR7, in addition to chemotaxis, controls the cytoarchitecture, the migratory speed, the endocytosis, and the survival of the mDCs (2–8, 43). The studies on the role of Mst1 in the immune system have focused on lymphocytes, and there is no information on the role of this kinase in other leukocytes (25). In this study, we have analyzed the role of Mst1 in the control of the CCR7-mediated functions in human mDCs. The results obtained indicate that downstream of CCR7, Mst1 controls in mDCs cytoarchitecture, endocytosis, and migratory speed but not sur-

vival or chemotaxis (Supplemental Fig. 1). These results provide useful information to develop strategies to modulate selectively the functions of CCR7 in mDCs and to better interpret recently described pathologies associated with the loss of function of Mst1 (44–46).

Recent reports show that alteration in Mst1 function may importantly affect the immune response. Patients bearing mutations of Mst1 that lead to a loss in the function of this kinase show recurrent bacterial and viral infections and symptoms of autoimmunity (44–46). Resembling the phenotype observed in Mst1-deficient mice (25), these patients show also T cell lymphopenia and impaired T cell responses. On the basis of these observations, most of the symptoms presented by the patients have been ascribed to deficient T cell function. However, in view of our results, it is possible that alterations in CCR7-depending signaling in mDCs could also contribute to the pathologies observed.

The information obtained in this paper supports our previous studies indicating that in mDCs the signaling modules controlling CCR7-dependent chemotaxis and survival are different of the modules controlling migratory speed (2, 4). The observation that downstream of CCR7 Mst1 modulates simultaneously cytoarchitecture, migratory speed, and endocytosis suggests that this kinase is high upstream the signaling pathway controlled by CCR7. Further studies will have to be performed to dissect the specific molecular components that selectively control each one of these three functions. We have also observed that two axes, namely, CCR7-$G_{\alpha 13}$ and CCR7-Gi-Mst1, converge to regulate RhoA and, consequently, actin dynamics, in mDCs (Supplemental Fig. 1). In summary, the results underline the key role of the regulation of the actin cytoskeletal network to control CCR7-dependent changes in cytoarchitecture, migratory speed, and endocytosis in DCs.

It has been shown that in thymocytes after phosphorylation by the kinases Mst1 or Mst2, the protein Mob1 binds and activates the Rac1 guanyl nucleotide exchanger Dock8, which is abundant in the thymus. Activated Dock8 promotes the activation of the small GTPase Rac, which controls the actin cytoskeleton and, consequently, the migratory response of the thymocytes (47). These results underline the key role of Mst1 in the regulation of the small GTPase Rac and the migration of thymocytes (47). Our results indicate that in DCs, downstream of CCR7 and Mst1, RhoA controls actin-dependent functions, including migratory speed, cytoarchitecture, and endocytosis. In future studies, it would be interesting to analyze whether in DCs Mst1 is also able to regulate Rac, as observed in thymocytes (47). Interestingly, when we analyzed in DCs the effect of knocking down Mst1 with siRNA on Dock8, we observed by Western blotting and immunofluorescence analysis that the reduction of Mst1 failed to affect the levels or localization of Dock8, suggesting alternative mechanisms to regulate Dock8 and/or Rac in DCs (results not shown).

We observed that reduction of Mst1 leads to reduced basal levels of mDC apoptosis, consistent with prior results showing that Mst1 could play proapoptotic roles in cells (18, 19). However, the reduction of Mst1 does not block CCR7-dependent activation of Akt or the induction of survival in mDCs, indicating that Mst1 does not mediate CCR7-dependent survival in these cells. The knocking down of Mst1 also failed to affect CCR7-dependent chemotaxis or the activation of Erk1/2, a key regulator of chemotaxis in mDCs (4). These observations are in contrast with results obtained in thymocytes and mature lymphocytes where has been shown that Mst1 controls CCR7-dependent chemotaxis (20, 21, 24, 47). These results point out differences in the role performed by Mst1 in different leukocytes and emphasize the importance of getting insight on the role of Mst1 in different cells of the immune system to develop selective strategies to intervene on these cells.

While this work was in progress, another group, using Mst1/2 KO mice models, has also shown that Mst1/2 is involved in the activation of RhoA in thymocytes (47). Because we used in our experiments monocyte-derived human mDCs and we focused on Mst1, together ours and the aforementioned results indicate that Mst1 can regulate RhoA both in lymphoid murine cells and human DCs. Finally, the results showing that $G_{\alpha i}$ and $G_{\alpha 13}$ converge in the regulation of RhoA are also of interest in view of prior contradictory data on this issue. Previously, it has been indicated that $G_{\alpha 13}$ regulates RhoA downstream of GPCRs (39–41), apparently challenging data obtained by other groups supporting that $G_{\alpha i}$ regulates RhoA downstream of GPCRs (48–50). Our results indicating that it is possible for a single GPCR, in this case CCR7, to use simultaneously both G_i and $G_{\alpha 13}$ to mediate the activation of RhoA, reconcile these apparently contradictory results. In summary, the data obtained provide further insights on the mechanisms used by CCR7 to regulate its functions in mDCs and on the role of Mst1 in these cells.

Acknowledgments

We thank P. Lastres for help with the cytometer and discussions, Alejandro Cuesta-Muriel for help in the experiments, and Génesis Andrea Altuve Urbina and Alba Adán Rojo for expert technical assistance. We sincerely thank the support of Dr. Miguel Angel Vega Palacios and Prof. Hiroyuki Osada.

Disclosures

The authors have no financial conflicts of interest.

References

1. Steinman, R. M., and J. Banchereau. 2007. Taking dendritic cells into medicine. *Nature* 449: 419–426.
2. Sánchez-Sánchez, N., L. Riol-Blanco, and J. L. Rodríguez-Fernández. 2006. The multiple personalities of the chemokine receptor CCR7 in dendritic cells. *J. Immunol.* 176: 5153–5159.
3. Sánchez-Sánchez, N., L. Riol-Blanco, G. de la Rosa, A. Puig-Kröger, J. García-Bordas, D. Martín, N. Longo, A. Cuadrado, C. Cabañas, A. L. Corbí, et al. 2004. Chemokine receptor CCR7 induces intracellular signaling that inhibits apoptosis of mature dendritic cells. *Blood* 104: 619–625.
4. Riol-Blanco, L., N. Sánchez-Sánchez, A. Torres, A. Tejedor, S. Narumiya, A. L. Corbí, P. Sánchez-Mateos, and J. L. Rodríguez-Fernández. 2005. The chemokine receptor CCR7 activates in dendritic cells two signaling modules that independently regulate chemotaxis and migratory speed. *J. Immunol.* 174: 4070–4080.
5. Escribano, C., C. Delgado-Martín, and J. L. Rodríguez-Fernández. 2009. CCR7-dependent stimulation of survival in dendritic cells involves inhibition of GSK3β. *J. Immunol.* 183: 6282–6295.
6. Yanagawa, Y., and K. Onoé. 2002. CCL19 induces rapid dendritic extension of murine dendritic cells. *Blood* 100: 1948–1956.
7. Yanagawa, Y., and K. Onoé. 2003. CCR7 ligands induce rapid endocytosis in mature dendritic cells with concomitant up-regulation of Cdc42 and Rac activities. *Blood* 101: 4923–4929.
8. Braun, A., T. Worbs, G. L. Moschovakis, S. Halle, K. Hoffmann, J. Bölter, A. Münk, and R. Förster. 2011. Afferent lymph-derived T cells and DCs use different chemokine receptor CCR7-dependent routes for entry into the lymph node and intranodal migration. *Nat. Immunol.* 12: 879–887.
9. Randolph, G. J., V. Angeli, and M. A. Swartz. 2005. Dendritic-cell trafficking to lymph nodes through lymphatic vessels. *Nat. Rev. Immunol.* 5: 617–628.
10. Comerford, I., Y. Harata-Lee, M. D. Bunting, C. Gregor, E. E. Kara, and S. R. McColl. 2013. A myriad of functions and complex regulation of the CCR7/CCL19/CCL21 chemokine axis in the adaptive immune system. *Cytokine Growth Factor Rev.* 24: 269–283.
11. Förster, R., A. Schubel, D. Breitfeld, E. Kremmer, I. Renner-Müller, E. Wolf, and M. Lipp. 1999. CCR7 coordinates the primary immune response by establishing functional microenvironments in secondary lymphoid organs. *Cell* 99: 23–33.
12. Condeelis, J. 2001. How is actin polymerization nucleated in vivo? *Trends Cell Biol.* 11: 288–293.
13. Bravo-Cordero, J. J., M. A. Magalhaes, R. J. Eddy, L. Hodgson, and J. Condeelis. 2013. Functions of cofilin in cell locomotion and invasion. *Nat. Rev. Mol. Cell Biol.* 14: 405–415.
14. Amano, M., M. Ito, K. Kimura, Y. Fukata, K. Chihara, T. Nakano, Y. Matsuura, and K. Kaibuchi. 1996. Phosphorylation and activation of myosin by Rho-associated kinase (Rho-kinase). *J. Biol. Chem.* 271: 20246–20249.
15. Kimura, K., M. Ito, M. Amano, K. Chihara, Y. Fukata, M. Nakafuku, B. Yamamori, J. Feng, T. Nakano, K. Okawa, et al. 1996. Regulation of myosin phosphatase by Rho and Rho-associated kinase (Rho-kinase). *Science* 273: 245–248.

16. Creasy, C. L., and J. Chernoff. 1995. Cloning and characterization of a human protein kinase with homology to Ste20. *J. Biol. Chem.* 270: 21695–21700.
17. Yin, H., Z. Shi, S. Jiao, C. Chen, W. Wang, M. I. Greene, and Z. Zhou. 2012. Germinal center kinases in immune regulation. *Cell. Mol. Immunol.* 9: 439–445.
18. Cheung, W. L., K. Ajiro, K. Samejima, M. Kloc, P. Cheung, C. A. Mizzen, A. Beeser, L. D. Etkin, J. Chernoff, W. C. Earnshaw, and C. D. Allis. 2003. Apoptotic phosphorylation of histone H2B is mediated by mammalian sterile twenty kinase. *Cell* 113: 507–517.
19. de Souza, P. M., and M. A. Lindsay. 2004. Mammalian Sterile20-like kinase 1 and the regulation of apoptosis. *Biochem. Soc. Trans.* 32: 485–488.
20. Katagiri, K., M. Imamura, and T. Kinashi. 2006. Spatiotemporal regulation of the kinase Mst1 by binding protein RAPL is critical for lymphocyte polarity and adhesion. *Nat. Immunol.* 7: 919–928.
21. Katagiri, K., T. Katakai, Y. Ebisuno, Y. Ueda, T. Okada, and T. Kinashi. 2009. Mst1 controls lymphocyte trafficking and interstitial motility within lymph nodes. *EMBO J.* 28: 1319–1331.
22. Ueda, Y., K. Katagiri, T. Tomiyama, K. Yasuda, K. Habiro, T. Katakai, S. Ikehara, M. Matsumoto, and T. Kinashi. 2012. Mst1 regulates integrin-dependent thymocyte trafficking and antigen recognition in the thymus. *Nat. Commun.* 3: 1098.
23. Zhou, D., B. D. Medoff, L. Chen, L. Li, X. F. Zhang, M. Praskova, M. Liu, A. Landry, R. S. Blumberg, V. A. Boussiotis, et al. 2008. The Nore1B/Mst1 complex restrains antigen receptor-induced proliferation of naïve T cells. *Proc. Natl. Acad. Sci. USA* 105: 20321–20326.
24. Dong, Y., X. Du, J. Ye, M. Han, T. Xu, Y. Zhuang, and W. Tao. 2009. A cell-intrinsic role for Mst1 in regulating thymocyte egress. *J. Immunol.* 183: 3865–3872.
25. Qin, F., J. Tian, D. Zhou, and L. Chen. 2013. Mst1 and Mst2 kinases: regulations and diseases. *Cell Biosci* 3: 31.
26. Riol-Blanco, L., C. Delgado-Martín, N. Sánchez-Sánchez, L. M. Alonso-C, M. D. Gutiérrez-López, G. M. Del Hoyo, J. Navarro, F. Sánchez-Madrid, C. Cabañas, P. Sánchez-Mateos, and J. L. Rodríguez-Fernández. 2009. Immunological synapse formation inhibits, via NF-κB and FOXO1, the apoptosis of dendritic cells. *Nat. Immunol.* 10: 753–760.
27. Delgado-Martín, C., C. Escribano, J. L. Pablos, L. Riol-Blanco, and J. L. Rodríguez-Fernández. 2011. Chemokine CXCL12 uses CXCR4 and a signaling core formed by bifunctional Akt, extracellular signal-regulated kinase (ERK)1/2, and mammalian target of rapamycin complex 1 (mTORC1) proteins to control chemotaxis and survival simultaneously in mature dendritic cells. *J. Biol. Chem.* 286: 37222–37236.
28. Gómez-Cabañas, L., C. Delgado-Martín, P. López-Cotarelo, L. M. Alonso-C, L. Riol-Blanco, and J. L. Rodríguez-Fernández. 2014. Detecting apoptosis of leukocytes in mouse lymph nodes. *Nat. Protoc.* 9: 1102–1112.
29. Rodríguez-Fernández, J. L., L. Sánchez-Martín, M. Rey, M. Vicente-Manzanares, S. Narumiya, J. Teixidó, F. Sánchez-Madrid, and C. Cabañas. 2001. Rho and Rho-associated kinase modulate the tyrosine kinase PYK2 in T-cells through regulation of the activity of the integrin LFA-1. *J. Biol. Chem.* 276: 40518–40527.
30. Frantz, C., G. Barreiro, L. Dominguez, X. Chen, R. Eddy, J. Condeelis, M. J. Kelly, M. P. Jacobson, and D. L. Barber. 2008. Cofilin is a pH sensor for actin free barbed end formation: role of phosphoinositide binding. *J. Cell Biol.* 183: 865–879.
31. Bailly, M., F. Macaluso, M. Cammer, A. Chan, J. E. Segall, and J. S. Condeelis. 1999. Relationship between Arp2/3 complex and the barbed ends of actin filaments at the leading edge of carcinoma cells after epidermal growth factor stimulation. *J. Cell Biol.* 145: 331–345.
32. Watabe, M., H. Kakeya, and H. Osada. 1999. Requirement of protein kinase (Krs/MST) activation for MT-21-induced apoptosis. *Oncogene* 18: 5211–5220.
33. Deng, Y., A. Pang, and J. H. Wang. 2003. Regulation of mammalian STE20-like kinase 2 (MST2) by protein phosphorylation/dephosphorylation and proteolysis. *J. Biol. Chem.* 278: 11760–11767.
34. Glantschnig, H., G. A. Rodan, and A. A. Reszka. 2002. Mapping of MST1 kinase sites of phosphorylation. Activation and autophosphorylation. *J. Biol. Chem.* 277: 42987–42996.
35. Davies, S. P., H. Reddy, M. Caivano, and P. Cohen. 2000. Specificity and mechanism of action of some commonly used protein kinase inhibitors. *Biochem. J.* 351: 95–105.
36. Kolch, W. 2005. Coordinating ERK/MAPK signalling through scaffolds and inhibitors. *Nat. Rev. Mol. Cell Biol.* 6: 827–837.
37. Bain, J., L. Plater, M. Elliott, N. Shpiro, C. J. Hastie, H. McLauchlan, I. Klevernic, J. S. Arthur, D. R. Alessi, and P. Cohen. 2007. The selectivity of protein kinase inhibitors: a further update. *Biochem. J.* 408: 297–315.
38. Jang, S. W., S. J. Yang, S. Srinivasan, and K. Ye. 2007. Akt phosphorylates MstI and prevents its proteolytic activation, blocking FOXO3 phosphorylation and nuclear translocation. *J. Biol. Chem.* 282: 30836–30844.
39. Tan, W., D. Martin, and J. S. Gutkind. 2006. The Gα13-Rho signaling axis is required for SDF-1-induced migration through CXCR4. *J. Biol. Chem.* 281: 39542–39549.
40. Gräler, M. H., R. Grosse, A. Kusch, E. Kremmer, T. Gudermann, and M. Lipp. 2003. The sphingosine 1-phosphate receptor S1P4 regulates cell shape and motility via coupling to Gi and G12/13. *J. Cell. Biochem.* 89: 507–519.
41. Worzfeld, T., N. Wettschureck, and S. Offermanns. 2008. G(12)/G(13)-mediated signalling in mammalian physiology and disease. *Trends Pharmacol. Sci.* 29: 582–589.
42. Sekine, A., M. Fujiwara, and S. Narumiya. 1989. Asparagine residue in the rho gene product is the modification site for botulinum ADP-ribosyltransferase. *J. Biol. Chem.* 264: 8602–8605.
43. Marsland, B. J., P. Bättig, M. Bauer, C. Ruedl, U. Lässing, R. R. Beerli, K. Dietmeier, L. Ivanova, T. Pfister, L. Vogt, et al. 2005. CCL19 and CCL21 induce a potent proinflammatory differentiation program in licensed dendritic cells. *Immunity* 22: 493–505.
44. Abdollahpour, H., G. Appaswamy, D. Kotlarz, J. Diestelhorst, R. Beier, A. A. Schäffer, E. M. Gertz, A. Schambach, H. H. Kreipe, D. Pfeifer, et al. 2012. The phenotype of human STK4 deficiency. *Blood* 119: 3450–3457.
45. Nehme, N. T., J. Pachlopnik Schmid, F. Debeurme, I. André-Schmutz, A. Lim, P. Nitschke, F. Rieux-Laucat, P. Lutz, C. Picard, N. Mahlaoui, et al. 2012. MST1 mutations in autosomal recessive primary immunodeficiency characterized by defective naive T-cell survival. *Blood* 119: 3458–3468.
46. Crequer, A., C. Picard, E. Patin, A. D'Amico, A. Abhyankar, M. Munzer, M. Debré, S. Y. Zhang, G. de Saint-Basile, A. Fischer, et al. 2012. Inherited MST1 deficiency underlies susceptibility to EV-HPV infections. *PLoS One* 7: e44010.
47. Mou, F., M. Praskova, F. Xia, D. Van Buren, H. Hock, J. Avruch, and D. Zhou. 2012. The Mst1 and Mst2 kinases control activation of rho family GTPases and thymic egress of mature thymocytes. *J. Exp. Med.* 209: 741–759.
48. Huang, S., L. Y. Chen, B. L. Zuraw, R. D. Ye, and Z. K. Pan. 2001. Chemoattractant-stimulated NF-κB activation is dependent on the low molecular weight GTPase RhoA. *J. Biol. Chem.* 276: 40977–40981.
49. Liu, F., A. D. Verin, P. Wang, R. Day, R. P. Wersto, F. J. Chrest, D. K. English, and J. G. Garcia. 2001. Differential regulation of sphingosine-1-phosphate- and VEGF-induced endothelial cell chemotaxis: involvement of G(iα2)-linked Rho kinase activity. *Am. J. Respir. Cell Mol. Biol.* 24: 711–719.
50. Vichalkovski, A., K. Baltensperger, D. Thomann, and H. Porzig. 2005. Two different pathways link G-protein-coupled receptors with tyrosine kinases for the modulation of growth and survival in human hematopoietic progenitor cells. *Cell. Signal.* 17: 447–459.

THE JOURNAL OF BIOLOGICAL CHEMISTRY VOL. 290, NO. 2, pp. 827–840, January 9, 2015

A Novel MEK-ERK-AMPK Signaling Axis Controls Chemokine Receptor CCR7-dependent Survival in Human Mature Dendritic Cells*

Received for publication, July 14, 2014, and in revised form, October 31, 2014 Published, JBC Papers in Press, November 25, 2014, DOI 10.1074/jbc.M114.596551

Pilar López-Cotarelo[‡1], Cristina Escribano-Díaz[‡2], Ivan Luis González-Bethencourt[‡], Carolina Gómez-Moreira[‡3], María Laura Deguiz[‡], Jesús Torres-Bacete[‡4], Laura Gómez-Cabañas[‡5], Jaime Fernández-Barrera[‡6], Cristina Delgado-Martín[‡7], Mario Mellado[§], José Ramón Regueiro[¶], María Eugenia Miranda-Carús[‖], and José Luis Rodríguez-Fernández[‡8]

From the [‡]CIB/CSIC (Centro de Investigaciones Biológicas, Consejo Superior de Investigaciones Científicas), 28040 Madrid, the [§]CNB/CSIC (Centro Nacional de Biotecnología/Consejo Superior de Investigaciones Cientificas,) 28049 Madrid, the [¶]School of Medicine, Universidad Complutense, 28040 Madrid, and the [‖]Department of Rheumatology, Hospital La Paz, 28046 Madrid, Spain

Background: Chemokine receptor CCR7 promotes survival in mature dendritic cells (mDCs).
Results: Activated AMP-dependent kinase (AMPK) induces apoptosis in mDCs; CCR7 uses the kinases MEK1/2-ERK1/2 to regulate phosphorylation of AMPK on Ser-485 and consequently its inhibition.
Conclusion: CCR7 uses a novel MEK1/2-ERK1/2-AMPK signaling axis to induce survival in mDCs.
Significance: AMPK is a potential target to regulate mDC-mediated immune responses.

Chemokine receptor CCR7 directs mature dendritic cells (mDCs) to secondary lymph nodes where these cells regulate the activation of T cells. CCR7 also promotes survival in mDCs, which is believed to take place largely through Akt-dependent signaling mechanisms. We have analyzed the involvement of the AMP-dependent kinase (AMPK) in the control of CCR7-dependent survival. A pro-apoptotic role for AMPK is suggested by the finding that pharmacological activators induce apoptosis, whereas knocking down of AMPK with siRNA extends mDC survival. Pharmacological activation of AMPK also induces apoptosis of mDCs in the lymph nodes. Stimulation of CCR7 leads to inhibition of AMPK, through phosphorylation of Ser-485, which was mediated by $G_i/G\beta\gamma$, but not by Akt or S6K, two kinases that control the phosphorylation of AMPK on Ser-485 in other settings. Using selective pharmacological inhibitors, we show that CCR7-induced phosphorylation of AMPK on Ser-485 is mediated by MEK and ERK. Coimmunoprecipitation analysis and proximity ligation assays indicate that AMPK associates with ERK, but not with MEK. These results suggest that in addition to Akt-dependent signaling mechanisms, CCR7 can also promote survival of mDCs through a novel MEK1/2-ERK1/2-AMPK signaling axis. The data also suggest that AMPK may be a potential target to modulate mDC lifespan and the immune response.

Mature dendritic cells (mDCs)[9] are potent antigen-presenting cells that stimulate naive T cells in the lymph nodes (1). It has been shown that the longevity of mDCs importantly affects the immune response. In this regard, both mice depleted of mDCs and mice that present aberrant long lived mDCs develop autoimmune diseases (2–6). However, between these two extremes, it is observed that the immune response improves as the longevity of the mDCs increases (3, 7). The aforementioned results suggest that obtaining information on the mechanisms that regulate mDC survival can be very useful to develop strategies to modulate the longevity of these cells and improve the immune response.

Chemokine receptor CCR7 (ligands CCL19 and CCL21) directs mDCs to the lymph nodes (LNs), attracted first by CCL21, which is expressed in the lymphatic vessels that lead to the LNs, and then by both CCL19 and CCL21, which are both expressed by stromal cells in the LNs (8, 9). Apart from directing the migration of mDCs, CCR7 also promotes survival in

* This work was supported by grants awarded by the Ministerio de Educación y Ciencia (SAF2005-00801), Ministerio de Ciencia e Innovación (SAF2008-01468), Ministerio de Economía y Competitividad (SAF2011-23890), Ministerio de Economía y Competitividad (SAF2011-23890), RIER (RETICS Program/Instituto de Salud Carlos III) (RD08/0075), and Consejería de Educación y Empleo from Comunidad de Madrid (Raphyme, S2010/BMD-2350).
[1] Supported by an FPI scholarship (Ministerio de Economía y competitividad).
[2] Recipient of an I3P contract (Consejo Superior de Investigaciones Científicas-Fondo Social Europeo).
[3] Supported by a contract associated with Grant Raphyme S2010/BMD-2350 (Consejería de Educación y Empleo, Comunidad de Madrid).
[4] Recipient of a JAEdoc contract (Consejo Superior de Investigaciones Científicas-Fondo Social Europeo).
[5] Supported by an FPU scholarship (Ministerio de Educación y Ciencia).
[6] Supported by scholarship I3P intro (Ministerio de Educación y Ciencia).
[7] Partially supported by an FPI fellowship, conferred by the Ministerio de Educación y Ciencia (Spain), and by a contract associated with grant RD08/0075 (RIER).
[8] To whom correspondence should be addressed: Centro de Investigaciones Biológicas, Consejo Superior de Investigaciones Científicas. C/Ramiro de Maeztu, 9, 28040 Madrid, Spain. Tel.: 34-91-8373112, Ext. 4302; Fax: 34-34-91-5360436; E-mail: rodrifer@cib.csic.es.

[9] The abbreviations used are: mDC, mature dendritic cell; ACC, acetyl coenzyme A carboxylase; mTOR, mammalian target of rapamycin; mTORC, mTOR complex; PTX, pertussis toxin; LN, lymph node; PLN, popliteal LN; FOXO, Forkhead box class O; AMPK, AMP-dependent kinase; S6K, S6 kinase; AICAR, 5-aminoimidazole-4-carboxamide ribonucleotide; CFSE, carboxyfluorescein diacetate succinimidyl ester; PLA, proximity ligation assay; DMSO, dimethyl sulfoxide; SR, sulforhodamine B; Z, benzyloxycarbonyl; VAD-FMK, Val-Ala-Asp(OMe)-fluoromethyl ketone; OMe, O-methyl ester; Akti, Akt1/2 inhibitor; RAPA, rapamycin; Abs, antibodies; p, phospho.

these cells (10–12), although the signaling mechanisms that regulate the latter function are starting to be defined. Previously, we showed that CCR7-regulated survival in mDCs is mediated by the G_i family of G proteins and the kinase Akt (10, 11). This kinase promotes survival through activation of the transcription factor NFκB and inhibition of several pro-apoptotic targets, including the transcription factors FOXO1/3 and the kinase GSK3β (10–12).

AMP-dependent kinase (AMPK) is considered a molecular sensor of cellular energy status (13, 14). Under conditions of low cellular energy status, AMPK becomes activated, resulting in the stimulation of ATP-producing (catabolic) pathways and the inhibition of ATP-consuming (anabolic) processes (13, 14), which together lead to the recovery of the ATP/ADP ratio of the cell. Recently, it has emerged that AMPK may also promote survival (*e.g.* Ref. 15) or apoptosis (*e.g.* Ref. 16) depending on the cell type. AMPK is activated upon phosphorylation of Thr-172, which is located on the activation loop of the catalytic α-subunit of the kinase (17), and it is inhibited by phosphorylation of Ser-485/491 (AMPKα1 on Ser-485 and AMPKα2 on Ser-491) (18–20). Phosphorylation of Ser-485/491 blocks the activity of AMPK, even when Thr-172 is phosphorylated, suggesting that phosphorylation of the aforementioned Ser residues exerts a dominant inhibitory role on activity of AMPK (21). It has been shown that the kinases Akt (18, 22, 23) or S6K (21) can inhibit AMPK by directly phosphorylating Ser-485/491 in different cell types. Herein we have studied whether the kinase AMPK plays a role in the regulation of the survival of mDCs. We show, first, that AMPK can play pro-apoptotic roles in mDCs both *in vitro* and *in vivo*; second, we show that the stimulation of CCR7 in mDCs leads to a rapid inhibition of AMPK through the phosphorylation of Ser-485; third, we show that MEK/ERK mediate the CCR7-dependent inhibition of AMPK; and fourth, we show that ERK, but not MEK, interacts with AMPK. Together, these results indicate that CCR7 can contribute to extend the survival of mDCs through the novel MEK1/2-ERK1/2-AMPK signaling axis. These results also suggest that the kinase AMPK may be a potential target to modulate the immune response.

EXPERIMENTAL PROCEDURES

Reagents and Materials—CCL19, CCL21 and TNFα were from PeproTech (Rocky Hill, NJ). GM-CSF and IL4 were purchased from ImmunoTools. Fluorescent dye carboxyfluorescein diacetate succinimidyl ester (CFSE) was obtained from Molecular Probes. FLIVO™ is Val-Ala-Asp(OMe)-fluoromethyl ketone (VAD-FMK). Sulforhodamine B (SR)-FLIVO (SR, λ_{abs} 565 nm; λ_{em} >600 nm), a form of FLIVO conjugated to sulforhodamine B, was obtained from Immunochemistry Technologies, LLC. Z-VAD-FMK was obtained from Enzo (Life Sciences). LY294002, Akt1/2 inhibitor, pertussis toxin, Hoechst 33342, propidium iodide, and the anti-α-tubulin antibodies were from Sigma. Compound C (24), UO126 and PD0325901, and ERK activation inhibitor peptide II, were from Calbiochem (Nottingham, UK). Rapamycin, KU0063794, Gallein, A769662 and FR180204 were obtained from Tocris Bioscience (Bristol, UK). CAY10561 was from Cayman Chemicals (Ann Harbor, MI). The anti-Bim antibody was from Affinity Bioreagents (Golden, CO). The MEK1, β-actin, 4E-BP1, ERK1, ERK2, and anti-AMPKα1 antibodies were from Santa Cruz Biotechnology Inc. (Santa Cruz, CA). The anti-Akt1, anti Bcl-$_{xL}$, anti-AMPKα, the anti-TSC2, anti-mTOR, anti-phospho-MEK1/2 (Ser-217/221), anti-phospho-ERK1/2 (Thr-202/Tyr-204 in ERK1, Thr-185/Tyr-187 in ERK2), anti-phospho-Akt1 (Ser-473), anti-phospho-AMPKα1 (Ser-485), anti-phospho-AMPKα (Thr-172), anti-phospho-TSC2 (Thr-1462), anti-phospho-mTOR (Ser-2448) and anti-phospho-4EBP1 (Thr-37/46), anti-phospho-p70-S6K (Thr-389), and anti-p70-S6K antibodies were from Cell Signaling Technology (Beverly, MA). The anti-phospho-acetyl CoA-carboxylase (Ser-79) was from Millipore. The anti-cleave caspase 3 was form Biorbyt (Cambridge, UK).

Mice—C57BL/6 mice (8–10 weeks) were maintained in the animal facility at the Centro de Investigaciones Biológicas and treated according to Animal Care Committee guidelines.

Purification of Murine DCs and Labeling of the Cells with Fluorescent Cell Trackers—Murine DCs were purified (97% $CD11c^+$) from spleens of donor mice using magnetic beads (Miltenyi) following the manufacturer's protocol. DCs used in the *in vivo* studies were labeled for 30 min at 37 °C with 2.5 μM of the fluorescent cell tracker probe CFSE in 0.1% BSA in PBS.

Cells and Culture Conditions—Human peripheral blood mononuclear cells were isolated from buffy coats from normal donors over a Lymphoprep (Nycomed, Norway). Monocytes were purified using anti-CD14 magnetic beads (Miltenyi) following the manufacturer's protocol and then induced to differentiate to DCs by adding GM-CSF and IL4 for 7 days as indicated previously (10, 11, 25–27). The DCs were induced to mature by adding TNFα as indicated previously (10, 11, 25–27).

Assays of Apoptotic Damage in Vitro—An equal number of live mDCs (determined by exclusion on trypan blue staining) were incubated in 0.1% BSA or 10% FCS in RPMI in the presence or absence of AMPK activators. Subsequently, the mDCs were harvested and plated for 40 min on polyornithine-coated coverslips. Apoptotic nuclear morphology was assessed using Hoechst 33342 staining as indicated previously (10, 11, 25, 26) or by analyzing the loss of nuclear DNA content by flow cytometry using propidium iodide as indicated elsewhere (28, 29).

Cell Lysis and Western Blot Analysis—To reduce the basal levels of activity of the molecules analyzed, mDCs (100×10^3 cells) were maintained in 0.1% BSA/RPMI for 30 min before starting the stimulation with chemokines. Mature DCs were then stimulated with chemokines for the indicated periods of time. The stimulation was terminated by solubilizing the cells in SDS-PAGE sample buffer (100 mM Tris/HCl, pH 6.8, 0.05 mM sodium orthovanadate, 3% SDS, 1 mM EDTA, 2% 2-β-mercaptoethanol, 5% glycerol) and boiled and then fractionated by SDS-PAGE and transferred to nitrocellulose membranes. After blocking with 5% nonfat milk protein in TBST (TBS plus 0.1% Tween 20), pH 7.5, membranes were incubated with the indicated antibodies in TBST and visualized with the appropriate HRP-conjugated secondary antibodies (Santa Cruz Biotechnology) and an ECL substrate (Pierce) detection system. Quantification of the blots was performed using MultiGauge software from Fujifilm.

Immunoprecipitation—Mature DC (~50×10^6 DCs) were dissolved in lysis buffer A (1% Nonidet P-40, 100 mM NaCl, 1 mM EDTA, 0.5 μM vanadate, and 20 mM Hepes, pH 7.4, includ-

ing a protease inhibition mixture (Sigma), and subjected to immunoprecipitation with anti-AMPKα antibody in the presence of TrueBlot™ anti-rabbit Ig agarose beads (TrueBlot™, eBioscience, San Diego, CA). Immunoprecipitates were washed five times in lysis buffer and then boiled in SDS-PAGE sample buffer supplemented with 50 mM dithiothreitol. After SDS-PAGE and transfer to nitrocellulose, the primary antibody step was followed by incubation with a horseradish peroxidase-conjugated antibody that recognizes native rabbit IgG (TrueBlot™, eBioscience).

SiRNAs and Nucleofections—Random control and AMPKα1 siRNAs were obtained from Santa Cruz Biotechnology. The siRNAs were transfected into mDCs by using nucleofection technology (Amaxa Biosystems) according to the manufacturer's instructions.

Proximity Ligation Assay (PLA)—The assay was performed on mDC seeded onto polyornithine-coated coverslips. The mDCs were treated with CCL21 and fixed in 4% paraformaldehyde. Staining with primary antibodies was performed as in conventional immunofluorescence. However, instead of using fluorescently labeled secondary antibodies, a PLA was carried following the manufacturer's instructions (30) (Duolink II *in situ* PLA detection kit, Olink Bioscience). Briefly, samples were incubated with secondary antibodies conjugated with DNA probes (MINUS and PLUS DNA probes). Probes were hybridized and ligated, followed by amplification of the DNA template in a rolling circle amplification reaction. A detection solution was added to identify amplified DNA. Finally, coverslips with the cells were prepared using mounting medium that includes DAPI to stain the nuclei. The coverslips were analyzed with a confocal microscope, and the interactions among ERK and AMPK proteins, detected as distinct fluorescent spots inside each DC, were subsequently quantified.

Two-photon Microscopy and Analysis of Apoptotic CFSE-labeled Dendritic Cells in the Lymph Nodes—The method has been described in detail previously (10, 25, 26, 31). Briefly, CFSE-labeled splenic mDCs (10^8 mDCs/ml) were dissolved in 20 μl of RPMI and injected subcutaneously along with LPS (1 μg/ml) into the hind footpad of recipient C57BL/6 mice (2×10^6 mDCs per footpad). After 36 h, when the mDCs have already reached the popliteal LNs (PLNs) (26, 32), treated or control animals were injected intraperitoneally, respectively, with the AMPK activator A769662 (3.6 mg/25 g of mice in DMSO) or with vehicle control DMSO. 40.5 h after initiation of the experiment, the mice were injected intravenously with SR-FLIVO (SR, λ_{abs} 565 nm; λ_{em} >600 nm), and after an additional 1 h, the mice were sacrificed, and the popliteal LNs were extracted from the mice and subsequently subjected to two-photon confocal analysis to visualize among the injected CFSE-mDCs those that present SR-FLIVO staining (see "Results"). Two-photon microscopy and analysis of apoptotic CFSE-DCs in the LNs was performed as described previously (31).

Statistics—Data are expressed as mean ± S.D., and significance of differences between two series of results was assessed using the Student's *t* test. Values of $p < 0.05$ were considered significant, and *ns* indicates non-significant differences.

RESULTS

AMPK Promotes Apoptosis in Mature Dendritic Cells in Vitro—To determine whether AMPK could regulate apoptosis in mDCs, we maintained the cells in complete medium in the absence or in the presence of the selective AMPK activators A769662 or AICAR. A769662 is a direct allosteric activator of AMPK (36). AICAR is an agent that is transported into cells where it is phosphorylated to form the AMP-mimetic *S*-aminoimidazole-4-carboxamida ribonucleoside monophosphate (ZMP), which activates AMPK without altering the intracellular levels of AMP or ATP (33) (Fig. 1*A*). Western blotting analysis using antibodies that recognize a phosphorylated/active AMPKα (p-AMPK (Thr-172)), or phosphorylated acetyl coenzyme A carboxylase (ACC) (p-ACC (Ser 79)), which is a direct target of active AMPK (34), confirmed that the treatment of mDCs with A769662 or AICAR induced activation of AMPK (Fig. 1*A*, *panel a*). We treated the mDCs with the AMPK activators and then measured the percentage of apoptosis by staining the nuclei of the cells with Hoechst 33342. DCs treated with Akti1/2, a potent inhibitor of the pro-survival kinase Akt (10, 11, 25), were used as positive controls of apoptosis. As shown in Fig. 1*A*, *panels b* and *c*, mDCs treated with pharmacological activators of AMPK displayed increased percentage of apoptosis. Similar results were obtained when, instead of Hoechst staining, apoptosis was measured by analyzing the loss of nuclear DNA content typical of apoptotic cells by flow cytometry using propidium iodide as label (28, 29) (Fig. 1*A*, *panel d*) or the activation of caspase-3, another well known apoptotic marker (Fig. 1*A*, *panel e*). When the pharmacological activators of AMPK were used to induce apoptosis in mDCs that had been pretreated with Z-VAD-FMK, a general caspase inhibitor, the effects of the AMPK activators on the apoptosis of the cells were abrogated, indicating that these agents induce caspase-dependent cell death (Fig. 1*B*). Finally, to corroborate that AMPK played pro-apoptotic roles in DCs, we reduced AMPK levels using siRNA (Fig. 1*C*, *panel a*). When DCs with normal or reduced levels of AMPK were shifted to 0.1% BSA/RPMI for 24 h and then stained with Hoechst 33342, it was observed that the mDCs that displayed reduced levels of AMPK (Fig. 1*C*, *panel b*) also presented a reduced percentage of apoptosis. Together, these results indicate that AMPK can promote apoptosis in mDCs.

We analyzed potential mechanisms whereby active AMPK could induce apoptosis in DCs. Previously, we reported that the kinase GSK3β may induce apoptosis in DCs by promoting the translocation to the nucleus of the transcription factor FOXO (10), which controls the expression of the pro-apoptotic Bcl2 family member Bim (10, 25, 26, 35). We tested whether similarly active AMPK could also promote the translocation of FOXO and induce overexpression of Bim in DCs. For this purpose, we transfected the DCs with FOXO1-GFP and then induced activation of AMPK by stimulating the DCs with AICAR or A769662. As shown in Fig. 2*A*, these agents induced a significant increase in the number of DCs that displayed FOXO-GFP in the nucleus. Consistent with these results, the stimulation of DCs with AICAR or A769662 also caused an increase in Bim levels in the DCs (Fig. 2*B*). In similar experi-

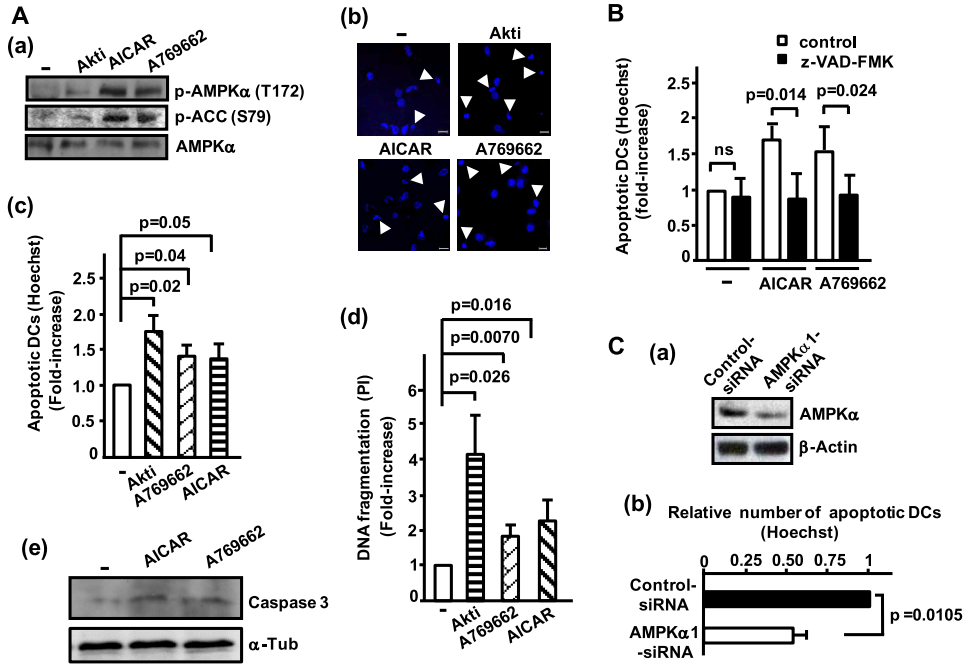

FIGURE 1. **AMPK induces apoptosis in dendritic cells.** *A*, *panel a*, DCs were suspended in 10% FCS in RPMI and then incubated for 24 h either in this medium alone (−) or in this medium plus Akti (5 μM), AICAR (1 mM), or A769662 (25 μM). Aliquots of DCs were subjected to a Western blotting analysis with Abs against phospho-AMPKα (Thr-172), phospho-ACC, or total AMPKα. *Panel b*, photographs taken from representative samples of the Hoechst 33342 stained DCs treated as in *panel a*. *Arrowheads* indicate apoptotic cells, showing condensed or fragmented nuclei. *Panel c*, DCs were suspended in 10% FCS in RPMI and then incubated in medium alone (−) or in medium plus Akti, AICAR, or A769662, as in *panel a*. The number represents -fold increase in the number of apoptotic DCs, determined by Hoechst 33342 staining, with respect to the control untreated DCs kept in 10% FCS in RPMI, which was considered as 1. Results shown represent the mean ± S.D. ($n = 4$). *Panel d*, the cells were treated or not with Akti, AICAR, or A769662 as in *panel b*. The number represents -fold increase in the number of DCs that presented DC fragmentation upon propidium iodide (*PI*) staining with respect to control untreated DCs kept in 10% FCS in RPMI. Results shown represent the mean ± S.D. ($n = 6$). *Panel e*, the DCs were suspended in 10% FCS in RPMI and then incubated for 33 h either in this medium alone (−) or in this medium plus AICAR or A769662 as in *panel a*. Aliquots of DCs were subjected to a Western blotting analysis with an antibody against caspase-3. The blots were probed with an antibody against α-tubulin to show equal loading. A representative experiment out of two performed is shown. *B*, DCs were suspended in 0.1% BSA in RPMI and then incubated for 40 h either in this medium alone (−) or in medium including AICAR (1 mM) or A769662 (25 μM), either in the absence (*control*) or in the presence of 10 μg/ml pan caspase inhibitor z-VAD-FMK. The apoptotic DCs observed in medium alone (−) untreated with z-VAD-FMK were given an arbitrary value of 1, and the -fold increase of apoptosis in the other samples was referred to this value. Results shown represent the mean ± S.D. ($n = 5$). *ns* indicates non-significant differences. *C*, mDCs were nucleofected either with random siRNA (control siRNA) or with a siRNA specific for AMPK (AMPKα1 siRNA). *Panel a*, 36 h after nucleofection, mDCs were washed in RPMI, and then an equal number of live DCs, determined by trypan blue exclusion, were subjected to Western blotting with an anti-AMPKα antibody. To confirm equal loading, the blots were reprobed with an antibody reacting with β-actin. *Panel b*, samples of DCs nucleofected either with control or with AMPKα1 siRNA were washed in RPMI, and then an equal number of live DCs, determined by trypan blue exclusion, were transferred to 0.1% BSA in RPMI for an additional 24 h. At the end of this period, the DCs were stained with Hoechst. The number of apoptotic DCs observed in the control siRNA nucleofected DCs was given an arbitrary value of 1, and the number of apoptotic DCs observed in AMPK siRNA-transfected DCs was referred to this value. Results shown represent the mean ± S.D. ($n = 3$).

ments, we did not observe any change in the expression of the pro-survival Bcl2 member Bcl-$_{xL}$ (not shown). Together, these results suggest that AMPK could induce apoptosis in DCs by promoting translocation of pro-apoptotic FOXO1 to the nucleus, which up-regulates the expression of the pro-apoptotic Bim.

Because it has been shown that AMPK inhibits the kinase mammalian target of rapamycin complex 1 (mTORC1) (36, 37), and mTORC1 has been shown to mediate the pro-survival signaling of the kinase Akt (38), we hypothesized that active AMPK may induce apoptosis by interfering with the pro-survival signaling induced from mTORC1 in DCs. To test this concept first, we analyzed whether mTORC1 plays a pro-survival role in DCs. Inhibition of mTORC1 by treating the DCs with the highly selective inhibitor rapamycin (RAPA) induces apoptosis, indicating that mTORC1 promotes survival in these cells (Fig. 2*C*). Next we studied whether CCR7 could also induce activation of mTORC1. As shown in Fig. 2*D*, simulation of CCR7 with CCL21 induces phosphorylation/inhibition of the mTORC upstream inhibitory molecule TSC2 and an increase in the phosphorylation of 4EBP1, a direct downstream target of mTORC (Fig. 2*D*), together indicating that CCR7 induces activation of mTORC1. Finally, we analyzed whether active AMPK could inhibit CCR7-dependent activation of mTORC1 (Fig. 2*E*). The treatment of the DCs with A769662 or AICAR, which, as indicated by the elevated levels of active/phosphorylated AMPK (Thr-172), induced activation of AMPK (Fig. 2*E*), also inhibited mTORC1 activity, as indicated by the reduction in the phosphorylation of 4EBP1 (Fig. 2*E*). Together, these results indicate that in DCs, active AMPK may also promote apoptosis by inhibiting mTORC1.

Stimulation of CCR7 Receptor Induces Phosphorylation/Inhibition of AMPK—As we have shown previously that stimulation of CCR7 protects mDCs from apoptosis (10, 11), we hypothesized that this receptor could also induce inhibition of pro-apoptotic AMPK in these cells. To test this hypothesis, the mDCs were treated with CCL21 for various times and then lysed in sample buffer. Subsequently, we examined the activity of AMPK using an antibody that recognizes the phosphorylated/inactive form of AMPKα1 (p-Ser-485). Stimulation with

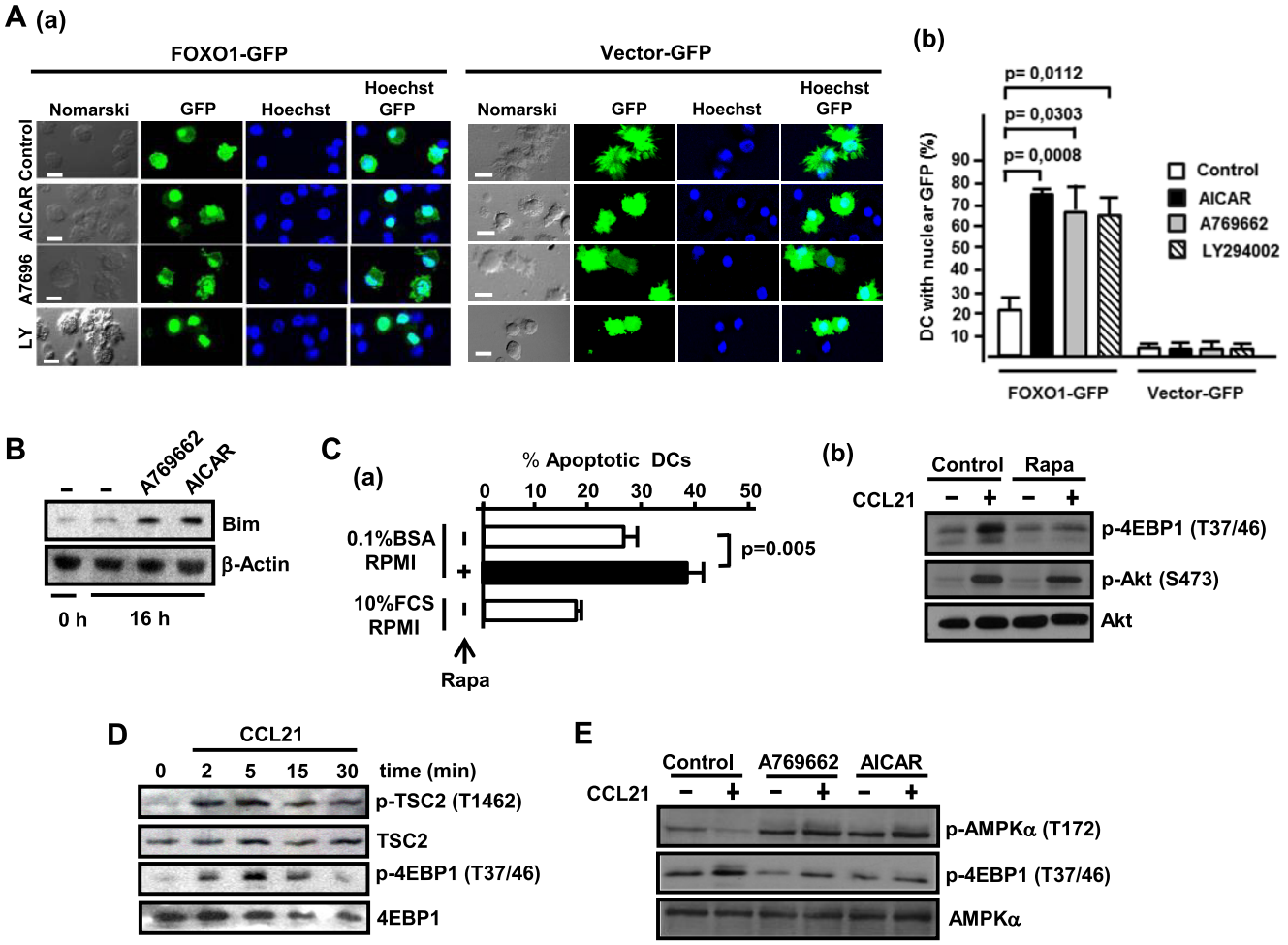

FIGURE 2. **Active AMPK may promote apoptosis by inducing translocation of FOXO1 to the nucleus and by inhibiting mTORC1.** *A*, *panel a*, the DCs were transfected with vector or FOXO1-GFP, and 6 h after transfection, the cells were resuspended in 10% FCS RPMI and then either kept untreated (*Control*) or treated with AICAR (1 mM), A769662 (25 μM), or LY294002 (*LY*, 100 μM) for an additional 2.5 h. Subsequently, the DCs were plated onto polyornithine-coated coverslips, fixed, permeabilized, and stained with Hoechst 33342. The DCs were examined with a fluorescence microscope. *Scale bar* represents 20 μm. *Panel b*, bar diagram representing the percentage of vector- or FOXO1-GFP-transfected DCs with GFP staining concentrated in the nucleus. Results shown represent the mean ± S.D. ($n = 3$). *B*, DCs were suspended in 0.1% BSA in RPMI and then kept untreated (−) or stimulated with A769662 (25 μM) or AICAR (1 mM) for 16 h. Aliquots of the DCs were subjected to a Western blot with an Ab against Bim. Blots were reprobed with an antibody reacting with β-actin to show equal loading (a representative experiment is shown). *C*, *panel a*, the DCs were suspended in 0.1% BSA in RPMI and then treated (+) or not (−) for 40 h with RAPA (100 nM). DCs maintained in 10% FCS in RPMI were used as negative controls. The DCs were plated on polyornithine-coated coverslips, fixed, and stained with Hoechst, and the apoptotic cells were examined as indicated under "Experimental Procedures." Results shown represent the mean ± S.D. ($n = 3$). *Panel b*, to confirm that RAPA inhibited mTORC1, aliquots of the control or RAPA-treated DCs from *panel a* were stimulated (+) or not (−) with CCL21 (15 nM). Subsequently, the DCs were lysed and analyzed by SDS-PAGE, followed by Western blotting. The blots were analyzed with Abs against phosphorylated 4EBP1 (Thr-37/46) or phosphorylated Akt (Ser-473). To show equal loading, the membranes were reprobed with an Ab against Akt. *D*, DCs (100,000 cells), suspended in 0.1% BSA in RPMI, were stimulated for the indicated times with CCL21 (15 nM) and then lysed and analyzed by SDS-PAGE, followed by Western blotting with Abs against phosphorylated TSC2 (Thr-1462) or phosphorylated 4EBP1 (Thr-37/46). To show equal loading, the membranes were reprobed with Abs against total 4EBP1. A representative experiment out of three performed is shown. *E*, the DCs were suspended in 0.1% BSA in RPMI and then kept untreated (*Control*) or treated with A769662 (25 μM) or AICAR (1 mM) for 60 min. Subsequently, the DCs were stimulated (+) or not (−) with CCL21 (15 nM) and then lysed and analyzed by SDS-PAGE, followed by Western blotting. The blots were analyzed with Abs against phosphorylated 4EBP1 (Thr-37/46) or phosphorylated AMPKα (Thr-172). To show equal loading, the membranes were reprobed with an Ab against AMPKα.

CCL21 (Fig. 3*A*) or CCL19 (not shown) induced inactivation of AMPK, which remained at relatively high levels until 60 min and only decayed after 120 min (Fig. 3*A*). Consistent with these results, stimulation of CCR7 caused also a reduction of the phosphorylation of the AMPK substrate ACC (Fig. 3*B*). When we used an antibody that recognizes the active form of AMPK (p-Thr-172), it was observed that stimulation of CCR7 also led to reduced levels of this active form of AMPK (Fig. 3*B*). Finally, the treatments of the mDCs with Compound C, a selective inhibitor of AMPK (24), blunted the phosphorylation of the active form of AMPK (p-Thr-172) (Fig. 3*C*, *panel a*), but failed to affect the CCR7-induced phosphorylation of Ser-485 on AMPK (Fig. 3*C*, *panel b*). Because AMPK activity is completely blunted after the treatment with Compound C, these results indicate that upon stimulation of CCR7, the phosphorylation of AMPK on Ser-485 was not due to an autophosphorylation event, but to the activity of an upstream kinase. In summary, these experiments indicate that stimulation of CCR7 in mDC causes phosphorylation on Ser-485 and inhibition of AMPK, which is mediated by an upstream kinase.

Activation of AMPK Induces Apoptosis of Murine DCs in the Lymph Nodes—We studied whether active AMPK could also play a pro-apoptotic role in the LNs, the setting where DCs present antigens to naive T-cells during the initiation of the

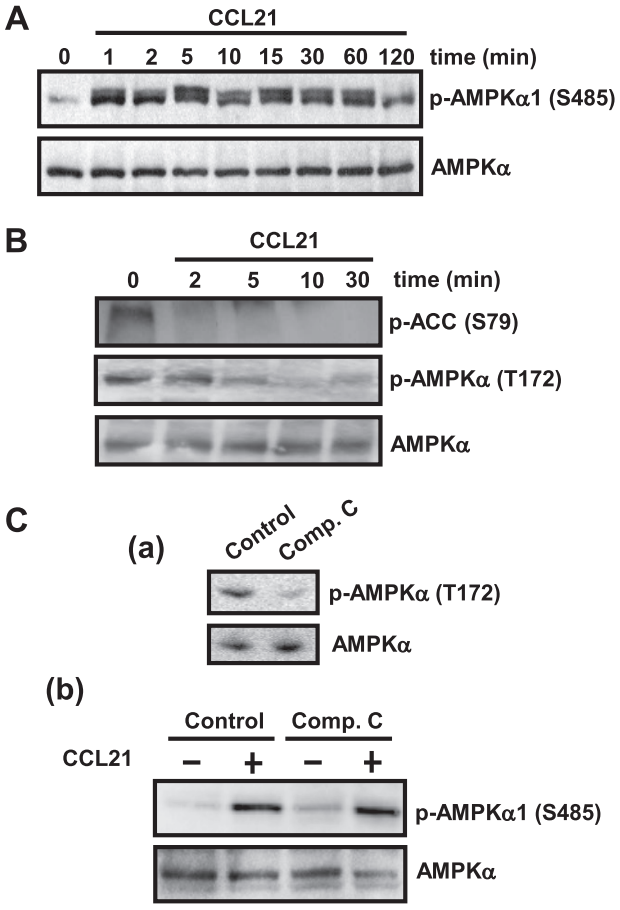

FIGURE 3. **Stimulation of CCR7 induces phosphorylation/inhibition of AMPK.** *A*, DCs (100,000 cells), suspended in 0.1% BSA in RPMI, were stimulated for the indicated times with CCL21 (15 nM) and then lysed and analyzed by SDS-PAGE, followed by Western blotting with Abs against phosphorylated/inhibited AMPKα1 (Ser-485). To show equal loading, the membranes were reprobed with Abs against total AMPKα. A representative experiment out of three performed is shown. *B*, DCs (100,000 cells), suspended as in *A*, were stimulated with CCL21 for the indicated times and then extracted and subjected to a Western blotting with Ab against phospho-ACC (Ser-79) and against phosphorylated/active AMPKα (Thr-172). To show equal loading, the membrane was reprobed with an Ab against total AMPKα. A representative experiment out of three performed is shown. *C*, *panel a*, DCs, suspended as in *panel a*, were either untreated (*Control*) or treated with AMPK inhibitor Compound C (*Comp. C*, 20 μM) for 60 min. Control and Compound C-treated DCs were stimulated with CCL21 (15 nM) for 5 min, and subsequently, lysed and subjected to Western blot analysis with Abs against phospho-AMPKα (Thr-172) and AMPKα. A representative experiment out of three performed is shown. *Panel b*, aliquots of the control or Compound C-treated samples, stimulated or not with CCL21, were used to analyze the activity of AMPK using the anti-phosphorylated AMPKα1 (Ser-485) antibody. To show equal loading, the membrane was reprobed with an Ab against total AMPKα.

immune response. Before performing the experiment *in vivo*, we first analyzed whether the treatment with AMPK activators also induced apoptosis in the splenic mDCs *in vitro*. Treatment with AICAR and A769662 significantly enhanced the activity of AMPK (Fig. 4*A*, *panel a*) and the apoptosis of the cells (Fig. 4*A*, *panel b*), indicating that active AMPK is also pro-apoptotic in splenic mDCs in culture. Furthermore, stimulation of splenic mDCs with murine CCL19 or CCL21 also induced, as in human mDCs, phosphorylation of AMPK on Ser-485 (Fig. 4*B*).

As it is known that conventional mDCs that arrive from peripheral tissues to the LNs become largely apoptotic in these regions (26, 39), we studied whether activators of AMPK could enhance the percentage of apoptotic mDCs inside the PLNs, which would indicate that active AMPK plays pro-apoptotic roles in these cells *in vivo*. For this purpose, C57BL/6 mice were injected subcutaneously in the hind footpad with CFSE-labeled splenic DCs. After 36 h, a time at which, as we previously demonstrated (26), there are a significant number of CFSE-labeled DCs positioned in the PLNs, the mice were injected intraperitoneally with 100 μmol of A769662. Control animals were injected with the same amount of vehicle (Fig. 4*C*, *panel a*). After an additional 4.5 h, the animals were injected intravenously with SR-FLIVO, a poly-caspase binding inhibitor probe (VAD-FMK) conjugated to a fluorescent dye that binds irreversibly to apoptotic caspases and allows the detection of apoptotic cells *in vivo* (10, 25, 26, 31). 1 h after the injection of SR-FLIVO, the mice were sacrificed, and the PLNs were obtained and analyzed by two-photon microscopy. In these experiments, if AMPK is pro-apoptotic, an enhanced SR-FLIVO staining in the mDCs in the PLNs obtained from the A769662-treated animals would be expected when compared with the vehicle-treated controls. Consistent with this prediction, mice injected with A769662 displayed a significant increase in the percentage of SR-FLIVO-labeled CFSE-DCs, indicating that active AMPK plays pro-apoptotic roles in the mDCs *in vivo* (Fig. 4*C*, *panels b* and *c*). We also observed induction of apoptosis in the DCs inside the PLNs when the mice were injected with AICAR (not shown). In summary, the prior experiments indicate that active AMPK promotes apoptosis of mDCs both *in vivo* and *in vitro*.

CCR7-dependent Inhibition of AMPK in mDCs Is Mediated by G_i and Gβγ, but Not by PI3K/Akt or S6K—In the next experiments, we studied the signaling pathway that could regulate the phosphorylation/inhibition of AMPK downstream of CCR7. As the G_i protein family of G proteins and the Gβγ dimers associated to these proteins mediate CCR7-dependent survival in mDCs (10, 11), we tested their involvement in the control of CCR7-dependent inhibition of AMPK. G_i-mediated signaling was blocked by treating the mDCs with the selective inhibitor pertussis toxin (PTX), and Gβγ-mediated signaling was blocked by treating the cells with Gallein (40). The observed inhibition of the CCR7-dependent phosphorylation of ERK1/2 (Fig. 5*A*, *panels a* and *b*), two kinases known to be regulated by G_i and Gβγ (10, 27), indicated that both PTX and Gallein efficiently blocked their targets. The treatment with PTX or Gallein also blunted the CCR7-induced phosphorylation of AMPK on Ser-485 (Fig. 5*A*, *panels a* and *b*), indicating that G_i and Gβγ regulate the phosphorylation of AMPK on Ser-485 downstream of CCR7.

Stimulation of CCR7 induces activation of Akt in mDCs (10, 11, 41), which is also controlled by the G_i family of proteins (10, 11). As Akt mediates the phosphorylation of Ser-485 on AMPK in a variety of cell types (18, 22, 23, 42), we analyzed whether it could also play a similar role downstream of CCR7 in mDCs. Surprisingly, the blocking of the activity of Akt, with the PI3K inhibitor LY294002 (Fig. 5*B*, *panel a*) or with the selective Akt inhibitor Akti1/2 (43) (Fig. 5*B*, *panel b*), failed to affect CCR7-dependent phosphorylation of AMPK on Ser-485, indicating that Akt does not mediate CCR7-dependent inhibition of AMPK in mDCs. Further emphasizing that Akt and AMPK are

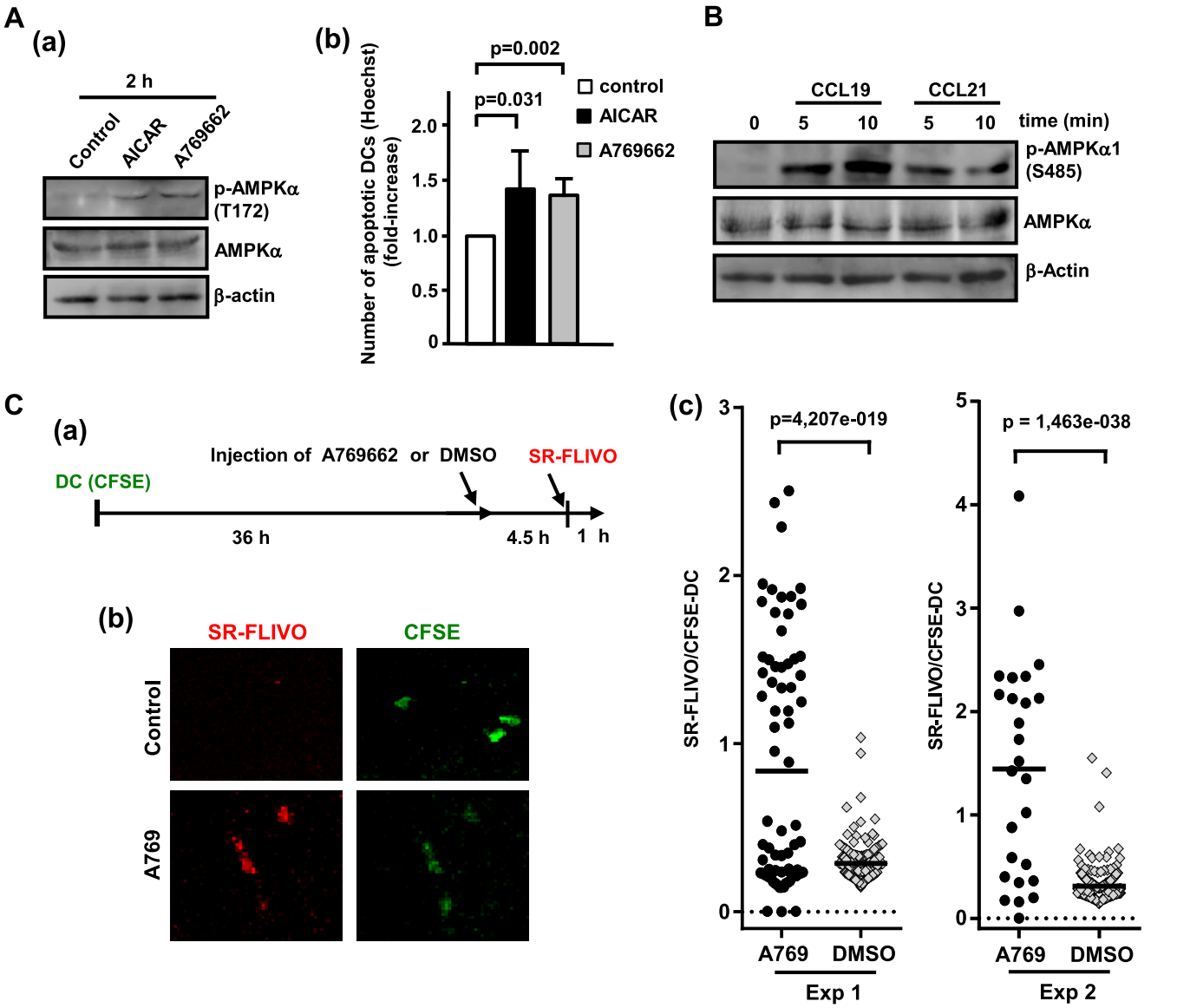

FIGURE 4. **Activation of AMPK increases the apoptosis of dendritic cells *in vitro* and in the lymph nodes.** *A*, *panel a*, splenic mDCs (500,000 cells) suspended in 10% FCS in RPMI were kept unstimulated (*Control*) or stimulated for the indicated times with AICAR (1 mM) or A769662 (25 μM) and then lysed and analyzed by SDS-PAGE, followed by Western blotting with Abs against phospho-AMPKα (Thr-172), total AMPKα and β-actin. A representative experiment out of five performed is shown. *Panel b*, aliquots of the splenic DCs treated as in *panel a* for 2 h were fixed and stained with Hoechst 33342 to detect apoptotic DCs. The number represents the -fold increase in the number of apoptotic DCs respect to the number of apoptotic DCs observed in the controls that was considered as 1. Results represent the mean $\pm$ S.D. ($n = 6$ experiments). *B*, splenic DCs (500,000 cells) suspended in 0.1% BSA in RPMI were stimulated for the indicated times with murine CCL19 or CCL21 (both at 15 nM) and then lysed and analyzed by SDS-PAGE, followed by Western blotting with Abs against phospho-AMPKα1 (Ser-485), total AMPKα, and β-actin. A representative experiment out of five performed is shown. *C*, *panel a*, experimental protocol. 2×10^6 CFSE-labeled splenic DCs were injected in the footpads of recipient mice. After 36 h, the animals were injected intraperitoneally with 100 μmol of A769662 or a similar volume of vehicle DMSO. After an additional 4.5 h, mice were injected (intravenously) with SR-FLIVO to stain apoptotic DCs in the LNs. After 1 h, the popliteal LNs were extracted, fixed, and subjected to two-photon analysis. *Panel b*, representative SR-FLIVO staining displayed by CFSE-labeled DCs obtained from the LNs of animals treated either with A769662 or with DMSO. The LNs of the mice were extracted and studied by two-photon microscopy as indicated under "Experimental Procedures." *Panel c*, the stacks of optical images of the LNs were examined with the Leica confocal software, and the values of the maximum amplitude of the SR-FLIVO and CFSE channel were obtained as indicated previously (see "Experimental Procedures"). Data from two experiments are presented. The data are represented as maximum intensity of SR-FLIVO over maximum intensity of CFSE for each individual DC in an LN. For A769662-treated animals, 74 DCs were analyzed in Experiment 1 (*Exp 1*), and 26 DCs were analyzed in Experiment 2 (*Exp 2*); for DMSO vehicle-treated animals, 171 DCs were analyzed in Experiment 1 (*Exp 1*), and 237 DCs were analyzed in Experiment 2(*Exp 2*).

independently regulated, the inhibition of AMPK, by treating the mDCs with Compound C, did not affect the CCR7-dependent phosphorylation of Akt (not shown).

Stimulation of CCR7 also induces activation of the mammalian target of rapamycin complex 1 (mTORC1) (Fig. 5*C*), which promotes survival in mDCs (Fig. 2*C*). Recently, it has been shown that S6K, a molecule that is regulated by mTORC1 (44), may also directly phosphorylate AMPK on Ser-485 (21). Therefore, we studied whether inhibition of S6K could block CCR7-dependent phosphorylation of AMPK on Ser-485. To inhibit S6K, we treated the mDCs with pharmacological agents that block either Akt (Akti) or mTORC1 (RAPA or KU0063794), both upstream regulators of S6K (44) (Fig. 5*D*). To analyze S6K activity, we used an antibody that recognizes a phosphorylated/

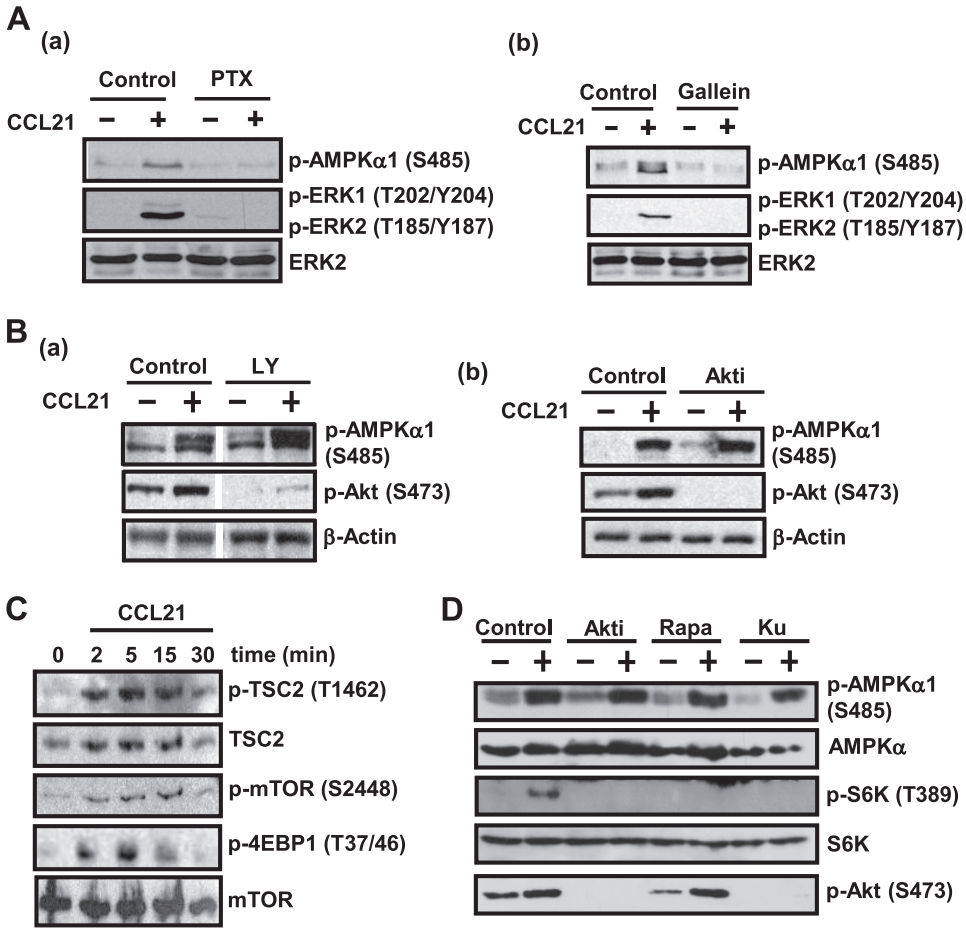

FIGURE 5. **Signaling downstream of CCR7 regulating the phosphorylation of AMPKα1 on serine 485.** *A*, *panel a*, DCs (100,000 cells) in complete medium were either kept untreated (*Control*) or treated with PTX (100 ng/ml) for 180 min. Subsequently, the DCs were washed and suspended in 0.1% BSA in RPMI. Control and PTX-treated DCs were stimulated with CCL21 (15 nM) for 5 min and subsequently lysed and subjected to Western blotting with the Ab against phosphorylated AMPKα1 (Ser-485) or phosphorylated ERK1/2 (Thr-202/Tyr-204 ERK1/Thr-185/Tyr-187 ERK2). ERK2 levels show equal loading of the gels. A representative experiment out of three performed is shown. *Panel b*, DCs, untreated or pretreated with the Gβγ inhibitor Gallein (40) for 15 min, were stimulated or not with CCL21 for 5 min and then lysed, and aliquots were subjected to Western blotting with an Ab against phosphorylated AMPKα1 (Ser-485) and phosphorylated ERK1/2 as in *panel a*. ERK2 levels show equal loading of the gels. A representative experiment out of three performed is shown. *B*, DCs suspended in 0.1% BSA in RPMI were either left untreated (*Control*) or pretreated for 60 min with the PI3K inhibitor LY294002 (*LY*, 100 μM, 60 min) (*panel a*) or Akti (5 μM) (*panel b*). The DCs were subsequently stimulated or not with CCL21 (15 nM) for 5 min and then lysed, and aliquots were subjected to Western blot with the Ab against phosphorylated/inhibited AMPKα1 (Ser-485) or against phosphorylated/active Akt1 (Ser-473). β-Actin levels show equal loading of the gels. A representative experiment out of three performed is shown. *C*, DCs (100,000 cells), suspended in 0.1% BSA in RPMI, were stimulated for the indicated times with CCL21 (15 nM) and then lysed and analyzed by SDS-PAGE, followed by Western blotting with Abs against phosphorylated TSC2 (Thr-1462), phosphorylated mTOR (Ser-2448), or phosphorylated 4EBP1 (Thr-37/46). To show equal loading, the membranes were reprobed with Abs against total TSC2 and mTOR. *D*, DCs suspended in 0.1% BSA in RPMI were either left untreated (*Control*) or pretreated for 60 min with Akti (5 μM), RAPA (100 nM), or KU0063794 (*Ku*) (500 nM). The DCs were subsequently stimulated or not with CCL21 (15 nM) for 5 min. The DCs were then lysed and analyzed by Western blotting with Abs against phosphorylated/inactive AMPKα1 (Ser-485), phosphorylated/active S6K (Thr-389), and phosphorylated/active Akt (Ser-473). Membranes were also probed with antibodies that recognize total S6K and AMPKα.

active form of this kinase (p-S6K (Thr-389)). Treatment of the mDCs with the inhibitors Akti1/2 (43), rapamycin (43, 45), and Ku (46), to inhibit Akt, mTORC1 and mTORC1/2, respectively, blunted, as expected, the activation of S6K. However, despite strong inhibition of S6K, the CCR7-dependent phosphorylation of AMPK on Ser-485 was not affected (Fig. 5*D*). These results indicate that Akt, mTORC1, mTORC2, and S6K do not mediate CCR7-dependent inhibition of AMPK in mDCs (see model in Fig. 9).

CCR7-dependent Inhibition of AMPK in DCs Is Mediated by MEK/ERK—Upon stimulation of the mDCs with CCL21, we observed similar kinetics in the activation of the kinases MEK1/2/ERK1/2 and phosphorylation of AMPK on Ser-485 (Fig. 6*A*). Therefore, we studied whether MEK1/2/ERK1/2 could mediate the phosphorylation of AMPK on Ser-485 downstream of CCR7. Treatment of the cells with UO126 (Fig. 6*B*) or PD03255901 (Fig. 6*C*), two potent and selective inhibitors of MEK1/2 (45) and, consequently of ERK1/2, the only known downstream targets of MEK1/2 (47), blunted CCR7-dependent phosphorylation of AMPK, indicating that MEK1/2 regulates the phosphorylation of AMPK on Ser-485 downstream of CCR7. In the next experiments, we studied whether ERK1/2 could also regulate AMPK phosphorylation on Ser-485. Our attempts to reduce the expression of ERK1 or ERK2 in mDCs using siRNAs were unsuccessful. Although the siRNAs used readily blunted ERK1 and ERK2 expression in HL-60 cells, we were unable to reduce the levels of these two kinases in mDCs (not shown). Therefore, we decided to use two pharmacological inhibitors to block ERK1/2 activity, namely, CAY10561 (Fig. 7*A*) and FR180204 (Fig. 7*B*). CAY10561 displays a high selec-

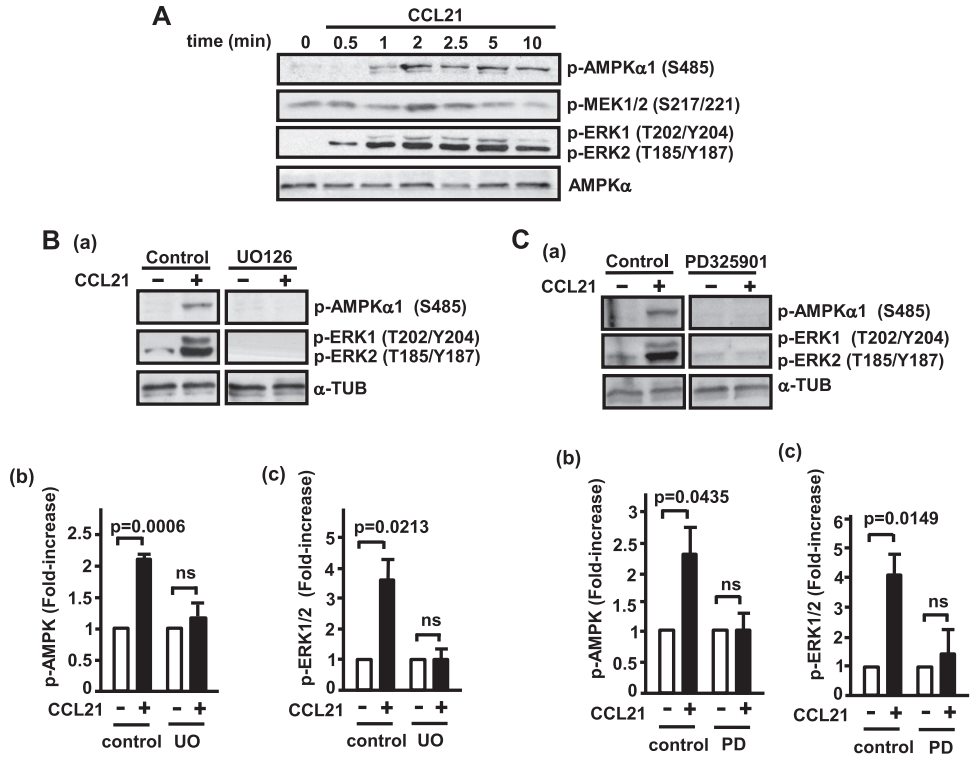

FIGURE 6. **CCR7-dependent phosphorylation/inhibition of AMPK is mediated by MEK.** *A*, DCs (100,000 cells) suspended in 0.1% BSA in RPMI were stimulated for the indicated times with CCL21 (15 nM) and then lysed and analyzed by SDS-PAGE, followed by Western blotting with Abs against phosphorylated AMPKα1 (Ser-485), MEK1/2 (Ser-217/221), or ERK1/2 (Thr-202/Thr-204 ERK1/Thr-185/Tyr-187 ERK2). To show equal loading, the membranes were reprobed with an Ab against AMPKα. A representative experiment out of three performed is shown. *B*, *panel a*, DCs suspended in 0.1% BSA in RPMI were either left untreated (*Control*) or pretreated with UO126 (2.5 μM, 60 min). The mDCs were subsequently stimulated or not with CCL21 for 5 min and then lysed, and the aliquots were subjected to Western blot with an antibody against phosphorylated/inactive AMPKα1 (Ser-485) or phosphorylated active ERK1/2 (Thr-202/Tyr-204 ERK1/Thr-185/Tyr-187 ERK2). α-Tubulin (*α-TUB*) levels show equal loading of the gels. A representative experiment out of three performed is shown. *Panel b*, -fold increase in the phosphorylation of AMPK in control and UO126 (*UO*)-treated mDCs, upon stimulation with CCL21. In both control and UO126-treated DCs, the degree of phosphorylation of the unstimulated DCs was given an arbitrary value of 1, and -fold increase in the CCL21-stimulated mDCs was represented. *Panel c*, similar to *panel b* with the difference that -fold increase in phosphorylation of ERK1/2 was examined. *C*, *panel a*, the experiments were performed as described in *B*, with the only difference that the DCs were treated with PD325901 (1 μM, 60 min). *Panels b* and *c*, similar to *panels b* and *c* in *B*, with the only difference that PD325901 was used. *ns* indicates non-significant differences.

tivity against ERK when tested against a panel of 184 related kinases (48, 49), and FR180 displays a high selectivity against ERK when tested against eight related kinases (50). As shown in Fig. 7, *A* and *B*, although the effects of CAY10561 and FR180 displayed higher variability when compared with the effects of the MEK1/2 inhibitors, both agents blocked CCR7-dependent phosphorylation of AMPK1a on Ser-485. Therefore, these results indicate that ERK1/2 can mediate the effects of MEK1/2 to induce inhibition of AMPK. As the pharmacological blocking of MEK1/2 and ERK1/2 prevents the phosphorylation/inhibition of AMPK, which plays pro-apoptotic roles, we predicted that treatment of the mDCs with the inhibitor would reduce the pro-survival effects induced by stimulation of CCR7. As shown in Fig. 7*C*, as expected, the pretreatment of the mDCs with the inhibitors of MEK1/2 or ERK1/2 reduced the pro-survival effects induced by the stimulation of CCR7, although at an extent slightly lower than that induced by inhibition of Akt.

ERK Associates to AMPK—As active MEK/ERK are required to observe phosphorylation of AMPK on Ser-485 downstream of CCR7, we studied the possibility that these molecules could associate to AMPKα in mDCs. We immunoprecipitated the endogenous AMPKα from cultures of mDCs and then carried out a Western blotting to analyze for the presence of ERK1 or MEK1 in the immunoprecipitates. As shown in Fig. 8*A*, we observed that AMPKα and ERK1 interacted both in unstimulated and in CCL21-stimulated mDCs, suggesting that these two proteins are able to associate, directly or indirectly, constitutively. In contrast, we did not detect MEK1 in the AMPKα immunoprecipitates (not shown). Because direct or indirect protein-protein associations cannot be discriminated by immunoprecipitation, to study whether AMPKα and ERK1 could interact directly each other, we performed a PLA (51, 52). This is a novel microscopy technique that allows detecting, with high specificity and sensitivity, close proximity between two proteins (<40 nm), suggesting direct interactions between these two molecules (30, 51, 52). The mDCs were plated on polyornithine-coated dishes, and then they were stimulated with CCL21 and finally subjected to a PLA analysis. Negative controls where single antibodies against ERK1 (Fig. 8*B*, *panel a*), AMPK1α (Fig. 8*B*, *panel a*), or MEK1 (Fig. 8*B*, *panel b*) were used showed no PLA fluorescence. Interestingly, we observed PLA fluorescence signal between the pair ERK1/AMPKα only in CCL21-stimulated mDCs, but not in unstimulated mDCs, suggesting that stimulation of CCR7 induces proximity between these two kinases (Fig. 8*B*, *panel c*). Consistent with immunoprecipitation results, we did not observe PLA fluorescent signal between the pair MEK1/AMPKα (not shown). Analysis of the interaction between ERK1 and MEK1, which was

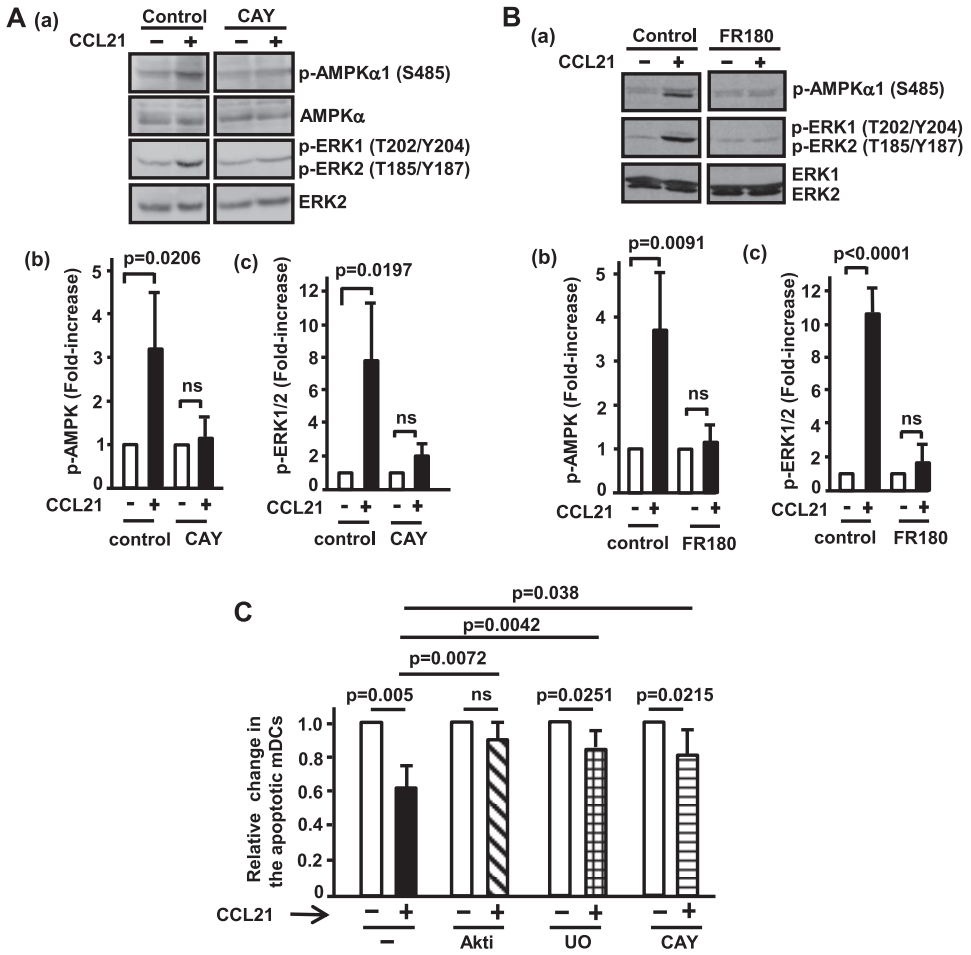

FIGURE 7. **CCR7-dependent phosphorylation/inhibition of AMPK is mediated by ERK.** *A*, *panel a*, DCs suspended in 0.1% BSA in RPMI were either left untreated (*Control*) or pretreated with CAY10561 (*CAY*, 20 μM, 2,5 h). The DCs were stimulated with CCL21 (15 nM) for 5 min and then lysed, and aliquots were subjected to Western blot with antibodies against phosphorylated/inactive AMPKα1 (Ser-485), total AMPKα, phosphorylated active ERK1/2 (Thr-202/Tyr-204 ERK1/Thr-185/Tyr-187 ERK2), or total ERK2. A representative experiment out of five performed is shown. *Panel b*, -fold increase in AMPK phosphorylation in control and CAY10561-treated mDCs, upon stimulation with CCL21. In both control and CAY10561-treated DCs, the degrees of phosphorylation of the unstimulated DCs were given an arbitrary value of 1, and the -fold increase in the CCL21-stimulated mDCs was represented. *Panel c*, similar to *panel b* with the difference that -fold increase in phosphorylation of Erk1/2 was examined. In *panels b* and *c*, the results represent the mean ± S.D. ($n = 5$ experiments). *ns* indicates non-significant differences. *B*, *panel a*, experiments were performed as described in *A*, with the differences that FR180 (100 μM, 60 min) was used and that anti-total ERK1/2 shows equal loading of the gels. A representative experiment out of three performed is shown. *Panel b*, similar to *panel b* in *A*, with the difference that -fold increase in AMPK phosphorylation was examined in the presence of FR180 as indicated in *panel a* in *B*. *Panel c*, experiments similar to *panel c* in *A* with the difference that -fold increase in phosphorylation of Erk1/2 was examined in the presence of FR180 as indicated in *panel a* in *B*. In *panels b* and *c*, the results represent the mean ± S.D. ($n = 3$ experiments). *ns* indicates non-significant differences. *C*, relative number of apoptotic DCs in unstimulated (−) and CCL21-stimulated DCs (+), after treating the mDCs with Akti, the MEK1/2 inhibitor UO126 (*UO*), or the ERK1/2 inhibitor CAY10561 (*CAY*). Results represent the mean ± S.D. ($n = 5$ experiments).

used as a positive control, also showed intense PLA fluorescence in the stimulated, but not in the unstimulated, mDCs (Fig. 8*B*, *panel d*). In summary, these results show that ERK and AMPK may be part of a similar protein complex, and in this complex, active ERK may control the phosphorylation of AMPK on Ser-485.

DISCUSSION

CCR7 directs mDCs to the LNs where the initiation of the immune response takes place. Previously, we showed that in addition to chemotaxis, CCR7 can promote survival in mDCs through the kinase Akt (10–12), which controls survival by inducing activation of NFκB and inhibition of FOXO1/3 and GSK3β (10–12). To get further insights on the mechanisms used by CCR7 to induce survival in mDCs, herein we have analyzed the involvement of the kinase AMPK in this process. Our results indicate that in mDCs, AMPK can play pro-apoptotic roles *in vitro* and *in vivo*.

The phenotypical features presented by the DCs that die after inducing activation of AMPK suggest that this kinase may induce an apoptotic type of death. In this regard, AMPK-dependent death is inhibited by the pan-caspase inhibitor z-VAD-FMK; it associates to caspase 3 activation, to the fragmentation of the nucleus, and to the increase in the expression of the pro-apoptotic Bcl2 family member Bim. Our results indicate that AMPK may promote apoptosis, at least partially, by inducing translocation to the nucleus of FOXO1, a transcription factor that plays pro-apoptotic roles in mDCs through the regulation of the expression of Bim (10, 25, 26), and by inhibiting mTORC1, a kinase complex controlled by CCR7 that also induces survival in mDCs (10, 26). In other cell types, AMPK has also been shown to be able to promote apoptosis using these two mechanisms (36, 53, 54).

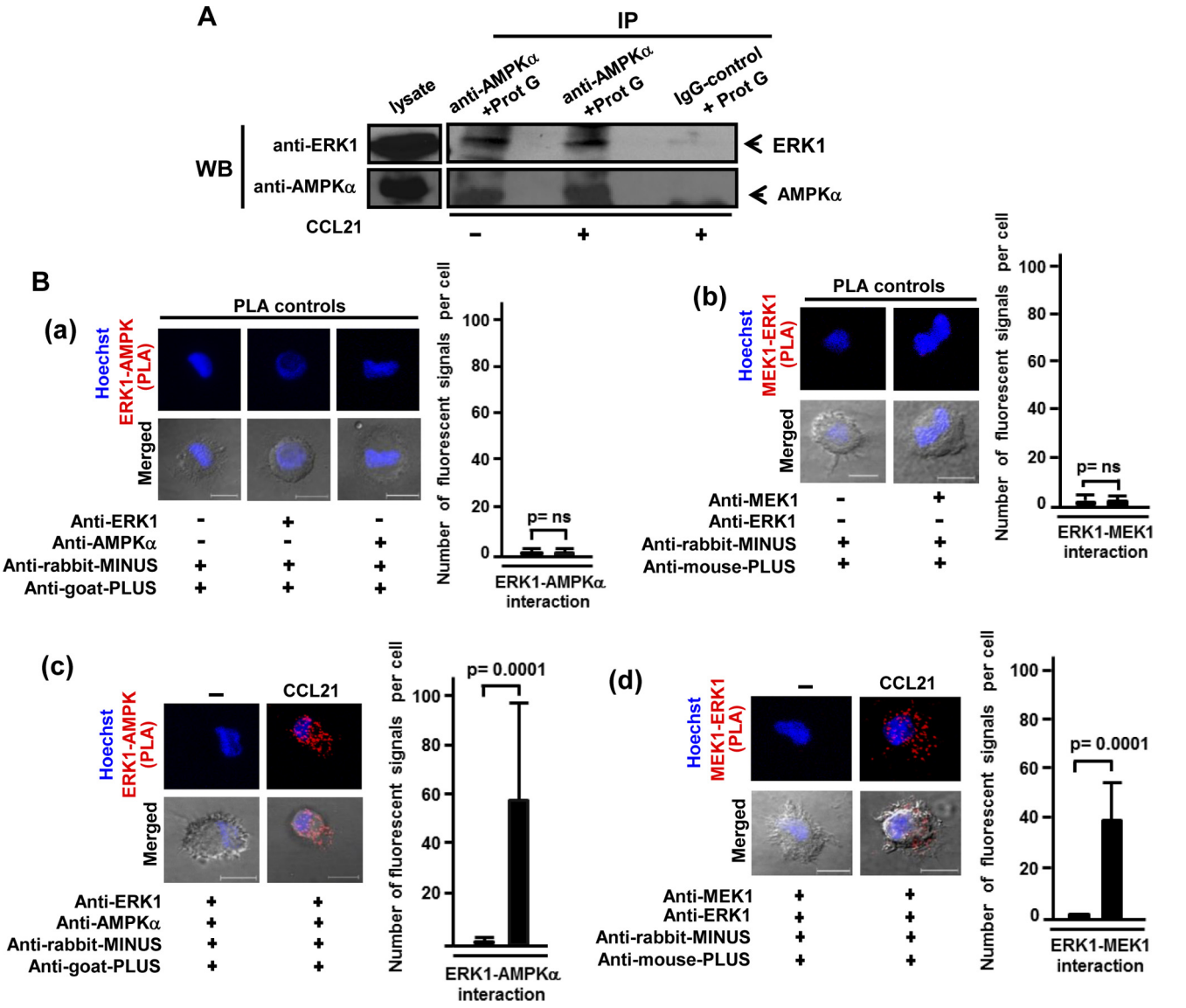

FIGURE 8. **AMPKα interacts with ERK1.** *A*, equal number of DCs, stimulated (+) or not (−) with CCL21 (15 nM), were subjected to immunoprecipitation (*IP*) with anti-AMPKα antibody or with IgG control, and subsequently, the immunoprecipitates were separated by SDS-PAGE, followed by Western blotting (*WB*) with anti-ERK1 or anti-AMPKα antibodies. A lysate of DCs was used as positive control. Aliquots of the lysates used to immunoprecipitate AMPK were analyzed for Western blotting for the presence of β-actin to demonstrate equal amount of proteins immunoprecipitated (not shown). *B*, interaction between ERK1 and AMPKα in mDCs was detected as fluorescent signals using the PLA. *Panels a* and *b*, PLA negative controls performed by labeling the DCs only with the anti-ERK1 or anti-AMPKα antibodies plus the anti-rabbit MINUS and the anti-goat PLUS (*panel a*) and the anti-MEK1 antibody and the anti-rabbit MINUS and the anti-mouse PLUS probes (*panel b*). Nomarski images and nuclei stained with Hoechst 33342 are also shown. *Scale bar*, 10 μm. In *panels a* and *b*, the number of fluorescent signals per cell was also quantified. At least 40 cells per field were counted. Results represent the mean ± S.D. ($n = 3$ experiments). *Panel c*, PLA fluorescent staining, indicating interaction between ERK1 and AMPKα, after CCL21 stimulation. *Panel d*, positive control. PLA fluorescent staining between MEK1 and ERK1 upon CCL21 stimulation is shown. Nomarski images and nuclei stained with Hoechst 33342 are also shown. *Scale bar*, 10 μm. In *panels c* and *d*, the number of fluorescent signals per cell was also quantified. At least 40 cells per field were counted. Results represent the mean ± S.D. ($n = 3$ experiments). *ns* indicates non-significant differences.

Consistent with its pro-survival role of the chemokine receptor CCR7 (11), we observed that its stimulation induces a rapid phosphorylation/inhibition of pro-apoptotic AMPK on Ser-485 (18–21). This inhibition of AMPK may promote DC survival through the effects that can be exerted on FOXO and mTORC1. Previously, we showed that stimulation of CCR7 induces activation of Akt, which, upon phosphorylating nuclear FOXO, induces its translocation to the cytoplasm (10, 11), preventing this factor from exerting pro-apoptotic effects through Bim. However, in contrast to Akt, active AMPK promotes, as shown above, the translocation of FOXO to the nucleus of DCs, from where it can regulate apoptosis. Thus, CCR7-mediated inhibition of AMPK may prevent this kinase from opposing the effects of Akt on FOXO, facilitating the complete translocation of FOXO to the cytoplasm. Moreover, CCR7-dependent inhibition of AMPK may also be able to prevent this kinase from inhibiting the pro-survival effects exerted by mTORC1. Thus, CCR7-mediated inhibition of AMPK may contribute to the extended survival of the DCs.

These results suggest that downstream of CCR7, the kinases MEK/ERK, but not Akt or S6K, mediate the phos-

phorylation of AMPK on Ser-485. Our results also indicate that ERK and AMPK may be components of a signaling complex where active ERK controls the phosphorylation of AMPK on Ser-485. Interestingly, these data contrast with prior results, obtained in other cell types, where it has been indicated that AMPK promotes inhibition of ERK (55–58), pointing out context-dependent differences in the mechanisms used by these two molecules to regulate each other. Previously, it has also been shown that infection of PK-15 cells with porcine circovirus type 2 (PCV2) also promotes interaction between AMPK and ERK (58). To the best of our knowledge, our work is the first study indicating that MEK/ERK can mediate the inhibition of AMPK by regulating Ser-485 phosphorylation.

The results obtained also indicate that MEK/ERK can regulate mDC survival. Until now, we had overlooked a role for MEK/ERK as regulators of CCR7-dependent survival in mDCs, probably due to the relatively less important role of these kinases as regulators of this function when compared with Akt. In most early experiments, the effects of MEK/ERK on mDC survival were analyzed after relatively short periods (6–10 h). Under these conditions, the effects of interfering with MEK/ERK on survival were negligible when compared with those induced by Akt inhibition. Only when apoptosis was analyzed after longer treatment with ERK1/2 inhibitors (24–40 h) did MEK/ERK emerge as a regulator of mDC survival, although still less potent than Akt. In Fig. 9, we present a model that summarizes the results obtained regarding the signaling mechanisms involved in the phosphorylation/inhibition of AMPK.

The results indicating that MEK/ERK, but not Akt, control AMPK phosphorylation on Ser-485 were unexpected for several reasons. First, we have shown previously that Akt is a key mediator of CCR7-dependent survival in mDCs (10, 11). Second, CCR7-mediated activation of Akt and phosphorylation of AMPK on Ser-485 were both mediated by G_i, suggesting that the CCR7-G_i-Akt axis may regulate the phosphorylation of AMPK. Third, Akt inhibits AMPK by directly phosphorylating Ser-485 on AMPK in several other cell types (18, 22, 23, 42). However, despite these prior results, we observe that inhibition of Akt or S6K, another kinase involved recently in the regulation of the phosphorylation of AMPK on Ser-485 (21), failed to block the phosphorylation of this residue upon stimulation of CCR7. In contrast, inhibition of MEK or its direct target ERK blocked CCR7-dependent phosphorylation of AMPK on Ser-485. Therefore, MEK/ERK emerge as novel regulators of the phosphorylation/inhibition of AMPK and, consequently, the survival of mDCs in addition to Akt. Interestingly MEK-ERK dependent phosphorylation of AMPK on Ser-485 seems cell- and/or receptor-specific because in granulosa cells, MEK/ERK inhibition was ineffective in preventing the FSH-mediated phosphorylation of AMPK on Ser-485 (22). These disparate results regarding the roles of Akt, S6K, and MEK/ERK on the phosphorylation of Ser-485 emphasize the combinatorial character of the signaling pathways and the importance of a detailed knowledge of the specific pathways used by specific receptors in each cell type. In summary, the data presented herein indicate that CCR7 may use the MEK-AMPK axis, in addition to Akt-dependent mechanisms (10–12), to promote survival in mDCs. These results add a novel component to the array of signals relayed from CCR7 to promote the survival of mDCs and provide new potential targets to modulate the function of these cells in the immune system.

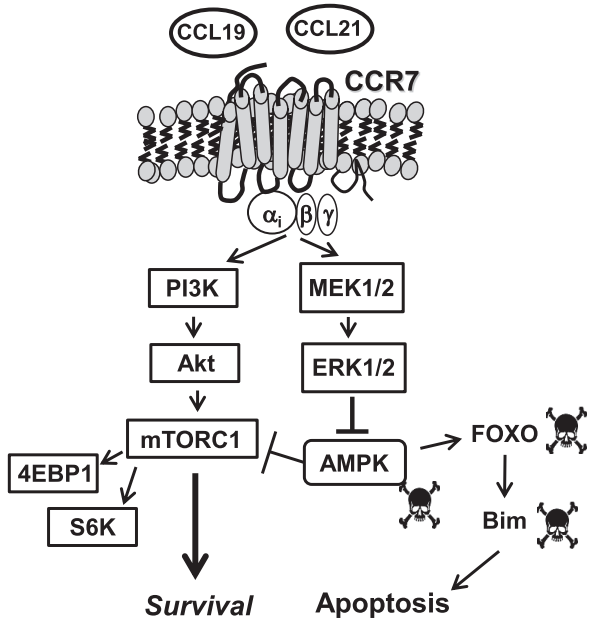

FIGURE 9. **CCR7-stimulated phosphorylation-inhibition of AMPK.** Stimulation of CCR7 with CCL19 or CCL21 induces $G_i G\beta\gamma$-mediated activation of the kinases MEK1/2/ERK1/2. CCR7 also induces activation of the PI3K/Akt/mTORC1/4EBP1 and S6K pathways, which promote survival in mDCs. Active AMPK induces apoptosis in mDCs by inhibiting the pro-survival effects of mTORC1 and by promoting translocation of the transcription factor FOXO to the nucleus, where it can control the expression of the pro-apoptotic Bcl2 family member Bim. Stimulation of CCR7 regulates, through the $G_i G\beta\gamma$/MEK1/2-ERK1/2 pathway (and independently of the PI3K/Akt/mTORC1pathway), the phosphorylation of the kinase AMPK on Ser-485, which results in the inhibition of this kinase and the consequent dampening of its pro-apoptotic effects. Therefore, CCR7 promotes survival in DCs through Akt-dependent mechanisms described previously (10–12) and by promoting MEK/ERK-dependent inhibition of AMPK.

Acknowledgments—We acknowledge P. Lastres for help with the cytometer and discussions and Génesis Andrea Altuve Urbina and Cristina Ruano Domínguez for expert technical assistance. We acknowledge Jill Suttles (University of Louisville School of Medicine) for kindly supplying reagents.

REFERENCES

1. Ueno, H., Klechevsky, E., Morita, R., Aspord, C., Cao, T., Matsui, T., Di Pucchio, T., Connolly, J., Fay, J. W., Pascual, V., Palucka, A. K., and Banchereau, J. (2007) Dendritic cell subsets in health and disease. *Immunol. Rev.* **219,** 118–142
2. Chen, M., Huang, L., and Wang, J. (2007) Deficiency of Bim in dendritic cells contributes to overactivation of lymphocytes and autoimmunity. *Blood* **109,** 4360–4367
3. Hildeman, D., Jorgensen, T., Kappler, J., and Marrack, P. (2007) Apoptosis and the homeostatic control of immune responses. *Curr. Opin. Immunol.* **19,** 516–521
4. Hou, W. S., and Van Parijs, L. (2004) A Bcl-2-dependent molecular timer regulates the lifespan and immunogenicity of dendritic cells. *Nat. Immunol.* **5,** 583–589
5. Nopora, A., and Brocker, T. (2002) Bcl-2 controls dendritic cell longevity *in vivo*. *J. Immunol.* **169,** 3006–3014

6. Ohnmacht, C., Pullner, A., King, S. B., Drexler, I., Meier, S., Brocker, T., and Voehringer, D. (2009) Constitutive ablation of dendritic cells breaks self-tolerance of CD4 T cells and results in spontaneous fatal autoimmunity. *J. Exp. Med.* **206,** 549–559
7. Kushwah, R., and Hu, J. (2010) Dendritic cell apoptosis: regulation of tolerance *versus* immunity. *J. Immunol.* **185,** 795–802
8. Randolph, G. J., Ochando, J., and Partida-Sánchez, S. (2008) Migration of dendritic cell subsets and their precursors. *Annu. Rev. Immunol.* **26,** 293–316
9. Comerford, I., Harata-Lee, Y., Bunting, M. D., Gregor, C., Kara, E. E., and McColl, S. R. (2013) A myriad of functions and complex regulation of the CCR7/CCL19/CCL21 chemokine axis in the adaptive immune system. *Cytokine Growth Factor Rev.* **24,** 269–283
10. Escribano, C., Delgado-Martín, C., and Rodríguez-Fernández, J. L. (2009) CCR7-dependent stimulation of survival in dendritic cells involves inhibition of GSK3β. *J. Immunol.* **183,** 6282–6295
11. Sánchez-Sánchez, N., Riol-Blanco, L., de la Rosa, G., Puig-Kröger, A., García-Bordas, J., Martín, D., Longo, N., Cuadrado, A., Cabañas, C., Corbí, A. L., Sánchez-Mateos, P., and Rodríguez-Fernández, J. L. (2004) Chemokine receptor CCR7 induces intracellular signaling that inhibits apoptosis of mature dendritic cells. *Blood* **104,** 619–625
12. Sánchez-Sánchez, N., Riol-Blanco, L., and Rodríguez-Fernández, J. L. (2006) The multiple personalities of the chemokine receptor CCR7 in dendritic cells. *J. Immunol.* **176,** 5153–5159
13. Hardie, D. G. (2011) AMP-activated protein kinase: an energy sensor that regulates all aspects of cell function. *Genes Dev.* **25,** 1895–1908
14. Hardie, D. G., Ross, F. A., and Hawley, S. A. (2012) AMPK: a nutrient and energy sensor that maintains energy homeostasis. *Nat. Rev. Mol. Cell Biol.* **13,** 251–262
15. Ido, Y., Carling, D., and Ruderman, N. (2002) Hyperglycemia-induced apoptosis in human umbilical vein endothelial cells: inhibition by the AMP-activated protein kinase activation. *Diabetes* **51,** 159–167
16. Campàs, C., Lopez, J. M., Santidrián, A. F., Barragán, M., Bellosillo, B., Colomer, D., and Gil, J. (2003) Acadesine activates AMPK and induces apoptosis in B-cell chronic lymphocytic leukemia cells but not in T lymphocytes. *Blood* **101,** 3674–3680
17. Woods, A., Vertommen, D., Neumann, D., Turk, R., Bayliss, J., Schlattner, U., Wallimann, T., Carling, D., and Rider, M. H. (2003) Identification of phosphorylation sites in AMP-activated protein kinase (AMPK) for upstream AMPK kinases and study of their roles by site-directed mutagenesis. *J. Biol. Chem.* **278,** 28434–28442
18. Horman, S., Vertommen, D., Heath, R., Neumann, D., Mouton, V., Woods, A., Schlattner, U., Wallimann, T., Carling, D., Hue, L., and Rider, M. H. (2006) Insulin antagonizes ischemia-induced Thr^{172} phosphorylation of AMP-activated protein kinase α-subunits in heart via hierarchical phosphorylation of $Ser^{485}/^{491}$. *J. Biol. Chem.* **281,** 5335–5340
19. Hurley, R. L., Barré, L. K., Wood, S. D., Anderson, K. A., Kemp, B. E., Means, A. R., and Witters, L. A. (2006) Regulation of AMP-activated protein kinase by multisite phosphorylation in response to agents that elevate cellular cAMP. *J. Biol. Chem.* **281,** 36662–36672
20. Pulinilkunnil, T., He, H., Kong, D., Asakura, K., Peroni, O. D., Lee, A., and Kahn, B. B. (2011) Adrenergic regulation of AMP-activated protein kinase in brown adipose tissue *in vivo*. *J. Biol. Chem.* **286,** 8798–9809
21. Dagon, Y., Hur, E., Zheng, B., Wellenstein, K., Cantley, L. C., and Kahn, B. B. (2012) p70S6 kinase phosphorylates AMPK on serine 491 to mediate leptin's effect on food intake. *Cell Metab.* **16,** 104–112
22. Kayampilly, P. P., and Menon, K. M. (2009) Follicle-stimulating hormone inhibits adenosine 5′-monophosphate-activated protein kinase activation and promotes cell proliferation of primary granulosa cells in culture through an Akt-dependent pathway. *Endocrinology* **150,** 929–935
23. Kovacic, S., Soltys, C. L., Barr, A. J., Shiojima, I., Walsh, K., and Dyck, J. R. (2003) Akt activity negatively regulates phosphorylation of AMP-activated protein kinase in the heart. *J. Biol. Chem.* **278,** 39422–39427
24. Zhou, G., Myers, R., Li, Y., Chen, Y., Shen, X., Fenyk-Melody, J., Wu, M., Ventre, J., Doebber, T., Fujii, N., Musi, N., Hirshman, M. F., Goodyear, L. J., and Moller, D. E. (2001) Role of AMP-activated protein kinase in mechanism of metformin action. *J. Clin. Invest.* **108,** 1167–1174
25. Delgado-Martín, C., Escribano, C., Pablos, J. L., Riol-Blanco, L., and Rodríguez-Fernández, J. L. (2011) Chemokine CXCL12 uses CXCR4 and a signaling core formed by bifunctional Akt, extracellular signal-regulated kinase (ERK)1/2, and mammalian target of rapamycin complex 1 (mTORC1) proteins to control chemotaxis and survival simultaneously in mature dendritic cells. *J. Biol. Chem.* **286,** 37222–37236
26. Riol-Blanco L, Delgado-Martín, C., Sánchez-Sánchez, N., Alonso-C, L. M., Gutiérrez-López, M. D., Del Hoyo, G. M., Navarro, J., Sánchez-Madrid, F., Cabañas, C., Sánchez-Mateos, P., and Rodríguez-Fernández, J. L. (2009) Immunological synapse formation inhibits, via NF-κB and FOXO1, the apoptosis of dendritic cells. *Nat. Immunol.* **10,** 753–760
27. Riol-Blanco, L., Sánchez-Sánchez, N., Torres, A., Tejedor, A., Narumiya, S., Corbí, A. L., Sánchez-Mateos, P., and Rodríguez-Fernández, J. L. (2005) The chemokine receptor CCR7 activates in dendritic cells two signaling modules that independently regulate chemotaxis and migratory speed. *J. Immunol.* **174,** 4070–4080
28. Nicoletti, I., Migliorati, G., Pagliacci, M. C., Grignani, F., and Riccardi, C. (1991) A rapid and simple method for measuring thymocyte apoptosis by propidium iodide staining and flow cytometry. *J. Immunol. Methods* **139,** 271–279
29. Riccardi, C., and Nicoletti, I. (2006) Analysis of apoptosis by propidium iodide staining and flow cytometry. *Nat. Protoc.* **1,** 1458–1461
30. Söderberg, O., Gullberg, M., Jarvius, M., Ridderstråle, K., Leuchowius, K. J., Jarvius, J., Wester, K., Hydbring, P., Bahram, F., Larsson, L. G., and Landegren, U. (2006) Direct observation of individual endogenous protein complexes *in situ* by proximity ligation. *Nat. Methods* **3,** 995–1000
31. Gómez-Cabañas, L., Delgado-Martín, C., López-Cotarelo, P., Escribano-Diaz, C., Alonso-C, L. M., Riol-Blanco, L., and Rodríguez-Fernández, J. L. (2014) Detecting apoptosis of leukocytes in mouse lymph nodes. *Nat. Protoc* **9,** 1102–1112
32. Mempel, T. R., Henrickson, S. E., and Von Andrian, U. H. (2004) T-cell priming by dendritic cells in lymph nodes occurs in three distinct phases. *Nature* **427,** 154–159
33. Corton, J. M., Gillespie, J. G., Hawley, S. A., and Hardie, D. G. (1995) 5-Aminoimidazole-4-carboxamide ribonucleoside: a specific method for activating AMP-activated protein kinase in intact cells? *Eur. J. Biochem.* **229,** 558–565
34. Winder, W. W., and Hardie, D. G. (1996) Inactivation of acetyl-CoA carboxylase and activation of AMP-activated protein kinase in muscle during exercise. *Am. J. Physiol.* **270,** E299–E304
35. Gilley, J., Coffer, P. J., and Ham, J. (2003) FOXO transcription factors directly activate *bim* gene expression and promote apoptosis in sympathetic neurons. *J. Cell Biol.* **162,** 613–622
36. Inoki, K., Zhu, T., and Guan, K. L. (2003) TSC2 mediates cellular energy response to control cell growth and survival. *Cell* **115,** 577–590
37. Gwinn, D. M., Shackelford, D. B., Egan, D. F., Mihaylova, M. M., Mery, A., Vasquez, D. S., Turk, B. E., and Shaw, R. J. (2008) AMPK phosphorylation of raptor mediates a metabolic checkpoint. *Mol. Cell* **30,** 214–226
38. Hung, C. M., Garcia-Haro, L., Sparks, C. A., and Guertin, D. A. (2012) mTOR-dependent cell survival mechanisms. *Cold Spring Harb. Perspect. Biol.* **4,** a008771
39. Kamath, A. T., Henri, S., Battye, F., Tough, D. F., and Shortman, K. (2002) Developmental kinetics and lifespan of dendritic cells in mouse lymphoid organs. *Blood* **100,** 1734–1741
40. Lehmann, D. M., Seneviratne, A. M., and Smrcka, A. V. (2008) Small molecule disruption of G protein $\beta\gamma$ subunit signaling inhibits neutrophil chemotaxis and inflammation. *Mol. Pharmacol.* **73,** 410–418
41. Iijima, N., Yanagawa, Y., Clingan, J. M., and Onoé, K. (2005) CCR7-mediated c-Jun N-terminal kinase activation regulates cell migration in mature dendritic cells. *Int. Immunol.* **17,** 1201–1212
42. Beauloye, C., Marsin, A. S., Bertrand, L., Krause, U., Hardie, D. G., Vanoverschelde, J. L., and Hue, L. (2001) Insulin antagonizes AMP-activated protein kinase activation by ischemia or anoxia in rat hearts, without affecting total adenine nucleotides. *FEBS Lett.* **505,** 348–352
43. Bain, J., Plater, L., Elliott, M., Shpiro, N., Hastie, C. J., McLauchlan, H., Klevernic, I., Arthur, J. S., Alessi, D. R., and Cohen, P. (2007) The selectivity of protein kinase inhibitors: a further update. *Biochem. J.* **408,** 297–315
44. Foster, K. G., and Fingar, D. C. (2010) Mammalian target of rapamycin (mTOR): conducing the cellular signaling symphony. *J. Biol. Chem.* **285,**

14071–14077
45. Davies, S. P., Reddy, H., Caivano, M., and Cohen, P. (2000) Specificity and mechanism of action of some commonly used protein kinase inhibitors. *Biochem. J.* **351,** 95–105
46. García-Martínez, J. M., Moran, J., Clarke, R. G., Gray, A., Cosulich, S. C., Chresta, C. M., and Alessi, D. R. (2009) Ku-0063794 is a specific inhibitor of the mammalian target of rapamycin (mTOR). *Biochem. J.* **421,** 29–42
47. Kolch, W. (2005) Coordinating ERK/MAPK signalling through scaffolds and inhibitors. *Nat. Rev. Mol. Cell Biol.* **6,** 827–837
48. Aronov, A. M., Baker, C., Bemis, G. W., Cao, J., Chen, G., Ford, P. J., Germann, U. A., Green, J., Hale, M. R., Jacobs, M., Janetka, J. W., Maltais, F., Martinez-Botella, G., Namchuk, M. N., Straub, J., Tang, Q., and Xie, X. (2007) Flipped out: structure-guided design of selective pyrazolylpyrrole ERK inhibitors. *J. Med. Chem.* **50,** 1280–1287
49. Hatzivassiliou, G., Liu, B., O'Brien, C., Spoerke, J. M., Hoeflich, K. P., Haverty, P. M., Soriano, R., Forrest, W. F., Heldens, S., Chen, H., Toy, K., Ha, C., Zhou, W., Song, K., Friedman, L. S., Amler, L. C., Hampton, G. M., Moffat, J., Belvin, M., and Lackner, M. R. (2012) ERK inhibition overcomes acquired resistance to MEK inhibitors. *Mol. Cancer Ther.* **11,** 1143–1154
50. Ohori, M., Kinoshita, T., Okubo, M., Sato, K., Yamazaki, A., Arakawa, H., Nishimura, S., Inamura, N., Nakajima, H., Neya, M., Miyake, H., and Fujii, T. (2005) Identification of a selective ERK inhibitor and structural determination of the inhibitor-ERK2 complex. *Biochem. Biophys. Res. Commun.* **336,** 357–363
51. Fredriksson, S., Gullberg, M., Jarvius, J., Olsson, C., Pietras, K., Gústafsdóttir, S. M., Ostman, A., and Landegren, U. (2002) Protein detection using proximity-dependent DNA ligation assays. *Nat. Biotechnol.* **20,** 473–477
52. Weibrecht, I., Leuchowius, K. J., Clausson, C. M., Conze, T., Jarvius, M., Howell, W. M., Kamali-Moghaddam, M., and Söderberg, O. (2010) Proximity ligation assays: a recent addition to the proteomics toolbox. *Expert Rev. Proteomics* **7,** 401–409
53. Greer, E. L., Oskoui, P. R., Banko, M. R., Maniar, J. M., Gygi, M. P., Gygi, S. P., and Brunet, A. (2007) The energy sensor AMP-activated protein kinase directly regulates the mammalian FOXO3 transcription factor. *J. Biol. Chem.* **282,** 30107–30119
54. Mihaylova, M. M., and Shaw, R. J. (2011) The AMPK signalling pathway coordinates cell growth, autophagy and metabolism. *Nat. Cell Biol.* **13,** 1016–1023
55. Du, J., Guan, T., Zhang, H., Xia, Y., Liu, F., and Zhang, Y. (2008) Inhibitory crosstalk between ERK and AMPK in the growth and proliferation of cardiac fibroblasts. *Biochem. Biophys. Res. Commun.* **368,** 402–407
56. Hwang, S. L., Jeong, Y. T., Li, X., Kim, Y. D., Lu, Y., Chang, Y. C., Lee, I. K., and Chang, H. W. (2013) Inhibitory cross-talk between the AMPK and ERK pathways mediates endoplasmic reticulum stress-induced insulin resistance in skeletal muscle. *Br. J. Pharmacol.* **169,** 69–81
57. Shen, C. H., Yuan, P., Perez-Lorenzo, R., Zhang, Y., Lee, S. X., Ou, Y., Asara, J. M., Cantley, L. C., and Zheng, B. (2013) Phosphorylation of BRAF by AMPK impairs BRAF-KSR1 association and cell proliferation. *Mol. Cell* **52,** 161–172
58. Zhu, B., Zhou, Y., Xu, F., Shuai, J., Li, X., and Fang, W. (2012) Porcine circovirus type 2 induces autophagy via the AMPK/ERK/TSC2/mTOR signaling pathway in PK-15 cells. *J. Virol.* **86,** 12003–12012

Am J Physiol Endocrinol Metab 310: E925–E937, 2016;
doi:10.1152/ajpendo.00503.2015.

Formoterol decreases muscle wasting as well as inflammation in the rat model of rheumatoid arthritis

Ana Belén Gómez-SanMiguel,[1]* Carolina Gomez-Moreira,[1]* María Paz Nieto-Bona,[2] Carmen Fernández-Galaz,[1] Maria Ángeles Villanúa,[1] Ana Isabel Martín,[1] and Asunción López-Calderón[1]

[1]*Department of Physiology, Faculty of Medicine, Complutense University, Madrid, Spain; and* [2]*Department of Basic Sciences in Health, Faculty of Health Sciences, Rey Juan Carlos University, Madrid, Spain*

Submitted 4 December 2015; accepted in final form 27 March 2016

Gómez-SanMiguel AB, Gomez-Moreira C, Nieto-Bona MP, Fernández-Galaz C, Villanúa MÁ, Martín AI, López-Calderón A. Formoterol decreases muscle wasting as well as inflammation in the rat model of rheumatoid arthritis. *Am J Physiol Endocrinol Metab* 310: E925–E937, 2016; doi:10.1152/ajpendo.00503.2015.—Adjuvant-induced arthritis is an experimental model of rheumatoid arthritis that is associated with body weight loss and muscle wasting. β_2-adrenergic receptor agonists are powerful anabolic agents that trigger skeletal muscle hypertrophy and have been proposed as a promising treatment for muscle wasting in human patients. The aim of this work was to determine whether formoterol, a selective β_2-adrenoreceptor agonist, is able to ameliorate muscle wasting in arthritic rats. Arthritis was induced in male Wistar rats by intradermal injection of Freund's adjuvant. Control and arthritic rats were injected daily with 50 μg/kg sc formoterol or saline for 12 days. Body weight change, food intake, and arthritis index were analyzed. After euthanasia, in the gastrocnemius mRNA was analyzed by PCR, and proteins were analyzed by Western blotting. Arthritis decreased gastrocnemius weight, cross-sectional area, and myofiber size, whereas formoterol increased those variables in both arthritic and control rats. Formoterol decreased the external signs of arthritis as well as NF-κB(p65) activation, TNFα, and COX-2 levels in the gastrocnemius of arthritic and control rats. Those effects of formoterol were associated with a decreased expression of myostatin, atrogin-1, and MuRF1 and in LC3b lipidation. Arthritis increased the expression of MyoD, myogenin, IGF-I, and IGFBP-3 and -5 in the gastrocnemius. In control and in arthritic rats, treatment with formoterol increased Akt phosphorylation and myogenin levels, whereas it decreased IGFBP-3 expression in the gastrocnemius. These data suggest that formoterol has an anti-inflammatory effect and decreases muscle wasting in arthritic rats through increasing Akt activity and myogenin and decreasing myostatin, the p-NF-κB(p65)/TNF pathway, and IGFBP-3.

cachexia; adjuvant-arthritis; β_2-adrenoreceptor; myogenin; insulin-like growth factor-binding protein-3

CHRONIC INFLAMMATORY ILLNESSES such as cancer, sepsis, and obstructive pulmonary disease are associated with a decrease in body weight and cachexia. Similarly, patients with rheumatoid arthritis have rheumatoid cachexia, which increases morbidity and mortality (33). Adjuvant-induced arthritis is an experimental model of rheumatoid arthritis that induces inflammatory cachexia. On *days 10* and *11* after adjuvant injection, rats stop gaining body weight and develop chronic inflammation, polyarthritis, anorexia, and cachexia due to whole body wasting, including muscle and fat tissue loss (6, 33). Skeletal muscle loss in arthritic rats is secondary to systemic inflammation and not to anorexia (7) or the reduction of spontaneous locomotion (15). Muscle wasting in several inflammatory illnesses is due to hyperactivation of the ubiquitin-proteasome pathway and autophagy lysosomal proteases, which are involved in protein degradation in skeletal muscle (22, 35). The two E3 ubiquitin ligases muscle RING-finger protein-1 (MuRF-1) and atrogin-1 are sensitive markers for muscular atrophy (35), and both are upregulated in arthritic rats (6). Moreover, arthritis also increased autophagic gene expression in muscle (18).

In addition to activating muscle proteolysis, the increased release of cytokines during chronic inflammation also promotes satellite cell activation and myogenesis (62). In this sense, we have reported that arthritis increases muscle regulatory factors and markers of satellite cell activation, myogenic differentiation factor D (MyoD), and myogenin (6), which play key roles in muscle plasticity and regeneration. The insulin-like growth factor-I (IGF-I)-insulin growth factor-binding protein (IGFBP) system in the skeletal muscle plays an important role in the maintenance of muscle mass (59). Adjuvant-induced arthritis is associated with alterations in the IGF-IGFBP system, and IGF-I administration to arthritic rats decreases muscle wasting as well as arthritis-induced increase in muscle IGFBP-3 mRNA (40, 41).

β_2-Adrenergic receptors are the main adrenergic receptors expressed in muscle cells, and their stimulation has well-known anabolic actions (for review, see Ref. 58). Activation of β_2-adrenergic receptors have also been shown to have anti-inflammatory effects in various inflammatory conditions, such as bronchial asthma, chronic obstructive pulmonary disease, and carrageen-induced paw oedema (14, 28, 63), as well as in several experimental models of sepsis (34). However, the role played by the sympathetic nervous system on arthritis development is not well known. It has been described that the timing of adrenergic drug administration is a critical factor in determining disease progression (21, 42). Sympathectomy or administration of β-adrenergic antagonist before the onset of arthritis decreases the severity of the illness in experimental arthritis (37, 38). However, when adrenergic therapy is given after disease onset, it decreases joint inflammation and bone destruction in the arthritic hind limbs (42). β_2-adrenoreceptor receptors are expressed in immune cells, and their stimulation decreases production of proinflammatory cytokines such as TNFα, whereas it increases the release of the anti-inflammatory interleukin-10 (10, 49). The anti-inflammatory effect of β_2-adrenergic stimulation was also evidenced in mice lacking β_2-adrenergic receptors, where there was decreased survival and increased inflammation in the endotoxemia setting (64).

* A. B. Gómez-SanMiguel and C. Gomez-Moreira contributed similarly to the study.

Address for reprint requests and other correspondence: A. López-Calderón, Departamento de Fisiología, Facultad de Medicina, Universidad Complutense, 28040, Madrid, Spain (e-mail: ALC@ucm.es).

Formoterol is a highly β_2-selective adrenergic receptor agonist that is capable of producing skeletal muscle hypertrophy at microgram doses (55). Its hypertrophic effect is mediated both by stimulating skeletal muscle synthesis and by decreasing muscle proteolysis (3, 25, 36). Accordingly, formoterol has been proposed as a possible pharmacological therapy for muscle loss (3, 26). Therefore, the purposes of this study were to *1*) analyze the possible anti-inflammatory effect of formoterol administration to arthritic rats and *2*) elucidate whether its effect on skeletal muscle is mediated by a decrease in proteolysis or/and by changes in myogenic regulatory factors and the IGF-IGFBP system.

MATERIALS AND METHODS

Animals. Arthritic and control male Wistar rats weighing 160 g (6 wk old) were purchased from Charles River Laboratories (Barcelona, Spain). Arthritis was induced in rats by an intradermal injection of 0.1 ml of heat-inactivated *Mycobacterium butyricum* (40 mg/ml in paraffin oil) in the right hindpaw under isoflurane anesthesia (6). Control animals were injected with vehicle. After arrival (*day 3* after adjuvant injection), rats were housed three per cage and maintained under standardized conditions of temperature (20–22°C) and light (lights on from 7:30 AM to 7:30 PM). The procedures followed the guidelines recommended by the European Union for the care and use of laboratory animals and were approved by the Complutense University Animal Care Committee.

In the first experiment, the effect of formoterol administration on arthritic rats was examined. On *day 11* after adjuvant injection, both control and arthritic rats were randomly divided into four groups, each with 20 rats. Control rats were subcutaneously (sc) injected daily with 250 μl of saline at 9 AM for 6 or 12 days and divided into *1*) control rats (C) fed ad libitum and *2*) pair-fed rats (PF) that received the same amount of food (g/100 g body wt) eaten on the previous day by

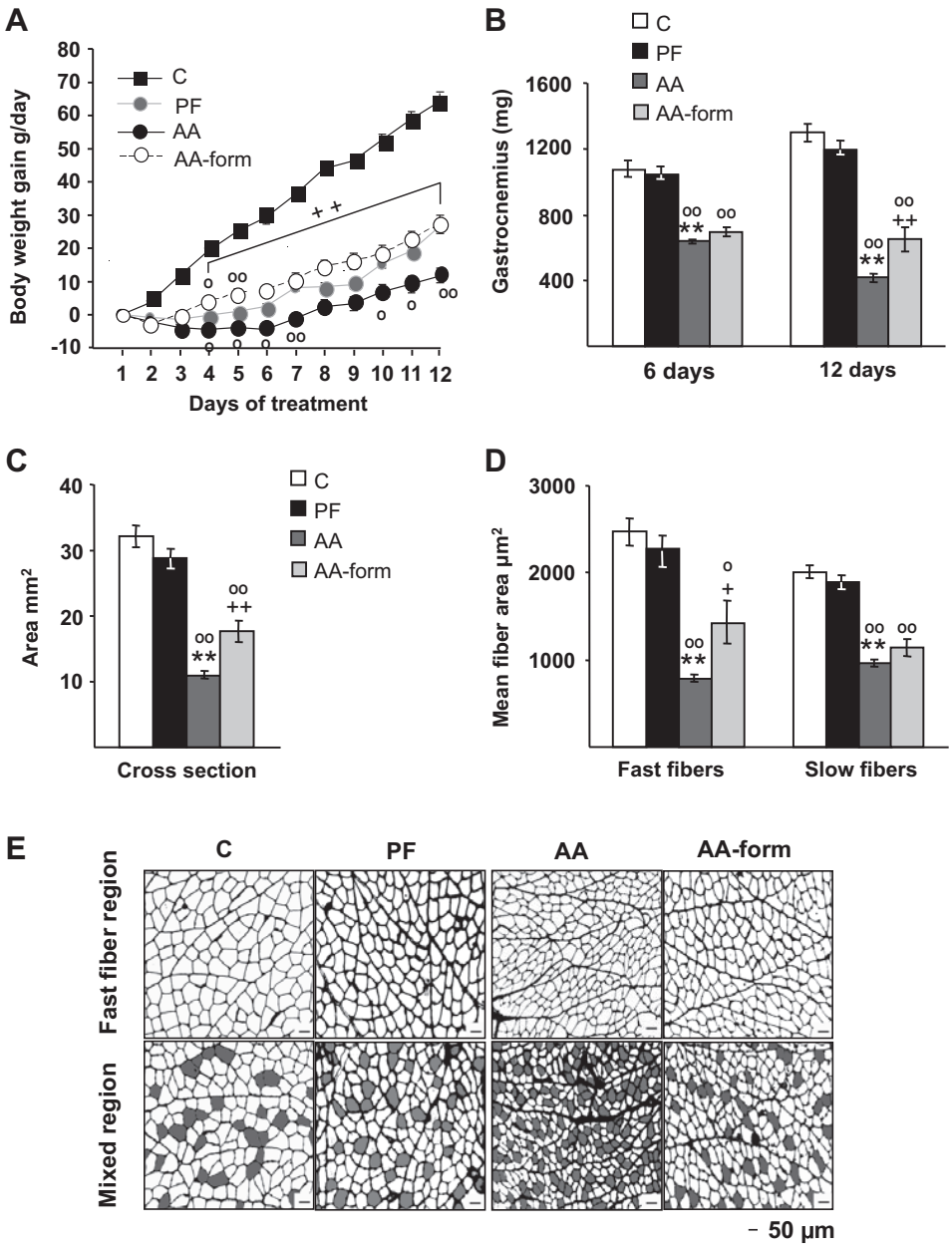

Fig. 1. *A–D*: effect of arthritis and formoterol administration (50 μg/kg sc) for 12 days on cumulative body weight gain (*A*), gastrocnemius weight (*B*), average cross-sectional area (*C*), and mean fast and slow fiber area (*D*). *E*: representative transverse sections from fast fiber region (*top*) and mixed region (*bottom*) of gastrocnemius muscle. Slow fibers (filled in gray resulting from slow type I MHC immunofluorescence) are mixed with fast fibers. All fibers are outlined by wheat germ agglutinin (black). Amplification of the inserts marked on each cross-section. Bar, 50 μm. C, control; PF, pair-fed; AA, arthritic rats; AA-form, arthritic rats treated with formoterol. AA rats had lower body weight gain than control and PF rats ($P < 0.01$). AA rats treated with formoterol had higher body weight gain than AA rats injected with saline and similar or higher body weight gain than PF rats. Arthritis decreased and formoterol treatment for 12 days increased gastrocnemius weight, cross-sectional area, and mean fast fiber area ($P < 0.01$). Data are expressed as means ± SE for $n = 7$–10 rats/group. $^{**}P < 0.01$ vs. control rats injected with saline; $^{\circ}P < 0.05$, $^{\circ\circ}P < 0.01$ vs. PF rats; $+P < 0.05$, $++P < 0.01$ vs. AA rats injected with saline. Least significant difference (LSD) multiple comparison test.

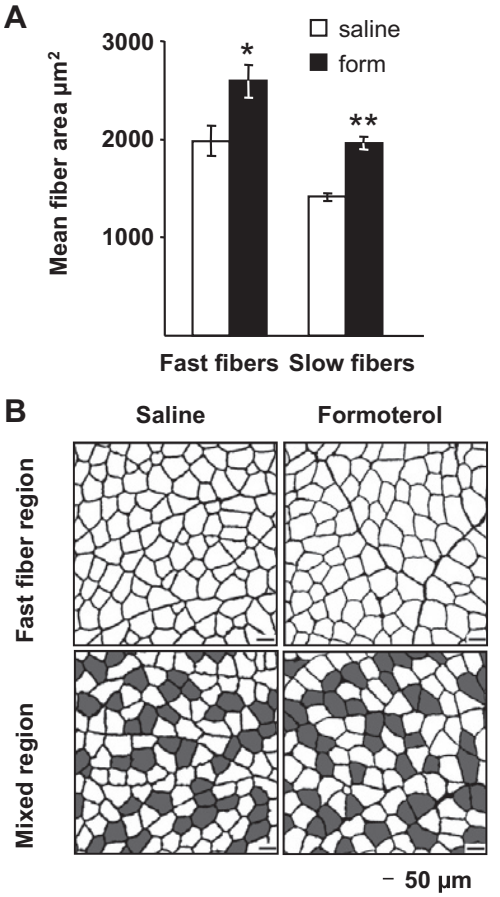

Fig. 2. *A*: formoterol administration (50 μg/kg) for 12 days to control rats increased gastrocnemius mean fast and slow fiber area. *B*: representative transverse sections from fast fiber region (*top*) and mixed region (*bottom*) of gastrocnemius muscle. Bar, 50 μm. Data are expressed as means ± SE for $n = 7$–9 rats/group. $^{*}P < 0.05$, $^{**}P < 0.01$ vs. saline.

arthritic rats treated with saline; arthritic groups were *3*) arthritis-saline (AA) and *4*) arthritis-formoterol (AA-form), which received a daily sc injection of 50 μg/kg formoterol (28) dissolved in saline for 6 or 12 days. We have observed that in arthritic rats the highest expression of atrogenes and myogenic regulatory factors in gastrocnemius muscle occurs between *days 15* and *16* after adjuvant injection, before the maximum values of both arthritis scores and muscle atrophy are reached (6). Accordingly, half of the rats in each group were euthanized by decapitation 16 days after adjuvant injection and after 6 days of formoterol treatment, 2.5 h after the last injection. The gastrocnemius muscle of the left hindpaw was removed, dissected, weighed, and frozen in liquid nitrogen and stored at −80°C until immunohistochemistry, RNA, and protein extraction were performed. Isolation and manipulation of tissues were always performed under sterile conditions. Although gastrocnemius expression of atrogin-1 and MuRF-1 transcripts peak around 16 days postadjuvant injection, muscle atrophy is more dramatic around *day 22* (6). Therefore, the second half of the rats from each group was euthanized by decapitation (on *day 22* after adjuvant injection and after 12 days of formoterol treatment) 2.5 h after the last injection. The gastrocnemius muscle of the left hindpaw was removed, dissected, weighed, and frozen in liquid nitrogen and stored at −80°C until analyses were performed.

Assessment of arthritis was performed by measuring the arthritis index of each animal, which was clinically scored by grading each paw from 0 to 4. Grading was determined as follows: 0, no erythema or swelling; 1, slight erythema or swelling of one or more digits; 2, swelling of paw; 3, swelling of entire paw and ankle; 4, ankylosis, incapacity to bend the ankle. The severity score was the sum of the clinical scores of each limb, the maximum value being 16 (6). Body weight, food intake, and arthritis index scores were examined daily. Food intake per cage was calculated by measuring the difference between the initial and the remaining amount of pellets in the feeder and expressed as grams per 100 grams body weight per day.

In a second experiment, we tested the effect of formoterol administration on control rats. Rats were euthanized by decapitation 2.5 h after the last injection, after being injected with 50 μg/kg sc or saline (250 μl) over 2, 6, or 12 days. The gastrocnemius muscle of the left hindpaw was removed, dissected, weighed, and frozen in liquid nitrogen and stored at −80°C until analyses were performed.

Muscle morphology and inmunohistochemistry. The gastrocnemius from the left hindpaw of the rats treated over 12 days was weighed, and the medial part was dissected, placed on a transparency film, glued at one end to a cork with gum tragacanth (Fibraguar; Fardi, Madrid, Spain), frozen in isopentane, cooled by liquid nitrogen, and stored at −80°C. Ten-micrometer cryostat sections taken from the midbelly region were fixed with 100% acetone and stained with hematoxylin-eosin. Parallel sections were kept at −80°C until further processing for immunohistochemical analysis. Four to six muscle hematoxylin-eosin stained sections were used to determine the whole cross-sectional area. Sections were scanned by transparency and converted to JPEG images (Epson scanner 4990). The area of each section was measured with ImageJ software, using the measure of the slide width (25 mm) to set the scale.

We used muscle fiber cross-sectional size as an index of type-specific fiber atrophy. Slow muscle fibers were detected with a monoclonal antibody against slow myosin heavy chain form (1:80; NCL-MHCs-Novocastra, Newcastle upon Tyne, UK) and secondary Alexa fluor 488 Goat antimouse IgG (A11001-Invitrogen, 1:100; Invitrogen, Madrid, Spain). The extracellular matrix was detected by wheat germ aglutinin labeled with Texas Red (W849, 1 μg/ml; Invitrogen). Sections were mounted with Prolong-Gold antifade reagent combined with DAPI (P36931; Invitrogen). Digital images were taken with a Leica DMI300 microscope. Several ×10 photomicrographs were used to compose fast fiber and mixed fiber regions with GIMP software. Complete sections were reconstructed in some cases. Compositions were made with at least two layers: WGA and slow myosine images. The WGA layer was used to border detection using Difference of Gaussians and inversion. After selecting the white WGA lines by tone, they were filled with black. Gaps on the

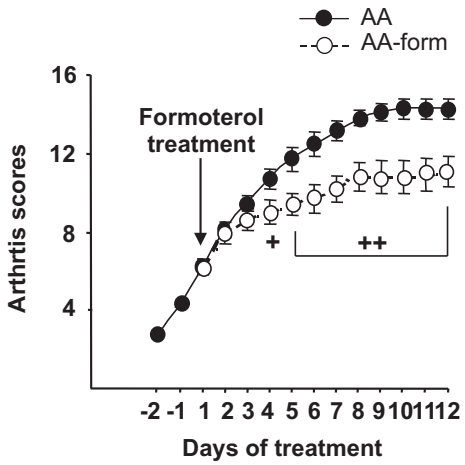

Fig. 3. Effect of formoterol (form) treatment (50 μg/kg body wt sc daily) to arthritic (AA) rats on arthritis index score evolution. Formoterol treatment decreased arthritis scores ($P < 0.01$). Data are expressed as means ± SE for $n = 9$–10 rats/group. $^{+}P < 0.05$, $^{++}P < 0.01$ vs. AA rats injected with saline. LSD multiple comparison test.

boundaries and connective tissue were corrected manually. Slow fibers on mixed areas were selected and filled with red (ff0000). The JPEG image with scale was first made binary to analyze particles with ImageJ software. This procedure allows measuring of the fast-fiber area. To analyze the area of the slow fibers from the mixed JPEG image, black boundaries were converted to white by color threshold and red fibers changed to black. At least two images from each region were selected for counting.

RNA extraction and real-time PCR. Gastrocnemius (100 mg) was homogenized, and total RNA was extracted using Ultraspec (Biotecx Laboratories, Houston, TX), following the manufacturer's protocol. The final concentration of RNA was determined (260 nm) with a BioPhotometer (Eppendorf, Germany), and the integrity of the RNA was confirmed by agarose gel electrophoresis. First-strand cDNA synthesis was performed using 1 μg of total RNA with a Quantiscript Reverse Transcription kit (Qiagen, Valencia, CA).

Real-time PCR for quantification of mRNA was performed on a SmartCycler (Cepheid, Sunnyvale, CA), using a SYBR Green protocol on the fluorescence temperature cycler. Each real-time PCR reaction consisted of 10 ng of total RNA equivalents, 1× Takara SYBR Green Premix Ex *Taq* (Takara Bio, Otsu, Shiga, Japan), and 300 nM forward and reverse primers in a reaction volume of 25.5 μl. Primers for real-time PCR were obtained from Roche (Madrid, Spain). The thermal cycling profile consisted of a preincubation step at 95°C for 10 s followed, by 40 cycles of 95°C denaturation steps for 15 s, 60°C annealing steps for 30 s, and 72°C extension steps for 30 s. Results were expressed relative to the control animals, where the relative mRNA abundance has been arbitrarily set to 1, using the cycle threshold 2 ($\Delta\Delta C_T$) method, with 18S as reference gene. PCR products were separated using agarose gel electrophoresis to confirm product presence and size.

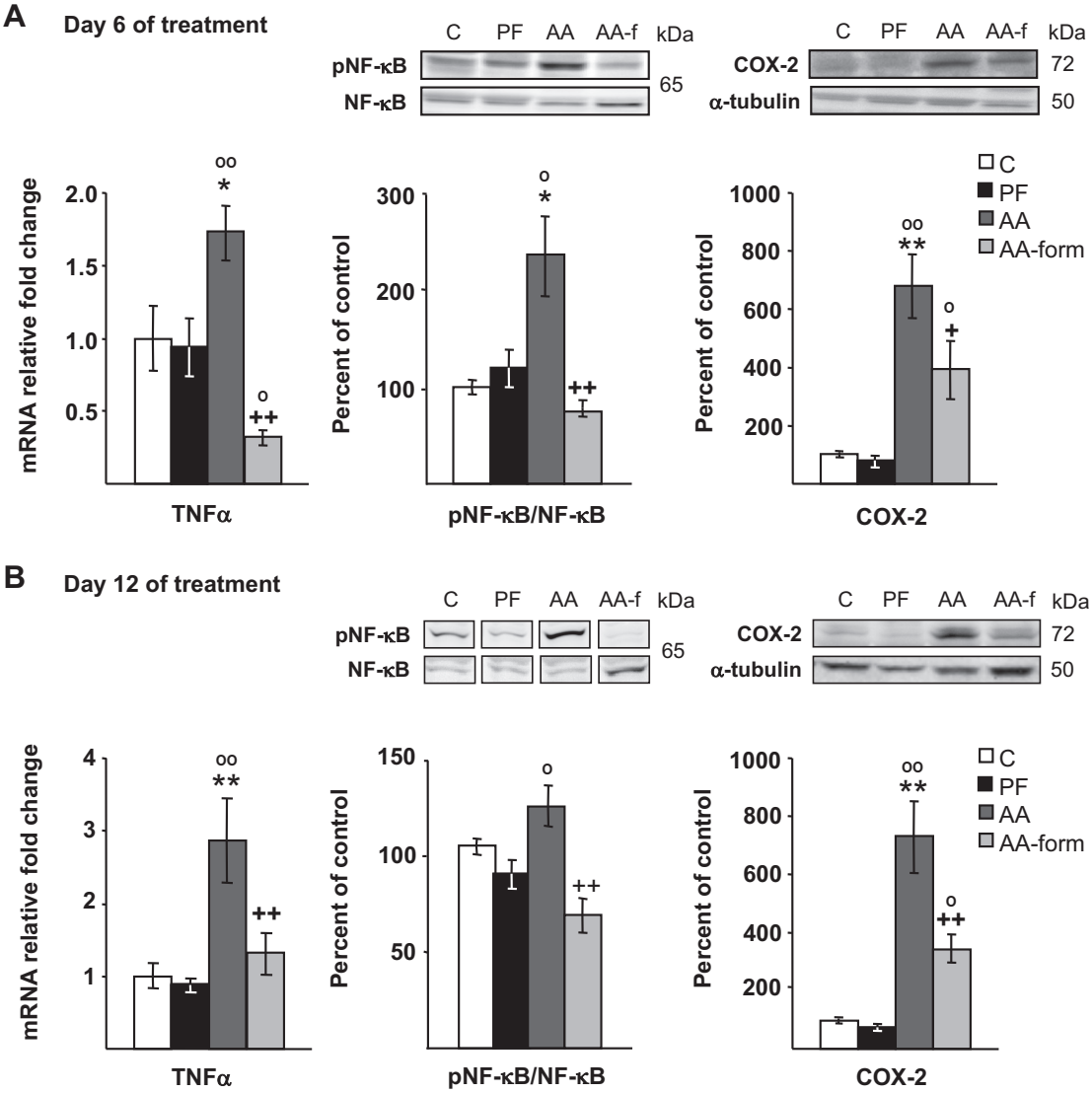

Fig. 4. Effect of formoterol (form) treatment (50 μg/kg body wt sc daily) to arthritic rats for 6 (*A*) or 12 (*B*) days on TNFα mRNA, NF-κB(p65) phosphorylation, and COX-2 in the gastrocnemius. C, control; PF, pair-fed; AA, arthritic rats; AA-f, arthritic rats treated with formoterol. TNFα mRNA was measured by PCR; p-NF-κB(p65), NF-κB(p65), and COX-2 were measured by Western blot. Representative Western blots are shown in *A* and *B*, *top*. Boxes through immunoblots represent spliced images to follow group and treatment order. Arthritis increased TNFα expression, NF-κB(p65) phosphorylation, and COX-2 levels in the gastrocnemius. Formoterol treatment for 6 or 12 days prevented arthritis-induced increase in TNFα and NF-κB(p65) phosphorylation and decreased COX-2 in the gastrocnemius ($P < 0.01$). Data represent means ± SE ($n = 6$–10). *$P < 0.05$, **$P < 0.01$ vs. control rats; °$P < 0.05$, °°$P < 0.01$ vs. PF rats; +$P < 0.05$, ++$P < 0.01$ vs. AA rats injected with saline. LSD multiple comparison test.

Western blot. Gastrocnemius was homogenized in RIPA buffer (10 μl/mg) with a protease inhibitor cocktail of 12.5 mM sodium deoxycolate, 100 mM phenylmethane sulfonyl fluoride, and 12.5 mM sodium orthovanadate and phosphatase inhibitors (Sigma-Aldrich, Madrid, Spain). The homogenate was later centrifuged at 13,000 rpm at 4°C for 30 min to remove tissue debris. Protein concentration was determined using the Bradford protein assay, with bovine serum albumin as standard. The protein extract was boiled for 5 min with a 1:1 volume of Laemmli loading buffer. Proteins (100 μg) were resolved by electrophoresis on 14% polyacrylamide gels under reducing conditions and then transferred onto nitrocellulose membranes that were blocked by incubation in 5% nonfat dry milk and 0.1% Tween (Sigma-Aldrich) in Tris-buffered saline. Ponceau S staining was performed to ensure equal transfer prior to blocking. Membranes were probed overnight at 4°C with antibodies against p-Aktser(473), COX-2 (D5H5), and microtubule-associated protein-1 light chain 3b (LC3b) (Cell Signaling Technology Inc, Boston, MA), Akt, p-NF-κB(p65) Ser^{536}, NF-κB p65 (C20), MuRF, MyoD, and myogenin (Santa Cruz Biotechnology, Santa Cruz, CA), and α-tubulin (Sigma-Aldrich). Membranes were then incubated for 90 min in the appropriate secondary antibody conjugated to horseradish peroxidase (anti-mouse IgG; Amersham Biosciences, Little Chalfont, UK), anti-rabbit IgG (GE Healthcare, Madrid, Spain), and anti-goat IgG (Santa Cruz Biotechnology), and peroxidase activity was detected using enhanced chemiluminescent reagent (Amersham Biosciences). Following ECL detection of phosphoproteins, membranes were stripped with stripping buffer (Restore Western Blot Stripping Buffer; Thermo Scientific Rockford, IL) and reprobed for total protein. Band intensities were quantified by densitometry using a PC-Image VGA24 program for Windows. The density of the protein band in each lane was expressed as the percentage of the mean density of control rats after load normalization using α-tubulin.

Statistical analysis. Results were compared using the statistics program Statgraphics plus for Windows. Normal distribution of data was assessed using a Shapiro-Wilks *W*-test. Data are presented as means ± SE. Statistical evaluation of the data was performed by one-way analysis of variance; post hoc comparisons were made using the least significant difference multiple range test. Statistical significance was set at $P < 0.05$.

RESULTS

As expected, arthritis decreased body weight gain ($P < 0.01$) because arthritic rats treated with saline had lower body weight gain than control and pair-fed rats from *days 2* and *4* of treatment, respectively (Fig. 1*A*). Formoterol administration to

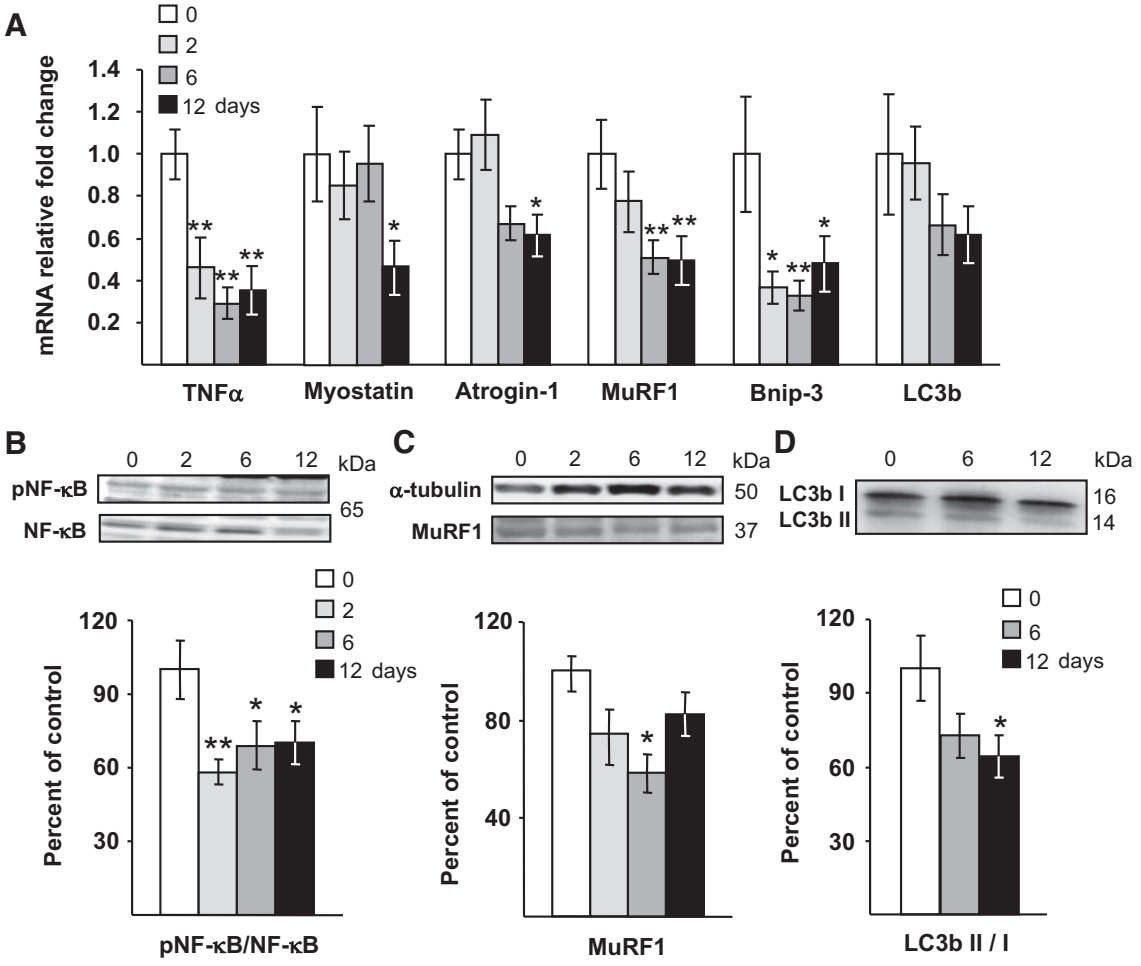

Fig. 5. Effect of formoterol administration (50 μg/kg body wt sc. daily) for 2, 6, and 12 days to control rats on gastrocnemius TNFα, myostatin, atrogin-1, muscle RING finger 1 (MuRF1), BCL2/adenovirus E1B 19-kDa protein-interacting protein-3 (Bnip-3), and light chain 3b (LC3b) mRNA (*A*), NF-κB(p65) phosphorylation (*B*), MuRF1 protein (*C*), and LC3b lipidation (*D*). mRNAs were measured by PCR and proteins by Western blot. Representative Western blots are shown in *B–D*, *top*. Formoterol treatment decreased TNFα, myostatin, atrogin-1, and Bnip-3 mRNA, MuRF1 mRNA and protein, NF-κB(p65) phosphorylation, and LC3b lipidation. Data represent means ± SE ($n = 8–10$). *$P < 0.05$, **$P < 0.01$ vs. control rats injected with saline. LSD multiple comparison test.

arthritic rats increased body weight gain, where these rats had higher body weight gain than pair-fed rats, on *days 4* and *5* of treatment. The stimulatory effect of formoterol treatment on body weight gain was not due to changes in food intake, since formoterol did not modify the inhibitory effect of arthritis on food intake (data not shown). Formoterol administration to control rats for 12 days also increased body weight gain from 69 ± 2.3 g in rats treated with saline to 82 ± 1.4 g in control rats treated with formoterol ($P < 0.01$), but it did not modify food intake (data not shown).

As expected, the decrease in body weight gain observed in arthritic rats was associated with muscle wasting. Evolution of gastrocnemius muscle wet mass on *days 6* and *12* of formoterol treatment is shown in Fig. 1*B*. Arthritis decreased gastrocnemius mass on *day 6* ($P < 0.01$) compared with both control and pair-fed rats. Gastrocnemius mass decreased further on *day 12* in arthritic rats treated with saline, having lower values than on *day 6* ($P < 0.01$). This decrease in skeletal muscle mass is not secondary to the decrease in food intake, since pair-fed rats have gastrocnemius mass similar to that of control rats fed ad libitum, and is higher than that of arthritic rats. Formoterol administration to arthritic rats for 6 days tended to increase gastrocnemius mass, but this increase was not statistically significant. However, formoterol treatment for 12 days increased gastrocnemius mass ($P < 0.01$) and prevented the decrease in gastrocnemius mass observed between *days 6* and *12* in arthritic rats treated with saline. Formoterol administration to control rats for 12 days increased gastrocnemius mass (1,257 ± 34 mg in rats treated with formoterol over 12 days vs. 1,066 ± 22 in rats treated with saline, $P < 0.01$).

Fig. 1, *C–E*, shows that arthritis induced a dramatic decrease in gastrocnemius cross-sectional area and in mean fast and slow fiber area ($P < 0.01$). As we have observed previously, myofiber atrophy was higher in fast than in slow fibers (8). Six days of treatment with formoterol did not significantly increase gastrocnemius mass or cross-sectional or fiber area (data not shown). However, the stimulatory effect of 12 days of formoterol treatment on gastrocnemius mass in arthritic rats was associated with an increase in gastrocnemius cross-sectional ($P < 0.01$) and mean fast fiber area ($P < 0.05$). In control rats, 12 days of formoterol treatment increased gastrocnemius cross-sectional area as well as mean fast and slow fiber area (Fig. 2, *A* and *B*).

As shown in Fig. 3, formoterol treatment decreased arthritis score index ($P < 0.01$), where the difference was significant from *day 4* of treatment with formoterol. Arthritis increased TNFα mRNA in the gastrocnemius muscle on both *day 6* and *day 12* of treatment ($P < 0.01$; Fig. 4, *A* and *B*). Formoterol prevented the stimulatory effect of arthritis on TNFα expression in the gastrocnemius muscle on both *day 6* and *day 12* ($P < 0.01$), where the arthritic rats treated with formoterol for 6 days had lower TNFα mRNA values than those of arthritic rats treated with saline and pair-fed rats. The inhibitory effect of formoterol on TNFα expression in the gastrocnemius was also observed in control rats from the 2nd day of treatment with formoterol ($P < 0.01$; Fig. 5*A*). Arthritis increased NF-

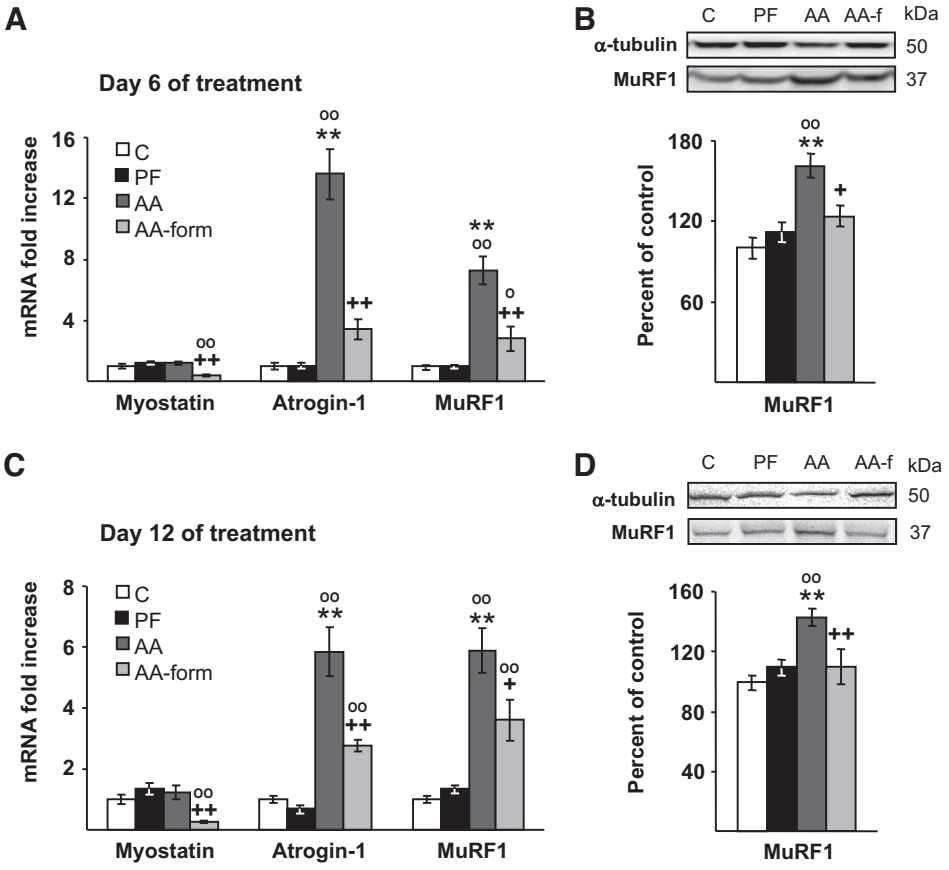

Fig. 6. Effect of formoterol (form) administration (50 μg/kg body wt sc daily) for 6 or 12 days to arthritic rats on myostatin, atrogin-1, and MuRF1 mRNA (*A* and *C*) and MuRF1 levels (*B* and *D*) in the gastrocnemius. C, control; PF, pair-fed; AA, arthritic rats; AA-f, arthritic rats treated with formoterol. Myostatin, atrogin-1, and MuRF1 mRNA were measured by PCR, and MuRF1 protein was measured by Western blot. Representative Western blots are shown in *B* and *D*, *top*. Arthritis increased atrogin-1 and MuRF1 expression ($P < 0.01$) in the gastrocnemius. Formoterol treatment for 6 or 12 days decreased myostatin, atrogin-1, and MuRF1 expression ($P < 0.01$) and prevented arthritis-induced increased in MuRF1 protein. Data represent means ± SE ($n = 6$–10). $^{**}P < 0.01$ vs. control rats, $^{\circ}P < 0.05$, $^{\circ\circ}P < 0.01$ vs. PF rats; $+P < 0.05$, $++P < 0.01$ vs. AA injected with saline. LSD multiple comparison test.

κB(p65) phosphorylation on both *day 6* and *day 12* ($P < 0.05$; Fig. 4, *A* and *B*), but the increase was higher on *day 6* of treatment (and 16 days after adjuvant injection) than on *day 12* of treatment (and 22 days after adjuvant injection). Arthritic rats treated with formoterol showed lower NF-κB(p65) phosphorylation in skeletal muscle on both days ($P < 0.01$). Formoterol was also able to decrease NF-κB(p65) phosphorylation in the gastrocnemius of control rats on all days analyzed (Fig. 5*B*). The arthritis-induced increase in COX-2 levels in the gastrocnemius was decreased by formoterol treatment on both *day 6* ($P < 0.05$; Fig. 4*A*) and *day 12* of treatment ($P < 0.01$; Fig. 4*B*). However, COX-2 levels in arthritic rats treated with formoterol were higher than in pair-fed rats. Pair-feeding the rats did not modify TNFα, COX-2, or pNF-κB(p65) levels in the gastrocnemius (Fig. 4, *A* and *B*).

As shown in Fig. 5*A*, formoterol administration to control rats for 12 days decreased the expression of myostatin, atrogin-1, MuRF1, and the autophagic marker gene BCL2/adenovirus E1B 19-kDa protein-interacting protein-3 (Bnip-3) as well as MuRF1 protein ($P < 0.05$; Fig. 5*C*). Lipidation, modification of LC3b from from LC3-I to the lipidated form (LC3b-II), has been widely used to indicate the occurrence of autophagy. Formoterol administration to control rats for 12 days decreased lipidation of LC3b, measured as the LC3b-II/LC3b-I ratio ($P < 0.05$; Fig. 5*D*). However, formoterol was not able to decrease LC3b expression in control rats (Fig. 5*A*).

The effect of arthritis and formoterol treatment on myostatin, atrogin-1, and MuRF1 in the gastrocnemius is shown in Fig. 6. Although myostatin mRNA was not modified by arthritis or pair-feeding the rats (Fig. 6, *A* and *C*), expression was decreased dramatically on *days 6* and *12* ($P < 0.01$) in arthritic rats treated with formoterol. Atrogin-1 and MuRF1 mRNA expression in the gastrocnemius of arthritic rats was higher than in control and in pair-fed rats on both *day 6* and *day 12* of treatment ($P < 0.01$; Fig. 6, *A* and *C*), where the increase was higher on *day 6* than on *day 12*. Formoterol treatment prevented arthritis-induced increase in atrogin-1 and MuRF1 mRNA, but to higher levels than those of pair-fed rats. Arthritis also increased MuRF1 protein in arthritic rats treated with saline ($P < 0.01$) but not in rats treated with formoterol (Fig. 6, *B* and *D*). Figure 7 shows the effect of arthritis and formoterol on the autophagic gene expression Bnip-3 and LC3b and on LC3b lipidation. Arthritis increased Bnip-3 and LC3b mRNA ($P < 0.01$; Fig. 7, *A* and *C*). Formoterol administration to arthritic rats prevented the effect of arthritis on Bnip-3 mRNA and decreased LC3b mRNA. Arthritis increased the conversion of LC3b-I to LC3b-II by lipidation (Fig. 7, *B* and *D*), and formoterol treatment for 6 and 12 days decreased LC3b-II, the lipidated form of the protein.

Arthritis did not modify protein kinase B (Akt) activity in the gastrocnemius muscle, since gastrocnemius of arthritic rats treated with saline had Akt phosphorylation similar to control

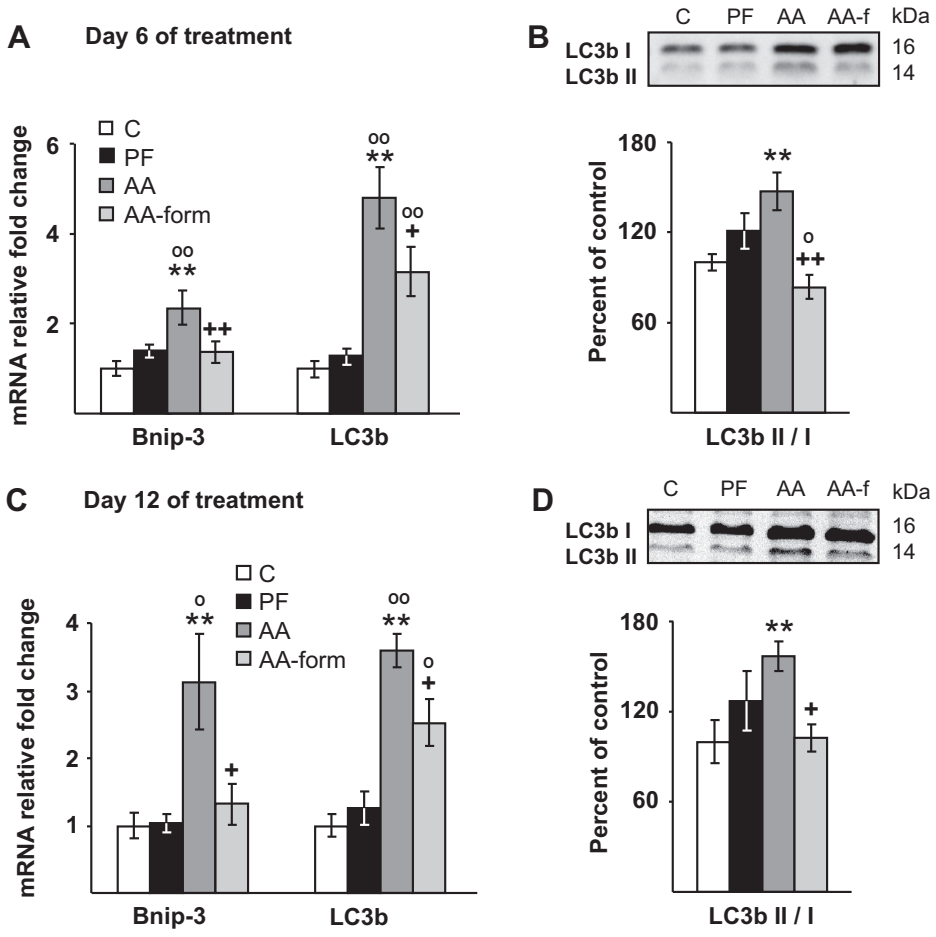

Fig. 7. Effect of formoterol (form) administration (50 μg/kg body wt sc daily) for 6 or 12 days to arthritic rats on Bnip-3 and LC3b mRNA (*A* and *C*) and on LC3b lipidation (*B* and *D*) in the gastrocnemius. C, control; PF, pair-fed; AA, arthritic rats. Bnip-3 and LC3b mRNA were measured by PCR and are presented as increase of the mean value in control rats. LC3b lipidation was represented as the LC3b II/LC3b I ratio measured by Western blot. Form treatment prevented arthritis-induced increase in Bnip-3 mRNA in LC3b lipidation and attenuated the increase in LC3b mRNA levels. Data represent means ± SE ($n = 6$ - 10). $^{**}P < 0.01$ vs. control rats; $^{\circ}P < 0.05$, $^{\circ\circ}P < 0.01$ vs. PF rats; $+P < 0.05$, $++P < 0.01$ vs. AA injected with saline. LSD multiple comparison test.

rats (Fig. 8, *A* and *C*). In contrast, in arthritic rats treated with formoterol for 6 or 12 days there was an increase in p-Akt levels as well as in the p-Akt/Akt ratio ($P < 0.01$). Similarly, formoterol increased p-Akt and p-Akt/Akt ratio after 6 and 12 days of treatment in control rats (Fig. 9*A*). On *day 6* of treatment there was an increase in MyoD expression in the gastrocnemius of arthritic rats regardless of whether they where treated with saline or formoterol ($P < 0.01$; Fig. 8*B*). However, the stimulatory effect of arthritis on MyoD expression was not seen on *day 12*, since MyoD levels were similar in all groups of rats (Fig. 8*D*). As shown in Fig. 9*B*, formoterol treatment did not significantly modify MyoD protein levels in the gastrocnemius of control rats. Arthritis increased myogenin levels on *days 6* and *12* ($P < 0.01$; Fig. 8, *B* and *D*). As has been reported (60), increased MyoD in muscle suggests that satellite cells are in a proliferative phase in arthritic rats on *day 6*. However, on *day 12* (22 after adjuvant injection), MyoD levels in the gastrocnemius were not increased in arthritic rats. In contrast, myogenin levels were increased on both days. Differences between MyoD and myogenin expression in arthritic rats on *day 12* of treatment can be due to the fact that MyoD acts on early stage of muscle regeneration, whereas myogenin is involved at a later stage of differentiation (30). Formoterol treatment for 12 days further increased myogenin in the gastrocnemius of arthritic rats ($P < 0.01$). Formoterol treatment for 6 and 12 days was also able to increase myogenin levels in control rats (Fig. 9*B*), but these increases were lower than those induced by arthritis.

The expression of IGF-I and IGFBPs mRNA in the gastrocnemius was modified by arthritis and formoterol treatment but not by pair-feeding the rats (Fig. 10, *A* and *B*). IGFBP-3 mRNA levels in the gastrocnemius of the arthritic rats treated with saline were markedly increased on both *day 6* and *day 12* ($P < 0.01$). In contrast, IGF-I mRNA levels were increased in arthritic rats treated with saline on *day 12* of treatment. Arthritis increased gastrocnemius IGFBP-5 levels mRNA in rats treated with saline on *day 6* ($P < 0.01$), and they increased further on *day 12* of treatment. The time course expression of IGFBP-5 in arthritic rats was modified in a pattern similar to that of IGF-I mRNA and myogenin, with their expression

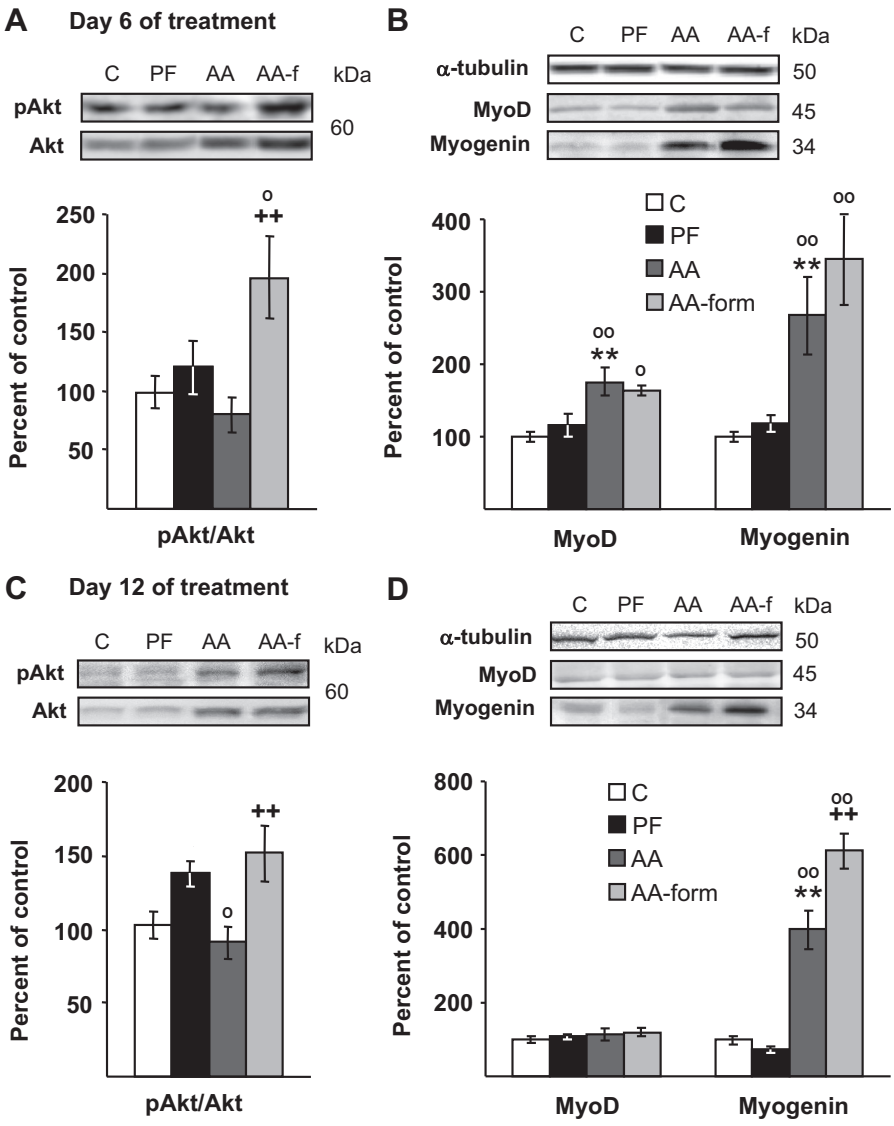

Fig. 8. Effect of formoterol (form) administration (50 μg/kg body wt sc daily) for 6 or 12 days to arthritic rats on Akt phosphorylation (p-Akt; *A* and *C*) and MyoD and myogenin levels (*B* and *D*) in the gastrocnemius. C, control; PF, pair-fed; AA, arthritic rats. Akt, p-Akt, myogenin, and MyoD were measured by Western blot. Representative Western blots are shown at the *top*. Arthritis increased MyoD levels only on *day 6* and myogenin on *days 6* and *12* ($P < 0.01$). Formoterol increased Akt phosphorylation on *days 6* and *12* and myogenin on *day 12* of treatment ($P < 0.01$). PF rats have a higher p-Akt/Akt ratio than control rats on *day 12* ($P < 0.05$). Data represent means ± SE ($n = 6$–10). $^{**}P < 0.01$ vs. control rats; $^{\circ}P < 0.05$, $^{\circ\circ}P < 0.01$ vs. PF rats; $^{++}P < 0.01$ vs. AA injected with saline. LSD multiple comparison test.

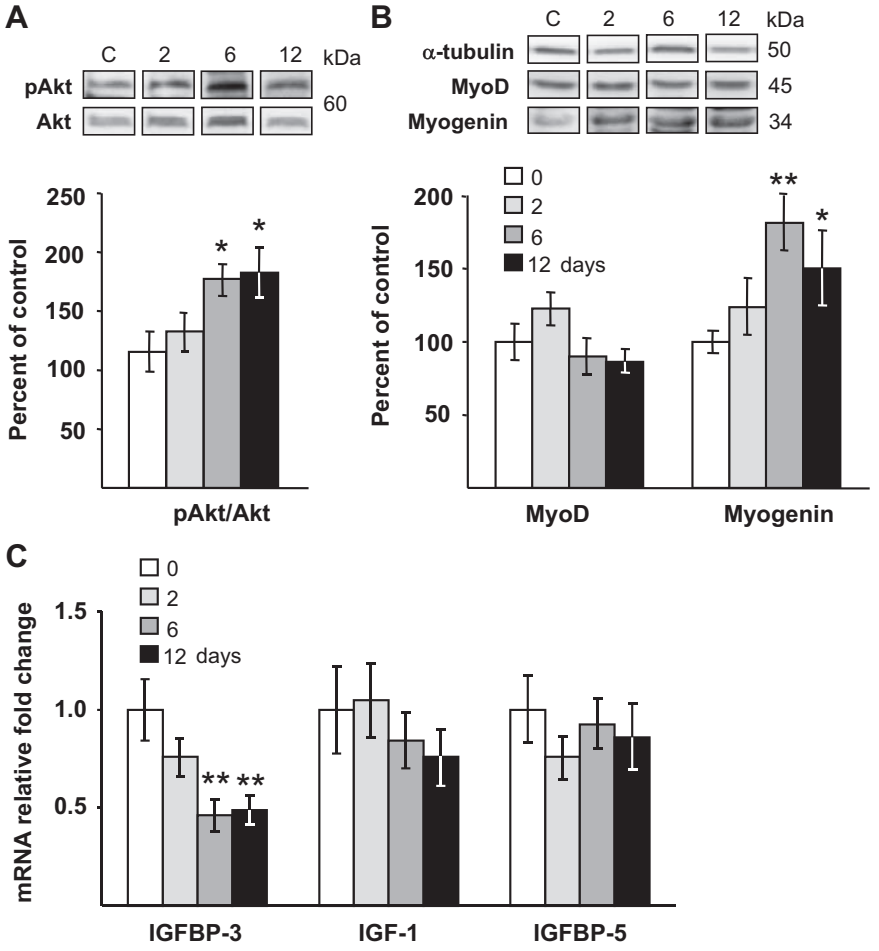

Fig. 9. Effect of formoterol administration (50 μg/kg body wt sc daily) for 2, 6, and 12 days to control rats on gastrocnemius Akt phosphorylation (*A*), myogenic differentiation factor D (MyoD) and myogenin levels (*B*), and insulin growth factor-binding protein (IGFBP)-3, IGF-I, and IGFBP-5 mRNA (*C*). mRNAs were measured by PCR and proteins by Western blot. Representative Western blots are shown at the *top*. Boxes through immunoblots represent spliced images to follow group and treatment order. Akt phosphorylation and myogenin levels were increased by 6 or 12 days of formoterol treatment. Formoterol decreased IGFBP-3 ($P < 0.01$). Data represent means ± SE ($n = 8$–10). *$P < 0.05$, **$P < 0.01$ vs. rats injected with saline. LSD multiple comparison test.

being higher on *day 12* than on *day 6*. The possible explanation for the highest expression being on *day 12* could be that IGFBP-5 and myogenin are related to the differentiation process in regenerating muscle (65), since knockdown of this IGFBP inhibits myogenic differentiation (54).

Formoterol administration to arthritic rats decreased IGFBP-3 expression ($P < 0.01$). Similarly, in control rats formoterol administration was able to decrease IGFBP-3 expression in the gastrocnemius ($P < 0.01$; Fig. 9*C*). Arthritic rats treated with formoterol had higher gastrocnemius IGFBP-5 than pair-fed rats but lower gastrocnemius IGFBP-5 than arthritic rats treated with saline on *day 6* ($P < 0.05$). However, on *day 12* of treatment, the two groups of arthritic rats had similar IGFBP-5 mRNA (Fig. 10*B*). In control rats, formoterol treatment did not modify IGF-I or IGFBP-5 mRNA in the gastrocnemius (Fig. 9*C*).

DISCUSSION

The present study indicates that formoterol administration to arthritic rats decreases inflammation and prevents inflammatory cachexia. The protective effect of formoterol on skeletal muscle mass is associated with decreased inflammation, myostatin, atrogenes, autophagic gene and IGFBP-3 expression, and LC3b lipidation together with Akt and myogenin activation.

Our data show that formoterol treatment decreases the severity of arthritis. These data are in accord with those reported previously in experimental models of arthritis, in which β_2-adrenergic stimulation inhibits inflammation during the chronic symptomatic phase of arthritis (for review, see Ref. 31). The anti-inflammatory effect of adrenergic stimulation has also been reported in rheumatoid arthritis patients who lose sympathetic nerve fibers, where catecholamine-producing cells in the synovial tissue start to replace sympathetic nerve fibers and have a strong anti-inflammatory effect (5). Formoterol has an anti-inflammatory effect on skeletal muscle of arthritic as well as of control rats, since it decreases NF-κB(p65) phosphorylation and the expression of TNFα and COX-2 in the gastrocnemius in both groups of rats. The anti-inflammatory effect of β_2-adrenergic stimulation has been reported in different cell types such as leukocytes, lung smooth muscle, and endothelial cells (28). In the skeletal muscle, it has been found that β-adrenergic blockade by propranolol treatment exacerbated sepsis-induced increase in muscle IL-6 and TNFα expression (34), suggesting an anti-inflammatory action of β-adrenergic activation in muscle.

In addition to its anti-inflammatory effect, formoterol treatment increased body and gastrocnemius weights. These data are in accord with the well-known antiatrophic actions of β_2-adrenergic agonist on skeletal muscle (26, 32). To our

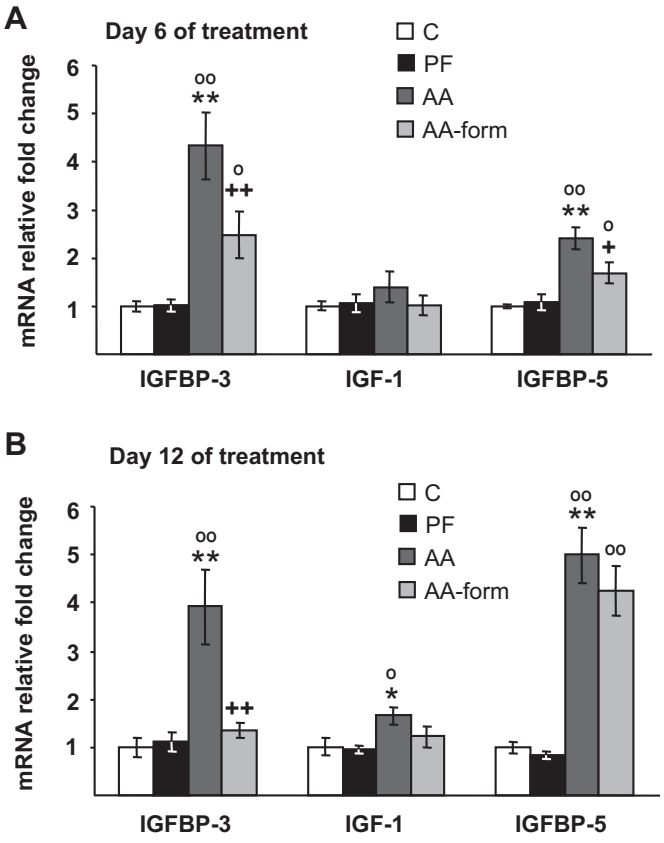

Fig. 10. Effect of formoterol (form) administration (50 μg/kg body wt sc daily) to arthritic rats for 6 (*A*) or 12 (*B*) days on IGFBP-3, IGF-I, and IGFBP-5 mRNA in the gastrocnemius. C, control; PF, pair-fed; AA, arthritic rats. mRNA was measured by PCR. Arthritis increased IGFBP-3 mRNA ($P < 0.01$), whereas form decreased its expression ($P < 0.01$). IGF-I mRNA was increased in AA treated with saline on *day 12* ($P < 0.05$). Arthritis increased IGFBP-5 mRNA ($P < 0.01$). Data represent means ± SE (n = 7–9). $*P < 0.05$, $**P < 0.01$ vs. control rats; $°P < 0.05$, $°°P < 0.01$ vs. PF rats; $+P < 0.05$, $++P < 0.01$ vs. AA injected with saline. LSD multiple comparison test.

knowledge, this is the first study directly showing the role of β_2-adrenergic activation in arthritis-induced muscle wasting.

As we have reported previously (6, 7), myostatin expression was not increased in arthritic rats. The lack of modification of myostatin in arthritic rats is in agreement with data reported in other conditions of muscle atrophy such as dexamethasone administration (23), muscle disuse (46), and some types of cancer (4). Formoterol was able to decrease myostatin expression in arthritic rats after 6 and 12 days of treatment and in control rats after 12 days of treatment. The inhibitory effect of formoterol on myostatin is well known (52), and it has been proposed that certain anabolic actions of formoterol in cancer-induced cachexia may be mediated via the myostatin system (4). In this sense, myostatin downregulation can contribute to the inhibitory effects of formoterol on muscle proteolysis, since myostatin upregulates atrogin-1 and MuRF1 expression, through the inhibition of Akt phosphorylation, thereby increasing the levels of active FoxO1 (47).

Arthritis increased atrogin-1, MuRF1, Bnip, and LC3B expression and LC3B-I conversion to LC3B-II by lipidation, suggesting an activation of the ubiquitin-proteasome and autophagic-lysosomal proteolytic pathways. Taking into account that arthritis does not modify Akt/FoxO3 phosphorylation (7), atrogenes and autophagy in arthritis can be induced through NF-κB activation, as it has been reported in hepatocytes after LPS administration (9). Formoterol significantly decreased arthritis-induced atrogin-1, MuRF1, Bnip-3, and LC3b expression in the gastrocnemius as well as LC3b lipidation. Similarly, β_2-adrenergic agonists have been reported to prevent cancer-induced muscle wasting and denervation-induced atrogin-1 and MuRF1 upregulation in muscle (3, 12, 19). Furthermore, chronic depletion of epinephrine exacerbates fasting-induced muscle proteolysis, increases atrogin-1, MuRF1, and LC3b expression and LC3b lipidation, and decreases p-Akt levels (20). The inhibitory effect of epinephrine on muscle proteolysis seems to be mediated by cAMP (50). Therefore, formoterol-induced MuRF1, atrogin-1, Bnip3, and LC3b repression can be mediated, as mentioned above, through the activation of AMPc/Akt and/or through downregulation of inflammation.

As reported previously, arthritis did not modify Akt phosphorylation in muscle (8). These data differ from those observed in other acute wasting conditions such as lipopolysaccharide (LPS) or glucocorticoid administration, which decrease Akt phosphorylation, whereas the transcription factors Forkhead box-containing protein O subclass (FoxO)-1 and -3a activities are increased (13, 44). In cachexia induced by chronic illnesses, the activity of the Akt/FoxO signaling pathway is not well known. It has been reported that FoxO1 and FoxO3 protein activity were unchanged in human cancer cachexia (61). Furthermore, in humans with chronic obstructive pulmonary disease, muscle atrophy is associated with an increase in Akt activation (17, 57). These and several other data indicate that under certain conditions Akt/FoxO and atrogene activity can be independent of each other. A possible explanation for these discrepancies can be that cachexia induced by a chronic process is not as rapid and severe as the acute muscle wasting observed in acute experimental models of muscle wasting. Accordingly, the physiological regulators may not be exactly the same. The fact that arthritis increased muscle TNFα expression and NF-κB(p65) phosphorylation suggests that this pathway can be responsible for arthritis-induced increased expression of atrogin-1 and MuRF1.

As reported previously with β_2-adrenoceptor agonists (29), 6 and 12 days of formoterol treatment also increased Akt activation in arthritic and control rats. It has been postulated that this stimulatory effect is mediated by an IGF-I-independent growth pathway through the $G_i\alpha/G\beta\gamma$/phosphatidylinositol 3-kinase signaling pathway (29, 56). Although some authors found that the stimulatory effect of formoterol on Akt phosphorylation decreases after 10 days of treatment (25), others reported that administration of formoterol is able to increase Akt phosphorylation after 28 days (31). Our data and those of Koopman et al. (31) suggest that some of the effects of formoterol on skeletal muscle mass are exerted via Akt signaling.

As we have reported previously, arthritis increases the myogenic regulatory factors MyoD and myogenin (6, 8). Upregulation of MyoD and myogenin together with an increase in inflammatory markers has also been reported in burn-induced muscle atrophy (53). Moreover, collagen-induced arthritis and immobilization increase muscle proteolysis and decrease muscle mass (15). However, whereas collagen-induced arthritis stimulated inflammation and myogenin expression, immobili-

zation did not modify the inflammatory response, and it decreased MyoD (15). These data are in accord with those showing that inflammation, although it induces muscle wasting, is also able to trigger muscle regeneration by activating satellite cell proliferation and differentiation, as indicated by Tidball (62). Stimulation of genes that regulate muscle development and growth, such as myogenin, has been reported in rats submitted to 5–14 days of an experimental intensive care unit model (39). These authors interpreted that result as a compensatory mechanism to reduce the excessive downregulation of sarcomeric proteins and upregulation of different proteolytic pathways.

A stimulatory effect of formoterol on muscle regeneration and on muscle regulatory factors has also been reported (11). The effects of formoterol on gastrocnemius do not seem to be mediated by MyoD, since MyoD expression in the gastrocnemius was not modified by formoterol administration to arthritic or to control rats. However, formoterol treatment was able to increase the expression of myogenin in the gastrocnemius of both arthritic and control rats. Similarly, in immobilized rat plantaris muscle, clenbuterol upregulated myogenin, whereas MyoD expression was unaffected (16). It has been reported previously that the inhibition of NF-κB activity increases Akt phosphorylation and promotes skeletal muscle regeneration by limiting inflammatory response and fibrosis (48). Therefore, it is possible that formoterol stimulates Akt and myogenin expression through its inhibitory action on NF-κB.

The effect of β_2-adrenoreceptor stimulation on the IGF-I system in skeletal muscle is not well known. Gonçalves et al. (19) found that clenbuterol did not change IGF-I levels in the soleus muscle. In contrast, clenbuterol has been reported to induce overexpression of IGF-I mRNA in the soleus and masseter muscles (1, 45). Arthritis increased IGFBP-5 in a way similar to myogenin, where the highest expression was observed on *day 12*. This could be explained by the fact that IGFBP-5 and myogenin are related to the differentiation process in regenerating muscle (65), since knockdown of this IGFBP inhibits myogenic differentiation (54). However, the present study shows that formoterol administration increases Akt activity, but it does not significantly modify IGF-I or IGFP5 in control or arthritic rats. Despite the aforementioned discrepancies, β_2-adrenoreceptor stimulation does not increase serum IGF-I levels but actually decreases circulating IGF-I (1, 2). These and our data are in accord with the second IGF-I-independent growth pathway involving the activation of β_2-adrenoceptors and subsequent Akt activation that has been mentioned above (29).

In contrast to the lack of effect of formoterol on IGF-I, formoterol decreased the arthritis-induced increase in gastrocnemius IGFBP-3 mRNA as well as IGFBP-3 expression in control rats. An inhibitory effect of clenbuterol on IGFBP-3 expression has been reported previously in the masseter muscle (45). IGFBP-3 is able to suppress myoblast proliferation through an IGF-I-independent mechanism (51). In different tissues, local IGFBP-3 is an inhibitor of cell growth and/or promoter of apoptosis by a non-IGF-dependent mechanism (27). Furthermore, IGFBP-3 upregulation is mediated by pro-apoptotic and growth inhibitory factors such as TNFα (27). Therefore, it is not surprising that muscle wasting induced by inflammation is associated with increased IGFBP-3 levels, as we have observed not only in arthritis but also after endotoxin injection (44). Taking into account that Akt is a negative regulator of IGFBP-3 (24), the inhibitory action of formoterol treatment on IGFBP-3 in the gastrocnemius can be mediated by the increase in p-Akt and/or the decrease in TNFα. Therefore, downregulation of IGFBP-3 levels in the gastrocnemius by formoterol treatment can contribute to skeletal muscle growth, development, and hypertrophy.

In summary, formoterol has an anti-inflammatory and hypertrophic action in skeletal muscle through increasing pAkt activity and myogenin and decreasing the p-NF-κB(p65)/TNFα pathway, myostatin, and IGFBP-3 in both arthritic and control rats. This study shows for the first time the effects of β-adrenergic agonist on muscle atrophy and transcription factors involved in muscle protein degradation in arthritis. Our observations suggest that formoterol treatment could be useful in reducing arthritis symptoms and in preserving muscle mass in rheumatoid arthritis patients. Further histological and functional studies are required to clarify the potential effect of formoterol on muscle regeneration and myogenesis.

ACKNOWLEDGMENTS

We are indebted to Christina Bickart for the English correction of the manuscript.

GRANTS

This work was supported by Grant BFU2012-38468 from MINECO and from Universidad Complutense of Madrid to A. B. Gómez-SanMiguel.

DISCLOSURES

No conflicts of interest, financial or otherwise, are declared by the authors.

AUTHOR CONTRIBUTIONS

A.B.G.-S., C.G.-M., M.P.N.-B., C.F.-G., M.A.V., A.I.M., and A.L.-C. performed experiments; A.B.G.-S., C.G.-M., M.P.N.-B., and C.F.-G. analyzed data; A.B.G.-S., C.G.-M., A.I.M., and A.L.-C. interpreted results of experiments; A.B.G.-S., C.G.-M., M.P.N.-B., C.F.-G., and A.L.-C. prepared figures; A.B.G.-S., C.G.-M., M.P.N.-B., C.F.-G., M.A.V., A.I.M., and A.L.-C. edited and revised manuscript; M.A.V., A.I.M., and A.L.-C. conception and design of research; A.L.-C. drafted manuscript; A.L.-C. approved final version of manuscript.

REFERENCES

1. **Awede BL, Thissen JP, Lebacq J.** Role of IGF-I and IGFBPs in the changes of mass and phenotype induced in rat soleus muscle by clenbuterol. *Am J Physiol Endocrinol Metab* 282: E31–E37, 2002.
2. **Bonefeld K, Hobolth L, Juul A, Møller S.** The insulin like growth factor system in cirrhosis. Relation to changes in body composition following adrenoreceptor blockade. *Growth Horm IGF Res* 22: 212–218, 2012.
3. **Busquets S, Figueras MT, Fuster G, Almendro V, Moore-Carrasco R, Ametller E, Argilés JM, López-Soriano FJ.** Anticachectic effects of formoterol: a drug for potential treatment of muscle wasting. *Cancer Res* 64: 6725–6731, 2004.
4. **Busquets S, Toledo M, Marmonti E, Orpí M, Capdevila E, Betancourt A, López-Soriano FJ, Argilés JM.** Formoterol treatment downregulates the myostatin system in skeletal muscle of cachectic tumour-bearing rats. *Oncol Lett* 3: 185–189, 2012.
5. **Capellino S, Cosentino M, Wolff C, Schmidt M, Grifka J, Straub RH.** Catecholamine-producing cells in the synovial tissue during arthritis: modulation of sympathetic neurotransmitters as new therapeutic target. *Ann Rheum Dis* 69: 853–860, 2010.
6. **Castillero E, Martín AI, López-Menduiña M, Granado M, Villanúa MA, López-Calderón A.** IGF-I system, atrogenes and myogenic regulatory factors in arthritis induced muscle wasting. *Mol Cell Endocrinol* 309: 8–16, 2009.
7. **Castillero E, Martín AI, López-Menduiña M, Villanúa MA, López-Calderón A.** Eicosapentaenoic acid attenuates arthritis-induced muscle

wasting acting on atrogin-1 and on myogenic regulatory factors. *Am J Physiol Regul Integr Comp Physiol* 297: R1322–R1331, 2009.

8. **Castillero E, Nieto-Bona MP, Fernández-Galaz C, Martín AI, López-Menduiña M, Granado M, Villanúa MA, López-Calderón A.** Fenofibrate, a PPARα agonist, decreases atrogenes and myostatin expression and improves arthritis-induced skeletal muscle atrophy. *Am J Physiol Endocrinol Metab* 300: E790–E799, 2011.
9. **Chen C, Deng M, Sun Q, Loughran P, Billiar TR, Scott MJ.** Lipopolysaccharide stimulates p62-dependent autophagy-like aggregate clearance in hepatocytes. *Biomed Res Int* 2014: 267350, 2014.
10. **Chou RC, Stinson MW, Noble BK, Spengler RN.** Beta-adrenergic receptor regulation of macrophage-derived tumor necrosis factor-alpha production from rats with experimental arthritis. *J Neuroimmunol* 67: 7–16, 1996.
11. **Conte TC, Silva LH, Silva MT, Hirabara SM, Oliveira AC, Curi R, Moriscot AS, Aoki MS, Miyabara EH.** The β2-adrenoceptor agonist formoterol improves structural and functional regenerative capacity of skeletal muscles from aged rat at the early stages of postinjury. *J Gerontol A Biol Sci Med Sci* 67: 443–455, 2012.
12. **Costelli P, García-Martínez C, Llovera M, Carbó N, López-Soriano FJ, Agell N, Tessitore L, Baccino FM, Argilés JM.** Muscle protein waste in tumor-bearing rats is effectively antagonized by a beta 2-adrenergic agonist (clenbuterol). Role of the ATP-ubiquitin-dependent proteolytic pathway. *J Clin Invest* 95: 2367–2372, 1995.
13. **Crossland H, Constantin-Teodosiu D, Gardiner SM, Constantin D, Greenhaff PL.** A potential role for Akt/FOXO signalling in both protein loss and the impairment of muscle carbohydrate oxidation during sepsis in rodent skeletal muscle. *J Physiol* 586: 5589–5600, 2008.
14. **de Montmollin E, Aboab J, Mansart A, Annane D.** Bench-to-bedside review: Beta-adrenergic modulation in sepsis. *Crit Care* 13: 230, 2009.
15. **de Oliveira Nunes Teixeira V, Filippin LI, Viacava PR, de Oliveira PG, Xavier RM.** Muscle wasting in collagen-induced arthritis and disuse atrophy. *Exp Biol Med (Maywood)* 238: 1421–1430, 2013.
16. **Delday M, Maltin CA.** Clenbuterol increases the expression of myogenin but not myoD in immobilized rat muscles. *Am J Physiol Endocrinol Metab* 272: E941–E944, 1997.
17. **Doucet M, Russell AP, Léger B, Debigaré R, Joanisse DR, Caron MA, LeBlanc P, Maltais F.** Muscle atrophy and hypertrophy signaling in patients with chronic obstructive pulmonary disease. *Am J Respir Crit Care Med* 176: 261–269, 2007.
18. **Gómez-SanMiguel AB, Martín AI, Nieto-Bona MP, Fernández-Galaz C, Villanúa MA, López-Calderón A.** The melanocortin receptor type 3 agonist D-Trp(8)-γ MSH decreases inflammation and muscle wasting in arthritic rats. *J Cachexia Sarcopenia Muscle* 7: 79–89, 2016.
19. **Gonçalves DA, Silveira WA, Lira EC, Graça FA, Paula-Gomes S, Zanon NM, Kettelhut IC, Navegantes LC.** Clenbuterol suppresses proteasomal and lysosomal proteolysis and atrophy-related genes in denervated rat soleus muscles independently of Akt. *Am J Physiol Endocrinol Metab* 302: E123–E133, 2012.
20. **Graça FA, Gonçalves DA, Silveira WA, Lira EC, Chaves VE, Zanon NM, Garófalo MA, Kettelhut IC, Navegantes LC.** Epinephrine depletion exacerbates the fasting-induced protein breakdown in fast-twitch skeletal muscles. *Am J Physiol Endocrinol Metab* 305: E1483–E1494, 2013.
21. **Härle P, Möbius D, Carr DJ, Schölmerich J, Straub RH.** An opposing time-dependent immune-modulating effect of the sympathetic nervous system conferred by altering the cytokine profile in the local lymph nodes and spleen of mice with type II collagen-induced arthritis. *Arthritis Rheum* 52: 1305–1313, 2005.
22. **Hosokawa S, Koseki H, Nagashima M, Maeyama Y, Yomogida K, Mehr C, Rutledge M, Greenfeld H, Kaneki M, Tompkins RG, Martyn JA, Yasuhara SE.** Title efficacy of phosphodiesterase 5 inhibitor on distant burn-induced muscle autophagy, microcirculation, and survival rate. *Am J Physiol Endocrinol Metab* 304: E922–E933, 2013.
23. **Jesinkey SR, Korrapati MC, Rasbach KA, Beeson CC, Schnellmann RG.** Atomoxetine prevents dexamethasone-induced skeletal muscle atrophy in mice. *J Pharmacol Exp Ther* 351: 663–673, 2014.
24. **Jin Q, Lee HJ, Min HY, Smith JK, Hwang SJ, Whang YM, Kim WY, Kim YH, Lee HY.** Transcriptional and posttranslational regulation of insulin-like growth factor binding protein-3 by Akt3. *Carcinogenesis* 35: 2232–2243, 2014.
25. **Joassard OR, Amirouche A, Gallot YS, Desgeorges MM, Castells J, Durieux AC, Berthon P, Freyssenet DG.** Regulation of Akt-mTOR, ubiquitin-proteasome and autophagy-lysosome pathways in response to formoterol administration in rat skeletal muscle. *Int J Biochem Cell Biol* 45: 2444–2455, 2013.
26. **Joassard OR, Durieux AC, Freyssenet DG.** β2-Adrenergic agonists and the treatment of skeletal muscle wasting disorders. *Int J Biochem Cell Biol* 45: 2309–2321, 2013.
27. **Jogie-Brahim S, Feldman D, Oh Y.** Unraveling insulin-like growth factor binding protein-3 actions in human disease. *Endocr Rev* 30: 417–437, 2009.
28. **Johnson M, Rennard S.** Alternative mechanisms for long-acting beta(2)-adrenergic agonists in COPD. *Chest* 120: 258–270, 2001.
29. **Kline WO, Panaro FJ, Yang H, Bodine SC.** Rapamycin inhibits the growth and muscle-sparing effects of clenbuterol. *J Appl Physiol* 102: 740–747, 2007.
30. **Koishi K, Zhang M, McLennan IS, Harris AJ.** MyoD protein accumulates in satellite cells and is neurally regulated in regenerating myotubes and skeletal muscle fibers. *Dev Dyn* 202: 244–254, 1995.
31. **Koopman R, Gehrig SM, Léger B, Trieu J, Walrand S, Murphy KT, Lynch GS.** Cellular mechanisms underlying temporal changes in skeletal muscle protein synthesis and breakdown during chronic {beta}-adrenoceptor stimulation in mice. *J Physiol* 588: 4811–4823, 2010.
32. **Koopman FA, Stoof SP, Straub RH, Van Maanen MA, Vervoordeldonk MJ, Tak PP.** Restoring the balance of the autonomic nervous system as an innovative approach to the treatment of rheumatoid arthritis. *Mol Med* 17: 937–948, 2011.
33. **Kremers HM, Nicola PJ, Crowson CS, Ballman KV, Gabriel SE.** Prognostic importance of low body mass index in relation to cardiovascular mortality in rheumatoid arthritis. *Arthritis Rheum* 50: 3450–3457, 2004.
34. **Lang CH, Nystrom G, Frost RA.** Beta-adrenergic blockade exacerbates sepsis-induced changes in tumor necrosis factor alpha and interleukin-6 in skeletal muscle and is associated with impaired translation initiation. *J Trauma* 64: 477–486, 2008.
35. **Lecker SH, Jagoe RT, Gilbert A, Gomes M, Baracos V, Bailey J, Price SR, Mitch WE, Goldberg AL.** Multiple types of skeletal muscle atrophy involve a common program of changes in gene expression. *FASEB J* 18: 39–51, 2004.
36. **Lee P, Birzniece V, Umpleby AM, Poljak A, Ho KK.** Formoterol, a highly β2-selective agonist, induces gender-dimorphic whole body leucine metabolism in humans. *Metabolism* 64: 506–512, 2015.
37. **Levine JD, Dardick SJ, Roizen MF, Helms C, Basbaum AI.** Contribution of sensory afferents and sympathetic efferents to joint injury in experimental arthritis. *J Neurosci* 6: 3423–3429, 1986.
38. **Levine JD, Coderre TJ, Helms C, Basbaum AI.** Beta 2-adrenergic mechanisms in experimental arthritis. *Proc Natl Acad Sci USA* 85: 4553–4556, 1988.
39. **Llano-Diez M, Gustafson AM, Olsson C, Goransson H, Larsson L.** Muscle wasting and the temporal gene expression pattern in a novel rat intensive care unit model. *BMC Genomics* 12: 602, 2011.
40. **López-Menduiña M, Martín AI, Castillero E, Villanúa MA, López-Calderón A.** Systemic IGF-I administration attenuates the inhibitory effect of chronic arthritis on gastrocnemius mass and decreases atrogin-1 and IGFBP-3. *Am J Physiol Regul Integr Comp Physiol* 299: R541–R551, 2010.
41. **López-Menduiña M, Martín AI, Castillero E, Villanúa MA, López-Calderón A.** Short-term growth hormone or IGF-I administration improves the IGF-IGFBP system in arthritic rats. *Growth Horm IGF Res* 22: 22–29, 2012.
42. **Lubahn CL, Schaller JA, Bellinger DL, Sweeney S, Lorton D.** The importance of timing of adrenergic drug delivery in relation to the induction and onset of adjuvant-induced arthritis. *Brain Behav Immun* 18: 563–571, 2004.
43. **Martín AI, Castillero E, Granado M, López-Menduiña M, Villanúa MA, López-Calderón A.** Adipose tissue loss in adjuvant arthritis is associated with a decrease in lipogenesis, but not with an increase in lipolysis. *J Endocrinol* 197: 111–119, 2008.
44. **Martín AI, Gómez-SanMiguel AB, Gómez-Moreira C, Villanúa MÁ, López-Calderón A.** αMSH blunts endotoxin-induced MuRF1 and atrogin-1 upregulation in skeletal muscle by modulating NF-κB and Akt/FoxO1 pathway. *Mediators Inflamm* 2014: 179368, 2014.
45. **Matsumoto T, Akutsu S, Wakana N, Morito M, Shimada A, Yamane A.** The expressions of insulin-like growth factors, their receptors, and binding proteins are related to the mechanism regulating masseter muscle mass in the rat. *Arch Oral Biol* 51: 603–611, 2006.

46. **McMahon CD, Popovic L, Oldham JM, Jeanplong F, Smith HK, Kambadur R, Sharma M, Maxwell L, Bass JJ.** Myostatin-deficient mice lose more skeletal muscle mass than wild-type controls during hindlimb suspension. *Am J Physiol Endocrinol Metab* 285: E82–E87, 2003.
47. **McFarlane C, Plummer E, Thomas M, Hennebry A, Ashby M, Ling N, Smith H, Sharma M, Kambadur R.** Myostatin induces cachexia by activating the ubiquitin proteolytic system through an NF-kB-independent, FoxO1-dependent mechanism. *J Cell Physiol* 209: 501–514, 2006.
48. **Mourkioti F, Kratsios P, Luedde T, Song YH, Delafontaine P, Adami R, Parente V, Bottinelli R, Pasparakis M, Rosenthal N.** Targeted ablation of IKK2 improves skeletal muscle strength, maintains mass, and promotes regeneration. *J Clin Invest* 116: 2945–2954, 2006.
49. **Muthu K, Deng J, Gamelli R, Shankar R, Jones SB.** Adrenergic modulation of cytokine release in bone marrow progenitor-derived macrophage following polymicrobial sepsis. *J Neuroimmunol* 158: 50–57, 2005.
50. **Navegantes LC, Resano NM, Migliorini RH, Kettelhut IC.** Role of adrenoceptors and cAMP on the catecholamine-induced inhibition of proteolysis in rat skeletal muscle. *Am J Physiol Endocrinol Metab* 279: E663–E668, 2000.
51. **Pampusch MS, Kamanga-Sollo E, White ME, Hathaway MR, Dayton WR.** Effect of recombinant porcine IGF-binding protein-3 on proliferation of embryonic porcine myogenic cell cultures in the presence and absence of IGF-I. *J Endocrinol* 176: 227–235, 2003.
52. **Pearen MA, Ryall JG, Lynch GS, Muscat GE.** Expression profiling of skeletal muscle following acute and chronic beta2-adrenergic stimulation: implications for hypertrophy, metabolism and circadian rhythm. *BMC Genomics* 10: 448, 2009.
53. **Quintana HT, Bortolin JA, da Silva NT, Ribeiro FA, Liberti EA, Ribeiro DA, de Oliveira F.** Temporal study following burn injury in young rats is associated with skeletal muscle atrophy, inflammation and altered myogenic regulatory factors. *Inflamm Res* 64: 53–62, 2015.
54. **Ren H, Yin P, Duan C.** IGFBP-5 regulates muscle cell differentiation by binding to IGF-II and switching on the IGF-II auto-regulation loop. *J Cell Biol* 182: 979–991, 2008.
55. **Ryall JG, Sillence MN, Lynch GS.** Systemic administration of beta2-adrenoceptor agonists, formoterol and salmeterol, elicit skeletal muscle hypertrophy in rats at micromolar doses. *Br J Pharmacol* 147: 587–595, 2006.
56. **Ryall JG, Church JE, Lynch GS.** Novel role for β-adrenergic signalling in skeletal muscle growth, development and regeneration. *Clin Exp Pharmacol Physiol* 37: 397–401, 2010.
57. **Sanders KJ, Kneppers AE, van de Bool C, Langen RC, Schols AM.** Cachexia in chronic obstructive pulmonary disease: new insights and therapeutic perspective. *J Cachexia Sarcopenia Muscle* 7: 5–22, 2016.
58. **Sato S, Shirato K, Tachiyashiki K, Imaizumi K.** Muscle plasticity and β_2-adrenergic receptors: adaptive responses of β_2-adrenergic receptor expression to muscle hypertrophy and atrophy. *J Biomed Biotechnol* 2011: 729598, 2011.
59. **Schulze PC, Fang J, Kassik KA, Gannon J, Cupesi M, MacGillivray C, Lee RT, Rosenthal N.** Transgenic overexpression of locally acting insulin-like growth factor-1 inhibits ubiquitin-mediated muscle atrophy in chronic left-ventricular dysfunction. *Circ Res* 97: 418–426, 2005.
60. **Srikuea R, Pholpramool C, Kitiyanant Y, Yimlamai T.** Satellite cell activity in muscle regeneration after contusion in rats. *Clin Exp Pharmacol Physiol* 37: 1078–1086, 2010.
61. **Stephens NA, Gallagher IJ, Rooyackers O, Skipworth RJ, Tan BH, Marstrand T, Ross JA, Guttridge DC, Lundell L, Fearon KC, Timmons JA.** Using transcriptomics to identify and validate novel biomarkers of human skeletal muscle cancer cachexia. *Genome Med* 2: 1, 2010.
62. **Tidball JG.** Inflammatory processes in muscle injury and repair. *Am J Physiol Regul Integr Comp Physiol* 288: R345–R353, 2005.
63. **Uzkeser H, Cadirci E, Halici Z, Odabasoglu F, Polat B, Yuksel TN, Ozaltin S, Atalay F.** Anti-inflammatory and antinociceptive effects of salbutamol on acute and chronic models of inflammation in rats: involvement of an antioxidant mechanism. *Mediators Inflamm* 2012: 438912, 2012.
64. **Walker-Brown J, Roberts MR.** Differential contribution of beta-adrenergic receptors expressed on radiosensitive versus radioresistant cells to protection against inflammation and mortality in murine endotoxemia. *Shock* 32: 541–547, 2009.
65. **Yamaguchi A, Sakuma K, Fujikawa T, Morita I.** Expression of specific IGFBPs is associated with those of the proliferating and differentiating markers in regenerating rat plantaris muscle. *J Physiol Sci* 63: 71–77, 2013.

Hindawi Publishing Corporation
Mediators of Inflammation
Volume 2014, Article ID 179368, 14 pages
http://dx.doi.org/10.1155/2014/179368

Research Article

αMSH Blunts Endotoxin-Induced MuRF1 and Atrogin-1 Upregulation in Skeletal Muscle by Modulating NF-κB and Akt/FoxO1 Pathway

Ana Isabel Martín, Ana Belén Gómez-SanMiguel, Carolina Gómez-Moreira, María Ángeles Villanúa, and Asunción López-Calderón

Department of Physiology, Faculty of Medicine, Complutense University of Madrid, 28040 Madrid, Spain

Correspondence should be addressed to Asunción López-Calderón; alc@ucm.es

Received 13 June 2014; Accepted 20 August 2014; Published 9 September 2014

Academic Editor: Alex Kleinjan

Alpha melanocyte stimulating hormone (αMSH) has been shown to have anti-inflammatory and anticachectic actions. We hypothesized that αMSH administration could attenuate the effect of lipopolysaccharide (LPS) on the skeletal muscle through modifications in IGF-Akt-FoxO1 pathway, or/and in serum corticosterone. Adult male Wistar rats were injected with LPS and/or αMSH. αMSH administration reduced LPS-induced increase in liver TNFα and serum nitrites as well as NF-κB activation in skeletal muscle. In contrast, αMSH was not able to prevent the stimulatory effect of LPS on serum concentration of ACTH and corticosterone. LPS decreased serum levels of IGF-I and IGFBP3 and their expression in the liver ($P < 0.01$). However IGFBP3 expression in the gastrocnemius was increased by LPS. Treatment with αMSH prevented the effects of LPS on IGFBP3 but not on IGF-I. In the gastrocnemius αMSH blocked LPS-induced decrease in pAkt as well as the increase in pNF-κB(p65), FoxO1, atrogin-1, and MuRF1 levels. These results suggest that αMSH blunts skeletal muscle response to endotoxin by downregulating atrogenes and FoxO1 at least in part by controlling NF-κB activation and Akt signalling, but not through modifications in the secretion of corticosterone or IGF-I.

1. Introduction

Inflammation induces skeletal muscle wasting leading to inflammatory cachexia that causes an increase in morbidity and mortality [1]. Critically ill patients with sepsis have a reduction in muscle mass within the first week [2]. This decrease in muscle mass is secondary to an increase in muscle proteolysis, whereas muscle protein synthesis rate does not seem to be affected [3]. Similarly, experimental sepsis induced by bacterial lipopolysaccharide (LPS) administration increases muscle proteolysis, but it does not decrease protein synthesis [4]. Of the major proteolytic systems, ubiquitin-proteasome pathway is increased, whereas calpain and caspase activities are not changed in sepsis [3]. Between the ubiquitin-proteasome system, two E3 ubiquitin ligases, muscle RING-finger protein-1 (MuRF1) and muscle atrophy F-box (MAFbx/atrogin-1), play an important role in muscle atrophy; they are called atrogenes and serve as early markers of skeletal muscle atrophy, aiding in the diagnosis of muscle disease [5]. Cytokines such as TNFα act as potent inducer of the inflammatory response transcription factor NF-κB that increases proteasome-dependent protein breakdown in skeletal muscle [6].

The Forkhead box containing protein O-subclass (FoxOs) are transcription factors that regulate cell proliferation, differentiation, and apoptosis. In their active unphosphorylated state, these proteins reside in the nucleus and promote gene expression of atrophy-stimulating genes such as atrogin-1 and MuRF1 [7]. Skeletal muscle FoxO nuclear localization and transcriptional activities are suppressed by insulin-like growth factor1 (IGF-I)/phosphatidyl inositol 3-kinase (PI3 K)/protein kinase B (Akt) pathway. Phosphorylation of FoxOs by Akt induces translocation from the nucleus and inactivation by degradation in the cytosol. Atrogene

induction through FoxO1 and FoxO3a activation is a crucial step in the process leading to muscle atrophy during sepsis [8]. In this sense, sepsis increases FoxO1 mRNA levels as well as nuclear FoxO1 levels and DNA binding activity in gastrocnemius muscle, but not in the heart [9, 10].

Although muscle wasting during sepsis seems to be secondary to multiple factors, the increased release of proinflammatory cytokines and glucocorticoids and the decreased release of IGF-I are important mediators of inflammatory cachexia. Inflammatory stress induced by LPS increases a number of proinflammatory cytokines that are released into the blood stream to activate the innate immune response. LPS administration also has a profound effect on the neuroendocrine system, leading to an increase in glucocorticoid secretion along with a decrease in circulating IGF-I [11–13]. Glucocorticoids are potent mediators of muscle atrophy [14, 15], through atrogin-1 and MuRF1 upregulation [16]. IGF-I is an important regulator of muscle mass; in addition to stimulating muscle protein synthesis through activation of PI3 K and Akt, it also reduces the expression of atrogin-1 and MuRF1 by inhibiting FoxO transcription factors [17, 18]. Taking into account that the IGF-I/Akt pathway is a crucial regulator of muscle mass, the decrease in IGF-I levels together with the increase in serum glucocorticoids can be the mechanism by which sepsis induces muscle wasting.

Alpha melanocyte stimulating hormone (αMSH) is a peptide that belongs to the melanocortins family that has many physiological functions, including immune function. αMSH has a potent anti-inflammatory activity; it decreases inflammatory mediators such as proinflammatory cytokines and nitric oxide production [19], whereas it increases anti-inflammatory cytokines [20]. It has been shown that the anti-inflammatory action of αMSH in a number of cell types is through blockade of NF-κB activation [20–22].

αMSH has been shown to ameliorate the course of inflammatory illnesses in experimental animals such as endotoxin-induced hepatitis [23], inflammatory bowel disease [24] and adjuvant-induced arthritis [25]. In addition to its anti-inflammatory activity, we have reported that αMSH is also able to prevent arthritis-induced muscle wasting, decreasing MuRF1 and atrogin-1 levels in skeletal muscle [26]. The aim of the present study was to analyze whether peripheral αMSH administration is able to prevent endotoxin-induced increase in atrogin-1, MuRF1, and FoxO1 and to analyze the possible role played by the IGF-I system and by endogenous glucocorticoids.

2. Material and Methods

2.1. Animals. All procedures on animals were carried out according to the guidelines recommended by the EU for the care and use of laboratory animals and were approved by the Complutense University Animal Care Committee (approval ID: CEA-UCM 16/12). Experimental design was performed to minimize suffering and the number of animals used. Male Wistar rats weighing 250–275 g were used in all experiments; they were purchased from Charles River Laboratories (Barcelona, Spain). Rats were housed 2-3 per cage, under controlled conditions of temperature (22°C) and light (lights on from 07:30 to 19:30 h). Rats were quarantined for 1 week before any experimental use.

Rats were randomly assigned to the following treatment groups of 10 rats and fed ad libitum: (1) control, i.p. injected with 250 μL sterile saline, (2) control + αMSH, i.p. injected with 100 μg/kg αMSH trifluoroacetate salt (Bachem, Bubendorf, Switzerland), (3) LPS, i.p. injected with 250 μg/kg LPS (serotype 055:B5, Sigma Chemical Co.), and (4) LPS + αMSH, which was simultaneously i.p. injected with both compounds in 250 μL saline. As LPS decreases food intake, a pair-fed (PF) group was added; it was injected with saline and received the same amount of food eaten by the group of rats injected with LPS. Rats received the treatments at 17:00 h and at 08:00 h the following day. This LPS administration protocol was shown to decrease levels of serum IGF-I and its mRNA in the liver [27]. All animals were euthanized by decapitation at 12:00 h, 19 h after the first, and 4 h after the second LPS and/or αMSH injection.

Trunk blood was collected and allowed to clot, and the serum was stored at −20°C for IGF-I, IGF binding protein 3 (IGFBP3), adrenocorticotropin hormone (ACTH), corticosterone, and nitrite assays. Spleens were removed, dissected, and weighed; liver and gastrocnemius muscle were removed, frozen immediately in liquid nitrogen, and stored at −80°C for isolation of mRNA and proteins.

2.2. RNA Extraction and Real-Time PCR. RNA was extracted using UltraspecTM (Biotecx Laboratories Inc. Houston, Texas, USA). The final concentration of RNA was determined with a BioPhotometer (Eppendorf, Germany), and the integrity of the RNA was confirmed by agarose gel electrophoresis. First-strand cDNA synthesis was performed using 1 μg of total RNA and the Quantiscript Reverse Transcription kit (Qiagen Combh Hilden, Valencia, CA, and USA). Real-time PCR for quantification of mRNA was performed on a SmartCycler (Cepheid, Sunnyvale, CA, USA) using a SYBR-Green protocol on the fluorescence temperature cycler. Each real-time PCR reaction consisted of 2.5 ng cDNA, 1x Takara SYBR Green Premix Ex Taq (Takara BIO INC, Otsu, Shiga, Japan), and 300 nM forward and reverse primers in a reaction volume of 25 μL. Primers for real-time PCR (Table 1) were obtained from Roche (Madrid, Spain) by using the EXIQON Universal Probe Library. The thermal cycling profile consisted of a preincubation step at 95°C for 10 s followed by 40 cycles of 95°C denaturation steps for 15 s, 60°C annealing steps for 30 s, and 72°C extension steps for 30 s. Results were expressed as fold changes in expression of each gene compared with control animals treated with saline using cycle threshold 2($\Delta\Delta$CT) method with 18S as reference gene.

2.3. Immunoblot. Gastrocnemius was homogenized in RIPA buffer (10 μL/mg) with protease inhibitors cocktail, sodium deoxycholate 12.5 mM, phenylmethane sulfonyl fluoride 100 mM, sodium orthovanadate 12.5 mM, and with phosphatase inhibitors (Sigma-Aldrich, Madrid, Spain) for pAkt/Akt and pFoxO1/FoxO1. Because of the

Table 1: Primers for real-time PCR.

Gene	Forward primer (5′ to 3′)	Reverse primer (5′ to 3′)	Product bp
18S	GGTGCATGGCCGTTCTTA	TCGTTCGTTATCGGAATTAACC	60
TNFα	TGAACTTCGGGGTGATCG	GGGCTTGTCACTCGAGTTTT	122
FoxO1	TCAGGCTAGGAGTTAGTGAGCA	GGGGTGAAGGGCATCTTT	95
Atrogin-1	GAACAGCAAAACCAAAACTCAGTA	GCTCCTTAGTACTCCCTTTGTGAA	74
MuRF1	TGTCTGGAGGTCGTTTCCG	ATGCCGGTCCATGATCACTT	58
IGF-I	GCTATGGCTCCAGCATTCG	TCCGGAAGCAACACTCATCC	62
IGFBP-3	GGAAAGACGACGTGCATTG	GCGTATTTGAGCTCCACGTT	78

low endogenous levels of total FoxO1 in skeletal muscle, accurate quantification of FoxO1 following nuclear and cytosolic fractionation of whole muscle remains difficult. Therefore, we determined it in the total protein extract. The protein extracts were boiled for 5 min in a 1 : 1 volume of Laemmli loading buffer. Proteins (100 μg) were resolved by electrophoresis on 10–12% polyacrylamide gels under reducing conditions and transferred onto nitrocellulose or polyvinylidene fluoride membranes (Bio-Rad, Madrid, Spain) that were blocked by incubation in 5% nonfat dry milk and 0.1% Tween (Sigma-Aldrich), in Tris-buffered saline. Ponceau-S staining was performed to ensure equal transfer prior to blocking. Membranes were probed overnight at 4°C sequentially with antibodies against pAkt (473), and pFoxO1 (256) (Cell Signalling Technology Inc, Boston, USA), Akt, FoxO1, NF-κBp65 (C20), pNF-κBp65 (536) and MuRF1 (Santa Cruz Biotechnology, Santa Cruz, CA, USA) with stripping of membranes, using stripping buffer (Restore Western Blot Stripping Buffer, Thermo-scientific Rockford, II, USA) before each new antibody. Membranes were incubated for 90 min in the appropriate secondary antibody conjugated to horseadish peroxidase (anti mouse IgG, Amersham Biosciences, Little Chalfont, UK; anti rabbit IgG, GE Healthcare, Madrid, Spain; or anti goat IgG, Santa Cruz) and peroxidase activity was detected using enhanced chemiluminescent reagent (Thermo Scientific, Rockford, IL, USA). Band intensities were quantified by densitometry using Gene Tools Analysis software.

2.4. Ligand Blot. Serum IGFBP3 levels were measured by ligand blot. Two microlitres of serum were diluted in sample buffer and boiled for 2 min at 90°C and loaded on to 1% SDS-12.5% polyacrylamide gels, and proteins were separated by electrophoresis under nonreducing conditions. Proteins were transferred onto nitrocellulose sheets (HybondTM-C extra, Amersham, UK). The membranes were dried and blocked for 1 h with 5% nonfat dry milk, 0.1% Tween (Sigma-Aldrich), in Tris-buffered saline. Membranes were probed overnight at 4°C with ^{125}I-labelled IGF-I (1.5×10^6 cpm/mL). The nitrocellulose sheets were then washed, dried, and exposed at −80°C to X-ray film (Kodak X-Omat AR, Eastman Kodak, Rochester, NY, USA). The film signals were quantified by densitometry using a PC-Image VGA24 program for Windows. The density of the IGFBP3 band in each lane was expressed as the percentage of the mean density of sera from control rats.

2.5. IGF-I, ACTH, Corticosterone, and TNFα Determinations. Serum IGF-I was measured using the antiserum to human IGF-I (UB2-495), from Dr. Underwood and Dr. Van Wik, and is distributed by the NIDDK Hormone Distribution Program through the National Hormone and Pituitary Program. Levels of IGF-I were expressed in terms of rat IGF-I from Gropep Ltd. (Adelaide, Australia). The intra-assay coefficient of variation was 8%. All samples from the same experiment were run in the same assay.

Serum ACTH and corticosterone was analyzed by a commercial kit from MP Biomedicals, LLC (Orangeburg, NY, USA), following the manufacturer's protocols. Liver TNFα was determined by ELISA with a kit from Amersham Biosciences (Barcelona, Spain).

2.6. Nitrite Determination. Nitrite and nitrate concentrations in serum were measured by a modified method of Griess assay [28]. Serum was deproteinized to reduce turbidity by centrifugation through a 30 kDa molecular weight filter using a Centrifree Micropartition Device with a YM-30 ultrafiltration membrane (Amicon Division, Millipore Corporation, Bedford, TX, USA), at 15000 rpm for 1 h at 37°C for 300 μL samples. One hundred μL of filtrated serum was mixed with 100 μL of vanadium chloride and was quickly followed by the addition of the Griess reagents. The determination was performed after incubation at 37°C for 30 min. The absorbance was measured at 540 nm. Nitrite and nitrate concentrations were calculated using a $NaNO_2$ standard curve.

2.7. Statistical Analysis. Statistics were computed using the statistics program STATGRAPHICS plus for Windows. Data are presented as means ± standard error of the mean and were tested with analysis of variance (ANOVA); *post-hoc* comparisons were made using the LSD multiple range test. Statistical significance was set at $P < 0.05$.

3. Results

3.1. Anti-Inflammatory Activity of αMSH Administration in Rats Injected with LPS. As shown in Figure 1(a), LPS administration increased spleen weight ($P < 0.01$) in rats treated with saline, but not in rats treated with αMSH. αMSH treatment to control rats did not modify spleen weight. LPS induced a significant increase in serum nitrite/nitrate levels ($P < 0.01$ Figure 1(b)). αMSH decreased nitrite/nitrate levels ($P < 0.01$)

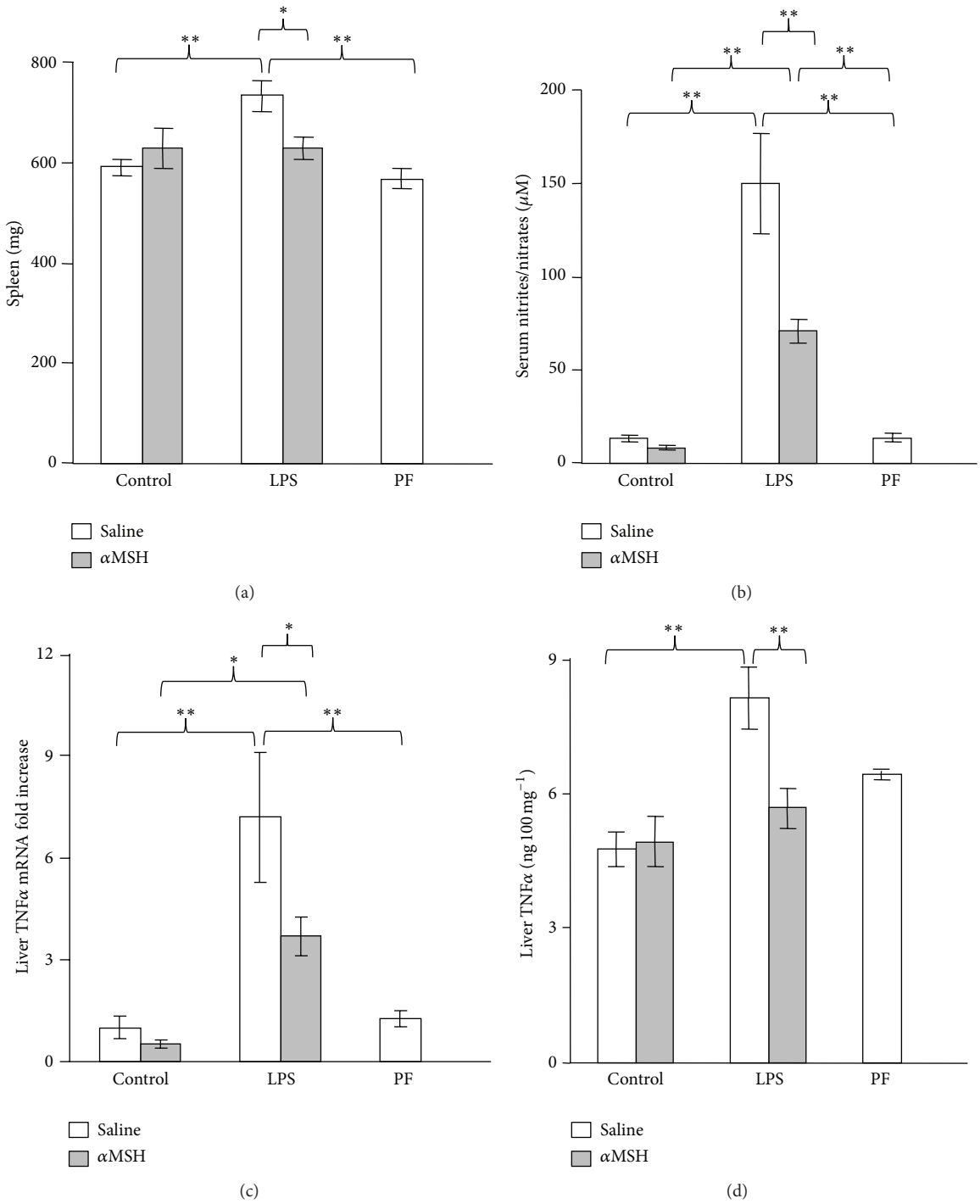

FIGURE 1: Effect of αMSH treatment (100 μg/kg) on spleen weight (a), serum concentrations of nitrites/nitrates (b), liver TNFα mRNA (c) and liver TNFα protein (d) in control rats or in rats treated with LPS (250 μg/kg). PF = pair-fed rats. αMSH treatment decreased the stimulatory effect of LPS administration on spleen weight, serum concentration of nitrites + nitrates, liver TNFα, and liver TNFα mRNA. Results are expressed as means ± SEM for 6–10 rats per group. $^{**}P < 0.01$ and $^{*}P < 0.05$, LSD multiple comparisons test.

in rats treated with LPS, but not in control rats. Pair-feeding the rats did not modify spleen weight or serum nitrite levels. LPS administration also increased liver TNFα as well as its mRNA ($P < 0.01$, Figures 1(c) and 1(d)). In rats treated with αMSH, LPS increased liver TNFα mRNA ($P < 0.05$) but to lower levels ($P < 0.05$) than those observed in rats injected with saline (Figure 1(c)). However, liver TNFα was not increased by LPS administration in rats treated with

Table 2: Effect of 0.1 mg/kg αMSH administration on body weight gain and food intake in control rats or in rats treated with 250 μg/kg LPS. PF = pair-fed rats. αMSH treatment attenuated the inhibitory effect of LPS administration on body weight gain and food intake. Results are expressed as means ± SEM for 10 rats per group. Values without the same letter are significantly different. LSD multiple comparisons test.

	Body weight gain g/19 h	Food intake g/19 h
Control-saline	4.3 ± 0.6^{a}	18.6 ± 0.35^{a}
Control-αMSH	6.1 ± 0.7^{a}	20.3 ± 0.45^{a}
LPS-saline	-21.7 ± 0.7^{b}	3.9 ± 0.67^{b}
LPS-αMSH	-14.3 ± 3.6^{c}	6.5 ± 1.4^{c}
PF	-14.7 ± 1.2^{c}	3.9

αMSH (Figure 1(d)). Liver TNFα mRNA and protein levels were similar in control rats treated with saline and in pair-fed rats.

3.2. αMSH Ameliorates LPS-Induced Decrease in Food Intake and Body Weight Gain. LPS administration decreased both food intake ($P < 0.01$) and body weight ($P < 0.01$, Table 2). This decrease in body weight gain is not only due to LPS-induced anorexia, since decrease in body weight gain was higher in the rats injected with LPS than in pair-fed rats ($P < 0.05$). In control rats αMSH treatment did not modify food intake or body weight gain. However, αMSH treatment attenuated the inhibitory effect of LPS on food intake ($P < 0.05$) and on body weight gain ($P < 0.01$).

3.3. Serum ACTH and Corticosterone after LPS and/or αMSH Administration. Serum levels of corticosterone and ACTH were not significantly modified by pair-feeding the rats or by administering 100 μg/kg αMSH to control rats (Figures 2(a) and 2(b)). LPS administration increased serum levels of ACTH and corticosterone ($P < 0.01$) in both groups of rats treated either with saline or with αMSH.

3.4. αMSH Administration Prevents the Effect of LPS on IGFBP3 but Not on IGF-I Levels. In rats treated with saline, LPS decreased circulating levels of IGF-I and IGFBP3 ($P < 0.01$, Figures 2(c) and 2(d)). αMSH administration prevented the inhibitory effect of LPS on circulating IGFBP3 levels, whereas it was unable to modify the effect of LPS on serum IGF-I levels. Neither serum concentrations of IGF-I nor IGFBP3 were affected by pair-feeding the rats or αMSH administration in control rats.

As observed in circulating IGF-I and IGFBP3, LPS administration decreased IGF-I and IGFBP3 expression in the liver ($P < 0.01$, Figures 3(a) and 3(c)). Treatment with αMSH did not modify the inhibitory effect of LPS on liver IGF-I mRNA. In contrast, αMSH attenuated LPS-induced decrease in liver IGFBP3, where the rats treated with LPS and αMSH had IGFBP3 mRNA levels between those of control rats and of the rats treated with LPS alone. Pair-feeding the rats or αMSH administration to control rats did not modify liver expression of IGF-I or IGFBP3.

Figures 3(b) and 3(d) show IGF-I and IGFBP3 expression in the gastrocnemius muscle. LPS had a different effect on IGF-I and IGFBP3 mRNA in the gastrocnemius than in the liver. Gastrocnemius IGF-I mRNA was not significantly affected by LPS, αMSH, or by pair-feeding the rats (Figure 3(b)). In contrast, LPS administration increased IGFBP3 mRNA in the gastrocnemius muscle ($P < 0.05$). αMSH treatment prevented the stimulatory effect of LPS on muscle IGFBP3, whereas it did not modify IGFBP3 mRNA in control rats.

3.5. αMSH Administration Prevents the Effect of LPS on NF-κB(p65), pAkt, FoxO1, MuRF1, and Atrogin-1 in the Gastrocnemius Muscle. The effects of LPS and αMSH administration on NF-κB(p65) and Akt in the gastrocnemius muscle are shown in Figures 4(a), 4(b), 4(c), and 4(d). LPS increased phosphoNF-κB(p65) in the rats treated with saline ($P < 0.01$, Figure 4(a)) but not in those treated with αMSH. There were no modifications in gastrocnemius NF-κB(p65) levels in none of the experimental groups (Figure 4(b)). LPS had a negative effect on Akt signalling, since it decreased phosphoAkt levels ($P < 0.01$, Figure 4(c)). αMSH treatment blocked the inhibitory effect of LPS on Akt phosphorylation. Neither αMSH nor pair-feeding the rats modified pAkt levels in the gastrocnemius muscle. All experimental groups had similar total Akt levels (Figure 4(d)).

LPS-induced decrease in muscle pAkt levels was associated with an increase in the muscle content of the active transcription factor FoxO1, as well as in its mRNA levels ($P < 0.01$, Figures 5(b) and 5(c)). αMSH treatment prevented the stimulatory effect of LPS on FoxO1 and FoxO1mRNA levels, since the rats treated with LPS and αMSH had lower FoxO1 content than the rats injected with LPS and saline and content similar to the levels of pair-fed rats. Pair-feeding the rats increased mean FoxO1 and its mRNA levels in the muscle, but this increase was not significant. LPS administration decreased pFoxO1 levels ($P < 0.05$, Figure 5(a)). LPS also decreased pFoxO1 levels in the rats treated with αMSH, but the decrease was not significant in comparison to the levels of control rats treated with αMSH.

Atrogenes expression coincides with the activity of the NF-κB and the Akt/FoxO1 pathway in the five groups of rats. Atrogin-1 mRNA was increased by LPS administration ($P < 0.01$, Figure 6(a)). Rats treated with both LPS and αMSH had lower gastrocnemius atrogin-1 mRNA than rats that received LPS alone ($P < 0.01$), and similar to pair-fed rats. LPS administration also increased muscle MuRF1 and its mRNA expression in the gastrocnemius muscle

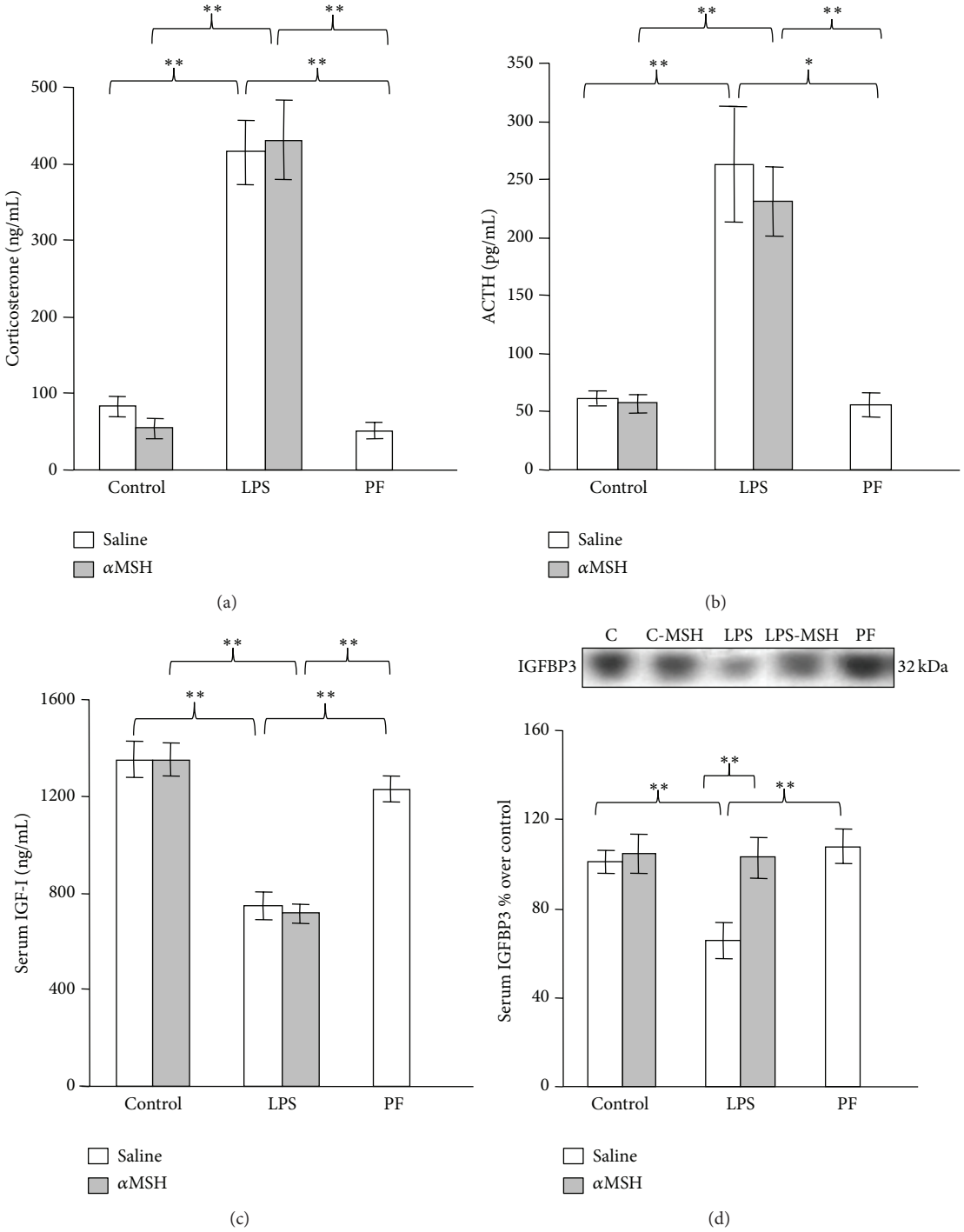

Figure 2: Effect of αMSH treatment (100 μg/kg) on serum concentration of corticosterone (a), ACTH (b), IGF-I (c), and IGFBP3 (d) in control rats or in rats treated with LPS (250 μg/kg). PF = pair-fed rats. LPS administration increased the serum concentrations of corticosterone and ACTH ($P < 0.01$), whereas αMSH had no significant effect either in control or LPS treated rats. Serum concentrations of IGF1 were decreased by LPS administration in both groups of rats treated with either αMSH or saline ($P < 0.01$). LPS treatment decreased serum concentration of IGFBP3 ($P < 0.01$). αMSH treatment prevented the effect of LPS on serum IGFBP3. Pair-feeding the rats did not modify serum corticosterone, ACTH, IGF-I, or IGFBP3 levels. Data are expressed as mean ± SEM for $n = 8$–10 rats per group. $^{**}P < 0.01$ and $^{*}P < 0.05$, LSD multiple comparisons test.

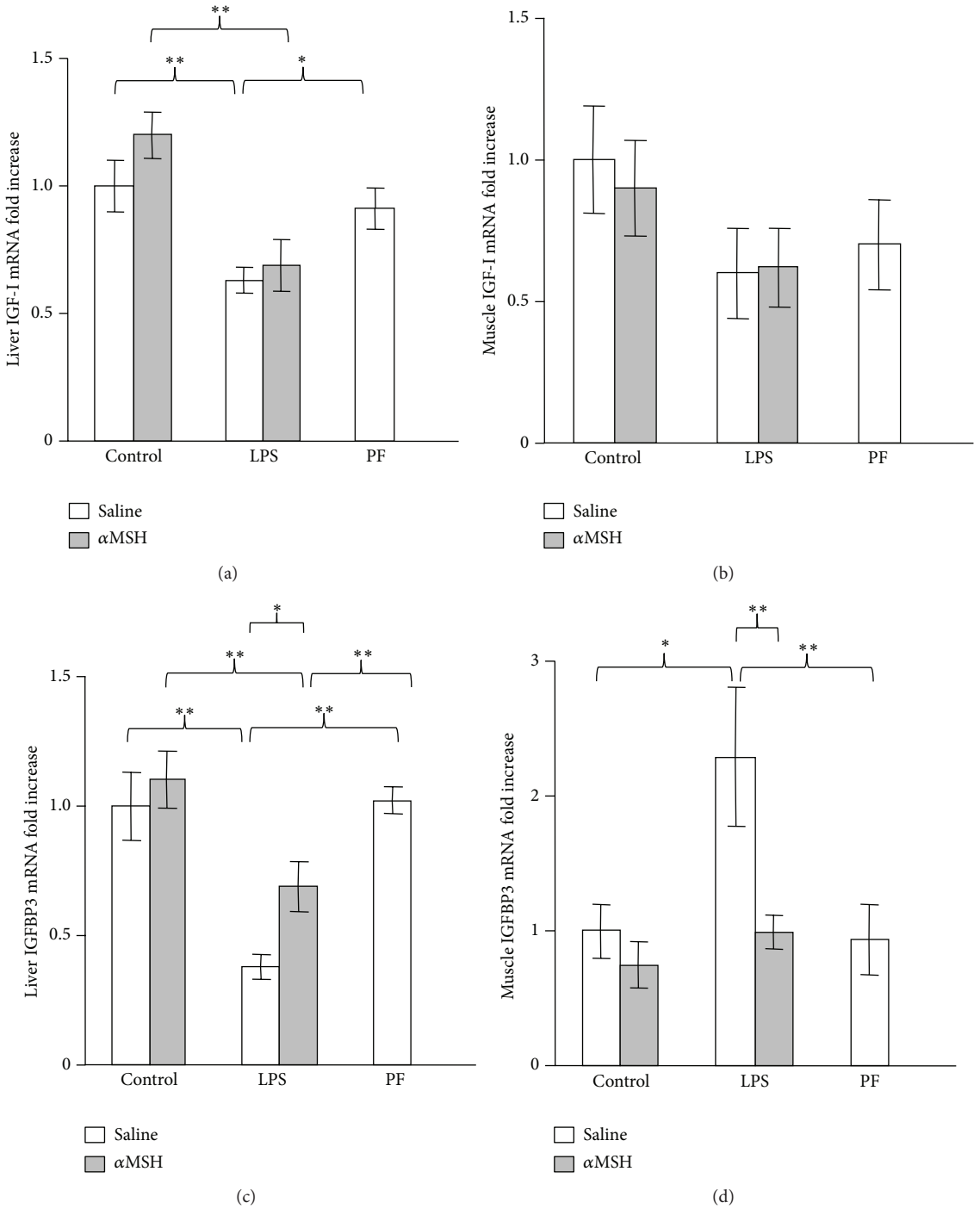

Figure 3: Effect of αMSH treatment (100 μg/kg) on IGF-I mRNA in liver (a) and gastrocnemius muscle (b) and on IGFBP3 mRNA in liver (c) and gastrocnemius muscle (d) in control rats or in rats treated with LPS (250 μg/kg). PF = pair-fed rats. Liver IGF-I mRNA was decreased by LPS administration in both groups of rats treated with either αMSH or saline ($P < 0.01$). LPS treatment decreased liver IGFBP3 mRNA ($P < 0.01$), but it increased muscle IGFBP3 mRNA ($P < 0.01$). αMSH treatment prevented the effect of LPS on muscle IGFBP3 mRNA, whereas it attenuated the inhibitory effect of LPS on liver IGFBP3 mRNA. Pair-feeding the rats did not modify IGF-I or IGFBP3 levels. Data are expressed as mean ± SEM for $n = 8$–10 rats per group. $^{**}P < 0.01$ and $^{*}P < 0.05$, LSD multiple comparisons test.

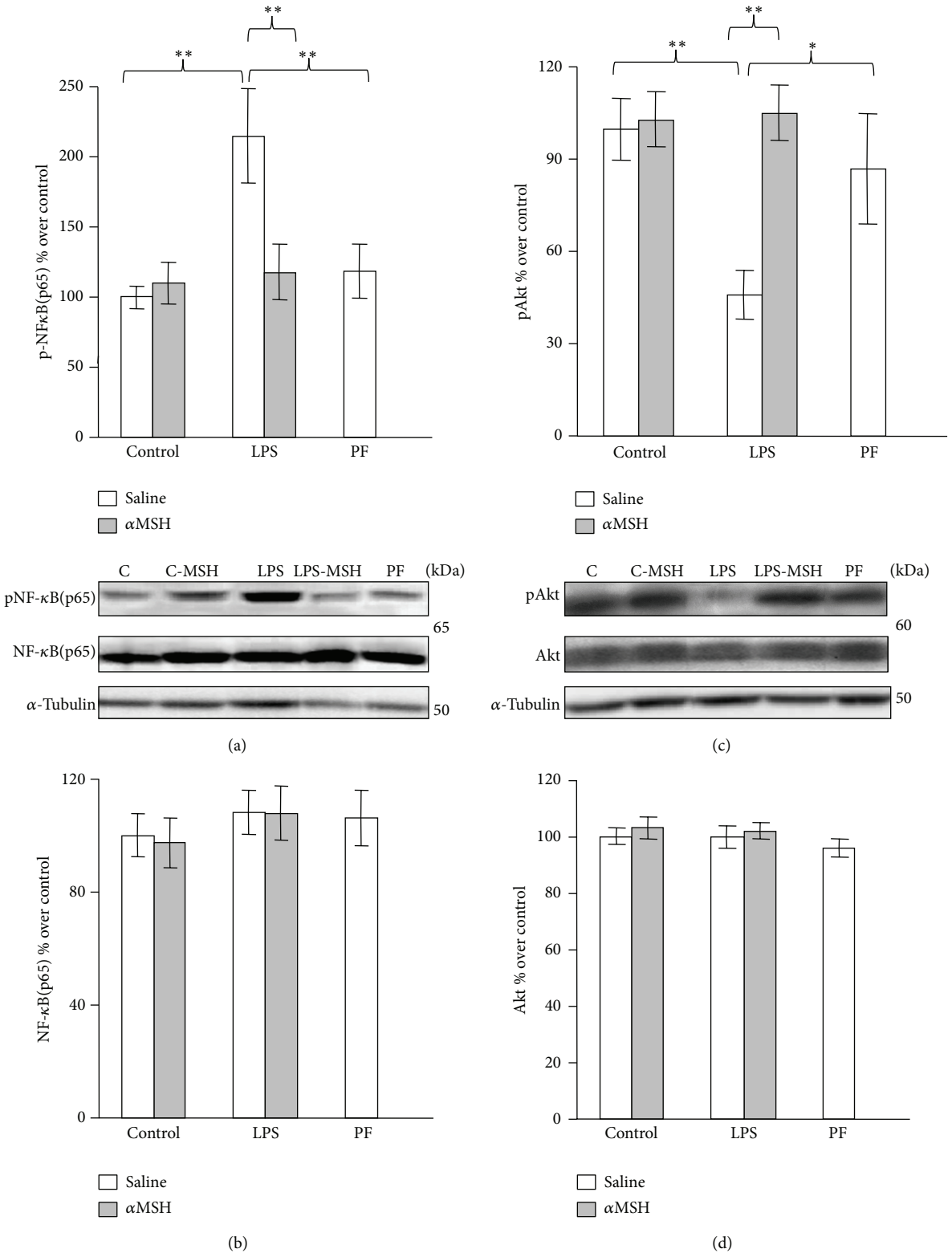

Figure 4: PhosphoNF-κB(p65) (a), NF-κB(p65) (b), phospho-Akt (c), and total-Akt (d) in gastrocnemius muscle of control, LPS and pair-fed (PF) rats treated with αMSH (100 μg/kg) or saline. LPS increased phosphoNF-κB(p65) ($P < 0.01$) and decreased pAkt ($P < 0.01$) in the rats treated with saline but not in rats treated with αMSH. Data represent mean ± SEM ($n = 7$–10 rats). $^{**}P < 0.01$ and $^{*}P < 0.05$, LSD multiple comparisons test.

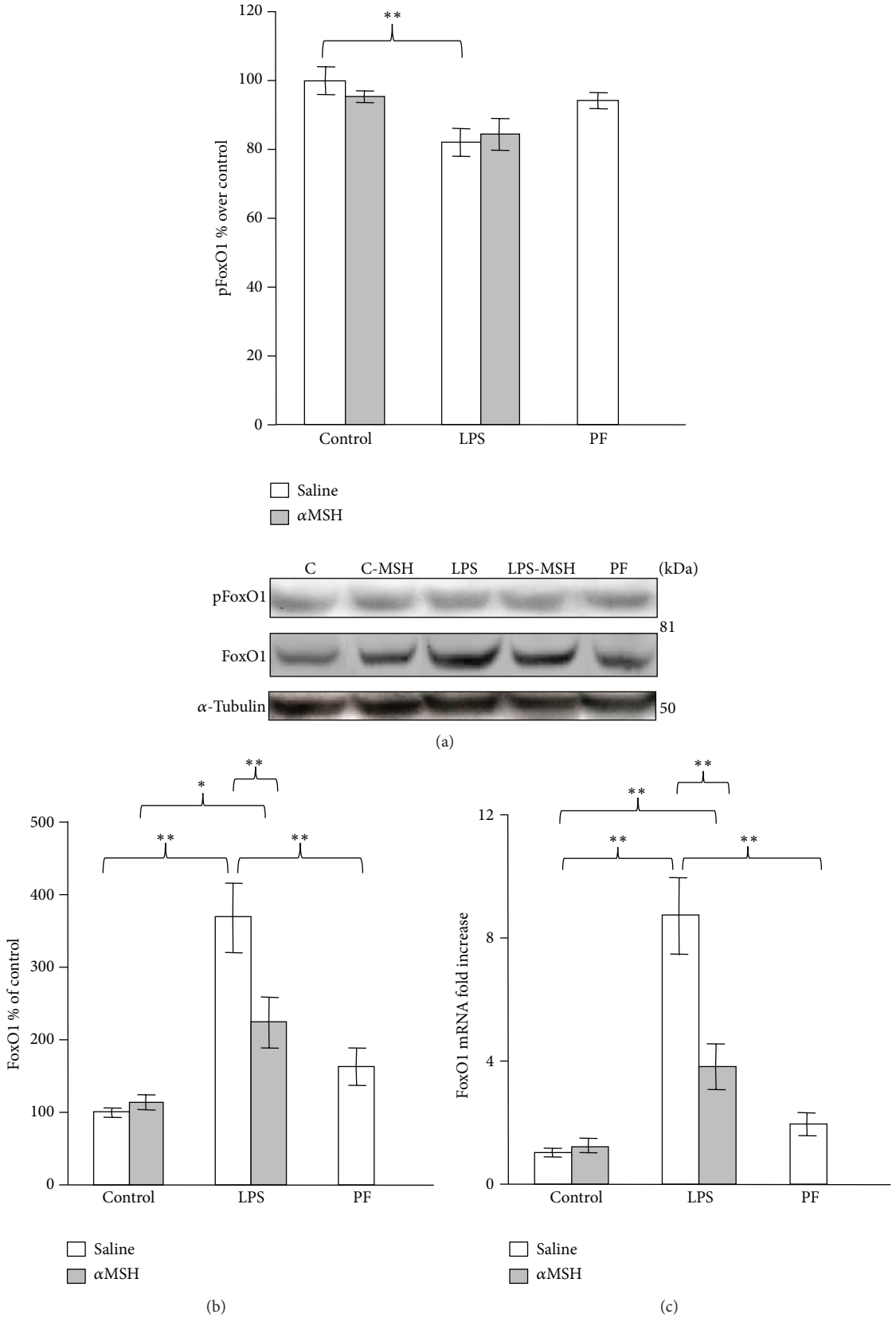

Figure 5: PhosphoFoxO1 (a), total FoxO1 (b), and FoxO1 mRNA levels (c) in gastrocnemius muscle of control, LPS and pair-fed (PF) rats treated with αMSH (100 μg/kg) or saline. LPS decreased pFoxO1 ($P < 0.05$), whereas it increased FoxO1 and FoxO1 mRNA ($P < 0.01$) in rats treated with saline. αMSH administration prevented LPS-induced increase in FoxO1 and its mRNA. Data represent mean ± SEM ($n = 8$–10 rats). $^{**}P < 0.01$ and $^{*}P < 0.05$, LSD multiple comparison test.

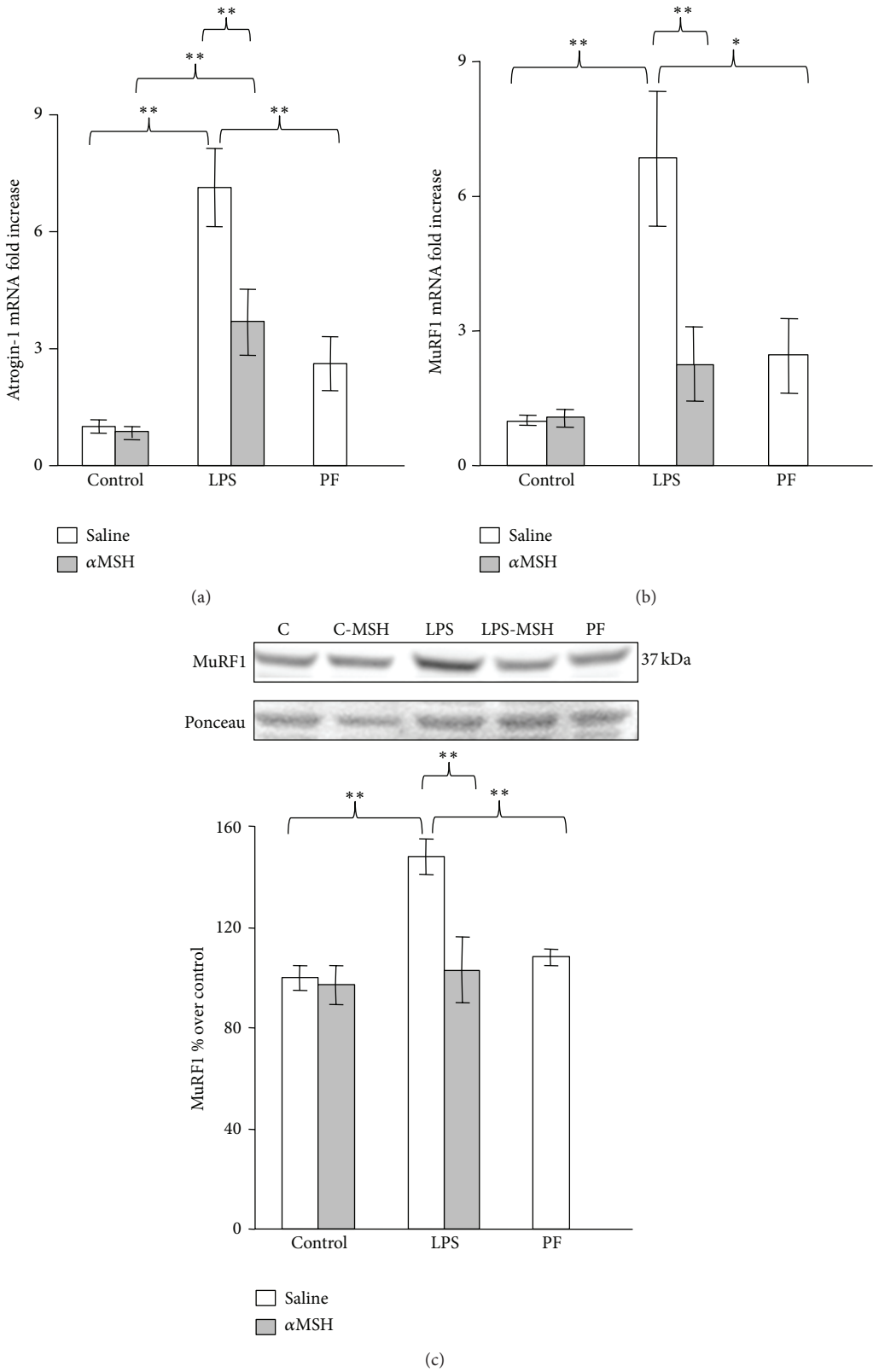

Figure 6: Atrogin-1 mRNA (a), MuRF1 mRNA (b), and MuRF1 (c) in gastrocnemius muscle of control, LPS and pair-fed (PF) rats treated with αMSH (100 μg/kg) or saline. LPS increased atrogin-1, MuRF1, and MuRF1 mRNA levels ($P < 0.01$), and αMSH administration prevented those increases. Data represent mean ± SEM (n = 7–10 rats). $^{**}P < 0.01$ and $^{*}P < 0.05$, LSD multiple comparison test.

($P < 0.01$, Figures 4(b) and 4(c)). αMSH treatment blocked LPS-induced increase in MuRF1 and in its mRNA in the gastrocnemius muscle.

4. Discussion

Our data show that αMSH treatment was not able to modify the stimulatory effect of LPS on circulating ACTH and corticosterone or the inhibitory effect of LPS on circulating and liver IGF-I. However, αMSH treatment induced anti-inflammatory changes in liver and muscle and prevented negative effects of LPS on skeletal muscle, such as inhibition of Akt phosphorylation and increase in IGFBP3 expression and in FoxO1, atrogin-1, and MuRF1 levels in the gastrocnemius muscle.

As previously reported [19, 20] αMSH prevented the increase in liver TNFα after LPS injection. The anti-inflammatory effect of αMSH was also evidenced by the ability of this hormone to decrease LPS-induced increase in spleen weight and serum concentration of nitrites/nitrates and to prevent NF-κB phosphorylation in muscle after LPS administration.

In accordance with data we have previously reported in arthritic rats [26], peripheral αMSH treatment attenuated LPS-induced anorexia and the decrease in body weight gain. On the contrary, intracerebroventricular administration of αMSH potentiates LPS-induced reduction in food intake during 6 h [29]. Those data and the fact that systemic αMSH treatment did not decrease food intake in control rats (present data and [26]) suggest that the ability of systemic αMSH to cross the blood brain barrier is low, as it has previously been reported [30], and the effects we observed are exerted at peripheral level.

In spite of its anti-inflammatory effect, peripheral administration of αMSH was not able to decrease the stimulatory effect of LPS administration on the adrenal axis. However, when centrally administered, αMSH has been reported to decrease the stimulatory effect of LPS on serum corticosterone levels, at a very low dosage [31, 32]. In addition, αMSH is not able to prevent the stimulatory effect of CRH on pituitary ACTH, suggesting a hypothalamic rather than pituitary site of action of αMSH on the hypothalamic-pituitary-adrenal axis [32].

In contrast to our data, an inhibitory effect of peripheral αMSH administration on LPS-induced increase in ACTH has been reported in mice [33]. Discrepancies can be due to the fact that these authors used a higher dosage of αMSH. We tested a higher dosage of αMSH (200 μg/kg), and again peripheral αMSH administration was not able to prevent the effect of LPS on circulating IGF-I, ACTH, and corticosterone (author's unpublished observation). Another possibility is that αMSH decreases the response to LPS within the first few minutes after administration. In this sense, Huang et al. [34] reported that in rats, 100 μg/kg αMSH partially blocks the stimulatory effect of LPS, since it prevents the increase in plasma corticosterone 60 min but not 30 or 120 min after LPS administration. Nevertheless, we cannot exclude that at a higher dosage peripheral administration of αMSH may be able to prevent the stimulatory effect of LPS on corticosterone levels.

As previously reported [11, 12, 27], LPS administration decreased circulating IGF-I and IGBP3 and their gene expression in the liver. Similar data have also recently been reported in septic patients [35]. LPS decreases serum IGF-I, acting both in the liver and at a central level [36, 37]. The effects of αMSH treatment on serum levels of IGF-I and IGFBP3 in rats injected with LPS were different, since αMSH was not able to modify the inhibitory effect of LPS on IGF-I, whereas it prevented the LPS-induced decrease in serum IGFBP3 and its expression in the liver. The different responses of both proteins to αMSH treatment may be due to the fact that they are regulated differently [38–40]. In addition, they are produced by different liver cells, whereas IGF-I is mainly produced in hepatocytes, IGFBP3 expression is only found in nonparenchymal cells [38, 41]. The effect of αMSH on liver IGFBP3 can be exerted directly, since liver cells express all αMSH receptors (MCRs) and their expression is upregulated during the acute phase response [42]. In addition, αMSH inhibits endotoxin-induced upregulation of the acute-phase cytokines (interleukin1 (IL1), IL6, and TNFα) in isolated Kupffer cells [42]. Therefore, αMSH can prevent LPS-induced decrease in IGFBP3 synthesis by nonparenchymal cells, although it is not able to prevent the decrease in IGF-I expression.

In contrast to the effect of LPS on liver IGFBP3 expression, local expression of IGBP3 was increased in skeletal muscle by LPS administration. These data indicate that regulation of IGFBP3 varies depending on the tissue. In chronic inflammation induced by arthritis we have found that IGFBP3 expression is also increased in the gastrocnemius muscle but not in the liver [43]. An increase in muscle IGFBP3 has also been reported 2 days after muscle injury, during the early phase of regeneration when muscle is invaded by inflammatory cells, especially by macrophages [44]. In peripheral tissues local IGFBP3 is a well-documented inhibitor of cell growth and/or promoter of apoptosis by a non-IGF-dependent mechanism (for review see [45]). IGFBP3 is produced by myogenic cell cultures and it suppresses proliferation in an IGF-dependent and -independent manner [46]. Accordingly, the increased expression of IGFBP3 in skeletal muscle can contribute to inflammation-induced muscle wasting. As in the case of circulating levels of IGFBP3, αMSH treatment was able to prevent LPS-induced increase in muscle IGFBP3 expression.

In the gastrocnemius muscle LPS decreased pAkt, whereas it increased pNF-κB(p65) and FoxO1 active protein and its mRNA. These data are in accordance with those previously reported by other authors [9, 47, 48]. As expected, the decrease in pAkt and the increase in pNF-κB and FoxO1 protein were associated with an increased expression in both atrogenes atrogin-1 and MuRF1. Treatment with αMSH prevented the effects of LPS on the muscle: the decrease in Akt phosphorylation and the increase in NF-κB(p65) phosphorylation and FoxO1, MuRF1, and atrogin-1, reaching levels similar to those found in pair-fed rats. All these data indicate that αMSH administration blocks LPS-induced alterations in Akt/FoxO1 signalling and downstream gene

targets of FoxO1, atrogin-1, and MuRF1 in gastrocnemius muscle. Similarly, in arthritic rats, αMSH administration prevents upregulation of both atrogin-1 and MuRF1 [26].

Taking into account that αMSH treatment prevented the inhibitory effect of LPS on pAkt in the gastrocnemius, we expected that αMSH would be able to modify the inhibitory effect of LPS on IGF-I. However, αMSH administration was unable to prevent LPS-induced decrease in serum and liver IGF-I expression. The possibility exists that normalization of Akt activity in gastrocnemius of the rats treated with LPS and αMSH is related to normalization of NF-κB activity and/or to muscle IGFBP3 levels. There are several data indicating that IGFBP3 can play an inhibitory role in the PI3K/Akt signalling pathway in different types of cancer cells, through an IGF-independent effect [49, 50]. IGFBP3 also decreases Akt phosphorylation in noncancer cell cultures such as adipocytes [51].

Although αMSH did not modify the effect of LPS on the main hormones related to muscle wasting (IGF-I and corticosterone), it had anti-inflammatory actions, and in the skeletal muscle it prevented the decrease in pAkt levels, the activation of NF-κB and FoxO1, and the upregulation of atrogin-1 and MuRF1. Because we analyzed the acute effects of LPS treatment, it was not possible to measure muscle atrophy. However, in arthritic rats chronic αMSH treatment decreases both muscle wasting and inflammation [26], in spite of not preventing the increase in serum concentrations of corticosterone and ACTH or the decrease in serum concentration of IGF-I (authors' unpublished observation). Another treatment that shows anti-inflammatory and anticachectic effects in arthritic rats is the PPAR-α agonist fenofibrate. Fenofibrate administration decreases skeletal muscle atrophy [52], but it is also unable to prevent the effects of arthritis on serum IGF-I and corticosterone levels [43].

It has been postulated that stimulation of muscle proteolysis requires two events, increased circulating glucocorticoid and/or impaired insulin signalling [53]. PI3K/Akt pathway, which had previously been shown to be sufficient to induce hypertrophy via activation of protein synthesis pathways, can also dominantly suppress the activation of atrophy pathways, determined by the induction of atrophy markers MuRF1 and atrogin-1 [54]. IGF-I, activated PI3K, or activated Akt is sufficient to inhibit the upregulation of MuRF1 and atrogin-1 induced by the glucocorticoid dexamethasone [18]. In our data, the preventive effect of αMSH on LPS-induced increase in atrogin-1 and MuRF1 levels can be explained by the normalization of NF-κB and Akt/FoxO1 pathways. This can be secondary to a reduced release of cytokines, as reflected by the normalization of pNF-κB levels, and/or to the normalization of IGFBP3 levels in the gastrocnemius.

5. Conclusion

Our data suggest that in rats injected with LPS, αMSH exerts anti-inflammatory and antiproteolytic activities in skeletal muscle downregulating FoxO1 and atrogene activation at least in part by controlling NF-κB and Akt activation. These results support αMSH as a novel potential therapeutic agent for clinical use in patients with sepsis that show a reduction in muscle mass. The pathways through which α-MSH blunts muscle wasting should be clarified by future studies analyzing the possible melanocortin receptors involved.

Conflict of Interests

The authors declare that there is no conflict of interests that could be perceived as prejudicing the impartiality of the research reported.

Authors' Contribution

Ana Isabel Martín and Ana Belén Gómez-SanMiguel contributed similarly to the study.

Acknowledgments

The authors are indebted to Christina Bickart for the English correction of the paper. This work was supported by Grants from FIS, no. PS09/00753, BFU2012-38468, and from UCM for Ana Belén Gómez-SanMiguel.

References

[1] L. A. Callahan and G. S. Supinski, "Sepsis-induced myopathy," *Critical Care Medicine*, vol. 37, no. 5, pp. S354–S367, 2009.

[2] J. B. Poulsen, K. Møller, C. V. Jensen, S. Weisdorf, H. Kehlet, and A. Perner, "Effect of transcutaneous electrical muscle stimulation on muscle volume in patients with septic shock," *Critical Care Medicine*, vol. 39, no. 3, pp. 456–461, 2011.

[3] M. Klaude, M. Mori, I. Tjäder, T. Gustafsson, J. Wernerman, and O. Rooyackers, "Protein metabolism and gene expression in skeletal muscle of critically ill patients with sepsis," *Clinical Science*, vol. 122, no. 3, pp. 133–142, 2012.

[4] M. Kovarik, T. Muthny, L. Sispera, and M. Holecek, "The dose-dependent effects of endotoxin on protein metabolism in two types of rat skeletal muscle," *Journal of Physiology and Biochemistry*, vol. 68, no. 3, pp. 385–395, 2012.

[5] S. H. Lecker, R. T. Jagoe, A. Gilbert et al., "Multiple types of skeletal muscle atrophy involve a common program of changes in gene expression," *FASEB Journal*, vol. 18, no. 1, pp. 39–51, 2004.

[6] B. Pijet, M. Pijet, A. Litwiniuk, M. Gajewska, B. Pajak, and A. Orzechowski, "TNF-α and IFN-s-dependent muscle decay is linked to NF-κB- and STAT-1α-stimulated Atrogin1 and MuRF1 genes in C2C12 myotubes," *Mediators of Inflammation*, vol. 2013, Article ID 171437, 18 pages, 2013.

[7] M. Sandri, C. Sandri, A. Gilbert et al., "Foxo transcription factors induce the atrophy-related ubiquitin ligase atrogin-1 and cause skeletal muscle atrophy," *Cell*, vol. 117, no. 3, pp. 399–412, 2004.

[8] S. A. Reed, P. B. Sandesara, S. M. Senf, and A. R. Judge, "Inhibition of FoxO transcriptional activity prevents muscle fiber atrophy during cachexia and induces hypertrophy," *FASEB Journal*, vol. 26, no. 3, pp. 987–1000, 2012.

[9] G. J. Nystrom and C. H. Lang, "Sepsis and AMPK activation by AICAR differentially regulate FoxO-1, -3 and -4 mRNA in striated muscle," *International Journal of Clinical and Experimental Medicine*, vol. 1, pp. 50–63, 2008.

[10] I. J. Smith, N. Alamdari, P. O'Neal, P. Gonnella, Z. Aversa, and P.-O. Hasselgren, "Sepsis increases the expression and activity of the transcription factor Forkhead Box O 1 (FOXO1) in skeletal muscle by a glucocorticoid-dependent mechanism," *International Journal of Biochemistry and Cell Biology*, vol. 42, no. 5, pp. 701–711, 2010.

[11] J. Fan, D. Char, A. J. Kolasa et al., "Alterations in hepatic production and peripheral clearance of IGF-I after endotoxin," *The American Journal of Physiology*, vol. 269, no. 1, pp. E33–E42, 1995.

[12] L. Soto, A. I. Martín, S. Millán, E. Vara, and A. López-Calderón, "Effects of endotoxin lipopolysaccharide administration on the somatotropic axis," *Journal of Endocrinology*, vol. 159, no. 2, pp. 239–246, 1998.

[13] T. Priego, I. Ibáñez de Cáceres, A. I. Martín, M. A. Villanúa, A. López-Calderón, and I. Ibáñez de, "Glucocorticoids are not necessary for the inhibitory effect of endotoxic shock on serum IGF-I and hepatic IGF-I mRNA," *Journal of Endocrinology*, vol. 172, no. 3, pp. 449–456, 2002.

[14] P.-O. Hasselgren, N. Alamdari, Z. Aversa, P. Gonnella, I. J. Smith, and S. Tizio, "Corticosteroids and muscle wasting: role of transcription factors, nuclear cofactors, and hyperacetylation," *Current Opinion in Clinical Nutrition and Metabolic Care*, vol. 13, no. 4, pp. 423–428, 2010.

[15] O. Schakman, S. Kalista, C. Barbé, A. Loumaye, and J. P. Thissen, "Glucocorticoid-induced skeletal muscle atrophy," *International Journal of Biochemistry and Cell Biology*, vol. 45, no. 10, pp. 2163–2172, 2013.

[16] E. Castillero, N. Alamdari, S. H. Lecker, and P.-O. Hasselgren, "Suppression of atrogin-1 and MuRF1 prevents dexamethasone-induced atrophy of cultured myotubes," *Metabolism: Clinical and Experimental*, vol. 62, no. 10, pp. 1495–1502, 2013.

[17] J. M. Sacheck, A. Ohtsuka, S. C. McLary, and A. L. Goldberg, "IGF-I stimulates muscle growth by suppressing protein breakdown and expression of atrophy-related ubiquitin ligases, atrogin-1 and MuRF1," *The American Journal of Physiology—Endocrinology and Metabolism*, vol. 287, no. 4, pp. E591–E601, 2004.

[18] T. N. Stitt, D. Drujan, B. A. Clarke et al., "The IGF-1/PI3K/Akt pathway prevents expression of muscle atrophy-induced ubiquitin ligases by inhibiting FOXO transcription factors," *Molecular Cell*, vol. 14, no. 3, pp. 395–403, 2004.

[19] C. Gonindard, C. Goigoux, E. Hollande, and L. D. D'Hinterland, "The administration of an α-MSH analogue reduces the serum release of IL-1α and TNFα induced by the injection of a sublethal dose of lipopolysaccharides in the BALB/c mouse," *Pigment Cell Research*, vol. 9, no. 3, pp. 148–153, 1996.

[20] T. Brzoska, T. A. Luger, C. Maaser, C. Abels, and M. Böhm, "Alpha-melanocyte-stimulating hormone and related tripeptides: biochemistry, antiinflammatory and protective effects in vitro and in vivo, and future perspectives for the treatment of immune-mediated inflammatory diseases," *Endocrine Reviews*, vol. 29, no. 5, pp. 581–602, 2008.

[21] S. K. Manna and B. B. Aggarwal, "α-melanocyte-stimulating hormone inhibits the nuclear transcription factor NF-κB activation induced by various inflammatory agents," *The Journal of Immunology*, vol. 161, no. 6, pp. 2873–2880, 1998.

[22] S.-N. Lee, J.-H. Ryu, J.-H. Joo et al., "α-Melanocyte-stimulating hormone inhibits tumor necrosis factor α-stimulated MUC5AC expression in human nasal epithelial cells," *The American Journal of Respiratory Cell and Molecular Biology*, vol. 44, no. 5, pp. 716–724, 2011.

[23] H. Chiao, S. Foster, R. Thomas, J. Lipton, and R. A. Star, "α-melanocyte-stimulating hormone reduces endotoxin-induced liver inflammation," *Journal of Clinical Investigation*, vol. 97, no. 9, pp. 2038–2044, 1996.

[24] N. Rajora, G. Boccoli, A. Catania, and J. M. Lipton, "α-MSH modulates experimental inflammatory bowel disease," *Peptides*, vol. 18, no. 3, pp. 381–385, 1997.

[25] G. Ceriani, J. Diaz, S. Murphree, A. Catania, and J. M. Lipton, "The neuropeptide alpha-melanocyte-stimulating hormone inhibits experimental arthritis in rats," *Neuroimmunomodulation*, vol. 1, no. 1, pp. 28–32, 1994.

[26] A. B. Gómez-SanMiguel, A. I. Martín, M. P. Nieto-Bona et al., "Systemic α-melanocyte-stimulating hormone administration decreases arthritis-induced anorexia and muscle wasting," *The American Journal of Physiology: Regulatory Integrative and Comparative Physiology*, vol. 304, no. 10, pp. R877–R886, 2013.

[27] M. Granado, A. I. Martín, T. Priego, M. A. Villanúa, and A. López-Calderón, "Inactivation of Kupffer cells by gadolinium administration prevents lipopolysaccharide-induced decrease in liver insulin-like growth factor-I and IGF-binding protein-3 gene expression," *Journal of Endocrinology*, vol. 188, no. 3, pp. 503–511, 2006.

[28] K. M. Miranda, M. G. Espey, and D. A. Wink, "A rapid, simple spectrophotometric method for simultaneous detection of nitrate and nitrite," *Nitric Oxide—Biology and Chemistry*, vol. 5, no. 1, pp. 62–71, 2001.

[29] Q.-H. Huang, V. J. Hruby, and J. B. Tatro, "Role of central melanocortins in endotoxin-induced anorexia," *The American Journal of Physiology—Regulatory Integrative and Comparative Physiology*, vol. 276, no. 2, pp. R864–R871, 1999.

[30] J. F. Wilson, "Low permeability of the blood-brain barrier to nanomolar concentrations of immunoreactive alpha-melanotropin," *Psychopharmacology*, vol. 96, no. 2, pp. 262–266, 1988.

[31] C. Caruso, C. Mohn, A. L. Karara et al., "Alpha-melanocyte-stimulating hormone through melanocortin-4 receptor inhibits nitric oxide synthase and cyclooxygenase expression in the hypothalamus of male rats," *Neuroendocrinology*, vol. 79, no. 5, pp. 278–286, 2004.

[32] A. B. Cragnolini, M. Perelló, H. B. Schiöth, and T. N. Scimonelli, "α-MSH and γ-MSH inhibit IL-1β induced activation of the hypothalamic-pituitary-adrenal axis through central melanocortin receptors," *Regulatory Peptides*, vol. 122, no. 3, pp. 185–190, 2004.

[33] C. Rivier, R. Chizzonite, and W. Vale, "In the mouse, the activation of the hypothalamic-pituitary-adrenal axis by a lipopolysaccharide (endotoxin) is mediated through interleukin-1," *Endocrinology*, vol. 125, no. 6, pp. 2800–2805, 1989.

[34] Q.-H. Huang, V. J. Hruby, and J. B. Tatro, "Systemic α-MSH suppresses LPS fever via central melanocortin receptors independently of its suppression of corticosterone and IL-6 release," *American Journal of Physiology—Regulatory Integrative and Comparative Physiology*, vol. 275, no. 2, pp. R524–R530, 1998.

[35] C. Papastathi, A. Mavrommatis, S. Mentzelopoulos, E. Konstandelou, M. Alevizaki, and S. Zakynthinos, "Insulin-like Growth Factor I and its binding protein 3 in sepsis," *Growth Hormone and IGF Research*, vol. 23, no. 4, pp. 98–104, 2013.

[36] T. Priego, M. Granado, I. Ibáñez de Cáceres, A. I. Martín, M. A. Villanúa, and A. López-Calderón, "Endotoxin at low doses

stimulates pituitary GH whereas it decreases IGF-I and IGF-binding protein-3 in rats," *Journal of Endocrinology*, vol. 179, no. 1, pp. 107–117, 2003.

[37] T. Priego, I. Ibáñez de Cáceres, A. I. Martín, M. A. Villanúa, and A. López-Calderón, "Endotoxin administration increases hypothalamic somatostatin mRNA through nitric oxide release," *Regulatory Peptides*, vol. 124, no. 1–3, pp. 113–118, 2005.

[38] A. Lelbach, J.-G. Scharf, and G. Ramadori, "Regulation of insulin-like growth factor-I and of insulin-like growth factor binding protein-1, -3 and -4 in cocultures of rat hepatocytes and Kupffer cells by interleukin-6," *Journal of Hepatology*, vol. 35, no. 5, pp. 558–567, 2001.

[39] T. Priego, I. Ibáñez de Cáceres, A. I. Martín, M. A. Villanúa, and A. López-Calderón, "Endotoxin decreases serum IGFBP-3 and liver IGFBP-3 mRNA: comparison between Lewis and Wistar rats," *Molecular and Cellular Endocrinology*, vol. 199, no. 1-2, pp. 23–28, 2003.

[40] A. I. Martín, M. López-Menduiña, E. Castillero, M. Granado, M. A. Villanúa, and A. López-Calderón, "Cyclooxygenase-2 activation by endotoxin mediates the decrease in IGF1, but not in IGFBP3, gene expression in the liver," *Journal of Endocrinology*, vol. 198, no. 2, pp. 385–394, 2008.

[41] E. M. Zimmermann, L. Li, E. C. Hoyt, J. B. Pucilowska, S. Lichtman, and P. K. Lund, "Cell-specific localization of insulin-like growth factor binding protein mRNAs in rat liver," *American Journal of Physiology: Gastrointestinal and Liver Physiology*, vol. 278, no. 3, pp. G447–G457, 2000.

[42] I. A. Malik, J. Triebel, J. Posselt et al., "Melanocortin receptors in rat liver cells: change of gene expression and intracellular localization during acute-phase response," *Histochemistry and Cell Biology*, vol. 137, no. 3, pp. 279–291, 2012.

[43] E. Castillero, M. López-Menduiña, A. I. Martín, M. A. Villanúa, and A. López-Calderón, "Comparison of the effects of the n-3 polyunsaturated fatty acid eicosapentaenoic and fenofibrate on the inhibitory effect of arthritis on IGF1," *Journal of Endocrinology*, vol. 210, no. 3, pp. 361–368, 2011.

[44] E. Jennische and C. M. Hall, "Expression and localisation of IGF-binding protein mRNAs in regenerating rat skeletal muscle," *APMIS*, vol. 108, no. 11, pp. 747–755, 2000.

[45] S. Jogie-Brahim, D. Feldman, and Y. Oh, "Unraveling insulin-like growth factor binding protein-3 actions in human disease," *Endocrine Reviews*, vol. 30, no. 5, pp. 417–437, 2009.

[46] M. S. Pampusch, E. Kamanga-Sollo, M. E. White, M. R. Hathaway, and W. R. Dayton, "Effect of recombinant porcine IGF-binding protein-3 on proliferation of embryonic porcine myogenic cell cultures in the presence and absence of IGF-1," *Journal of Endocrinology*, vol. 176, no. 2, pp. 227–235, 2003.

[47] H. Crossland, D. Constantin-Teodosiu, S. M. Gardiner, D. Constantin, and P. L. Greenhaff, "A potential role for Akt/FOXO signalling in both protein loss and the impairment of muscle carbohydrate oxidation during sepsis in rodent skeletal muscle," *The Journal of Physiology*, vol. 586, no. 22, pp. 5589–5600, 2008.

[48] O. Schakman, M. Dehoux, S. Bouchuari et al., "Role of IGF-I and the TNFα/NF-κB pathway in the induction of muscle atrogenes by acute inflammation," *The American Journal of Physiology—Endocrinology and Metabolism*, vol. 303, no. 6, pp. E729–E739, 2012.

[49] N. Alami, V. Page, Q. Yu et al., "Recombinant human insulin-like growth factor-binding protein 3 inhibits tumor growth and targets the Akt pathway in lung and colon cancer models," *Growth Hormone and IGF Research*, vol. 18, no. 6, pp. 487–496, 2008.

[50] M. Cortés-Sempere, M. P. De Miguel, O. Pernía et al., "IGFBP-3 methylation-derived deficiency mediates the resistance to cisplatin through the activation of the IGFIR/Akt pathway in non-small cell lung cancer," *Oncogene*, vol. 32, no. 10, pp. 1274–1283, 2013.

[51] S. S. Y. Chan, S. M. Twigg, S. M. Firth, and R. C. Baxter, "Insulin-like growth factor binding protein-3 leads to insulin resistance in adipocytes," *Journal of Clinical Endocrinology & Metabolism*, vol. 90, no. 12, pp. 6588–6595, 2005.

[52] E. Castillero, M. P. Nieto-Bona, C. Fernández-Galaz et al., "Fenofibrate, a PPARα agonist, decreases atrogenes and myostatin expression and improves arthritis-induced skeletal muscle atrophy," *American Journal of Physiology—Endocrinology and Metabolism*, vol. 300, no. 5, pp. E790–E799, 2011.

[53] Z. Hu, H. Wang, H. L. In, J. Du, and W. E. Mitch, "Endogenous glucocorticoids and impaired insulin signaling are both required to stimulate muscle wasting under pathophysiological conditions in mice," *The Journal of Clinical Investigation*, vol. 119, no. 10, pp. 3059–3069, 2009.

[54] S. C. Bodine, T. N. Stitt, M. Gonzalez et al., "Akt/mTOR pathway is a crucial regulator of skeletal muscle hypertrophy and can prevent muscle atrophy in vivo," *Nature Cell Biology*, vol. 3, no. 11, pp. 1014–1019, 2001.

JOURNAL OF PHYSIOLOGY AND PHARMACOLOGY 2012, 63, 6, 649-659
www.jpp.krakow.pl

A.I. MARTIN[1], M.P. NIETO-BONA[2], E. CASTILLERO[1], C. FERNANDEZ-GALAZ[1], M. LOPEZ-MENDUINA[1], A.B. GOMEZ-SANMIGUEL[1], C. GOMEZ-MOREIRA[1], M. ANGELES VILLANUA[1], A. LOPEZ-CALDERON[1]

EFFECT OF CYCLOOXYGENASE-2 INHIBITION BY MELOXICAM, ON ATROGIN-1 AND MYOGENIC REGULATORY FACTORS IN SKELETAL MUSCLE OF RATS INJECTED WITH ENDOTOXIN

[1]Department of Physiology, Faculty of Medicine, Complutense University of Madrid, Madrid, Spain;
[2]Department of Histology, Faculty of Health Sciences, Rey Juan Carlos University, Madrid, Spain

Cyclooxygenase-2-induction by inflammatory stimuli has been proposed as a mediator of inflammatory cachexia. We analyse whether cyclooxygenase-2 inhibition by meloxicam administration is able to modify the response of skeletal muscle to inflammation induced by lipopolysaccharide endotoxin (LPS). Male rats were injected with 1 mg kg^{-1} LPS at 17:00 h and at 10:00 h the following day, and euthanized 4, 24 or 72 hours later. Atrogin-1, MuRF1, myogenic regulatory factors and cyclooxygenase-2 in the gastrocnemius were determined by real time-PCR (mRNA) and Western blot (protein). In a second experiment the effect of meloxicam administration (1 mg kg^{-1}) was analyzed. Meloxicam was administered either in a preventive manner, 1 hour before each endotoxin injection, or in a therapeutic manner, starting 2 hours after the second LPS injection and at 24 and 48 hours afterwards. There was a marked increase in MuRF1 mRNA ($P<0.01$) 4 hours after LPS, and in atrogin-1 mRNA 4 hours ($P<0.01$) and 24 hours ($P<0.01$) after LPS. Cyclooxygenase-2 was increased, whereas MyoD was decreased at 4, 24 and 72 h. Both types of meloxicam treatment blocked LPS-induced increase in atrogin-1. Preventive, but not therapeutic, meloxicam decreased myostatin ($P<0.01$) and increased Pax7 ($P<0.01$) and MyoD ($P<0.05$). Therapeutic meloxicam treatment decreased gastrocnemius myogenin. These data suggest that cyclooxygenase-2 inhibition by meloxicam administration can prevent the increase in atrogin-1 and the decrease in MyoD induced by LPS administration. However, prolonged therapeutic meloxicam treatment seems to be less effective, since it can inhibit myogenic regulatory factors.

Key words: *cyclooxygenase-2, gastrocnemius muscle, lipopolysaccharide, MyoD, meloxicam, myostatin, myogenin, skeletal muscle, sepsis*

INTRODUCTION

Skeletal muscle is a plastic organ that can increase or decrease in volume in accordance with modifications in energy balance and environmental factors. Inflammatory illnesses such as sepsis, cancer and arthritis are associated with muscle wasting (1-3). Sepsis induces myopathy characterized by a reduction in muscle force-generating capacity and muscle wasting (3). Moreover, myopathy and its related syndromes are a major cause of mortality and long-term morbidity in critically ill patients (3). Critically ill patients with sepsis can have a 20% reduction in muscle mass within the first week (4). These patients have a normal muscle protein synthesis rate, whereas muscle proteolysis is increased up to 160% (5). Of the major proteolytic systems, ubiquitin-proteasome pathway is increased, whereas calpain and caspase activities are not changed in sepsis (5). The two E3 ubiquitin ligases, muscle RING-finger protein-1 (MuRF-1) and atrogin-1 are sensitive markers for muscular atrophy (6). The mechanisms by which chronic inflammatory diseases activate the ubiquitin-proteasome pathway are through the release of cytokines (2) or myostatin, a negative regulator of muscle mass (7).

Cyclooxygenases (COXs) are key enzymes in regulating the biosynthesis of prostaglandins. COX-2 isoform is inducible by pro-inflammatory cytokines and other stimuli, not only in immune cells, but also in other tissues such as skeletal muscle (8). COX-2 activation plays an important role in cachexia induced by experimental arthritis (3). Inhibition of COX-2, by meloxicam administration, ameliorates muscle wasting by preventing arthritis-induced upregulation of muscle atrogin-1 and MuRF1 (3). COX inhibitors are also able to improve cancer cachexia in both experimental animals and in humans (9, 10), by acting on the ubiquitin-proteasome pathway (11).

In spite of the anti-cachetic effect of anti-inflammatory therapy with COX-2 inhibitors, these drugs can have adverse effects on muscle regeneration and growth after muscle injury (12). COX-2 activation plays an important role in muscle regeneration after muscle injury (13). The role of COX-2 in muscle regeneration seems to be related to the fact that inflammatory response facilitates myogenesis (14). Although the role of COX-2 activation in sepsis is not well known, COX-2 inhibition prevents lipopolysaccharide-induced decrease in serum and liver IGF-I and decreases pro-inflammatory cytokines and liver injury in septic rats (15, 16).